Understanding the role of NOS1AP on ECG parameters and arrhythmogenesis: insights from mice and men

Thesis submitted for the degree of

Doctor of Philosophy

University of Oxford

Parag R. Gajendragadkar

Division of Cardiovascular Medicine

Radcliffe Department of Medicine

&

Hertford College





Supervisors

Professor Barbara Casadei

Professor Jemma C Hopewell

Dr Jillian N Simon

January 2022

Acknowledgements

The work presented here would not be possible without a number of people. Firstly, thanks to the British Heart Foundation for funding the research initially. Secondly, heartfelt thanks to my supervisors - Barbara Casadei for continuously setting higher standards for me to push myself towards and Jemma Hopewell for taking a chance on me and nurturing my development in a very different environment. To my final supervisor Jillian Simon - a big thank you for your patience and friendship at all times, both at work and outside. Also, I felt extremely privileged to have all the staff in the various research teams selflessly welcome me and make my time with them fun and fruitful.

Finally, and most importantly, my heartfelt gratitude to my whole family and especially my young children for their tolerance, support and understanding. They dealt with the things that needed dealing with, and got on with life whilst I was busy (yet again) 'doing work for my DPhil thesis'.

Abstract

Understanding the role of NOS1AP on ECG parameters and arrhythmogenesis: insights from mice and men

Thesis submitted for degree of DPhil in Medical Sciences, November 2021

Of the parameters on a surface ECG, the QT interval, which represents ventricular repolarisation, has arguably been the most studied. In humans, observational data suggests both short and long QT intervals are associated with a higher risk of ventricular and atrial arrhythmias. However, these observational studies are subject to limitations such as confounding and reverse causality, so the causal relevance is unclear. Unexpectedly, the strongest common non-coding genetic variants associated with a longer QT interval across populations map within an enhancer of the Nitric Oxide Synthase 1 Adaptor Protein (*NOSIAP*) gene, which are associated with higher myocardial *NOSIAP* transcript expression. However, the mechanism by which the NOSIAP protein affects the QT interval and the risk of arrhythmia remains unclear.

The aim of this thesis was to investigate the mechanistic effects of cardiac-limited *NOSIAP* over-expression on ECG parameters and arrhythmogenesis in a transgenic mouse model and subsequently investigate the causal relevance of ECG parameters more broadly in human arrhythmogenesis using large-scale population data.

A transgenic mouse overexpressing human *NOSIAP* in the myocardium (NOSIAP-Tg) was generated and phenotyped. NOSIAP-Tg showed a modest increase in NOSIAP protein (~2.5-fold) in all cardiac chambers. Subsequent phenotyping revealed a longer P-wave duration, PR interval and QRS interval, but a shorter measured QT interval on ECG. The mice had a higher propensity to induced *ex-vivo* ventricular arrhythmias and *in-vivo* atrial arrhythmias in the absence of echocardiographic differences in cardiac structure or function. Investigation of the cardiac electrical substrate resulting from *NOSIAP* overexpression revealed no significant difference in action potential durations (APD) between genotypes at physiological heart rates, although a shorter APD was seen at slower heart rates in NOSIAP-Tg hearts. There was a significant reduction in conduction velocity in the left ventricles of transgenic mice in the absence of an increase in cardiac fibrosis. The slower conduction velocity in NOSIAP-Tg was associated with lower connexin-43 protein content at the intercalated disc. No differences in calcium handling, NOSI content or NOS activity were detected between genotypes. Exploratory analyses did not suggest gross differences in the rapid sodium current I_{Na}.

We subsequently investigated the causal relevance in humans of altered ECG parameters (observed in NOSIAP-Tg mice) and risks of development of atrial fibrillation (AF). To overcome limitations from existing observational data, we employed Mendelian randomisation techniques using weighted genetic scores for P-wave duration, PR interval and QT interval representing lifelong differences in cardiac electrical parameters. We showed novel evidence supporting causal relationships between lifelong differences in electrical parameters and risks of developing both AF and non-AF supraventricular tachycardias in large human population datasets. Unexpectedly, results supported a causal association between lifelong differences in ECG parameters representing longer atrial conduction times within the normal range, and a lower risk of AF.

Overall, the findings suggested that NOSIAP impairs cardiac electrical conductance and coupling by reducing connexin-43 protein stability and highlight the need for investigations of the impact of gene variation on NOSIAP protein and subcellular localisation in the human myocardium. Future investigation of the electrical substrate using an integrative combination of fundamental molecular knowledge, genetics and electrophysiology may yield novel insights and new therapeutic options.

Declaration

I declare that all the work presented in this thesis is the result of my own work, except for work done with significant collaboration as declared below, with other assistance specified and clearly acknowledged in the text throughout.

- As declared in **Section 3.2**, generation of the transgenic mouse model was performed by Dr. Ben Davies, Transgenic Core Head at the Wellcome Centre for Human Genetics, University of Oxford and his group at our request.
- As declared in **Section 4.2.4** and **Section 4.2.8**, Dr Jakub Tomek from the Department of Physiology, Anatomy and Genetics at the University of Oxford analysed optical mapping and quantitative connexin-43 immunofluorescence data in a blinded manner on my behalf.
- As declared in **Section 4.2.8**, Dr Jillian Simon from the Department of Cardiovascular Medicine at the University of Oxford significantly assisted me with optimisation of the immunofluorescence experiments.
- As declared in **Section 4.2.9**, Dr Xing Liu performed experiments and analysed data regarding exploratory sodium current analyses.
- The work presented in **Chapter 6** resulted in a publication:
    - **Gajendragadkar PR**, Von Ende A, Ibrahim M, Valdes-Marquez E, Camm CF, Murgia F, Stiby A, Casadei B, Hopewell JC. Assessment of the causal relevance of ECG parameters for risk of atrial fibrillation: A Mendelian randomization study. PLoS Med. 2021; 18(**5**):e1003572. doi: 10.1371/journal.pmed.1003572. PMID: 33983917.
    - Whilst the data, figures and analyses presented in the thesis are my own, I acknowledge the contribution of my co-authors across a variety of data curation, software and bioinformatic aspects in helping me obtain these data and publish the paper above.

I declare the work presented here is not substantially the same as any that I have submitted, or, is being concurrently submitted for a degree or diploma or other qualification at the University of Oxford or any other University or similar institution.

Table of Contents

Chapter 1: Introduction 1

Summary 1

1.1 Parameters on the electrocardiogram 2

1.2 The QT interval and ventricular arrhythmias 3

1.2.1 First descriptions 3

1.2.2 Contemporary views about the QT interval on surface ECG 4

Drug induced long QT syndrome 4

Congenital long QT syndromes 5

Sudden death and the QT interval in the general population 6

1.3 The QT interval and atrial arrhythmias 8

1.4 Genetics of the QT interval 8

1.5 Genetic variation in *NOS1AP* and the QT interval 9

1.5.1 Insights from genome-wide association studies 9

1.5.2 Genetic insights from specific populations 11

Relevance of variation in NOS1AP to the QT interval across other populations 11

Relevance of variation in NOS1AP to risk of sudden death in the general population 12

Relevance of variation in NOS1AP to risk of drug-induced QT prolongation 12

Relevance of variation in NOS1AP to those with 'Mendelian' long QT syndromes 13

1.5.3 Functional consequences of *NOS1AP* polymorphism 16

1.6 Function of the NOS1AP protein 19

1.6.1 Insights from neurobiology 19

1.6.2 NOS1AP and electrophysiology 20

Cardiac sympathetic neurons 20

Experiments in cardiac tissues 21

NOS1AP:NOS1 interactions in cardiac tissues 22

1.7 Aims and objectives 25

Chapter 2: General laboratory methods 26

Summary 26

2.1 Assessment of gene expression 27

2.1.1 RNA isolation 27

2.1.2 Reverse transcription to cDNA 27

2.1.3 Quantitative real-time PCR 27

2.1.4 Quantification of gene expression results 27

2.2 Assessment of protein expression by Western blotting 28
2.2.1 Sample preparation 28
2.2.2 Estimation of sample protein content 28
2.2.3 Protein separation and transfer to membranes 28
2.2.4 Quantification of protein content 29
2.3 Myocyte isolation 29

Chapter 3: Phenotype of Tg(*Myh6-hNOS1AP*) 30
Summary 30
3.1 Introduction 31
3.2 Methods of mouse model generation 34
3.2.1 Cloning of the overexpression construct 34
3.2.2 Genotyping PCR for screening 35
3.2.3 Pronucleus microinjection 37
3.2.4 Screening for transgenic founders 38
3.2.5 Breeding of Tg(*Myh6-hNOS1AP*) 39
3.2.6 Genotyping protocol for breeding 39
3.2.7 Tissue collection 40
3.3 Chapter specific methods 42
3.3.1 Assessment of gene expression 42
3.3.2 Assessment of protein expression 42
3.3.3 Echocardiography 43
3.3.4 Electrocardiography 44
3.3.5 Ventricular arrhythmia induction *ex-vivo* 45
3.3.6 Statistical methods 46
3.4 Results 48
3.4.1 The transgenic mouse model has myocardial specific gene and protein overexpression of NOS1AP 48
Gene expression profile 48
Protein expression profile 48
3.4.2 Cardiac structure or function was unaffected in the transgenic mouse model 51
3.4.3 Surface ECG parameters are altered in transgenic mice with myocardial *NOS1AP* overexpression 51
3.4.4 The probability of *ex-vivo* pacing induced ventricular arrhythmias is increased in transgenic mice 55
3.5 Discussion 57
3.5.1 Summary of results 57

3.5.2 Comparing NOS1AP expression in mouse model and humans 57
Gene expression *57*
Protein expression *58*
3.5.3 Comparing ECG parameters in NOS1AP-Tg and humans 60
ECG parameters representing ventricular repolarisation *60*
ECG parameters representing depolarisation and conduction velocity *61*
Sex-specific differences *62*
3.5.4 Ventricular arrhythmias in transgenic model compared to humans 62

Chapter 4: Mechanisms underlying the cardiac electrical phenotype in Tg(*Myh6-hNOS1AP*) 65
Summary 65
4.1 Introduction 66
4.1.1 ECG parameters and the electrical substrate 66
4.1.2 NOS1AP and calcium handling 67
4.1.3 NOS1AP and NOS1 67
4.2 Chapter specific methods 69
4.2.1 Total collagen assay 69
4.2.2 Ventricular monophasic action potential measurements 69
Measurements *69*
Analysis *69*
4.2.3 Calcium transient measurements 70
Measurements *70*
Analysis *71*
4.2.4 Conduction velocity measurements using optical mapping 71
Measurements *71*
Analysis *74*
4.2.5 Assessment of gene expression 76
4.2.6 Assessment of protein expression 76
4.2.7 NOS activity assay 77
Measurements *77*
Analysis *77*
4.2.8 Immunofluorescence 78
General Methods *78*
Connexin-43 quantification *79*
4.2.9 Single-cell I_{Na} current measurements 80
4.2.10 Statistical methods 81
Sample size calculations *81*

Statistical testing *81*
4.3 Results 83
4.3.1 Differences in left ventricular collagen content do not explain arrhythmogenic phenotype 83
4.3.2 Left ventricular monophasic action potential durations are shorter in transgenic mice at slower, but not physiological heart rates 84
4.3.3 Calcium handling in ventricular cardiomyocytes is not affected by myocardial overexpression of *NOS1AP* 89
4.3.4 Transgenic mice have slower left ventricular epicardial conduction as measured by optical mapping 90
4.3.5 Myocardial overexpression of *NOS1AP* is associated with a reduction in connexin-43 92
Gene expression *92*
Protein expression *93*
Localisation *94*
4.3.6 Myocardial overexpression of *NOS1AP* is not associated with changes in NOS1 gene or protein expression or alterations in NOS1 activity 96
Gene expression *96*
Protein expression *97*
NOS activity in left ventricular tissue homogenates *97*
Immunofluorescence *98*
4.3.7 Exploratory sodium current data 99
4.4 Discussion 104
4.4.1 Action potential duration 104
Specifics of APD measurements *104*
Species-specific differences *106*
Repolarisation reserve *107*
4.4.2 Calcium handling 108
4.4.3 Conduction velocity 109
Tissue architecture *109*
Myocyte coupling via gap junctions *110*
Depolarising sodium current I_{Na} *113*
4.4.4 NOS1AP and NOS1 114
NOS1AP-NOS1 interaction *114*
NOS1 protein levels *115*
NOS1 activity *115*
NOS1AP-NOS1 localisation *117*
4.4.5 Sex-specific differences 118

Chapter 5: Atrial arrhythmias in Tg(*Myh6-hNOS1AP*) 120
Summary 120
5.1 Introduction 121
5.1.1 ECG parameters in murine models of atrial arrhythmias 121
5.1.2 NOS1AP, QT interval and AF in humans 121
5.2 Chapter specific methods 123
5.2.1 Atrial fibrillation induction *in-vivo* 123
5.2.2 Assessment of protein expression 123
5.2.3 Statistical methods 124
5.3 Results 125
5.3.1 The probability of *in-vivo* pacing induced atrial arrhythmias is increased in transgenic mice 125
5.3.2 Exploratory data on atrial connexin-40 protein levels 129
5.4 Discussion 130
5.4.1 Atrial Arrhythmogenesis in NOS1AP-Tg 130
5.4.2 Implications for human atrial arrhythmogenesis 131

Chapter 6: Causal relevance of ECG parameters and atrial arrhythmias in humans . 133
Summary 133
6.1 Introduction 134
6.1.1 Historical perspective of ECG parameters and atrial fibrillation 134
6.1.2 Contemporary perspective of mechanisms of atrial fibrillation and ECG parameters 135
Triggers for atrial fibrillation 135
Substrate for sustaining atrial fibrillation 135
The ECG in atrial fibrillation 136
6.1.3 Observational data linking ECG parameters and AF 136
P-wave duration and AF 136
PR interval and risk of AF 137
QT interval and risk of AF 138
6.1.4 Limitations of observational data 139
6.1.5 Mendelian randomisation 139
6.2 Methods 141
6.2.1 Study populations and outcome definitions 141
UK Biobank 141
Defining AF, SVT, and other outcomes in UK Biobank 143

6.2.2 Selection of genetic variants 146
Selection of genetic variants for P-wave duration score 147
Selection of genetic variants for PR interval duration score 147
Selection of genetic variants for QT interval score 148
Selection of genetic variants for ion channel scores 148
6.2.3 Statistical analysis 152
UK Biobank 152
Power calculations 152
External replication dataset 154
Sensitivity analyses in UK Biobank 154
6.2.4 Standard protocol approvals, registration and patient consent 159
6.3 Results 160
6.3.1 UK Biobank participant characteristics 160
6.3.2 Genetic scores associated with measured 12-lead ECG parameters 160
6.3.3 Genetically predicted differences in ECG parameters and risk of AF 162
6.3.4 Genetically predicted differences in ECG parameters and risk of SVT 167
6.3.5 Genetically predicted ECG parameter score associations with left atrial size on cardiac MRI 169
6.3.6 Genetically predicted ECG parameters, via ion channel pathways, and risk of AF, lone AF and SVT 169
6.3.7 Independent replication and meta-analysis 169
6.3.8 Sensitivity analyses 172
Genetically predicted risk of AF and effect on 12-lead ECG parameters 172
Sensitivity analyses for pleiotropy and other assumption violations 172
6.4 Discussion 180
6.4.1 ECG parameters as predictors of AF 180
6.4.2 Mechanistic insights into pathophysiology of arrhythmias 181
6.4.3 Limitations 183
6.4.4 Conclusion 185
6.4.5 Implications for NOS1AP-Tg 185

Chapter 7: Conclusions 186
Summary 186
7.1 Discussion of key findings 187
7.1.1 Summary 187
7.1.2 NOS1AP and the electrical substrate 188
Conduction velocity and depolarisation 188
Conduction velocity and repolarisation 189

Mapping repolarisation in humans *190*
Intercalated disc and QT interval *191*
7.1.3 Mechanisms of arrhythmogenesis 192
NOS1AP and arrhythmia triggers *192*
NOS1AP and the autonomic system *193*
7.1.4 ECG parameters and arrhythmias 193
7.2 Limitations 195
7.2.1 Transgenic mouse model 195
Rationale for generation *195*
Generation of model *195*
Fundamental use of murine model *195*
7.2.2 Population science work 196
7.3 Future work 196

List of Figures

Chapter 1: Introduction 1
Figure 1.1 – Einthoven's ECG tracing 2
Figure 1.2 – Representative ECG complex 3
Figure 1.3 – Regional association with QT interval around *NOS1AP* gene 10
Figure 1.4 – Associations between genetic QT scores and long QT syndrome 15
Figure 1.5 – eQTL data showing gene expression for *NOS1AP* polymorphisms 16
Figure 1.6 – *NOS1AP* gene expression across different tissues by allele 17
Figure 1.7 – Initial proposed mechanisms of NOS1AP (CAPON) action in neurons 19
Chapter 3: Phenotype of Tg(*Myh6-hNOS1AP*) 30
Figure 3.1 – Plasmid map of pMyh6-NOS1AP 35
Figure 3.2 – Screening PCR 36
Figure 3.3 – Oocyte microinjection 37
Figure 3.4 – Screening for transgenic founders 39
Figure 3.5 – Validation of genotyping protocol 40
Figure 3.6 – Representative echocardiography image 43
Figure 3.7 – Representative ECG trace denoting interval measurements 45
Figure 3.8 – Gene expression profile of *NOS1AP* in Tg(*Myh6-hNOS1AP*) colony 49
Figure 3.9 – Protein expression profile of NOS1AP in Tg(*Myh6-hNOS1AP*) colony 50
Figure 3.10 – Qualitative differences in ECG traces for Tg(*Myh6-hNOS1AP*) colony 52
Figure 3.11 – ECG parameter values for Tg(*Myh6-hNOS1AP*) colony 52
Figure 3.12 – ECG parameter values by sex 54
Figure 3.13 – Ventricular arrhythmias in *ex-vivo* hearts of Tg(*Myh6-hNOS1AP*) colony .. 56
Chapter 4: Mechanisms underlying the cardiac electrical phenotype in Tg(*Myh6-hNOS1AP*) 65
Figure 4.1 – Action potential duration measurements from monophasic action potential . 70
Figure 4.2 – Optical mapping setup 73
Figure 4.3 – Example analysis of optical mapping data 75
Figure 4.4 – Example traces from NOS activity assay 78
Figure 4.5 – Left ventricular collagen content for Tg(*Myh6-hNOS1AP*) colony 83
Figure 4.6 – Left ventricular monophasic action potential duration (APD) comparisons ... 85
Figure 4.7 – Left ventricular *ex-vivo* monophasic action potential durations 86
Figure 4.8 – Left ventricular APD_{90} values by sex 88
Figure 4.9 – Example calcium transient traces 89
Figure 4.10 – Data from left ventricular optical mapping experiments 91

Figure 4.11 – Gene expression profile of *Gja1* in Tg(*Myh6-hNOS1AP*) colony 93
Figure 4.12 – Connexin-43 protein expression 94
Figure 4.13 – Cx43 and N-cadherin in left ventricular myocytes 95
Figure 4.14 – Gene expression profile of *Nos1* in Tg(*Myh6-hNOS1AP*) colony 96
Figure 4.15 – NOS1 protein expression..... 97
Figure 4.16 – NOS activity (L-NAME inhibitable fraction) in the left ventricle 98
Figure 4.17 – NOS1AP and NOS1 in left ventricular myocytes..... 99
Figure 4.18 – Example raw tracings for sodium current measurements..... 100
Figure 4.19 – Sodium current characteristics..... 102
Figure 4.20 – Effects of SMTC on the sodium current 103
Chapter 5: Atrial arrhythmias in Tg(*Myh6-hNOS1AP*) 120
Figure 5.1 – Representative ECG trace showing burst pacing induced atrial arrhythmia 125
Figure 5.2 – Probabilities of atrial arrhythmia induction for Tg(*Myh6-hNOS1AP*) colony 127
Figure 5.3 – Duration of induced atrial arrhythmias for Tg(*Myh6-hNOS1AP*) colony..... 128
Figure 5.4 – Probability of atrial arrhythmia induction for Tg(*Myh6-hNOS1AP*) colony by sex 129
Figure 5.5 – Exploratory atrial connexin-40 protein expression..... 129
Chapter 6: Causal relevance of ECG parameters and atrial arrhythmias in humans. 133
Figure 6.1 – Example overview of Mendelian randomisation 140
Figure 6.2 – Generation of main analyses datasets..... 142
Figure 6.3 – Details of genetic variant selection..... 146
Figure 6.4 – Distribution of genetic scores in UK Biobank Population..... 153
Figure 6.5 – Associations between genetic scores and 12-lead ECG parameters in UK Biobank 161
Figure 6.6 – Effects of genetically predicted ECG parameters on risk of atrial fibrillation in UK Biobank 163
Figure 6.7 – Effects of genetically predicted ECG parameters on risk of ‘lone’ atrial fibrillation in UK Biobank..... 165
Figure 6.8 – Effects of genetically predicted ECG parameters on risk of ‘lone’ atrial fibrillation in UK Biobank..... 166
Figure 6.9 – Effects of genetically predicted ECG parameters on risk of supraventricular tachycardias in UK Biobank..... 168
Figure 6.10 – Effects of genetically predicted ECG parameters on risk of atrial fibrillation in UK Biobank and AFGen 171
Figure 6.11 – Funnel plot for SNPs in P-wave duration score..... 177
Figure 6.12 – Funnel plot for SNPs in PR interval score 178
Figure 6.13 – Funnel plot for SNPs in QT interval score 179

Chapter 7: Conclusions 186
Figure 7.1 – Genetic associations across ECG timepoints 199

List of Tables

Chapter 3: Phenotype of Tg(*Myh6-hNOS1AP*) 30
Table 3.1 – Details of screening primers for PCR 36
Table 3.2 – Screening PCR reaction details 36
Table 3.3 – Microinjections performed 38
Table 3.4 – Genotyping PCR protocol 40
Table 3.5 – Correction formulae used for QT interval 45
Table 3.6 – Echocardiography parameters for Tg(*Myh6-hNOS1AP*) colony 51
Table 3.7 – Heart rate corrected QT intervals for Tg(*Myh6-hNOS1AP*) colony 53
Chapter 4: Mechanisms underlying the cardiac electrical phenotype in Tg(*Myh6-hNOS1AP*) 65
Table 4.1 – Conditions for immunofluorescence staining 79
Table 4.2 – Left ventricular action potential durations at 90% repolarisation (APD_{90}) 84
Table 4.3 – Slope coefficients for cycle length vs action potential duration 86
Table 4.4 – Calcium transient parameters in Tg(*Myh6-hNOS1AP*) colony 89
Chapter 6: Causal relevance of ECG parameters and atrial arrhythmias in humans . 133
Table 6.1 – Phenotype codes for definition of atrial fibrillation 144
Table 6.2 – Phenotype codes for other definitions 145
Table 6.3 – SNPs included in P-wave duration score 149
Table 6.4 – SNPs included in PR interval score 149
Table 6.5 – SNPs included in QT interval score 150
Table 6.6 – Power calculations for genetic ECG scores 154
Table 6.7 – SNPs included in AF score 156
Table 6.8 – Baseline characteristics of participants in UK Biobank 160
Table 6.9 – Baseline characteristics of participants with SVT in UK Biobank 167
Table 6.10 – Effect of genetic risk score for atrial fibrillation on 12-lead ECG parameters 172
Table 6.11 – Sensitivity analyses for estimate of ECG score effects on atrial fibrillation in UK Biobank 174
Table 6.12 – Phenoscanner derived details for non-ECG parameter associated traits for SNPs in ECG scores 175

Common Abbreviations

AF	Atrial fibrillation
ANOVA	Analysis of variance
APD	Action potential duration
AV	Atrio-ventricular
$[Ca^{2+}]_i$	Calcium transient
CAPON	C-terminal adaptor protein for nitric oxide synthase 1
CI	Confidence interval
Cx40	Connexin-40
Cx43	Connexin-43
DNA	Deoxyribose nucleic acid
ECG	Electrocardiogram
eQTL	Expression quantitative trait loci
ERP	Effective refractory period
GWAS	Genome-wide association study
I_{Na}	Depolarising sodium current
LA	Left atrium
LV	Left ventricle
LD	Linkage disequilibrium
L-NAME	*N*ω-nitro-L-arginine methyl ester chloride
LQT	Long QT (syndrome)
LV	Left ventricle
MAP	Monophasic action potential
MR	Mendelian randomisation
MRI	Magnetic resonance imaging
mRNA	Messenger ribose nucleic acid
NOS1 / nNOS	Nitric oxide synthase 1 / Neuronal nitric oxide synthase
NOS1AP	Nitric oxide synthase 1 adaptor protein
NOS1AP-Tg	NOS1AP overexpressing transgenic mouse [Tg(*Myh6-hNOS1AP*)]
OR	Odds ratio
PCR	Polymerase chain reaction
RA	Right atrium
RV	Right ventricle
SD	Standard deviation
SMTC	S-Methyl-L-thiocitrulline
SNP	Single nucleotide polymorphism
SVT	Supraventricular tachycardia
Tg	Transgenic
UKB	UK Biobank
VF / VT	Ventricular fibrillation / Ventricular tachycardia
WT	Wild-type

1

Introduction

Summary

The QT interval on the electrocardiogram predominantly represents cardiac ventricular electrical repolarisation. Prolongation of this, either due to congenital genetic defects taking the form of long QT syndromes or due to medications, are linked to an increased incidence of ventricular arrhythmias. Variation in the QT interval within the healthy population may also predict risk of sudden death but there is marked variability. Genome-wide association studies now suggest that a significant proportion of variation in the QT interval is hereditary and explained in a polygenic manner, which may have further relevance to those with long QT syndromes. Surprisingly, the strongest genetic associations with the QT interval in healthy populations were linked to variants increasing the expression of *NOSIAP* (Nitric Oxide Synthase 1 Adaptor Protein), which had not previously been recognised as being of relevance to cardiac physiology. Following on from initial descriptions from neurobiology, NOSIAP has been somewhat inconsistently linked in cell models to alterations in myocyte electrophysiology, possibly mediated by NOSI. Thus, the development of a whole organ model which could investigate the potential alteration of cardiac electrical substrate and mechanisms of arrhythmogenesis related to NOSIAP overexpression is needed.

1.1 Parameters on the electrocardiogram

The electrocardiogram (ECG) is a recording that represents the spread of electrical activity through the heart and is, nowadays, used routinely in clinical practice. Around the turn of the 20th century, Dutch physician Willem Einthoven improved upon Augustus D Waller's early methods to record the electrical activity of the heart and demonstrated five deflections which he designated PQRST (**Figure 1.1**), named after Descartes' original mathematical traditions, which led to him being awarded the Nobel Prize for Physiology or Medicine in 1924 [1-3]. Subsequent improvements in lead placement and technology over the next fifty years finally led to the current 12-lead ECG being standardised by the American Heart Association in 1954 [4].

Figure 1.1 – Einthoven's ECG tracing

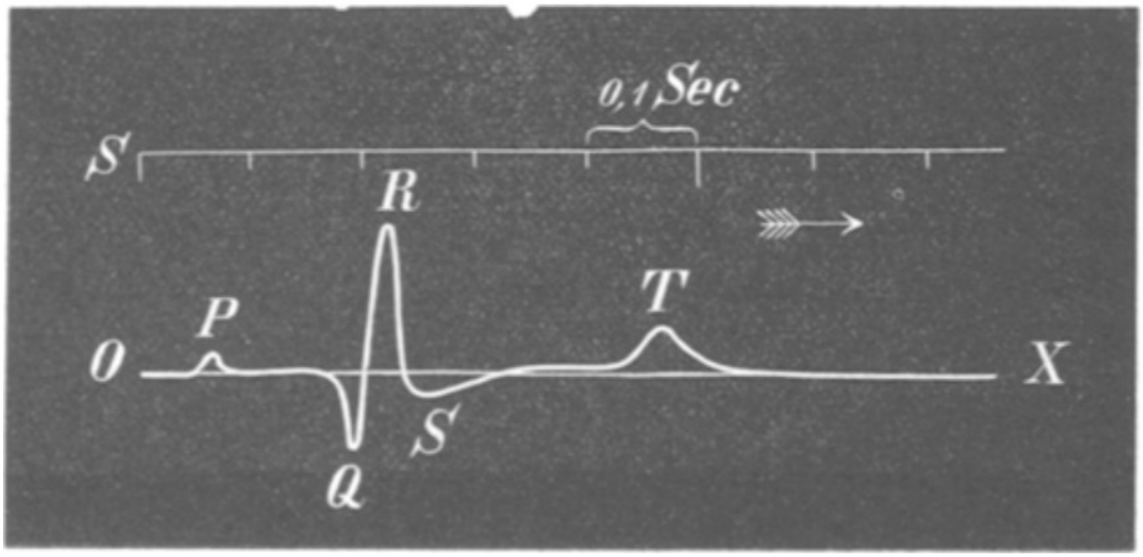


Figure 1.1: Einthoven's corrected P-Q-R-S-T deflections representing the spread of electrical activity through a human heart over one heartbeat, measured using a capillary electrometer [2].

Broadly speaking, the P-wave and the QRS complex represent atrial and ventricular depolarisation respectively. The PR or PQ interval represents the total time taken for electrical activity to transit through the atria and atrio-ventricular node, whilst the QT interval represents the time taken for the ventricles to depolarise and repolarise (**Figure 1.2**). However, as the time taken for ventricular depolarisation is normally very short, in common practice the QT interval is primarily taken to represent ventricular repolarisation.

Figure 1.2 – Representative ECG complex

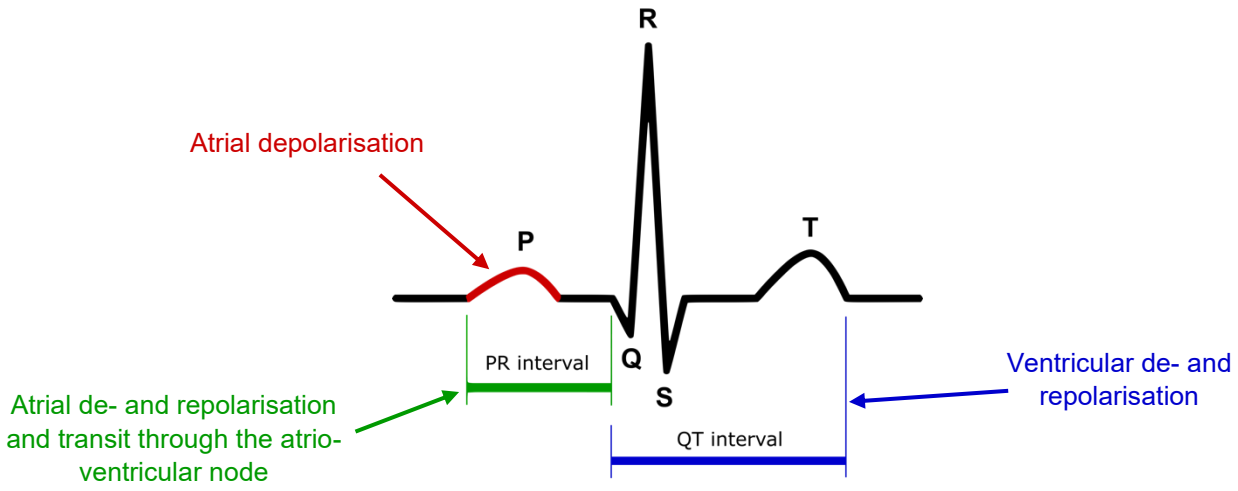


Figure 1.2: Representative single ECG complex showing key parameters and the presumed underlying electrical activity.

1.2 The QT interval and ventricular arrhythmias

Ventricular arrhythmias in the form of ventricular tachycardia (VT) or ventricular fibrillation (VF) result in inefficient or chaotic mechanical contraction of the ventricles, leading to a reduced or non-existent cardiac output and cardiac arrest. These lethal ventricular arrhythmias are thought to be the final mechanism in 15-20% of all deaths globally, being the leading cause of death in patients with pre-existing cardiovascular disease and are thought to be the cause of the syndrome of 'sudden cardiac death' or 'spontaneous cardiac arrest' [5-7].

1.2.1 First descriptions

It took some time for the links between a long QT interval and an increased risk of ventricular arrhythmias to be made. The first descriptions of prolonged QT interval on an ECG being associated with sudden death came in 1957 and 1960, when Jervell and Lange-Nielsen and then Romano and Ward described familial syndromes involving "fainting attacks" followed by sudden cardiac death with associated prolongations of the QT interval, but crucially without capturing the malignant arrhythmia [8]. In 1960, ventricular fibrillation as a result of an R wave falling on a T-wave was described by Smirk and Palmer [9]. By contrast, they did not show any connection with

prolonged QT intervals. Meanwhile, the first description by Selzer and Wray of paroxysmal VT and VF due to quinidine (then used for atrial arrhythmias) in 1964 [10] was followed by Desertenne in 1966 coining the term 'torsades de pointes' to describe polymorphic VT in those with atrio-ventricular block [11]. However, it wasn't until the 1970s that prolonged QT intervals were recognised as being fundamental to the pathology of polymorphic VT and that drug induced long QT syndrome was recognised more formally [12].

Given its familial clustering from the original descriptions, a genetic basis for long QT syndrome was long suspected, but it wasn't until the 1990s that, using linkage analysis, mutations in the *KCNQ1* gene were identified as responsible [13-15]. This set the scene for the contemporary understanding of defects in repolarising currents affecting the QT interval in these presumed Mendelian disorders. In parallel, for drug induced acquired QT prolongation, an individual's predisposition was always suspected as a risk factor, but it wasn't until the 1980s that it was noted that those who were at risk of developing drug induced torsades de pointes had QT intervals at the upper limit of the normal range and block of the inward rectifier potassium current (I_{Kr}) was identified as causative [16].

1.2.2 Contemporary views about the QT interval on surface ECG

Drug induced long QT syndrome

Drug-induced long QT syndrome is now a well recognised entity that is a key feature of drug safety and development [17,18]. Briefly, after further work identified the gene for *KCNH2* (formerly termed *HERG*) as encoding the channel responsible for I_{Kr} and inherited long QT syndrome type 2 [19], it became apparent that most drugs leading to long QT syndrome inhibited this particular repolarising current [20]. The risk of drug induced long QT syndrome leading to polymorphic VT and VF is however, not universal. Firstly, not all QT prolongation appears to confer an increased arrhythmic risk – for instance the use of amiodarone does not result in arrhythmias despite prolonging the QT interval [20]. Secondly, it is clear that not every person develops drug induced QT prolongation with the same medications, and the risk of arrhythmias is also very variable [20].

To explain these findings, Dan Roden coined the term 'repolarisation reserve' [21,22]. Evidence suggests that repolarisation is not solely accomplished by a single current and that a multitude of currents contribute to this complex phenomenon, such that some accommodation for impaired repolarisation might be possible if other mechanisms were intact [22,23]. Mechanisms that may reduce repolarisation reserve include acquired ones such as hypokalaemia and bradycardia. There is also now some genetic evidence supporting the concept of repolarisation reserve with suggestion that the variation in response to drug induced QT prolongation may be partially explained by common genetic variants affecting the QT interval [24].

Congenital long QT syndromes

Whilst mutations in 17 distinct genes had previously been described to result in subtypes of congenital long QT syndrome (LQT), recent re-appraisals confirmed only three genes as definitively causative – *KCNQ1* (LQT1), *KCNH2* (LQT2) and *SCN5A* (LQT3), accounting for approximately 80% of cases with another four genes showing strong evidence of causation (*CALM1-3*, *TRDN*) [25-28]. A number of mutations in each gene have been described, with the severity of the clinical condition thought to be related to their corresponding 'position' within the subsequent protein and its functional significance [25,26]. It is clear nowadays that there is variable penetrance within families – i.e. family members are affected differently by the same mutations, both in terms of the length of the QT interval as well as the clinical course [25-27].

The different subtypes of LQT have been classically described as having differing T-wave morphologies on the ECG, different triggers for ventricular arrhythmias, and differing clinical courses [27]. Specifically, individuals with LQT1 generally have a more favourable course and response to treatment than those with LQT2 or LQT3 [27]. Whilst an extremely long heart-rate corrected QT_c interval (i.e. > 500 ms) makes the diagnosis of a long QT syndrome extremely likely, it is possible that such extreme values may not be seen at rest or at all, and that a failure of a mildly prolonged QT interval to shorten on exercise may be the only obvious ECG feature in the context of syncopal episodes representing ventricular arrhythmias [25,27]. The 'Schwartz-score' also proposes notching on the T-wave as a feature lending itself to aid in the diagnosis, suggesting not

all risk is captured simply by the length of the QT interval [25,27]. Lahrouchi *et al*. [29] found that patients with long QT syndrome without a recognised pathogenic mutation (so called 'genotype negative'; comprising ~20% of diagnoses) had a significantly increased burden of 'common' variants associated with QT prolongation when compared either with patients with long QT syndrome who had a defined pathogenic variant, or healthy controls. This suggests that genotype negative long QT syndrome may be a polygenic condition, with accumulation of numerous smaller factors ultimately reducing the repolarisation reserve and prolonging the QT interval.

The interaction between the specific LQT subtype and the autonomic nervous system appears to have an important bearing on clinical outcomes. Patients with LQT1 syndrome appear to have arrhythmias triggered by sympathetic stimulation such as exercise, responding well to beta-blockade and left cardiac sympathetic denervation [30-32]. By contrast, those with LQT3 are typically described as experiencing ventricular arrhythmias at times of higher vagal tone and slower heart rates such as during sleep, with beta-blockers being reported to sometimes worsen symptoms [31].

Overall, these findings suggest that even in long QT syndrome, the QT interval is a complex representation of a number of underlying cardiac electrical processes, likely modified by other genetic and autonomic influences, and is not the sole determinant of ventricular arrhythmogenesis.

Sudden death and the QT interval in the general population

With insights from drug induced long QT and congenital long QT syndromes, the question of whether an individual's QT interval is associated with risk of sudden death has been studied in observational studies over many years with variable results.

Observational studies suggested that a prolonged QT interval in patients with pre-existing structural heart disease was a risk factor for sudden death [33,34], but data from the Framingham heart study reported that QT interval was not associated with any risks of all-cause mortality, sudden death or cardiovascular mortality [35]. Other studies then confirmed that a significant

proportion of the risk seen with an increased QT interval in the general population was associated with concomitant coronary disease [36]. This highlights the problem of confounding when considering observational data – in this case coronary heart disease affecting both the QT interval and the risk of sudden death.

In a systematic review of the prospective studies investigating QT interval and cardiovascular outcomes, Montanez *et al.* [37] commented that there were inconsistent associations reported across the studies using variable definitions of a 'prolonged' QT interval with variable subgroups defining age and inconsistent definitions of end-points. The heterogeneity in part relates to practical definitions as to how the QT interval is measured (longest in any lead or averaging across all leads with different machine algorithms) and also results from the fact that the determination of end-points such as sudden arrhythmic death from routinely collected health data for thousands of people is challenging, particularly in the era before electronic health records.

Using more detailed and rigorous phenotypes of sudden death, Straus *et al.* [38] suggested that a QT_c interval above 450 ms in men and 470 ms in women was associated with a three-fold increased risk of sudden death after adjustment for a multitude of known confounders, and a subsequent meta-analysis including ~36,000 people suggested that across the population, an increase of 50 ms in the QT_c conferred an increased relative risk of sudden death of 25% [39]. Using Mendelian randomisation methods, genetic scores corresponding to a longer QT interval have been associated with a modest increase in risk of sudden death [40]. There is also modest evidence suggesting that a prolonged QRS duration (as part of the QT interval) may be associated with risk of sudden death, but considerable controversy as to whether this is truly causal pr just reflecting left ventricular impairment [41-43].

Overall, the data suggests higher risks of sudden cardiac death related to longer QT intervals in a general population, but does suggest significant inter-individual variability.

1.3 The QT interval and atrial arrhythmias

In those with long QT syndromes, an increased incidence of atrial arrhythmias has been described, presumed to be due to shared associations between atrial and ventricular substrates [44-46]. On a population level, observational studies have suggested that long and short QT intervals both are associated with a higher risk of developing atrial fibrillation (AF) [47-50]. These studies were observational and all have limitations (e.g. confounding, reverse causality) when it comes to assessing causality. Therefore, whether differences in QT interval somehow cause atrial arrhythmias or are a biomarker is unknown.

1.4 Genetics of the QT interval

ECG parameters are thought to have a heritable component, and for the QT interval, approximately 30-40% of the variability has been estimated as being heritable [51]. The familial clustering of the long QT syndromes led to recognition and identification of a number of the genes involved in regulating the QT interval as described earlier.

Initial approaches to investigate the heritability of the QT interval in the general population focused on candidate gene approaches. Here, selected polymorphisms in candidate genes known to encode potassium channels and relevant to long QT syndromes were investigated for their associations with the QT interval in normal individuals [52]. Pfeufer *et al*. [52] found significant associations with the QT interval mostly in non-coding polymorphisms located upstream of *KCNQ1* and *KCNH2*. However, these specific variants accounted for <1% of total variance of the QT interval, and even in those with clinically diagnosed long QT syndromes, approximately 20% are termed 'genotype negative', indicating that a known significant pathogenic mutation was not identified [53]. Thus, there is a significant gap between our understanding of the mechanisms underlying the normal regulation of the QT interval beyond insights gained from the more severe long QT syndromes.

Utilising datasets at a population level, genome-wide association studies (GWAS) investigated the genetic basis of the QT interval in 2006 [54], 2014 [55], and a further GWAS in 2021 awaiting peer-

review [56]. Here, using larger ECG datasets and restricting QT intervals to those within the normal range, genetic polymorphisms can be imputed across the whole genome and associations with QT interval made in an unbiased manner, with strict statistical adjustments for multiple testing.

Arking *et al*. [54,55] described 68 independent polymorphisms occurring at common frequencies (defined as >1%) in the population at a stringent discovery threshold ($P < 1 \times 10^{-8}$) and estimated that in total they explained ~10% of all variation in the QT interval. However, they estimated that in total and at more lenient statistical thresholds, contemporary genetic assays captured around 20% of all the variation within the QT interval [55].

Across the QT interval, polymorphisms within genes encoding ion channels associated with long QT syndromes (*KCNQ1, KCNH2, SCN5A* and others) were significantly associated with the QT interval in normal individuals, giving biological plausibility to the GWAS findings and replicating effects seen using candidate gene approaches [54,55]. However, again, genes in ion channels only accounted for a small proportion of the total heritability of the QT interval suggesting many other mechanisms were involved.

1.5 Genetic variation in *NOS1AP* and the QT interval

1.5.1 Insights from genome-wide association studies

Unexpectedly, Arking *et al*. consistently [54,55] identified that the most significant associations with the QT interval in normal individuals were found with common non-coding polymorphisms associated with the gene *NOSIAP* on chromosome 1q. This gene encodes the protein Nitric Oxide 1 Synthase Adaptor Protein (NOSIAP) which was first described in neuronal tissue and was known as CAPON (C-terminal Adaptor Protein for Nitric Oxide Synthase 1) [57]. At the time, however, its role in cardiac electrophysiology had not previously been recognised.

Inferring association between 'statistical' hits across the genome, typically in non-coding regions and putative genes and biological pathways is not always straightforward. Initial fine-mapping of the *NOSIAP* locus confirmed that the statistically significant polymorphisms were confined to a

region just upstream of the 5' coding region of *NOSIAP*. Further modelling of the association towards the 3' region of the nearby *OLFML2B* gene showed a significant drop of association with the QT interval [54]. The authors felt that this all strongly contributed to suggesting that non-coding but regulatory elements in *NOSIAP* affected the QT interval with their data identifying 11 distinct genetic variants in *NOSIAP* contributing to the QT interval, occurring at frequencies of between 5 – 26% in the general population, with each allele contributing between 1 – 5 ms to the QT interval [55]. The first GWAS [54] identified the single nucleotide polymorphism (SNP) rs10494366 associated with *NOSIAP* as having the strongest association with the QT interval with more detailed mapping in subsequent studies [55,58] identifying the SNP rs12143842 tagged to *NOSIAP* as having the strongest association with the QT interval ($P = 1 \times 10^{-213}$) of all SNPs across the genome. A plot of association with QT interval of the *NOSIAP* gene and surrounding gene is shown in **Figure 1.3**.

Figure 1.3 – Regional association with QT interval around *NOS1AP* gene

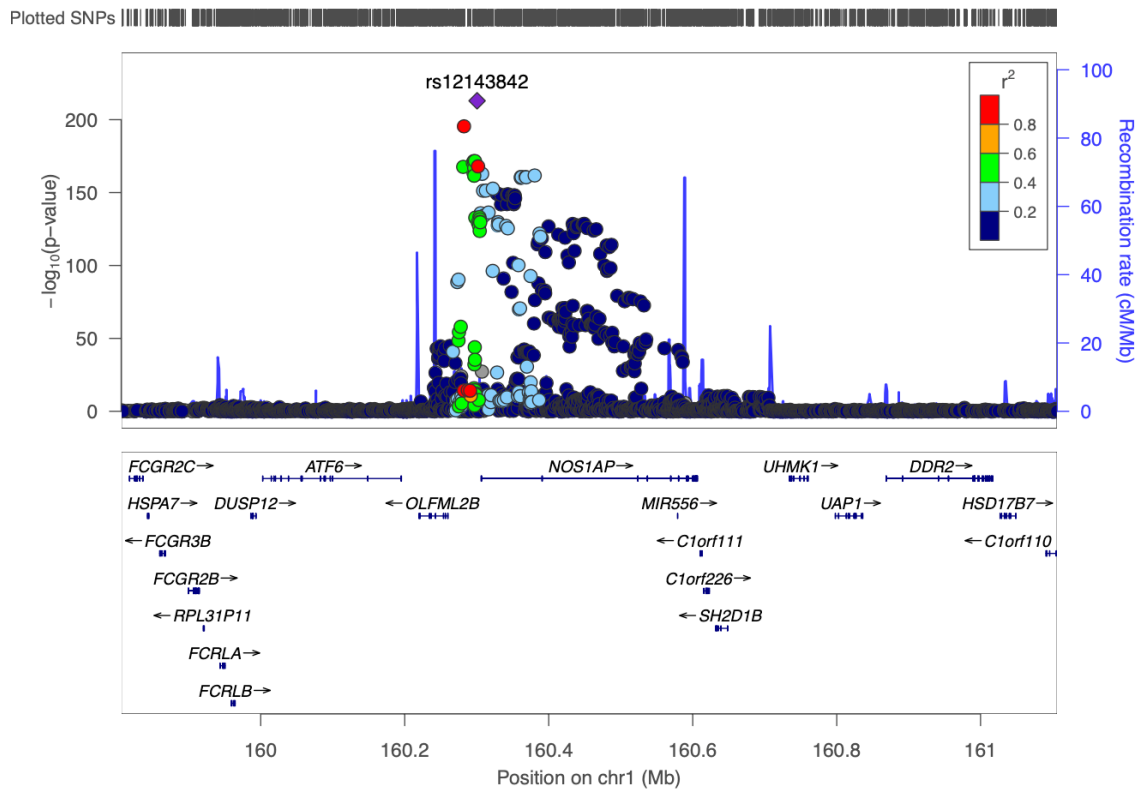


Figure 1.3: Regional association plot showing area around *NOS1AP* gene and variant association with QT interval created using LocusZoom (http://csg.sph.umich.edu/locuszoom/) and using data from QT interval GWAS [55].

1.5.2 Genetic insights from specific populations

Subsequent to the description of the importance of *NOSIAP* in regulating the QT interval, a number of subsequent descriptions of associations between specific polymorphisms in *NOSIAP* and QT interval or risk of sudden death followed. Broadly speaking, these could be grouped into (i) those that extended the applicability of the SNPs described from the GWAS population of otherwise normal Caucasians of European ancestry to different populations, or (ii) those studies from which further mechanistic understanding might be inferred.

Relevance of variation in NOS1AP to the QT interval across other populations

Four separate studies initially confirmed the association between NOS1AP polymorphisms and the QT interval in separate populations [59-62], with Shah *et al.* [63] extending this to include significant associations within a multi-ethnic cohort, although the specific polymorphism identified to be significant varied based on ethnicity. Subsequent larger studies using genome-wide approaches provided further evidence that common variations in *NOSIAP* contributed to the QT interval in multi-ethnic populations [64-66], adding substantial weight to the hypothesis that *NOSIAP*'s association with the QT interval is not ethnicity or population specific.

It has been well recognised since initial ECG recordings that after puberty, males shorten their QT interval and adult women have a longer QT interval than adult men in the absence of an increased risk of sudden death [67,68]. The reasons for this sex-specific finding have been extensively investigated without a specific consensus, but are thought to be related to differences in sex-specific hormones occurring post-puberty and seem to still be relevant even in patients with long QT syndromes [69]. Two small studies [70,71] using limited genotyping reported conflicting results regarding sex-interactions of the QT prolonging effects of *NOSIAP* polymorphisms. Tobin *et al.* [70] suggested females had longer QT intervals associated with the single *NOSIAP* polymorphism that was tested whilst Winbo *et al.* [71] reported that the single *NOSIAP* polymorphism they tested only associated with the QT interval in male patients, despite them having a shorter QT interval compared to females. More robustly, the GWAS studies adjusted the measured QT intervals for sex

prior to testing for genetic association so the main *NOSIAP* polymorphisms found to be significant should be relevant to both sexes.

Relevance of variation in NOS1AP to risk of sudden death in the general population

As discussed earlier, as the measured QT interval does not capture all the risk associated with sudden death, the identification in the GWAS of potential genetic modifiers led to a number of studies to investigate whether *NOSIAP* influenced the risk of sudden death.

Unfortunately, the results from studies using limited genotyping and in cohorts of different ethnicities have been conflicting [59,72-76]. Taking a different approach, Noseworthy *et al*. [77] constructed a weighted QT interval genetic score comprising of 15 distinct variants (including one in *NOSIAP*) previous reported as being associated with QT interval. They confirmed associations between the genetic score and measured QT interval in a Finnish population, but found no association between the genetic score and risk of sudden death.

These studies all suffered from the same limitations – namely that sudden death due to ventricular arrhythmias is difficult to define precisely (leading to inclusion of misclassified diagnoses or too few cases if very strict definitions) and detailed biobanks and phenotyping are lacking beyond small datasets. Additionally, most sudden death occurring in later life is in the context of structural cardiac changes (e.g. secondary to ischaemic cardiomyopathy) with environmental factors dominating over genetics.

Relevance of variation in NOS1AP to risk of drug-induced QT prolongation

With limited insights to be gained from associations between genetic polymorphisms and sudden death in the general population, studies explored whether these polymorphisms may have more relevance when considering sudden death in populations at higher risk.

Considering drug induced QT syndrome, van Noord *et al*. [78] reported in a population study an interaction effect of a *NOSIAP* polymorphism on QT interval prolongation in verapamil users (after adjustment for some cardiovascular disease confounders). After testing a panel of *NOSIAP* polymorphisms spanning the gene, Jamshidi *et al*. [79] found associations between certain

polymorphisms in *NOS1AP* and the risk of drug induced long QT syndrome. Of note, those with drug induced QT syndrome did have a longer QT interval at baseline compared with controls, but the association persisted after adjustment for this, albeit with smaller magnitude of effect. The authors suggested that the effects of the polymorphisms in *NOS1AP* may be both via the baseline QT but also via a specific effect on drug induced QT prolongation. In a human experimental study of healthy volunteers, Strauss *et al*. [24] constructed a weighted QT interval genetic score comprising 61 common genetic variants (including *NOS1AP*) and found that this explained ~25-30% of the variation in baseline QT and also ~25-30% of the response to controlled injection of three known QT prolonging anti-arrhythmic medications. Interestingly, they found no correlation between baseline QT interval and risk of drug-induced QT prolongation, but acknowledged this may be related to statistical power. Using data from a cohort of patients with known drug-induced long QT syndrome, they found the genetic QT score to be significantly associated with risk of torsade de pointes, explaining 12% of the total variation in risk. Overall, this suggests that common genetic polymorphisms individually accounting for small differences in the QT interval may be useful in aggregate for understanding and predicting the heterogeneity of responses in addition to conventional non-genetic risk stratification.

Relevance of variation in NOS1AP to those with 'Mendelian' long QT syndromes

A number of studies subsequently investigated whether common genetic polymorphisms in *NOS1AP* affecting the normal QT interval were still of relevance in people with significantly abnormal repolarisation in the form of long QT syndromes.

Crotti *et al*. [80] selected 5 *NOS1AP* polymorphisms to investigate in a founder family all with long QT type 1 syndrome sharing the same *KCNQ1* pathogenic mutation. They found associations between two *NOS1AP* polymorphisms and baseline QT interval as well as risks of development of cardiac symptoms and risk of life-threatening events. The effects of *NOS1AP* on the QT interval were seen despite significant QT prolongation and led to the authors suggesting that variants in *NOS1AP* were a 'modifier' of risk in those with long QT syndrome. Tomas *et al*. [81] investigated selected *NOS1AP* polymorphisms across a wide range of patients with different types of long QT

syndromes, including those in whom no pathogenic mutation was found. In this large mixed population of ~900 patients, after conducting unbiased classification tree analysis, they found that *NOS1AP* polymorphisms had additional predictive value in terms of cardiac events only in those with a corrected QT interval of <500 ms. However, when limiting the analysis to those with long QT type 1-3 syndromes, they found evidence that polymorphisms in *NOS1AP* offered additional risk prediction on top of the clinical features of QT interval >500 ms, female sex and type of long QT syndrome. Earle *et al*. [82] found that in a Pacific islander population with long QT syndrome, *NOS1AP* polymorphisms were associated with clinical events, but interestingly found no association between those polymorphisms and baseline QT interval. Kolder *et al*. [83] used a much larger panel of polymorphisms and found significant associations between *NOS1AP* and QT interval and risk of cardiac events in patients with pathogenic mutations in *KCNH2* leading to long QT type 2 syndrome. At face value, these data suggest that polymorphisms in *NOS1AP* had additional risk predictive value in those with long QT syndromes.

A significantly clearer insight into the genetic architecture of long QT syndrome came after Lahrouchi *et al*. [29] performed a GWAS looking for common variants affecting the QT interval in proband participants diagnosed with long QT syndrome. Using a case-control design initially, they found that the previously reported *NOS1AP* polymorphism at rs12143842 was also the most significantly associated with risk of long QT syndrome, along with two others already reported as significant in the general population. In fact, most of the genetic variants relevant in the general population to the QT interval predicted risk of long QT syndrome, but just at more modest significance thresholds. A weighted genetic risk score of common polymorphisms predicting the QT interval in the normal population was constructed and found to predict risk of long QT syndrome in a dose-response manner. Additionally, those with identified pathogenic mutations and long QT syndrome had higher values of the polygenic QT risk score than controls, and those in whom no mutation was identified had even higher values overall (**Figure 1.4 A**). Looking at specific polymorphisms, those that conferred a greater change in the QT interval were associated with a higher risk of diagnosis of long QT syndrome in a linear fashion (**Figure 1.4 B**).

Figure 1.4 – Associations between genetic QT scores and long QT syndrome

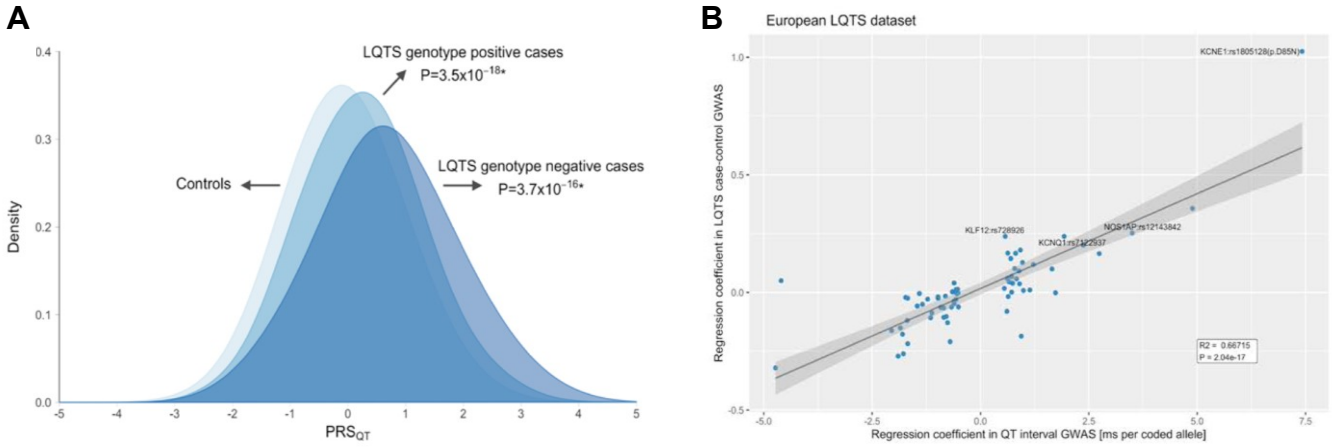


Figure 1.4: Adapted from Lahrouchi *et al.* [29]. (**A**) shows values of weighted polygenic risk score against frequency for QT interval (PRS_{QT}) across groups of controls and those affected by long QT syndrome (LQTS) with or without identified pathogenic genetic mutations in those of European ancestry. (**B**) shows the individual genetic polymorphism's effect on the QT interval reported in other genome-wide association studies (GWAS) against their predicted risk for diagnosis of LQTS in the authors' cohort of LQTS probands.

The previous 'disease-modifying' role of *NOSIAP* polymorphisms in long QT syndrome was not borne out in the study by Lahrouchi *et al.* [29]. When conducting the GWAS to predict the risk of arrhythmic events in people with long QT syndrome, no significant genomic loci were found and interestingly, no association between the polygenic genetic QT score and measured QT interval overall in those with long QT syndrome was found. The authors acknowledged this to be unusual compared to previous studies and suggested that this may have been due to a lack of statistical power due to a lack of QT variability following their decision to include only probands (and not family members) in the long QT cases, whilst other studies included both.

Overall, the evidence suggests that the QT interval is an intermediate phenotype in long QT syndrome and that aggregation of common genetic variants (including those in *NOSIAP*), significantly alter the phenotype meaning that our view of LQT syndrome as a monogenic Mendelian disease is likely to be a biological oversimplification. Additionally, the evidence suggests that the biological mechanism by which variation in *NOSIAP* affects the QT interval

might still be relevant even in those with significant defects in ion-channel mediated repolarisation.

1.5.3 Functional consequences of *NOS1AP* polymorphism

The GWAS confirmed that the polymorphisms associated with QT interval were located in non-coding regions of *NOSIAP* [55], a common finding in polygenic genetic traits. Evidence for a common 'cis' effect (i.e. that these polymorphisms affect *NOSIAP* and not another gene), and that they are likely involved in regulation of gene expression comes from a variety of sources.

Expression quantitative trait loci (eQTL) analysis, where gene expression is measured across many genotyped participants showed that in non-diseased hearts, polymorphisms of *NOSIAP* associated with longer QT intervals are associated with an increased amount of gene expression in left ventricular tissues (**Figure 1.5**; courtesy of Professor Connie Bezzina [84,85]).

Figure 1.5 – eQTL data showing gene expression for *NOS1AP* polymorphisms

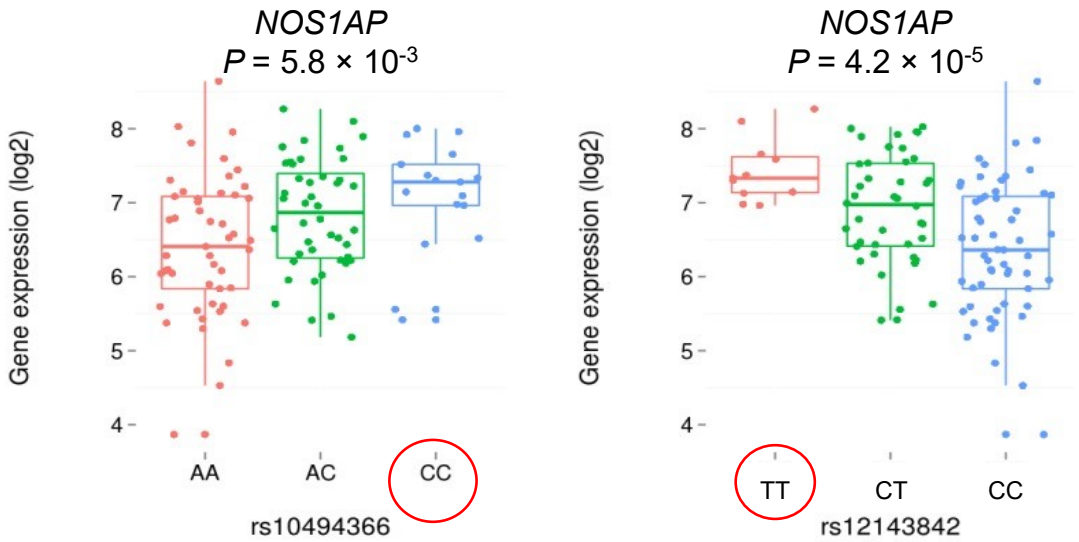


Figure 1.5: Expression quantitative trait loci (eQTL) analysis showing gene expression of *NOS1AP* in left ventricular tissue from non-diseased hearts for key independent *NOS1AP* polymorphisms (LD r^2 0.16) significantly associated with QT interval [84,85]. Red circles highlight alleles associated with longer QT interval in GWAS [54,55].

Using an eQTL public database (www.gtexportal.org), this can be confirmed across a range of other tissues, other *NOSIAP* polymorphisms, and in more participants (**Figure 1.6**).

Figure 1.6 – *NOS1AP* gene expression across different tissues by allele

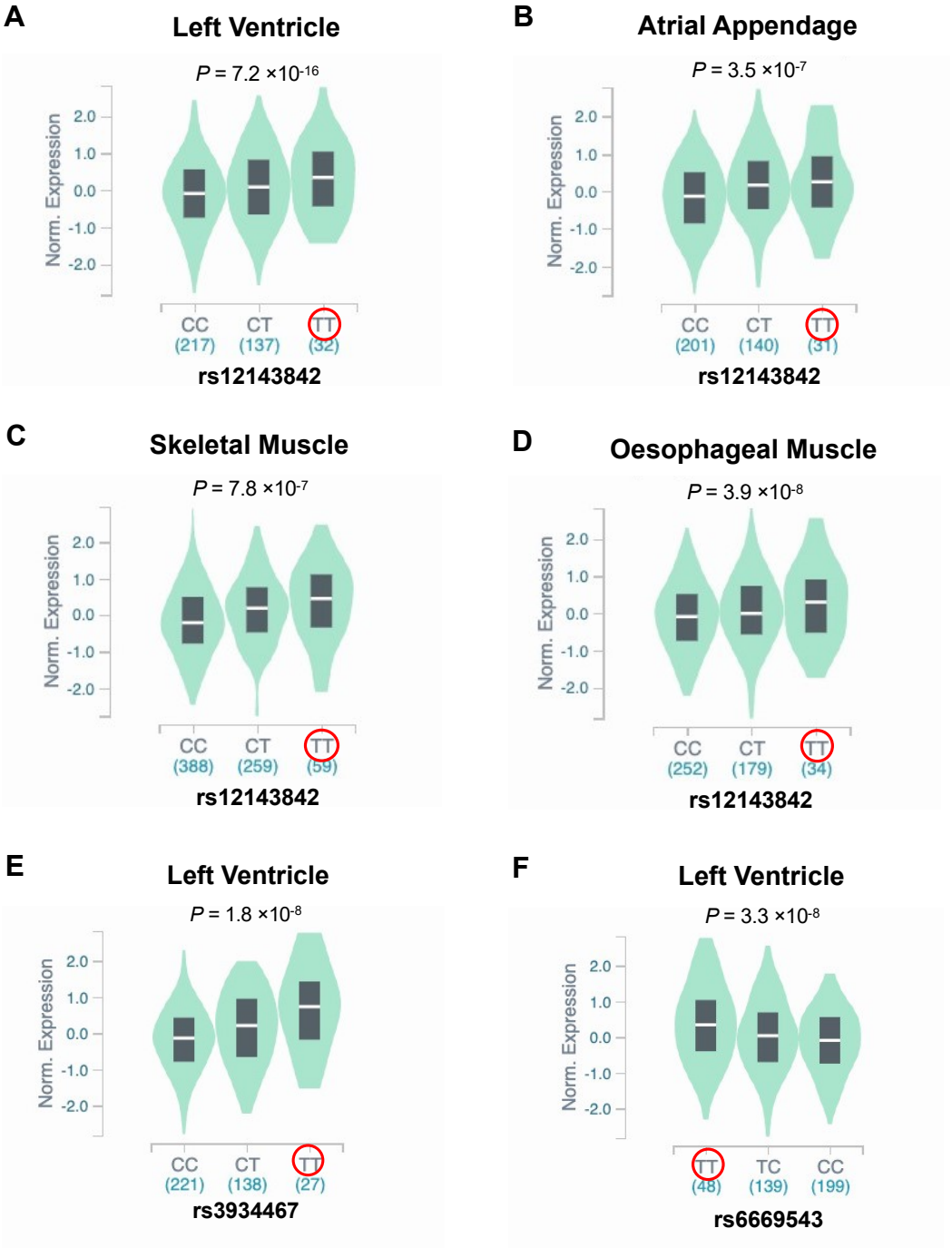


Figure 1.6: Panels (**A**) to (**D**) show *NOS1AP* gene expression in cardiac and non-cardiac tissues for the main rs12133842 polymorphism associated with QT interval. Panels (**E**) and (**F**) show gene expression in left ventricular tissue for two other GWAS significant independent *NOS1AP* polymorphisms (LD r^2 for rs3934467 with rs1213842 0.07 and with rs6669543 0.004) associated with QT interval. QT prolonging alleles circled in red with number of individual samples in brackets below. *P*-value is for trend across alleles, with median and interquartile range represented by white line and dark green bars, and density plot of other values represented by lighter green clouds. All graphs adapted from www.gtexportal.org.

It is noticeable that in a general population, the degree of change of *NOS1AP* gene expression when split by single alleles is modest and that there is a significant degree of biological variability in *NOS1AP* gene expression. This is entirely in keeping with the fact that it is likely that multiple polymorphisms (as well as other regulators of gene expression such as DNA methylation etc.) contribute to any individual's quantitative gene expression of *NOS1AP*.

Whilst the alleles reported in the GWAS have the most significant associations, this does not necessarily mean they are the truly functional alleles due to the possibility of them being in linkage disequilibrium (LD) with the true functional allele (i.e. they are always inherited together and not randomly). This necessitates the use of more detailed mapping and laboratory experiments.

Kapoor *et al*. [86] performed further fine-mapping of the area around the rs12143842 locus reported as consistently showing the strongest associations with the QT interval. Combining fine-mapping across different cohorts and overlaying regions with multiple genomic 'maps' representing enhanced chromatin accessibility (a hallmark of functional regulators), they identified 12 polymorphisms around the locus for further functional assessment. Using a mouse cardiomyocyte cell line as well as a non-cardiac cell line and cloning the polymorphisms into luciferase reporter constructs, they identified a single polymorphism functionally associated with modest (~1.9 fold) but consistently significant differential allelic gene expression across cell lines. This was then confirmed to hold true in human cardiac tissue, and then by expression in zebrafish embryos. Specific base pair deletions around the polymorphism altered transcriptional activity, suggesting that the variant base as well as a short 11 base pair flanking sequence likely act as a binding site for a hitherto unidentified protein affecting transcriptional regulation.

Overall, there is strong evidence that the *NOS1AP* polymorphisms associated with a prolonged QT interval are associated with increases in *NOS1AP* gene expression.

1.6 Function of the NOS1AP protein

Following on from increased gene expression of *NOSIAP*, it is therefore likely that more NOSIAP protein is somehow involved in prolonging cardiac repolarisation. Prior to identification as being relevant to the QT interval, NOSIAP was first described in the area of neurobiology.

1.6.1 Insights from neurobiology

NOSIAP was first described and termed CAPON by Jaffrey *et al.* [57] during investigations of nitric oxide synthase 1 (NOSI or neuronal NOS) coupling in neurons. Subsequent studies in neurons [87,88] suggested that NOSIAP may function as a structural modulator of NOSI signalling, either by competitively binding NOSI via its own C-terminal PDZ domain and altering enzyme localisation, or by docking other proteins via a phosphotyrosine binding (PTB) domain and modulating downstream signal transduction (**Figure 1.7**).

Figure 1.7 – Initial proposed mechanisms of NOS1AP (CAPON) action in neurons

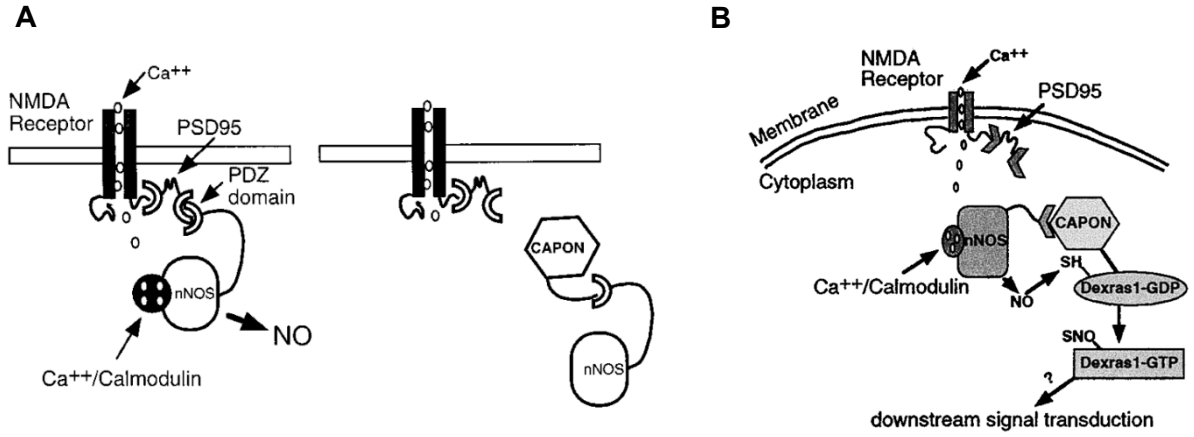


Figure 1.7: Proposed mechanisms of NOS1AP (CAPON) interaction with NOS1 (nNOS) in neurons from initial work by (**A**) Jaffrey *et al.* [57] and (**B**) showing putative downstream interactions of NOS1AP from work by Fang *et al.* [87].

Interest in NOSIAP increased significantly after reports suggesting that non-coding polymorphisms in the gene may be associated with risk of schizophrenia and that there was a higher expression of *NOSIAP* in the cortex due of those who suffered from the condition due to functional overexpression associated with the risk polymorphism, although this has not yet been replicated at GWAS significance thresholds [89-92]. The molecular consequences of increased

NOS1AP in neurons appeared to be related to altering growth patterns of neurons by interaction with structural components and possibly via effects on NOS1 [93-95]. Interestingly, molecular disruptors of the NOS1AP:NOS1 interaction showed efficacy as pain-killers and for anxiolysis in experimental models [96-99]. Part of this effect is thought to be related to modulation of NOS1 related NMDA receptor gated Ca^{2+} influx into neurons, with some evidence that disruption of the NOS1AP:NOS1 interaction may have a beneficial effect in post-stroke Ca^{2+} influx mediated neurotoxicity [100,101].

Investigations detailing the molecular interactions between NOS1AP and NOS1 suggest more complexity than previously appreciated. Candemir *et al.* [94] tested different lengths of NOS1AP peptides for interaction with NOS1 and noticed that the functional interaction was dependent on both the PDZ domain and the PTB domain, but was not accompanied by differences in NOS1 enzymatic activity. Using a variety of methods, Li *et al.* [102] showed that the C-terminus PDZ domain of NOS1AP was not necessary or sufficient for binding to NOS1, but did promote the stability of the complex. They described a new domain they called the 'ExF' domain as being critical to the binding with subsequent studies [103] showing that NOS1AP:NOS1 binding was significantly reduced using denatured NOS1AP, suggesting a tertiary structural element to the interactions.

Overall, although NOS1AP was first described within neurobiology as an 'adaptor protein' interacting with NOS1, it does appear to be capable of more complex interactions than previously appreciated with mixed evidence of its ability to significantly alter NOS1 biology.

1.6.2 NOS1AP and electrophysiology

Cardiac sympathetic neurons

Cardiac repolarisation is a complex process and the polymorphisms identified as being relevant to the QT interval are not specific to cardiac tissues. In a letter, Herring and Paterson [104] suggested that NOS1AP may possibly regulate NOS1 mediated sympathetic neurotransmission and alter cardiac physiology, providing a link between some of the neurobiological observations and possible myocyte mechanisms of action.

Following on from this, Lu *et al.* [105] investigated the role of NOSIAP in rat cardiac sympathetic neurons. They hypothesised that NOSI mediated neurotransmitter release of norepinephrine may be modulated by NOSIAP in diseased states and found a reduction in NOSIAP expression in the stellate ganglia of spontaneously hypertensive rats. Using cultured sympathetic neurons, they found adenoviral-mediated overexpression of *NOSIAP* led to increases in NOSI activity and reductions in neuronal I_{Ca} and a reduction in calcium transient amplitude ($[Ca^{2+}]_i$). By overexpressing *NOSIAP* using an *in-vivo* percutaneous adenoviral injection into the right atrium of spontaneously hypertensive rats, Lu *et al.* [105] also found a reduction in norepinephrine production using an excised atrial preparation. Whilst not the primary focus of their work, they suggested that NOSIAP associated changes in autonomic reactivity may play a role in modulating cardiac electrophysiology, such as by altering the beta-adrenergic sensitivity of I_{Ks} [106].

Experiments in cardiac tissues

From the existing literature, a few explanations have been offered regarding the specific mechanisms as to how NOSIAP may affect electrophysiological parameters. The first study by Chang *et al.* [107] used adenoviral overexpression of *NosIap* in isolated guinea pig ventricular cardiomyocytes suggested that single cell APDs at 10%, 50%, 75% and 90% total repolarisation were all shortened compared with controls. Subsequently, Milan et al. [108] knocked down 90% of *nosIap* gene expression using morpholinos in zebrafish embryos. They used optical mapping in whole zebrafish hearts and, contrary to the findings of Chang *et al.* [107], showed that knockdown of *nosIap* was associated with a shortening of APDs with a slowed upstroke. Kapoor *et al.* [86] used neonatal rat ventricular myocyte monolayers and found that viral overexpression of *NOSIAP* was associated with a shortened APD and increased conduction velocity, more consistent with Chang *et al.*'s [107] work. In tissue sections of human hearts, Kapoor *et al.* [86] also suggested that NOSIAP localised to the intercalated disc, suggesting that it may somehow be associated with the differences in conduction velocity they observed in their *in-vitro* model. In contrast to Chang *et al.* [107] and Lu *et al.*'s [105] observations, Treuer and Gonzalez [109] suggested that knockdown of *NosIap* in neonatal rat ventricular myocytes was associated with a reduced $[Ca^{2+}]_i$. A single report

exists of a global *Nos1ap* knockout murine model, which reported no differences in ECG parameters when compared to wild-type mice, although the authors did not report confirmation of *Nos1ap* gene or protein knockout [110].

Recently, using human induced pluripotent cardiomyocyte stem cells (hiPSCs), Ronchi *et al*. [111] suggested that *NOS1AP* alleles associated with prolonged QT interval affected NOS1 mediated repolarisation. They used cell lines from two different individuals with the same pathogenic mutation resulting in long QT syndrome type 1 but differing in major/minor allele at two *NOS1AP* loci (with both having been previously been described as being linked to QT interval, although not at GWAS thresholds) and attributed observed differences to allelic variation at the *NOS1AP* loci. The finding of significant individual variability in *NOS1AP* gene expression (suggesting either other polymorphisms or other factors affecting NOS1AP protein levels) and the findings of Lahrouchi *et al*. [29] suggesting a polygenic inheritance of the long QT syndrome may somewhat attenuate the conclusions drawn using this methodology.

Overall, these somewhat contradictory findings may suggest differing effects when using single cell or cell culture systems from different species to investigate cardiac electrophysiology. There are likely multiple cellular factors which could work in conjunction to influence whole-organ electrophysiology, and this is not addressed by approaches thus far focused on overexpression or knockdown in isolated cell systems.

NOS1AP:NOS1 interactions in cardiac tissues

In cardiac tissues, there is evidence indicating that NOS1AP co-localises with NOS1 and may play a role in both directing NOS1 to sub-cellular compartments and modulating nitric oxide (NO) production [112]. Due to its evanescent nature, NO signaling is likely to occur over a limited spatial range within cardiac myocytes, (estimated to be in the sub-micrometer range [113]) suggesting localisation of NOS isoforms is therefore a critical factor determining the targets of NOS1-derived NO.

In murine left ventricular (LV) myocytes, NOS1 is localised to the sarcoplasmic reticulum (SR) [114] and, to a lesser extent, the sarcolemmal membrane [115,116]. However, subcellular localisation of NOS1 in cardiomyocytes is highly dynamic and NOS1 has been reported to translocate to the sarcolemmal membrane in the presence of ischaemia/reperfusion injury and beta-adrenergic stimulation [117] or LV remodelling following a myocardial infarction [118,119]. Intracellular redistribution of NOS1 in the injured myocardium requires the formation of a complex with NOS1AP [112]. In human atrial myocytes, NOS1 is predominantly located on the sarcolemmal membrane, where it interacts with scaffold adaptors such as dystrophin, α-syntrophin [116] and caveolin-3 via its PDZ domain [120]. Whether this reflects species- or heart chamber-related differences in NOS1AP subcellular localisation is unknown.

As described in neurons, NOS1 also plays a significant role in the regulation of Ca^{2+} fluxes in the myocardium [121]. In particular, NOS1-derived NO increases the rate of SR Ca^{2+} reuptake, by increasing phospholamban phosphorylation (*via* a cGMP-independent effect on phosphatase activity) [122,123] and decreases the sarcolemmal L-type Ca^{2+} current (I_{Ca}) [124,125]. On the basis of this evidence, one would expect the results of Chang *et al.* [107], where myocardial NOS1 activity was enhanced by NOS1AP overexpression, with a reduction in I_{Ca} and a shortening of action potential duration (APD). However, these findings would imply that *NOS1AP* variants may prolong cardiac repolarisation and the QT interval by decreasing the expression level of *NOS1AP* in the heart, leading to a reduction in NOS1 activity and an increase in I_{Ca} and APD. Similarly, a reduction in NOS1AP abundance in sympathetic neurons would be expected to increase noradrenaline release and compound the pro-arrhythmic phenotype. This would be contradictory to the findings of *NOS1AP* polymorphisms associated with a longer QT interval being associated with increased gene expression (**Figure 1.6**), suggesting that either NOS1AP or NOS1 may have other effects on myocardial electrical properties.

Subsequent data indicate that APD is shorter in murine atrial $NOS1^{-/-}$ cardiomyocytes and that NOS1 inhibition or knockdown in human and murine atrial myocytes leads to a shorter APD and loss of APD rate-dependent adaptation by increasing K^+ currents, such as I_{Kur}, I_{to} and I_{Kl} [126].

Furthermore, NOS1-derived NO has been reported to increase the ryanodine receptor (RyR) open probability (P_o) [125,127]. Although this would not be expected to prolong APD, a higher RyR P_o has been associated with an increased propensity to arrhythmias [128] and may constitute a 'second hit' promoting life threatening arrhythmogenesis in patients with an existing long QT interval. Indeed, ventricular arrhythmia inducibility and Ca^{2+} sparks are increased in a murine model where NOS1 activity is enhanced by myocardial overexpression of *GCH1* (the enzyme encoding for the NOS1 co-factor tetrahydrobiopterin) [125]. Finally, increased *S*-nitrosation of the sodium channel, SCN5A, resulting from altered NOS1 coupling to its inhibitor (the sarcolemmal Ca-ATPase subtype 4b or PMCA4b) due to α1-syntrophin mutations, has been shown to increase the late sodium current (I_{Na}) and prolong the QT [129].

These findings suggest that downstream of increased myocardial expression of NOS1AP, NOS1-derived NO may influence myocardial APD and excitability through effects on multiple sarcolemmal ion channels and Ca^{2+} release from the sarcoplasmic reticulum *via* the RyR.

1.7 Aims and objectives

Based on the current evidence presented, the mechanisms by which increased human *NOSIAP* gene expression alters cardiac electrophysiology and arrhythmogenesis are still uncertain and the aim of this thesis was to investigate this.

Specifically, the objectives of the thesis were to answer the following questions:

1. **Does NOSIAP protein overexpression in the myocardium lead to a cardiac electrical phenotype?** It was hypothesised that the development and phenotyping of a mouse model of cardiomyocyte-limited human *NOSIAP* gene expression would allow better whole-organ investigation of a complex electrical substrate. This would also allow focus on arrhythmogenesis at a tissue level and allow distinction of effects inherent to the cardiomyocyte vs those driven by potential autonomic changes [**Chapter 3**; Phenotype of Tg*(Myh6-hNOSIAP)* and **Chapter 5**; Atrial arrhythmias in Tg*(Myh6-hNOSIAP)*].
2. **How might NOSIAP affect cardiac electrophysiology, and are its effects NOSI mediated?** It was hypothesised that NOSIAP overexpression may alter multiple parameters affecting arrhythmogenesis, and that these would be at least partially modulated by NOSI. This would be investigated at both a cellular and tissue level by using the transgenic mouse model [**Chapter 4**; Mechanisms underlying the cardiac electrical phenotype in Tg*(Myh6-hNOSIAP)*].
3. **Are any of the findings from the mouse model relevant to arrhythmogenesis in human populations?** It was hypothesised that the altered ECG parameters seen in the mouse might be relevant in humans as regarding risks of arrhythmogenesis. This would be investigated using large human population datasets [**Chapter 6**; Causal relevance of ECG parameters and atrial arrhythmias in humans].

2

General laboratory methods

Summary

A general outline of laboratory methods used is presented. Chapter-specific methods and details are provided in the relevant sections.

2.1 Assessment of gene expression

2.1.1 RNA isolation

The mirVana kit (ThermoFisher Scientific) was used as per the manufacturer's instructions for total RNA isolation. Briefly, tissue samples stored at -80°C were kept on ice and homogenised in lysis buffer using beads. Following acid-phenol:chloroform organic extraction, the resulting RNA was purified and total RNA extracted in RNAse free water. RNA quality and quantification was performed using a nanodrop spectrophotometer (Nano Drop ND-1000, ThermoFisher) by assessment of 260/280nm absorbance ratio (requiring ratio 1.8 – 2.15) for quality and absorbance at 260nm for quantity of RNA respectively. RNA sample concentrations were then normalised to 25ng/µl and stored at -80°C until the next stage of processing.

2.1.2 Reverse transcription to cDNA

Using a total of 500ng of freshly extracted RNA, cDNA was generated on the same day using the QuantiTect reverse transcription kit (Qiagen) after a pre-clearing genomic DNA wipeout step as per manufacturer's instructions. cDNA was stored at a concentration of 10 ng/ml.

2.1.3 Quantitative real-time PCR

One nanogram of cDNA was used per sample and added to 5 µl of TaqMan fast advanced master mix (ThermoFisher Scientific), 3.5 µl of nuclease free water and 0.5 µl of relevant TaqMan probe (FAM-MGB dye, ThermoFisher Scientific) in a standard 96 or 384 well plate. Each sample was assayed in duplicate, alongside water containing negative controls and housekeeping genes whose gene expression was known to not vary in the target tissues of interest. Reactions were performed using the ABI Prism system (Applied Biosystems).

2.1.4 Quantification of gene expression results

During specific PCR probe amplification, each sample generated a cycle threshold (Ct) value defined as the cycle when the fluorescence of the PCR product is greater than the background signal (in the exponential phase of the reaction), which is inversely proportional to the amount of PCR product and probe-specific mRNA in the sample. These values were averaged for each

sample's technical duplicates. After subtracting the housekeeping gene's Ct (whose expression levels typically do not vary) from the Ct of the gene of interest to give a △Ct, as the Ct values are logarithmic, relative expression of the gene of interest to a housekeeping gene was expressed as $2^{-\triangle Ct}$.

2.2 Assessment of protein expression by Western blotting

2.2.1 Sample preparation

Tissue samples were removed from -80°C storage and homogenised using beads in 150-200 µl of RIPA buffer (10x stock, Sigma Aldrich) along with protease inhibitors (ThermoFisher Scientific). The homogenates were spun at 13 g in a centrifuge at 4°C for 8 minutes. The supernatant was removed from the cellular debris and kept on ice for further processing.

2.2.2 Estimation of sample protein content

Sample protein content was estimated using the bicinchoninic acid assay (BCA, ThermoFisher Scientific). Briefly, the colourimetric change after incubation of the reagent solution for 30 minutes with an aliquot of sample was assayed in a 96 well flat-bottomed plate using a plate reader and absorbance at 562 nm. A set of standards of known concentrations were also prepared by serial dilution using bovine serum albumin (BSA) and a standard curve drawn. Linear regression was used to draw a line of best fit and the averages of the technical duplicates of the sample protein readings used to calculate the corresponding sample protein concentrations.

2.2.3 Protein separation and transfer to membranes

Depending on the protein of interest and type of tissue, samples to run in the gel were prepared with 20-40 µg of protein along with loading buffer (LDS, ThermoFisher Scientific) and reducing agent (ThermoFisher Scientific). After heating the samples to 95°C for 5 minutes the samples were cooled and thoroughly vortexed. Depending on the protein of interest samples were either loaded onto 4-12% or 10% Bis-Tris NuPage gels (ThermoFisher Scientific), 4-12% Tris-Acetate gels (ThermoFisher Scientific), or 12% Criterion Tris-Glycine gels (Bio-Rad) with appropriate running buffers and a protein ladder (Amersham ECL Rainbow Marker, Merck) and separated using

electrophoresis. The gel proteins were transferred onto nitrocellulose membranes with specific details provided in relevant sections.

2.2.4 Quantification of protein content

After blocking of non-specific binding, nitrocellulose membranes were incubated overnight with primary antibodies against the protein of interest. After washing the membranes the next day, these were then incubated with horse-radish peroxidase (HRP) conjugated secondary antibodies directed against the species the primary antibodies were raised in. After addition of appropriate development solutions, the band intensities were recorded using the ChemiDoc Imaging system (Bio-Rad). Band intensities were quantified using Image Lab software (version 6, Bio-Rad) and expressed as a ratio of the protein of interest relative to that of a loading control.

2.3 Myocyte isolation

Isolation of murine ventricular myocytes was performed using Langendorff apparatus and enzymatic digestion. Mice had 1000 units of heparin injected intraperitoneally a short while before cervical dislocation. Subsequently, the heart was rapidly excised and placed in Ca^{2+}-free Tyrode solution (130 mmol/L NaCl, 5.6 mmol/L KCl, 3.5 mmol/L $MgCl_2$, 5 mmol/L HEPES, 0.4 mmol/L Na_2PO_4, 20 mmol/L taurine, 10 mmol/L glucose; pH 7.4). The aorta was cannulated and initially perfused with a Ca^{2+}-free Tyrode solution to clear the blood for 3 minutes followed by perfusion with a solution containing collagenase for between 7-9 minutes. After removing the hearts from the perfusion system, the left ventricle was dissected out. Pieces were placed in a further digestion solution with collagenase and gently triturated for 3 minutes to disperse the ventricular myocytes. The presence of live myocytes was confirmed by microscopic visualisation. The solution was centrifuged and then resuspended in storage solution with experiments carried out on the myocytes shortly thereafter.

3

Phenotype of Tg(*Myh6-hNOS1AP*)

Summary

Alleles of *NOS1AP* associated with longer QT intervals and ventricular arrhythmia in humans have been associated with increased myocardial gene expression. To investigate whether the latter is sufficient to prolong ventricular repolarisation and result in a proarrhythmic phenotype, we generated a transgenic mouse overexpressing human *NOS1AP* in the myocardium (NOS1AP-Tg). NOS1AP-Tg showed human *NOS1AP* mRNA levels that were ~800-fold larger than the endogenous murine *Nos1ap* mRNA and a modest increase in NOS1AP protein (~2.5-fold) in all cardiac chambers. Subsequent phenotyping revealed altered surface ECG parameters and an increased propensity to the induction *ex-vivo* ventricular arrhythmias in the absence of echocardiographic changes in cardiac structure or function.

3.1 Introduction

Alleles of *NOS1AP* associated with longer QT intervals and presumed ventricular arrhythmias (manifesting as the phenotype of unexplained sudden death) are associated with increased gene expression in cardiac tissues (**Figure 1.6**). Until now, functional characterisation of NOS1AP's effects on ventricular repolarisation have come from *in-vitro* studies using viral overexpression or RNA knockdown of NOS1AP in isolated guinea-pig cardiomyocytes [107], neonatal rat ventricular myocytes [86,109], zebrafish cardiomyocytes [108] or rat cardiac sympathetic neurons [105].

The human phenotype of the QT interval is a complex, whole organism phenotype which is difficult to entirely recapitulate from single-cell experiments. The isolation, culture and viral transfection of isolated cardiomyocytes may also contribute to adaptations which may affect functional readouts. This may be relevant when reconciling the seemingly opposite effects of NOS1AP on action potential duration [86,107,108], as well NOS1 levels and activity [105,107,111] that have been reported in single-cell experiments across different species using viral overexpression of *NOS1AP*. Inferring the effects of differing single alleles of *NOS1AP* using human iPSC cardiomyocytes may seem attractive [111], but fails to take into account that the genetic background of individuals from which the cell lines are derived is different, including the inheritance of other functional *NOS1AP* alleles (in the latest genome-wide association study for QT interval, eleven distinct *NOS1AP* polymorphisms were identified [55]). Unless individuals have an identical genetic background except for the single *NOS1AP* allele, the variation in inheritance of other alleles throughout the genome that might otherwise affect electrical parameters or NOS1 activity means that attributing differences in iPSC cell lines to a single *NOS1AP* allele is flawed. There are also limitations to assessing cell-cell coupling and electrical propagation in such systems when compared to whole organ systems.

Therefore, the use of a model organism has the significant advantage of being able to evaluate complex phenotypes *in-vivo*. Although a technical description of the generation of a cre recombinase-conditional murine *Nos1ap*-overexpressing transgenic mouse has been previously published [130], no further details of the phenotype of this mouse have been reported. By contrast,

there is a single report of a global murine *Nos1ap* knockout model [110] which showed evidence of more severe cardiac dysfunction and increased mortality after intraperitoneal doxorubicin injection (25 mg/kg body weight), with no evidence of cardiac electrical or structural changes under basal conditions, suggesting that NOS1AP may protect against anthracycline-induced cardiotoxicity.

We generated a transgenic murine model of human *NOS1AP* overexpression targeted to the myocardium. In humans, genetic variation in *NOS1AP* would naturally occur across all tissue types. In particular, previous work has shown that NOS1AP may play a role in regulating sympathetic neurotransmission [105]. Cardiac neuronal tissue such as sympathetic neurons have the ability to modulate cardiac electrical parameters, and therefore, limiting *NOS1AP* overexpression to the myocardium in our model does not entirely recapitulate the human phenotype and is a limitation of our methodology. By contrast, there is very little NOS1 in the cardiac sympathetic system in mice [131], and overall, cardiomyocyte-limited overexpression has the benefit of being able to make more specific inferences about myocardial versus neuronal NOS1AP effects. These factors all contributed to the decision to use a background of a commonly studied inbred mouse strain (C57Bl6/J) to generate a myocardial-specific *NOS1AP* overexpressing murine model - Tg(*Myh6-hNOS1AP*). Expressing the human protein allowed for more reliable differentiation of gene and protein expression compared to the endogenous form, however, the relevance of the model relies on the protein being capable of functional interactions with endogenous murine proteins. There is a 95% amino acid sequence homology between murine and human proteins (UniProt alignment of murine and human CAPON – uniport.org/align) with conservation of both the C-terminus PDZ binding domain and additional key 'ExF' motif, both of which are important for NOS1AP interaction with NOS1 [57,98,102].

In this chapter, I report the steps taken to generate and characterise Tg(*Myh6-hNOS1AP)* mice. In particular, I validated the model's cardiomyocyte-limited *NOS1AP* overexpression by examining the gene and protein expression of endogenous murine *Nos1ap* and human *NOS1AP* across a variety of tissues. Subsequently, I investigated cardiac structure and function using echocardiography and

baseline electrical parameters using electrocardiography. To gain some understanding of the potential arrhythmic nature of the model, together with Dr Jillian Simon, I setup and tested an *ex-vivo* Langendorff perfusion system and performed ventricular burst pacing in the presence of atrio-ventricular block to investigate the model's susceptibility to ventricular arrhythmias.

3.2 Methods of mouse model generation

Cloning of the overexpression construct and pronuclear injections to generate the founder mouse was done by Dr. Ben Davies, Transgenic Core Head at the Wellcome Centre for Human Genetics, University of Oxford and his group at our request. Subsequent breeding, development of the genotyping protocol and colony management was my own work.

3.2.1 Cloning of the overexpression construct

The NOS1AP cDNA was amplified from human cDNA using primers which contained 5'SalI and 3'MluI restriction sites for cloning (5' - GTCGACACCATGCCTAGCAAAACCAAGTACAACCT - 3' and 5' - ACGCGTCTACACGGCGATCTCATCATCCAG - 3'). The resulting polymerase chain reaction (PCR) product was cloned into a PCR cloning vector and sequenced to verify the expected sequence and lack of PCR-induced mutations. The ~1.5 kb cDNA was cloned using the SalI and MluI sites into a plasmid vector pMyh6-PL containing the 5.4 kb upstream region of the mouse *Myh6* gene, a polylinker containing a unique SalI and MluI restriction site and a downstream human growth hormone polyadenlylation sequence (**Figure 3.1**).

The transgenic construct was isolated from the plasmid backbone via NotI digestion. The resulting 7.7 kb fragment was isolated, purified, filtered using a micro-filtration unit (Millipore) and diluted to a concentration of 2 ng/µl in microinjection buffer (10 mM Tris-HCl pH 7.4, 0.1 mM EDTA). The construct purity and the concentration were verified by agarose gel electrophoresis.

Figure 3.1 – Plasmid map of pMyh6-NOS1AP

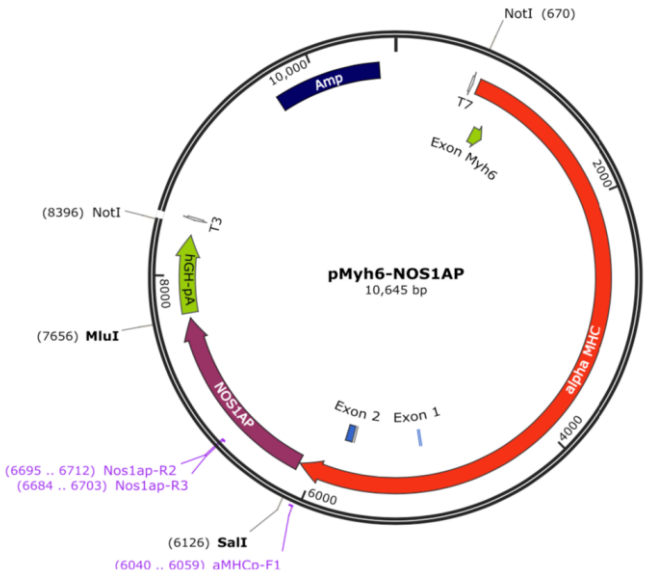


Figure 3.1: Plasmid map of pMyh6-NOS1AP showing the Myh6 promoter sequence in red, the NOS1AP cDNA sequence in mauve and the polyadenylation sequence in green. The primer locations for genotyping the transgenic pups are shown in purple, along with the relevant restriction sites used for construction and purification of the transgenic construct.

3.2.2 Genotyping PCR for screening

To establish the PCR screening for genotyping the generated transgenic mice, primer combinations were designed by amplifying a specific PCR product of ~670 bp from the Myh6-NOS1AP transgene. The forward primer, aMHCp-F1, binds to the 3' end of the Myh6 promoter and the reverse primers, NOS1AP-R2 and NOS1AP-R3, bind to the 5' end of the NOS1AP cDNA cassette. PCR amplification was therefore specific to the transgenic cassette sequence and should not amplify the orthologous sequence from the mouse. To confirm that the screening PCR was sufficiently sensitive at the level of genomic DNA, the transgenic vector DNA was serially diluted with 100 ng of wild-type genomic DNA. The PCR was sufficiently sensitive to clearly detect the transgene at a dilution of 100 fg in 100 ng, equivalent to a dilution factor of 1×10^6, and was sufficient to detect a single copy of the 7.7 kb transgene in the mouse genome. The primer sequences and the optimised PCR conditions are listed in **Table 3.1** and **Table 3.2**, whilst **Figure 3.2** shows the result of the sensitivity screen. Primers aMHCp-F1 and Nos1ap-R2 were selected for the genotyping.

Table 3.1 – Details of screening primers for PCR

Name	Sequence
aMHCp-F1	5′ - GTA GGA AAG TCA GGA CTT CA - 3′
NOS1AP-R2	5′ - TTG CTG TTC CTC TCG CTC - 3′
NOS1AP-R3	5′ - CTC TCG CTC TCT CCA TCT TC - 3′

Table 3.1: PCR primer sequences used for screening.

Table 3.2 – Screening PCR reaction details

Reaction mix			Reaction conditions			
			Step	Temp (°C)	Time (s)	Cycles
Genomic mouse cDNA	100	ng	Denaturing	94	300	× 1
Primers	10	pmol	Denaturing	94	60	
dNTPs	0.16	mM	Annealing	55	60	× 35
Reaction buffer	0.1	Vol	Extension	72	40	
$MgCl_2$	3	mM	Completion	72	360	× 1
Taq polymerase (Immolase)	1	U	Hold	4	-	
Total reaction volume	20	µl				

Table 3.2: Details of reaction mix on the left-hand side and thermal cycler protocol on the right. dNTP: deoxyribose nucleoside triphosphate.

Figure 3.2 – Screening PCR

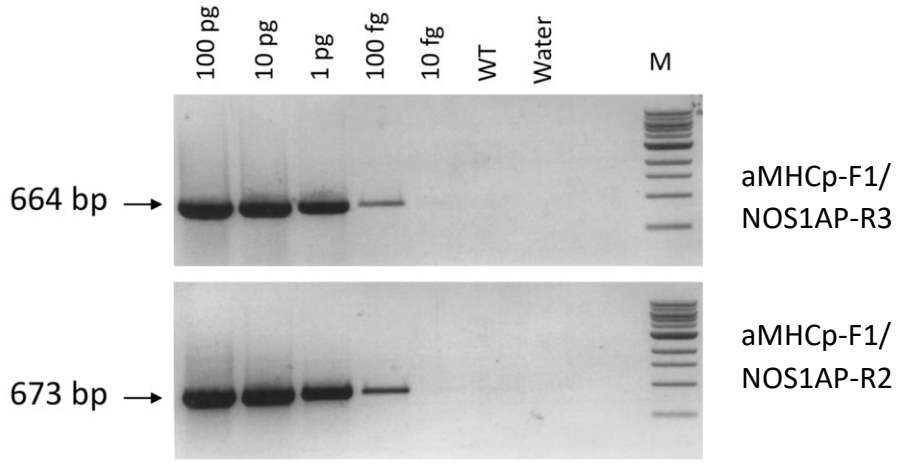


Figure 3.2: Agarose gel electrophoresis results for establishment of the PCR screen to verify the specificity and sensitivity of transgene detection. Concentration of transgenic vector DNA (100 pg – 10 fg) diluted within 100ng of wild-type genomic DNA across top row with wild-type (WT) genomic DNA alone and water as controls and marker (M). Combinations of primers used to amplify transgene shown on right. aMCHp-F1/NOS1AP-R2 ultimately selected for screening purposes. [Image courtesy of Dr Ben Davies].

3.2.3 Pronucleus microinjection

Three-week-old female C57Bl6/J mice were superovulated and mated with male mice from the same background. The resulting fertilized oocytes were collected from the oviduct of plugged female mice and cultured until two clear pronuclei were visible. The purified transgenic construct was microinjected into one of the pronuclei (**Figure 3.3**) and injected embryos were cultivated overnight to the two-cell stage.

Figure 3.3 – Oocyte microinjection

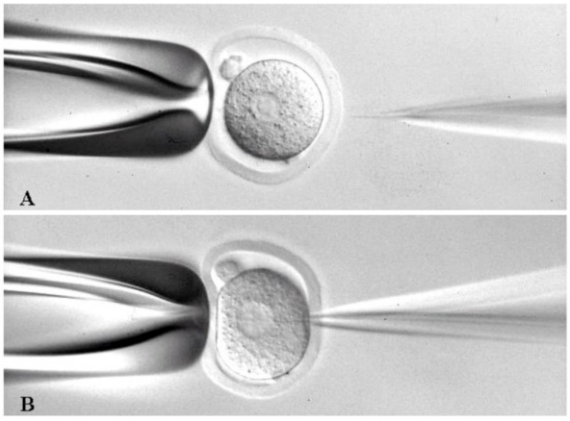


Figure 3.3: (**A**) Oocyte before injection with visible male pronucleus. (**B**) Oocyte after injection with enlarged male pronucleus demonstrating successful injection. [Image courtesy of Dr Ben Davies].

Two-cell embryos were then re-implanted into the oviduct of pseudo-pregnant CD1 foster mothers at 0.5 days post-coitum. Between 18 and 19 days later, pups were born from the foster mothers.

Table 3.3 summarises the DNA microinjections which were performed.

Table 3.3 – Microinjections performed

Transfer date	Embryos transferred	Date of Birth	Number of pups born	Transgenic founders
22-Oct-15	32	12-Nov-15	3	
22-Oct-15	32	12-Nov-15	8	
19-Nov-15	22	10-Dec-15	6	
15-Jan-16	30	05-Feb-16	3	
17-Mar-16	32	07-Apr-16	6	
26-May-16	16	16-Jun-16	TLL	
26-May-16	16	16-Jun-16	10	
17-Nov-16	28	08-Dec-16	TLL	
17-Nov-16	29	08-Dec-16	12	
22-Dec-16	13	12-Jan-17	1	
28-Mar-17	24	18-Apr-17	4	
28-Mar-17	25	17-Apr-17	5	1
04-Apr-17	19	25-Apr-17	6	
04-Apr-17	19	25-Apr-17	7	
09-May-17	32	30-May-17	3	
09-May-17	32	30-May-17	4	
11-May-17	34	01-Jun-17	Not pregnant	
11-May-17	32	01-Jun-17	Not pregnant	
13-Jun-17	31	04-Jul-17	TLL	
13-Jun-17	30	04-Jul-17	1	
20-Jun-17	24	11-Jul-17	3	
20-Jun-17	28	11-Jul-17	4	
06-Jul-17	28	27-Jul-17	1	
		TOTALS	87 pups born	1 Tg founder

Table 3.3: Summary of microinjections performed over ~18 months. TLL: Total litter loss.

3.2.4 Screening for transgenic founders

A total of 87 mice were born. Tail biopsies from weaned pups were prepared and DNA was extracted using E.Z.N.A. DNA tissue extraction kit (Omega). PCR amplification was performed and a specific 673 bp PCR product was obtained when the transgenic construct had integrated into the host genome (**Figure 3.4**). In addition, a second PCR was performed with control DNA to ensure sufficient DNA quality. However, the overall transgenic efficiency was very low. After investigation, it was felt it may have been related to impurities in the DNA. Although subsequently resolved, only one founder mouse [C57Bl6/J-Tg(*Myh6-hNOS1AP*)] could be identified using the transgene specific PCR. The usual transgenesis frequencies for the C57Bl6/J background used are between 5 – 10%.

Figure 3.4 – Screening for transgenic founders

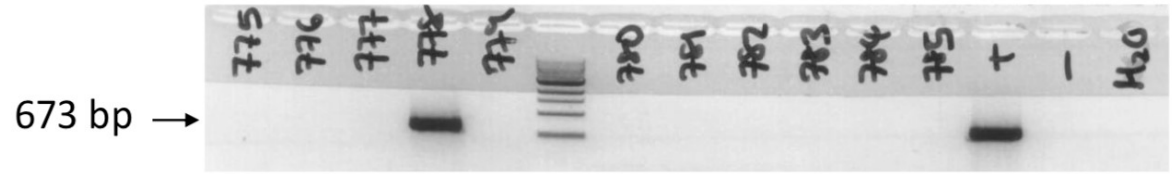


Figure 3.4: Agarose gel electrophoresis of DNA from tails of pups born. PCR with the primers aMHCp-F1 and NOS1AP-R2 was performed. Only 1 pup out of 87 born had successful transgene integration. [Image courtesy of Dr Ben Davies].

3.2.5 Breeding of Tg(*Myh6-hNOS1AP*)

I bred the single female F0 founder mouse (Tg/$^{+}$) with a male C57Bl6/J ($^{+}/^{+}$). Consequently, F1 offspring were transgenic (Tg/$^{+}$) or wild-type ($^{+}/^{+}$) at expected Mendelian frequencies of 50% of each genotype. Subsequent breeding was between transgenic and wild-type offspring. Breeding and ear-notching of the transgenic strain was undertaken in compliance with the UK Home Office Guidance on the Operation of Animals (Scientific Procedures) Act 1986 under Project Licence 30/3374 and P52BA7BA2. Mice were housed and cared for in approved facilities in compliance with UK Home Office regulations, had unlimited access to food and water and were subject to twelve-hour light/dark cycles. The original transgenic founder mouse lived for 2 years at which point she was humanely culled.

3.2.6 Genotyping protocol for breeding

Using the aMHCp-F1 and NOS1AP-R2 PCR primers listed earlier in **Table 3.1**, I optimised the genotyping protocol using DNA extracted from murine ear notches collected for routine identification. DNA extraction was performed using the HotSHOT technique [132]. Ear notches had 75µl of alkaline lysis buffer added (25 mM NaOH, 0.2mM disodium EDTA) and were then heated to 95°C for one hour. Samples were cooled to 4°C and 75 µl neutralizing solution then added to each sample (40 mM Tris-HCl). PCR reactions were carried out as in **Table 3.4** and the product run in 2% agarose gels with TAE/TBE with 12 µl of GelRed at 120 V for 50 minutes and developed using the Chemidoc system (Bio-Rad). A 673 bp product was seen in transgenic mice (**Figure 3.5**).

Table 3.4 – Genotyping PCR protocol

Reaction mix per sample			Reaction conditions			
			Step	Temp (°C)	Time (s)	Cycles
HotSHOT extracted DNA	5	µl	Denaturing	95	600	× 1
Bioline Red mix	12.5	µl	Denaturing	94	60	
aMHC-F1 Primer	0.5	µl	Annealing	57	60	× 32
NOS1AP-R2 Primer	0.5	µl	Extension	72	30	
$MgCl_2$	0.5	µl	Completion	72	600	× 1
Nuclease free water	1	µl	Hold	4	-	
Total reaction volume	20	µl				

Table 3.4: Details of reaction mix on the left-hand side and thermal cycler protocol on the right.

Figure 3.5 – Validation of genotyping protocol

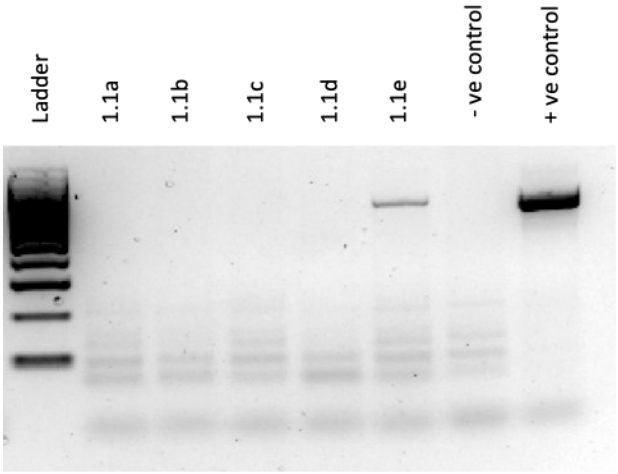


Figure 3.5: Agarose gel electrophoresis of PCR products from DNA extracted from ear notches of first transgenic litter using transgene primers. Pup 1.1e expresses the transgene with a PCR product at the appropriate level with the positive control of genomic DNA.

3.2.7 Tissue collection

Mice were euthanised under Schedule 1 using cervical dislocation with confirmation of death by exsanguination. The chest was opened and after transection of the descending aorta, the heart was perfused with ~5 ml of ice-cold phosphate-buffered saline (PBS) through both the right and left ventricles to clear any blood. Hearts were then removed and the atria and ventricles dissected and snap-frozen separately in cryo-tubes on dry ice. A portion of the lungs were then removed and frozen after which the abdomen was opened and portions of the liver, spleen and kidneys were removed and snap-frozen. After retraction of overlying skin, a portion of the quadriceps femoris

from the hind legs was resected and snap frozen. Finally, after incision and splitting of the skull, a portion of the cerebrum was also snap-frozen. Samples were all stored at -80°C until needed. Tissues were subsequently homogenised in the appropriate buffers on ice using a stainless-steel bead and a Tissue Lyser bead mill (Qiagen) at 50Hz for 2-3 minutes.

3.3 Chapter specific methods

3.3.1 Assessment of gene expression

Gene expression was assessed using quantitative real-time PCR using TaqMan gene expression probes as described in **Section 2.1**. The specific probes used were Mm01290688_m1 for murine *Nos1ap*, Hs00928956_m1 for human *NOS1AP*, Mm00437762_m1 for murine *B2m*, Mm99999915_g1 for murine *Gapdh* and Mm02342430_g1 for murine *Ppia* (all probes from ThermoFisher Scientific).

For quantification of transgenic gene expression relative to wild-type, the mean △Ct for wild-type was subtracted from the mean △Ct for a corresponding transgenic sample and relative gene expression of transgenic genes to wild-type expressed as $2^{-\triangle\triangle Ct}$.

3.3.2 Assessment of protein expression

Protein expression was assessed using Western blotting as described in **Section 2.2**. Specifically, protein homogenates from tissues were separated on 4-12% Bis-Tris NuPage gels (ThermoFisher Scientific) using gel electrophoresis at 180 V for ~90 minutes at room temperature. A human NOS1AP purified recombinant protein with an N-terminal His tag (NM_014697, Origene) was used as a positive control. Samples were then transferred onto nitrocellulose membranes in transfer buffer with 15% methanol at 250 mA for 120 min at 4 °C. After cutting membranes at appropriate molecular weights, blocking of non-specific binding was performed using 5% skimmed milk in phosphate buffered saline with 0.1% Tween-20 (ThermoFisher Scientific) followed by incubation with the primary antibodies (mouse monoclonal anti-CAPON C-9 sc-374504, Santa Cruz Biotechnology, at 1:1000 dilation or rabbit polyclonal anti-GAPDH PA1-987, ThermoFisher Scientific, at 1:50000) overnight at 4 °C. After washing, appropriate species-specific secondary antibodies at 1:25000 for anti-mouse and 1:50000 for anti-rabbit were added for one hour and then washed off. Membranes were developed using Dura extended duration substrate (ThermoFisher Scientific), with imaging performed using a ChemiDoc Imager (BioRad) and band intensities quantified via the ImageLab software (BioRad).

3.3.3 Echocardiography

Mice aged 16 – 20 weeks were anaesthetised initially using 5% isoflurane/O_2 mix followed by maintenance using a 2% isoflurane/O_2 mixture and placed on a heated table with integrated ECG monitoring. An appropriate depth of anaesthesia was maintained and echocardiography performed using a VisualSonics Vevo 2100 system and a 18-38 MHz MS400 transducer probe (FUJIFILM VisualSonics Inc, Toronto). Left ventricular (LV) systolic function was assessed under light anaesthesia, aiming for a heart rate of approximately 450bpm. All measurements were taken using M-mode echocardiography in a short axis view at the level of the papillary muscles (**Figure 3.6**).

Figure 3.6 – Representative echocardiography image

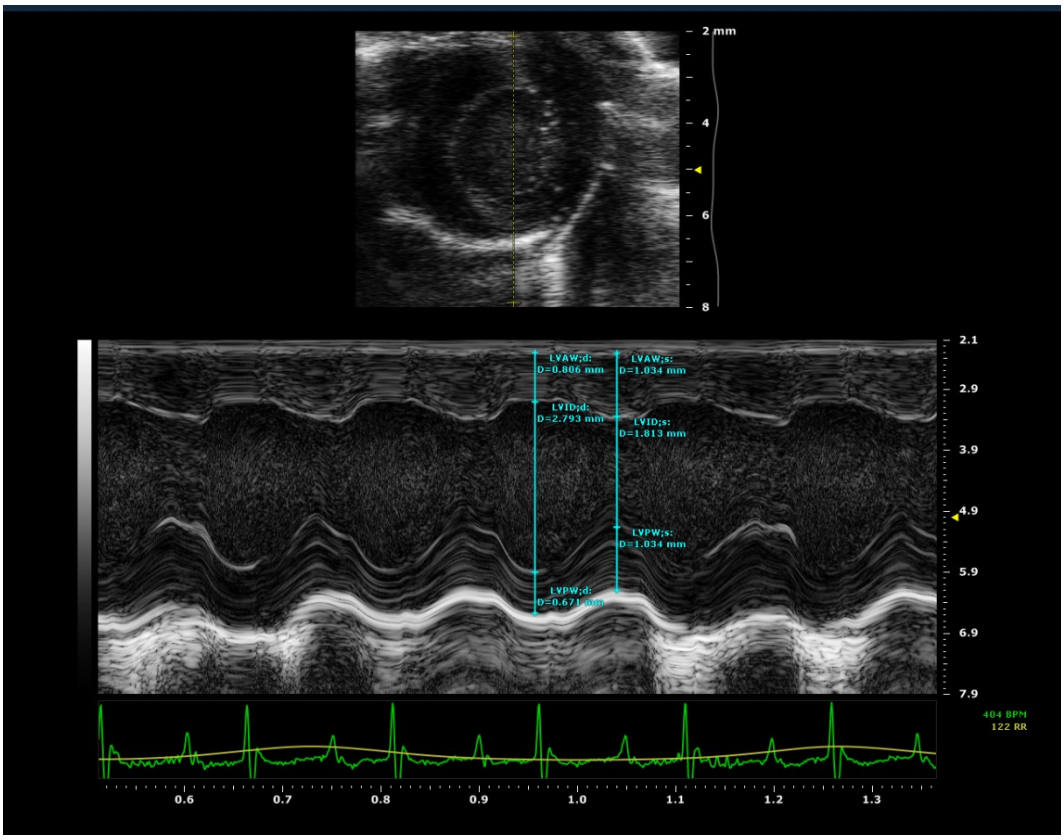


Figure 3.6: M-mode parasternal short-axis echocardiography image from anaesthetised wild-type mouse. LVAW;d: Left ventricular anterior wall; diastole. LVID;d: Left ventricular internal diameter; diastole. LVPW;d: Left ventricular posterior wall; diastole. LVAW;s: Left ventricular anterior wall; systole. LVID;s: Left ventricular internal diameter; systole. LVPW;s: Left ventricular posterior wall; systole.

LV size measurements as detailed in **Figure 3.6** were measured on six different cycles and the values averaged using Vevo LAB analysis software (FUJIFILM VisualSonics Inc, Toronto). After

automated calculation of left ventricular volumes using the Teicholz method, left ventricular ejection fraction was calculated according to the formula below:

$$\text{Ejection Fraction (\%)} = \frac{End\ diastolic\ volume - End\ systolic\ volume}{End\ diastolic\ volume} \times 100$$

Fractional shortening was calculated as follows:

$$\text{Fractional shortening (\%)} = \frac{LV\ internal\ diameter;\ diastole - LV\ internal\ diameter;\ systole}{LV\ internal\ diameter; diastole} \times 100$$

Left ventricular mass was calculated using the uncorrected cube formula where LV mass = [(LVID;d + LVAW;d + LVPW;d)^3 – LVID;d^3] × 1.055 and 1.055 was the gravity of myocardium [133].

3.3.4 Electrocardiography

Mice aged 16 – 20 weeks were anaesthetised initially using 5% isoflurane/O_2 mix followed by maintenance using a 2% isoflurane/O_2 mixture and placed on a heated pad. Subcutaneous needle electrodes (platinum F-E7, Grass Technologies) were inserted into all four limbs and connected to an Iso-DAM8A amplifier (World Precision Instruments) and a CED Power 1401-3A interface (Cambridge Electronic Design). ECG data was continuously acquired from a lead II configuration using Spike2 software (Cambridge Electronic Design) for the duration of the protocol.

A 30-second period under steady-state conditions was used for signal averaging using Spike2. ECG intervals were measured from this averaged trace for each mouse. As shown in **Figure 3.7**, and as previously defined [134], ECG measurements of P-wave duration, PR interval (defined as from the start of the P-wave till the first ventricular deflection), QRS duration (defined as from the start of the first ventricular deflection until the S wave crosses the baseline from below, before the start of the T-wave) and QT interval (defined from the start of the first ventricular deflection until the point the ECG trace reached baseline before the next P-wave) were taken as well as an averaged heart rate or R-R interval for the 30 second recording. As the QT interval is traditionally thought to alter with heart rate (although this may not be as relevant in mice [135]), a variety of commonly used correction formulae were used to 'correct' the QT interval values for each mouse as detailed in **Table 3.5**.

Figure 3.7 – Representative ECG trace denoting interval measurements

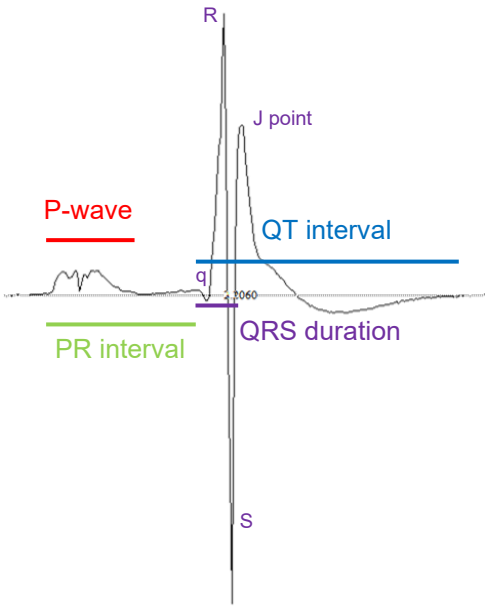


Figure 3.7: Representative ECG tracing from wild-type mouse showing the measurement of common ECG intervals from signal averaged murine ECG lead II. Note the initial small q-wave, R-wave then deep S-wave with a high J point or prominent J-wave.

Table 3.5 – Correction formulae used for QT interval

Name of formula	Formula
Bazzett*	$QT_c = \frac{QT}{\sqrt{RR/100}}$
Fridericia*	$QT_c = \frac{QT}{\sqrt[3]{RR/100}}$
Framingham	$QT_c = QT + 0.154(1 - RR)$

Table 3.5: Formulae used for calculation of 'corrected' QT interval (QT_c) using heart rate, expressed as RR interval in milliseconds. *Bazzett and Fridericia formulas modified for murine heart rate by dividing RR interval by 100 as previously described [136].

3.3.5 Ventricular arrhythmia induction *ex-vivo*

After cervical dislocation, murine hearts from mice aged 16 – 20 weeks were excised from the chest and the aorta rapidly cannulated (< 3 minutes) and sutured in an ice-cold solution of Krebs-Henseleit (K-H) buffer that was bubbled with 95% O_2 / 5% CO_2. The cannulated heart was then connected to a Langendorff perfusion system and kept warm using a heated water-jacketed chamber (IH-SRL, Harvard Apparatus). Aortic pressure was maintained at 60 mmHg throughout

the experiment using constant perfusion of K-H buffer (with 95% O_2 / 5% CO_2), kept warmed to 37°C. Following a 3-minute stabilisation period, spring loaded recording electrodes were placed on the right and left ventricular free walls and spontaneous (i.e. unpaced) monophasic action potentials (MAPs) were recorded for 5 minutes. Subsequently, a small incision was made in the right atrium and forceps were inserted and used to crush the atrio-ventricular (AV) node. Recording electrodes were placed once again on the right and left ventricular surfaces of the heart and an octapolar electrophysiology catheter (CIBer mouse EP catheter, NuMed Inc.) passed into the right atrium, crossing the tricuspid valve, with the distal electrodes in the apex of the right ventricle and the proximal electrodes in the right atrium. AV block was confirmed by the presence of dissociated atrial and ventricular electrical signals. After a 5-minute monitoring period, the pacing threshold from the distal right ventricular apex catheter electrodes was determined and burst pacing performed at twice threshold. As per published protocols for murine ventricular arrhythmia stimulation [137,138], 2 seconds of burst pacing starting at 40 ms coupling intervals with each subsequent burst's coupling interval decreasing by 2 ms until a minimum interval of 20 ms were delivered, representing eleven distinct pacing trains. The protocol was paused if ventricular tachycardia (VT) or ventricular fibrillation (VF) was induced and not restarted until sinus rhythm was restored.

For subsequent analyses, the data for each mouse was reviewed (IsoHeart software, Harvard Biosciences). An episode of VT or VF was deemed to have occurred if more than 3 consecutive beats were observed. The proportion of wild-type or transgenic mice developing any episode of VT or VF was calculated, as well as the probability of any given pacing train to induce VT or VF in any mouse (number of episodes of VT or VF/total pacing trains expressed as a percentage).

3.3.6 Statistical methods

For the main outcome of probability of VT/VF induction, power calculations for group sizes were determined using GPower 3.1 (Universitat Dusseldorf, Germany). Using a power of 90% and a 5% significance level ($\alpha = 0.05$) to detect an absolute difference in arrhythmia induction of 20% (10%

vs 30%) between the groups with a standard deviation of 15% (based on previous experiments [139-141]) gave a minimum sample size of 14 per group.

Data were analysed using GraphPad Prism 7 (GraphPad Software Inc.). Normality of data was assessed using the D'Agostino Pearson test. Statistical testing between groups was performed by two-tailed unpaired *t*-tests for normally distributed data, Mann-Whitney tests for non-parametric data, or chi-squared tests or Fisher's exact test for proportions. Two-way analysis of variance (ANOVA) was used to test for genotype differences across sex, with data being confirmed to be normally distributed or, if not, log transformed prior.

Data were expressed as mean and standard deviation for normally distributed data, and median and interquartile ranges for non-normally distributed data. Echocardiography and VT/VF induction were performed and analysed by me whilst blinded to genotype.

3.4 Results

3.4.1 The transgenic mouse model has myocardial specific gene and protein overexpression of NOS1AP

Gene expression profile

I quantified the gene expression of murine *Nos1ap* and human *NOS1AP* in a range of tissues in transgenic mice and their wild-type littermates. Murine *Ppia* was selected as the housekeeping gene for normalisation as it was found to have the lowest standard deviation in Ct values across all tissue samples and genotypes (1.7 vs 2.7 for *Gapdh* and 3.3 for *B2m*).

As shown in **Figure 3.8**, the endogenous expression of murine *Nos1ap* mRNA was highest in cardiac and central nervous system tissue, with no differences between genotypes. The transgenic mouse showed that cardiac *NOS1AP* mRNA expression was ~800-fold higher than endogenous murine *Nos1ap* mRNA levels. *NOS1AP* expression was detected only in cardiac and lung tissue. The mean Ct value for *NOS1AP* in lung tissue in transgenic mice was 26 (compared with ~17 for cardiac tissues, ~500-fold lower expression) and it was seen in all lung tissue samples. The expression of endogenous *Nos1ap* was unaffected by the transgenic *NOS1AP* expression, across all tissue types.

Protein expression profile

Using Western blotting, protein expression of endogenous murine and human NOS1AP was quantified with the use of an antibody detecting both species' proteins (directed against amino acids 304-503 mapping the C-terminus of the protein in rats) in a variety of tissues. The recombinant purified human NOS1AP protein used as a positive control for transgene expression as well as the overexpressed human NOS1AP protein in cardiac tissues had higher molecular weights (~75kDa) compared with murine NOS1AP (~56kDa), confirmed using different antibodies. This was despite similar lengths of amino acid sequences (506 in human vs 503 in mice) and the same predicted molecular weight and open-source databases not suggesting significant differences in post-translational modifications. Overall, protein expression of human NOS1AP was ~2.5 fold higher in cardiac tissues compared to the endogenous murine protein (**Figure 3.9**).

Figure 3.8 – Gene expression profile of *NOS1AP* in Tg(*Myh6-hNOS1AP*) colony

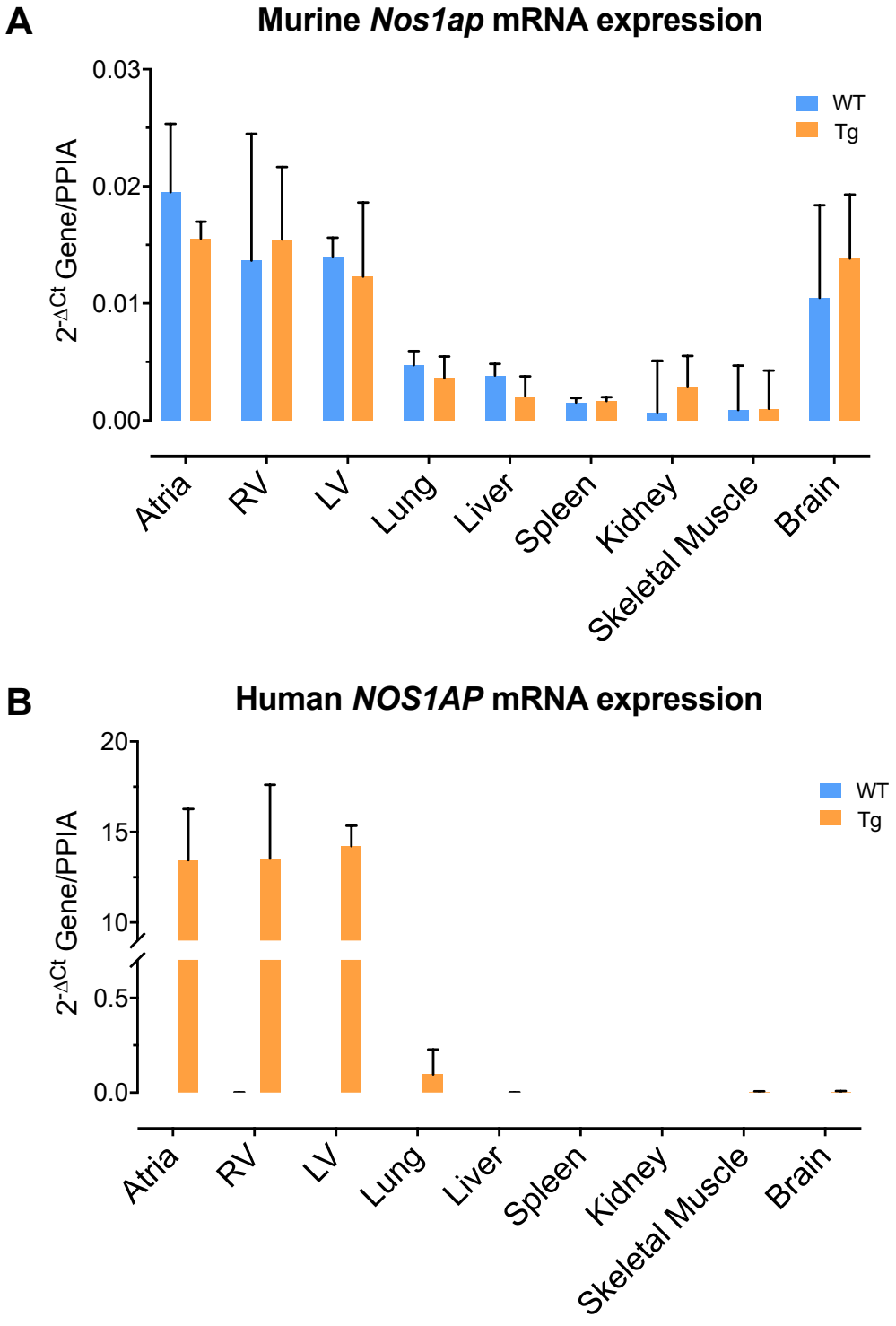


Figure 3.8: Gene expression in a variety of tissues of endogenous murine *Nos1ap* (**A**) and human *NOS1AP* (**B**) in wild-type (WT; n=8) and transgenic (Tg; n=6) mice as measured by RT-qPCR and displayed as median and interquartile ranges. (**A**) There were no significant changes in gene expression between WT and Tg mice for endogenous murine *Nos1ap* in all tissue types (Mann-Whitney tests). (**B**) Atrial, right ventricular (RV), left ventricular (LV) and lung tissue had significantly higher human *NOS1AP* gene expression in Tg mice compared to WT littermates ($P<0.001$; Mann-Whitney test). The mRNA was undetectable in other tissue types for both genotypes.

Figure 3.9 – Protein expression profile of NOS1AP in Tg(*Myh6-hNOS1AP*) colony

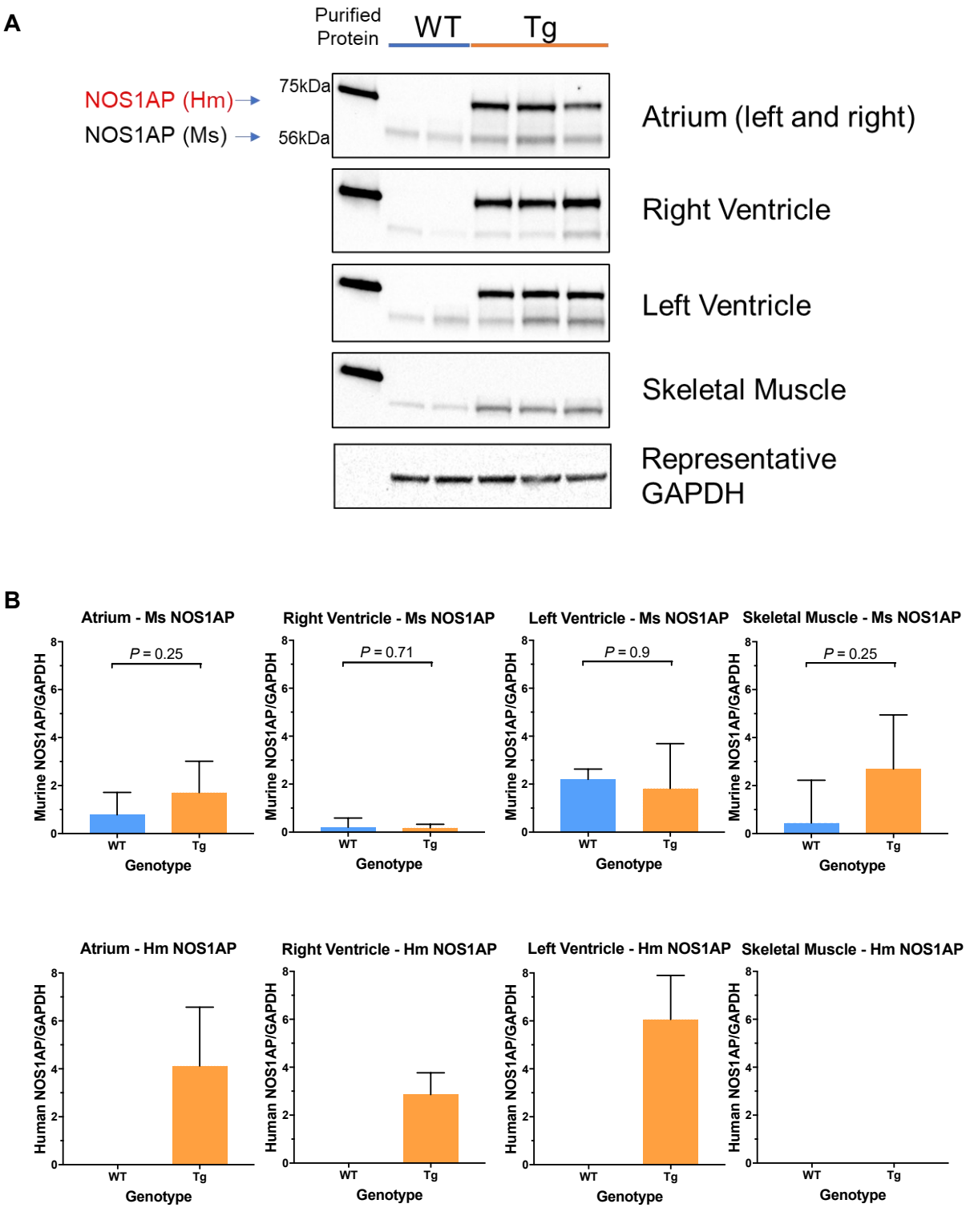


Figure 3.9: Human (Hm) and murine (Ms) NOS1AP protein content in cardiac and skeletal muscle tissues in wild-type mice (WT) and transgenic (Tg) littermates. Atrial tissue is a mixture of right and left atrium. (**A**) Representative Western blots of tissues showing human purified NOS1AP protein lane with WT and Tg tissues, with GAPDH shown for skeletal muscle (**B**) Quantification of changes in murine NOS1AP normalised to GAPDH in WT (n=3) and Tg (n=6) mice with median and interquartile ranges shown; Mann-Whitney test.

3.4.2 Cardiac structure or function was unaffected in the transgenic mouse model

To compare cardiac structure and function in mice from both genotypes, I performed trans-thoracic echocardiography in mice aged 16 – 20 weeks old. As shown in **Table 3.6**, there were no significant differences in left ventricular structure or systolic function between transgenic and wild-type littermates.

Table 3.6 – Echocardiography parameters for Tg(*Myh6-hNOS1AP*) colony

Parameter	Wild-type (n=10)	Transgenic (n=12)	*P* for difference
M:F ratio	6 : 4	6 : 6	-
Mean heart rate (bpm)	460 ± 47	460 ± 24	0.99
Body weight (g)	28.6 ± 5.1	27.4 ± 3.4	0.50
LVAWd (mm)	0.99 ± 0.11	0.93 ± 0.13	0.25
LVIDd (mm)	2.99 ± 0.70	3.14 ± 0.50	0.57
LVPWd (mm)	0.92 ± 0.13	0.87 ± 0.17	0.41
LVAWs (mm)	1.33 ± 0.27	1.30 ± 0.27	0.82
LVIDs (mm)	2.09 ± 0.75	2.06 ± 0.67	0.91
LVPWs (mm)	1.31 ± 0.23	1.31 ± 0.28	0.98
Ejection Fraction (%)	59.1 ± 18.7	64.1 ± 18.2	0.54
Fractional Shortening (%)	31.5 ± 12.2	35.5 ± 13.3	0.47
LV mass (mg)	95.7 ± 28.0	94.9 ± 24.4	0.94
LV mass per g body weight (mg/g)	3.46 ± 1.1	3.50 ± 0.95	0.94

Table 3.6: Details of echocardiography parameters; LVAW: Left ventricular anterior wall; LVID: Left ventricular internal dimension; LVPW: Left ventricular posterior wall; d: diastole, s: systole. Values presented as mean ± standard deviations. Unpaired *t*-test for comparison.

3.4.3 Surface ECG parameters are altered in transgenic mice with myocardial *NOS1AP* overexpression

Investigation of the surface ECG in 21 wild-type (13 male and 8 female) and 19 transgenic mice (7 male and 12 female) aged 16 – 20 weeks old showed that qualitatively, the ECG trace was altered in transgenic mice, lacking the negative component of the T-wave and with more deflections within the QRS complex (**Figure 3.10**). Signal-averaged surface ECG recordings (~250 complexes) revealed that transgenic mice had a longer P wave duration (26 ± 5 ms vs 21 ± 4 ms, $P = 0.004$) and longer PR interval (41 ± 3 ms vs 38 ± 3 ms, $P = 5\times10^{-4}$) compared with wild-type littermates. However, there was no change in the PR isoelectric interval (16 ± 6 ms vs 15 ± 4 ms, $P = 0.63$) between genotypes, suggesting that the changes in the PR interval were secondary to the changes

in P-wave duration and not atrio-ventricular nodal conduction. Transgenic mice had slightly longer QRS complexes than their wild-type littermates (11 ± 1 ms vs 10 ± 1 ms, $P = 0.02$), with shorter QT intervals (50 ± 12 ms vs 60 ± 11 ms, $P = 0.006$) which were unrelated to differences in RR intervals under general anaesthesia (124 ± 16 ms vs 121 ± 12 ms, $P = 0.60$; **Figure 3.11**).

Figure 3.10 – Qualitative differences in ECG traces for Tg(*Myh6-hNOS1AP*) colony

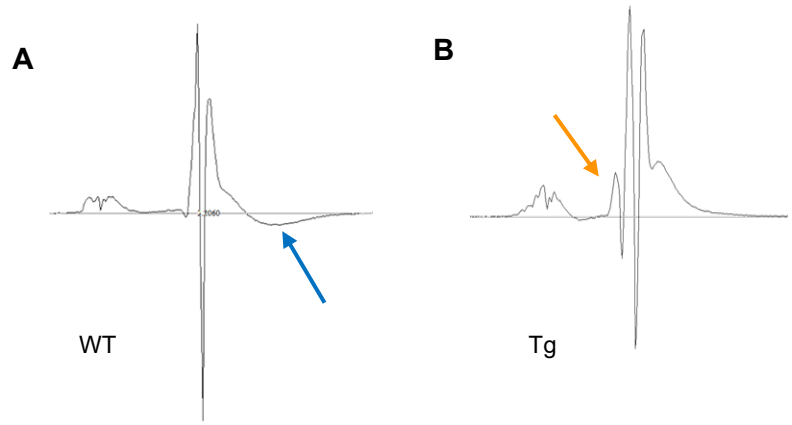


Figure 3.10: Representative signal-averaged ECG recordings from (**A**) wild-type (WT) and (**B**) transgenic (Tg) mice. Tg mice lacked the negative component of the T-wave seen in WT mice (blue arrow) and had extra deflections within the QRS complex, possibly representing bundle branch block (orange arrow) compared to WT littermates.

Figure 3.11 – ECG parameter values for Tg(*Myh6-hNOS1AP*) colony

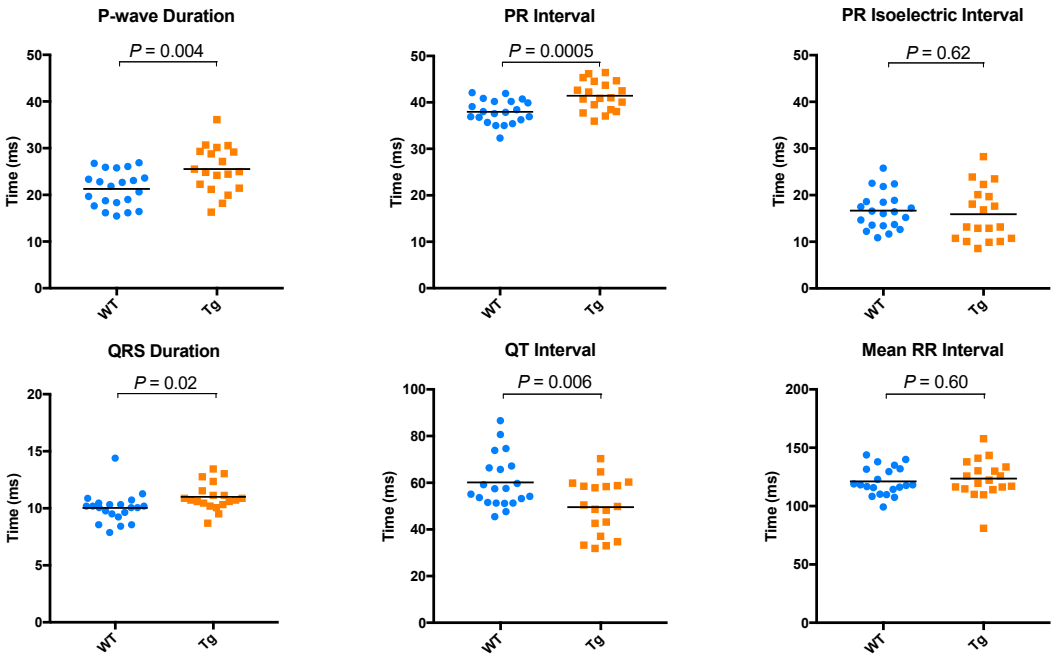


Figure 3.11: Signal averaged ECG parameters measured in 21 wild-type (WT) and 19 transgenic (Tg) mice under general anaesthesia. Horizontal lines are mean values, unpaired *t*-test for comparisons.

Overall, there was only a modest correlation between the mean RR interval and the measured QT interval across both genotypes (Pearson's r +0.37; 95% Confidence Interval [CI] 0.07 -0.61, *P*=0.02). Further correction of QT intervals for the RR interval with a variety of formulae did not alter the findings (**Table 3.7**).

Table 3.7 – Heart rate corrected QT intervals for Tg(*Myh6-hNOS1AP*) colony

Method of correction	Wild-type QT	Transgenic QT	*P* for difference
Uncorrected	60 ± 11	50 ± 12	0.006
Bazzett	55 ± 9	45 ± 10	0.002
Fridericia	56 ± 10	46 ± 10	0.003
Framingham	42 ± 10	31 ± 11	0.002

Table 3.7: Heart rate corrected QT intervals using popular correction formulae. Values displayed as mean ± standard deviation. Unpaired *t*-test for comparisons.

Electrical parameters and the QT interval in particular are known to vary between sexes. As seen in **Figure 3.12**, although the QT interval was *shorter* in females versus males of the same genotype, there was no evidence of genotype interaction with sex for any of the ECG parameters. I did also find a longer PR interval (but not P-wave) in Tg females vs WT females and Tg males.

Overall, these findings suggest that, under basal conditions, mice with myocardial overexpression of human NOS1AP have atrial and ventricular ECG parameters reflecting altered depolarisation and conduction as well as repolarisation, independent of changes in cardiac structure or function. Most notably, transgenic mice had shorter measured QT intervals but longer QRS and atrial ECG parameters (P-wave duration and PR interval).

To evaluate any propensity to spontaneous sudden cardiac death in later life, we aged a cohort of mice over a period of time. Twelve transgenic mice and thirteen wild-type littermates were aged to between 8 months and 1-year-old without any evidence of sudden death or animal welfare issues observed, making spontaneous malignant ventricular arrhythmias and cardiac arrest unlikely.

Figure 3.12 – ECG parameter values by sex

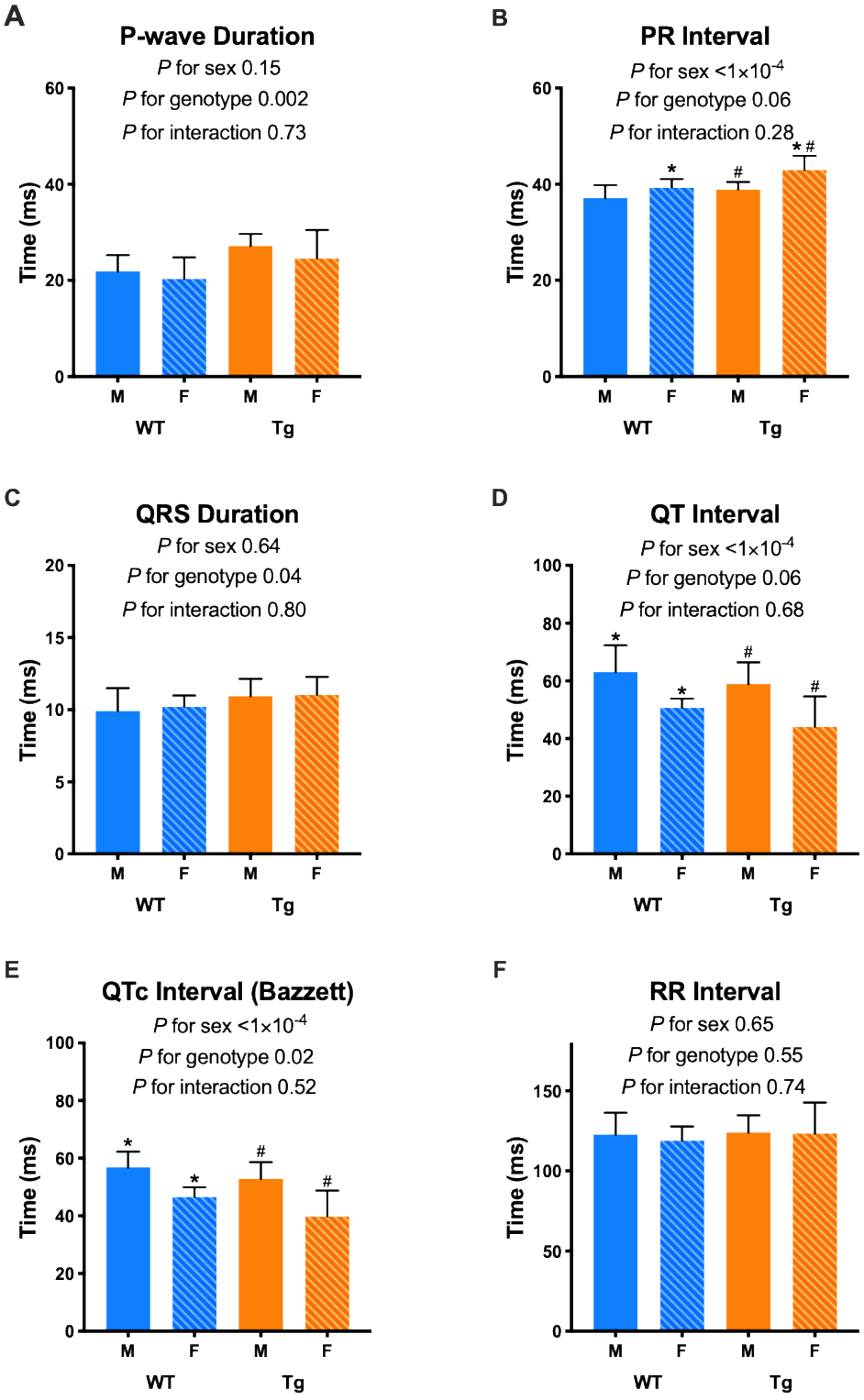


Figure 3.12: (**A**) to (**F**): ECG parameters measured in 13 wild-type (WT) males and 8 WT females as well as 7 transgenic (Tg) males and 12 Tg females. *P*-values from two-way analysis of variance with terms for genotype and sex with post-hoc comparisons adjusted using Sidak's method for multiple comparisons. For PR interval (**B**): **P*-value of 5×10^{-3} (WT female vs Tg female) and $^{\#}3\times10^{-3}$ (Tg male vs female). For QT interval (**D**): **P*-value of 5×10^{-3} (WT male vs female) and $^{\#}2\times10^{-3}$ (Tg male vs female). For QT_c (**E**): **P*-value of 2×10^{-3} (WT male vs female) and for $^{\#}3\times10^{-4}$ (Tg male vs female).

3.4.4 The probability of *ex-vivo* pacing induced ventricular arrhythmias is increased in transgenic mice

Given the association in humans between increased myocardial *NOSIAP* expression and longer QT interval with increased incidence of sudden death [72,73,77], I compared the propensity to develop *ex-vivo* pacing induced ventricular arrhythmias between genotypes in 18 wild-type (8 male and 10 female) and 18 transgenic mice (8 male and 10 female) aged 16 – 20 weeks old. Arrhythmogenesis is a stochastic process and accordingly, I assessed the probability of developing arrhythmias after any single burst of pacing out of a number of bursts (representative trace - **Figure 3.13 A**).

Ventricular arrhythmias were typically non-sustained and of very short duration (<1 second) with VT being typically monomorphic. The probability of developing VT/VF after any burst of pacing was significantly higher in transgenic mice compared to wild-type littermates (27% vs 9%, P=0.0012; **Figure 3.13 B**). Additionally, more transgenic mice developed VT/VF in response to burst pacing compared to their wild-type littermates (89% vs 56%, P=0.06; **Figure 3.13 C**), although this did not reach statistical significance. There were no significant differences between males and females in each group and there was no interaction between genotype and sex (**Figure 3.13 D** and **E**).

Figure 3.13 – Ventricular arrhythmias in *ex-vivo* hearts of Tg(*Myh6-hNOS1AP*) colony

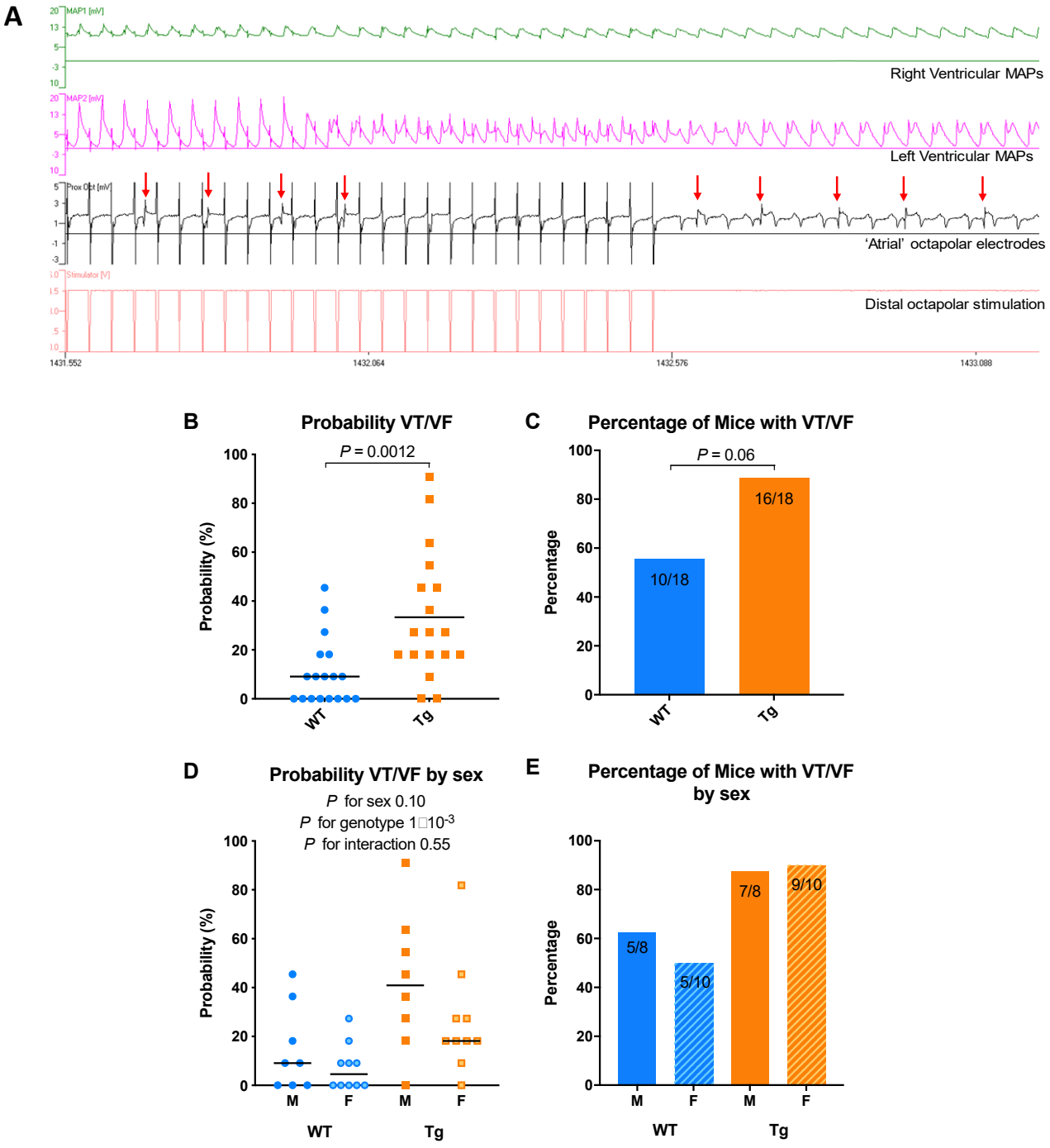


Figure 3.13: (**A**) shows representative tracing of ventricular tachycardia (VT) induction after pacing from the distal octapolar electrode (red trace) with recording of epicardial right and left ventricular monophasic action potentials (MAPs; green and pink traces). The atrial octapolar electrodes (black trace) show pacing artefact and near-field atrial electrograms (red arrows) independent of ventricular activity confirming successful atrioventricular nodal crush. (**B**) shows probability of any burst pacing train inducing VT or ventricular fibrillation (VF) in wild-type (WT) or transgenic (Tg) genotypes; horizontal lines represent median values, Mann-Whitney test for comparison. (**C**) shows percentage of mice with VT/VF in WT or Tg littermates; Fisher's exact test for comparison. (**D**) shows same data as in **B** grouped by sex (both genotypes with M:F ratio of 8:10); horizontal lines represent median values. *P* for interaction using two-way analysis of variance with terms for genotype and sex after transformation of data to normal distribution using addition of a constant. (**E**) shows same data as in **C** grouped by sex.

3.5 Discussion

3.5.1 Summary of results

The Tg(*Myh6-hNOSIAP*) model was confirmed to have cardiac gene overexpression of human *NOSIAP* translating into a ~2.5-fold increase in protein expression of human NOSIAP over endogenous murine NOSIAP in cardiac tissues. Transgenic mice had a cardiac electrical phenotype on surface ECG, although, unexpectedly, a shorter measured QT interval when compared to wild-type littermates. They also had a longer P-wave duration, longer PR intervals, a longer QRS duration and qualitatively different QRS-T complexes with no changes in heart rate when compared with wild-type littermates. Isolated perfused hearts from transgenic mice also had an increased probability to develop ventricular arrhythmias in response to burst pacing when compared with wild-type littermates.

3.5.2 Comparing NOS1AP expression in mouse model and humans

Gene expression

The assumption in generating this transgenic overexpressing model was that human genetic variants in *NOSIAP* would be associated with altered NOSIAP protein expression. The genetic variants showing significant associations between *NOSIAP* and QT interval lie in non-coding regions of the genome and are likely to have *cis*-regulatory functions on gene expression, as evidenced by increased chromatin accessibility in this region (assessed by DNaseI hypersensitivity) and other functional assays [86]. These findings do not rule out possible effects of the genetic variants on silencing RNA or micro-RNA; however, human gene expression data from left ventricular and left atrial appendage tissues (obtained from personal communication [84] and the GTEx portal) shown in **Figure 1.5** and **Figure 1.6** show that the alleles associated with a prolonged QT interval display an approximately 1.2 to 1.5-fold increase in *NOSIAP* mRNA transcript per allele. Modest differences in *NOSIAP* expression are consistent with the effects of common genetic variation in a healthy population, especially with variation in non-protein coding regions of the genome [29].

Notably, single variants in alleles of *NOSIAP* are associated with a range of *NOSIAP* mRNA expression across individuals. For instance, measured *NOSIAP* mRNA in individuals homozygous for G/G at the rs12143842 allele can be different by 16-fold at the top versus bottom of the range (**Figure 1.5**). Whilst there is a trend across the population that variants associating with a longer QT have higher *NOSIAP* gene expression, it is likely that any individual's myocardial *NOSIAP* gene expression is influenced by multiple variants (by cis-regulation from other alleles within *NOSIAP* or trans-effects from other genes) rather than driven by a single polymorphism. This highlights the relevance of inbred mouse strains in understanding biology and highlights a limitation of human iPSC cells where conclusions can be difficult to draw unless the cell lines are genetically identical and differ only by a single *NOSIAP* polymorphism which may be possible by using isogenic pairs [142].

Specific to our model, a very low level of transgene expression of human *NOSIAP* was detected in the lung tissue of transgenic mice. The *Myh6* promoter for Myosin heavy chain 6 is considered to be cardiomyocyte-specific but there are reports from transgenic mouse models in the literature where *Myh6* gene expression is localised to the thick intimal wall of pulmonary veins and venules, closest to the heart, the so-called 'pulmonary myocardium' [143-145]. Alternatively, my results might plausibly represent a contaminant from tissue collection due to the proximity of cardiac and lung tissues, the high levels of human *NOSIAP* gene expression and the extremely sensitive nature of the polymerase chain reaction. A further limitation is that the cardiac tissues used for gene expression and indeed protein expression testing were homogenates and not isolated cardiomyocytes. Particularly for murine atria with embedded parasympathetic nuclei, this may affect measured endogenous *Nosiap* or *NosI* gene and protein expression. However, by using cardiomyocyte-limited human *NOSIAP* overexpression, any functional differences between genotypes should be the result of cardiomyocyte NOSIAP alone.

Protein expression

There are no specific data in humans of the consequences of changes in *NOSIAP* gene expression on protein levels. The Tg(*Myh6-hNOSIAP*) model significantly overexpresses the mRNA of human

NOS1AP. Unfortunately, due to difficulties generating the founder, and despite further attempts, the Transgenic Core lab were unable to generate further lines with potentially varying levels of *NOS1AP* transgene overexpression. However, at a protein level, at face value, the current line's ~2.5-fold increase in human NOS1AP compared to the endogenous murine protein is relatively modest.

Ultimately, gene and protein expression are not linearly related. Although for most endogenous genes across a variety of cells, there are more protein copies compared to mRNA copies (i.e. a single mRNA transcript is likely translated into peptides multiple times) [146,147], the correlation between mRNA levels and protein levels is known to be surprisingly variable [148]. In the 'steady state', the primary determinant of protein levels are usually mRNA levels [147] so in our NOS1AP-Tg model one may speculate that the 'excess' mRNA was not translationally efficient, or saturated the specific cellular translation machinery and was not translated into protein.

Despite close homology in amino acid sequences and the same 'predicted' molecular weights using online tools, human NOS1AP protein was consistently seen at a higher molecular weight compared to the endogenous murine form. Open-source databases (dbPTM and UniProt) predict both human and murine proteins to undergo phosphorylation at similar residues across the proteins and do not highlight other predicted areas of post-translational modification. Interestingly, the human recombinant purified protein I used as a positive control was also seen at the higher molecular weight and was generated in *Escherichia Coli* bacteria. Studies that used viral transduction of human *NOS1AP* saw similar molecular weights as seen by us across a variety of tissues [105,107], suggesting that this is not limited to the transgenic model. Ultimately, Western blot-based assessment of molecular weights can be affected by protein charge as well as post-translational modifications such as glycosylation, phosphorylation or ubiquitination. Further investigation would be needed to accurately determine the cause and indeed whether this has any functional relevance.

Thus, whilst the gene and protein expression of NOSIAP in the murine myocardium may not be a direct replica of human physiology, it does provide an *in-vivo* system to try to understand the role of the human NOSIAP protein commensurate with modest changes in protein expression.

3.5.3 Comparing ECG parameters in NOS1AP-Tg and humans

ECG parameters representing ventricular repolarisation

Given that increased *NOSIAP* gene expression is associated with a longer QT interval in humans, it may seem surprising that this appears to have the opposite effect in our transgenic murine model. A number of reasons may explain this unexpected finding.

In humans, the QT interval is a surrogate for ventricular repolarisation. A number of studies have shown that in mice, this is not necessarily the case. Mice have a high heart rate and consequently, the murine action potential is very short [149]. Depolarisation in some parts of the heart occurs simultaneously with repolarisation in others [150] and, importantly the duration of the QT interval in transgenic mice does not necessarily correlate with action potential duration in individual cells [151]. Particularly for repolarisation, there exists a gradient across the heart, occurring earlier at the apex than the basal regions and also earlier in the epicardium than the endocardium [149]. For murine studies, we used a single limb lead of the ECG to reflect the sum of the electrical vector through the whole myocardium. Therefore, if there were changes in electrical activity localised to specific areas of the heart, these may have been missed or under-represented in a single lead ECG (e.g. ECG changes in Brugada syndrome in humans typically confined to certain leads only).

As noted in **Figure 3.10**, the QRS-T segment in our transgenic mice was morphologically different to that seen in wild-type littermates. In particular, in the wild-type mice, the terminal part of the QT interval was comprised of a negative T-wave deflection gradually reaching the isoelectric baseline. This deflection was not seen in the transgenic mice whose ECGs had a more abrupt transition back to baseline, remaining mainly positive. Therefore, the QT intervals measured in the transgenic model were shorter when measured using similar methods to the human ECGs, which may or may not truly represent shortened repolarisation. As there is an additional discrepancy

between murine QT intervals and action potential durations at cell or tissue level [151], further investigation of markers of repolarisation is needed.

ECG parameters representing depolarisation and conduction velocity

Transgenic mice had longer P-wave durations, PR intervals and QRS durations compared to their wild-type littermates. The duration of the isoelectric component of the PR interval was not different between genotypes, suggesting that the changes in the PR interval were primarily driven by changes in the P-wave and time taken for atrial depolarisation to occur rather than atrio-ventricular nodal conduction. Similarly, the longer QRS duration in transgenic mice would ordinarily reflect slower or abnormal ventricular depolarisation. The shortened QT interval measured in transgenic mice was not affected by the finding of a slightly longer QRS interval, so further methods to 'correct' the QT interval for this were not pursued.

NOSIAP genetic variants have not been implicated as yet in other human ECG parameters beyond the QT interval, at least at GWAS significance thresholds. However, the largest GWAS of P-wave duration only identified 9 genetic variants at GWAS significance threshold which explained a total of ~2% of the total variance [152]. This suggests that a large proportion of genetic variance remains unexplained for this trait, mainly due to small sample size which is contributed to by difficulty in reliably recording P-wave duration on clinical ECGs. For QRS duration, shared genetic associations with PR interval and QT interval have been noted [153,154], suggesting a degree of common heritability which is not surprising, given a degree of overlap between atrial and ventricular electrical physiology. Stringent multiple-testing significance thresholds for reporting GWAS also mean that there are likely to be 'true' effects of other genetic variants that are not reported, but which may nonetheless contribute to the much-described phenomenon of 'missing' heritability in complex polygenic traits, especially in those whose genetic architecture is dependent on common variants with small individual effects [155]. Again, absence of evidence does not mean evidence of absence.

The effects on atrial ECG parameters in our transgenic model may not be unusual as murine atrial and ventricular depolarisation are similarly dependent on the rapid inward sodium current, I_{Na},

then the transient outward current I_{to} and subsequently on the L-type calcium current $I_{Ca,\,L}$ [156]. Other major determinants of the speed of depolarisation on a tissue level are gap junctions formed by connexin hexamers [157]. Different pro-arrhythmic murine models due to mutations in sodium channels replicating Brugada syndrome or LQT3 [158,159], reductions in connexin-40 [160,161], or connexin-43 [162-165] have also been associated with both atrial and ventricular ECG parameter changes and differences in measured electrical conduction velocities. Thus, any effects of NOS1AP on these parameters would likely affect both atrial and ventricular cardiomyocytes.

Sex-specific differences

Unexpectedly, female mice had shorter measured QT intervals across both genotypes when compared to their male littermates. In adult humans, females are recognised as having longer QT intervals compared to males [67]. There have been limited studies in the murine literature directly comparing sex-specific differences of the QT interval but in general, the data are conflicting [68]. This may be due to difficulties in the measurement of ECG parameters in mice and also perhaps as QT differences are more pronounced at lower heart rates which are not normally seen in mice.

In our experiments, the shorter QT interval didn't translate into sex-specific statistical differences in ventricular arrhythmia inducibility, although the experiments were not powered to detect these.

3.5.4 Ventricular arrhythmias in transgenic model compared to humans

As reported, the transgenic mice did not exhibit features of premature or sudden cardiac death, suggesting that spontaneous episodes of sustained ventricular fibrillation are unlikely in these animals. However, the NOS1AP-Tg hearts were significantly more likely to develop ventricular arrhythmias in response to burst pacing compared with their wild-type littermates, suggesting that NOS1AP overexpression leads to an increased propensity to initiate arrhythmias in response to triggers, without necessarily altering the ability of arrhythmia to self-sustain.

In our mouse model, overexpression of NOS1AP did not result in gross changes in cardiac structure or left ventricular systolic function as measured by echocardiography. Whilst this does not rule out subtle changes in cardiac function, the absence of an overt heart failure or sudden death

phenotype in aged mice makes cardiac structural abnormalities unlikely to be a cause of any differences seen between genotypes when the mice were younger. A study by Sugiyama *et al.* [110] described the generation of a mouse model with global *Nos1ap* knockout (*Nos1ap*$^{-/-}$) based on disruption of exon 3 of *Nos1ap*. Interestingly, they found no baseline changes in cardiac function or ECG parameters or spontaneous arrhythmias when the knockout mice were compared to wild-type. They did not however report confirmation of gene and protein knockout and so it is unclear whether their targeted exon disruption strategy was entirely successful.

Drawing major conclusions about ventricular arrhythmia sustainability in murine models is challenging. Previous theories relying on macroscopic concepts of mechanisms of fibrillation held that a critical size of chamber would be required for a fibrillatory wave to propagate and therefore, that the murine heart might not be able to do so [149]. Whilst no longer felt to be accurate, it is generally accepted that most murine models of arrhythmogenesis do not develop sustained ventricular arrhythmias comparable to those seen in humans [166,167]. For instance, even in mice with mutations in potassium channel genes and prolonged QT intervals on ECG, ventricular arrhythmias typically last for about a second [168,169].

As discussed in **Section 1.4.2**, genetic variants in *NOSIAP* have been associated with an increased incidence of sudden cardiac death in some human populations [72,73,77]. An explanation for this might be that the *NOSIAP*-related QT prolongation causes lethal ventricular arrhythmias. However, as discussed in **Section 1.2.2**, longer QT intervals are not consistently associated with an increased risk of sudden death in all populations [37,170]. Additionally, the associations between the alleles prolonging QT interval and risk of sudden cardiac death are inconsistent, and not attenuated by adjustment for the QT interval [72,73,171]. Overall, this suggests that some pro-arrhythmic effects of *NOSIAP* may occur independently of QT prolonging mechanisms.

To date, the current theories surrounding the mechanisms by which NOSIAP may alter the electrical substrate have been derived from studies in isolated cardiomyocytes and have focused on changes in NOS1-sensitive repolarising currents [107,111]. Our model suggests that at a whole heart

level, changes in ECG parameters may reflect differences in the electrical substrate underlying the pro-arrhythmic tendency.

Chapter 4 describes further work investigating the mechanisms by which NOSIAP might lead to the development of a pro-arrhythmic electrical substrate.

4

Mechanisms underlying the cardiac electrical phenotype in Tg(*Myh6-hNOSIAP*)

Summary

Investigation of the cardiac electrical substrate resulting from *NOSIAP* overexpression surprisingly revealed no significant difference in ventricular myocytes action potential durations between genotypes at physiological heart rates, although a shorter APD was seen at slower heart rates. There was a significant reduction in conduction velocity in the left ventricles of transgenic mice without an increase in cardiac fibrosis. This slowing of conduction velocity was not obviously explained by changes in the rapid sodium current I_{Na}, although transgenic mice had slower inactivation characteristics of the current. Slower conduction velocity in the transgenic mice was accompanied by lower ventricular content of connexin-43, particularly at the intercalated discs. No differences in calcium handling or NOS activity were detected between genotypes.

4.1 Introduction

Coumel's classical triangle of arrhythmogenesis highlights three factors – substrate, triggers, and modulating factors (particularly the autonomic nervous system) as critical in arrhythmogenesis [172]. In the case of *ex-vivo* burst pacing-induced ventricular arrhythmias, as shown in the NOS1AP-Tg mouse in **Figure 3.13**, the primary source of this finding would likely be changes in the myocardial substrate, potentially representing both electrical and structural properties [173]. Electrical parameters which offer the most likely arrhythmogenic substrate in this context include (i) an altered APD; (ii) altered calcium handling (which may also contribute to changes in APD); and (iii) altered conduction velocity. Thus far, studies from cell culture models have been inconsistent with regard to which of these substrates is most affected by changes in myocardial NOS1AP expression (whether it be by gene silencing or overexpression), limiting our ability to draw firm conclusions at present as to how, in humans, NOS1AP may alter arrhythmic susceptibility.

4.1.1 ECG parameters and the electrical substrate

The NOS1AP-Tg mice had longer P-wave, PR interval and QRS interval durations but a shorter measured QT interval. The primary component of the QT interval is the T-wave but despite many years of debate in the literature, the specific electrophysiological mechanisms underlying its generation remain unclear [174-176]. Broadly speaking, it is felt that varying gradients of ventricular repolarisation, both endo-epicardial as well as apico-basal contribute to the generation and therefore duration of the T-wave [175]. Whilst direct mapping and measurement of these gradients is inherently difficult, from our understanding of inherited and acquired long QT syndrome it is clear that altered individual cellular repolarisation, leading to changes in cellular action potential duration (APD) can be reflected by differences in the QT interval on the ECG [177,178].

Following on from this, in cardiac chambers of a similar size, differences in the duration of ECG parameters representing depolarisation (e.g. P-wave duration and QRS interval as seen in NOS1AP-Tg) should represent changes in the speed of travel of the electrical impulse. For repolarisation

parameters such as the QT interval, the relationship to conduction velocity is more difficult to conceptualise as there is not an obvious spreading electrical wavefront of repolarisation. However, differences in time to depolarisation of different myocardial regions may alter the time taken for repolarisation to complete. This may be heterogenous across the myocardium and lead to changes in the surface ECG, as has been proposed to explain the localised ECG changes in the ST and QT segments seen in Brugada syndrome [175,179,180]. Therefore, I focused upon comparing left ventricular APDs and conduction velocity between the NOS1AP-Tg mice and their wild type littermates.

4.1.2 NOS1AP and calcium handling

Altered evoked intracellular calcium ($[Ca^{2+}]_i$) transients have been described in relation to arrhythmogenesis in human long QT syndrome [181-183]. Indeed, alterations in $[Ca^{2+}]_i$ have been associated with changes in *Nos1ap* gene expression in various cell models. Treuer and Gonzalez [109] showed a reduced amplitude of evoked $[Ca^{2+}]_i$ transients after silencing RNA-induced knock down of *Nos1ap* gene expression in neonatal rat ventricular cardiomyocyte culture. Contrastingly, using rat cardiac sympathetic neuron culture, Lu *et al.* [105] showed that adenoviral overexpression of *NOS1AP* resulted in a reduction in peak total neuronal calcium current I_{Ca} and consequent lower amplitude of depolarisation-induced $[Ca^{2+}]_i$ transients compared with controls.

Given the described associations and the increased incidence of evoked ventricular arrhythmias seen in the NOS1AP-Tg mouse, I also investigated potential changes in $[Ca^{2+}]_i$ transients due to *NOS1AP* overexpression in the transgenic model.

4.1.3 NOS1AP and NOS1

Whilst NOS1AP was first described as an adaptor protein for NOS1 in neuronal tissues [57], whether NOS1AP's effects on cardiac physiology are NOS1 dependent is less certain. In human and murine atrial myocytes, disruption of NOS1 signalling (as observed in the presence of atrial fibrillation) is associated with a shorter right atrial APD_{90} due to an increase in I_{Kur} density [126], whereas in guinea-pig ventricular cardiomyocytes, NOS1 blockade using S-Methyl-L-thiocitrulline acetate (SMTC) has been shown to prolong APD_{90} by enhancing $I_{Ca,L}$ and $I_{Na,L}$ [111].

Initially, Chang *et al.* [107] suggested that after adenoviral overexpression of *Nos1ap* in cultured guinea pig ventricular myocytes, NOS1 protein levels may have been maintained by NOS1AP overexpression. Using immunofluorescence-based methods, they also reported a small increase in NOS1 activity in the *NOS1AP* overexpressing myocytes. Finally, they found that the significant APD shortening described earlier in *NOS1AP* overexpressing myocytes was completely reversed by the non-isoform specific NOS inhibitor *N*ω-nitro-L-arginine methyl ester chloride (L-NAME). Lu *et al.* [105] used the NOS1 inhibitor N-[(4S)-4-Amino-5-[(2-aminoetyl) amino]pentyl]-N′-nitroguanidine (AAAN) to suggest that most of the effects seen on I_{Ca} and $[Ca^{2+}]_i$ in rat cardiac sympathetic neurons due to adenoviral mediated *NOS1AP* overexpression were NOS1 dependent.

Therefore, I investigated potential alterations in NOS1 gene and protein expression and activity levels in the NOS1AP-Tg mice. Furthermore, given the limited diffusion range of NO in cardiomyocytes [113], data indicating that NOS1 subcellular localisation may determine NOS1's downstream targets [184], and evidence suggesting that NOS1AP may contribute to altering the sub-cellular localisation of NOS1 (at least under conditions of stress) [112], I also examined the sub-cellular distribution of NOS1AP and its possible co-localisation with NOS1.

Overall, the work presented in this chapter focusses on investigating the hypothesis that there is an altered left ventricular electrical and structural substrate accompanying cardiac *NOS1AP* overexpression in the transgenic mouse model that explains the altered ECG parameters and ventricular arrhythmogenesis seen.

4.2 Chapter specific methods

4.2.1 Total collagen assay

The total collagen assay (QuickZyme Biosciences) was used as per manufacturer's instructions for quantitative measurement of hydroxyproline as an indicator of total collagen content. Briefly, 15 – 30 mg of left ventricular tissue were weighed for each sample of interest and added to 6M HCl in a ratio of 1mg tissue: 10µl HCl and incubated at 95°C for 20 hours. After cooling and centrifugation, the supernatant was diluted, a detection agent added and the absorbance at 570 nm measured. Comparisons for each sample were made with a standard set of known collagen concentrations and the total collagen in µg per weight of tissue (in mg) was calculated.

4.2.2 Ventricular monophasic action potential measurements

Measurements

Hearts were excised from mice aged 16 – 20 weeks and perfused on a Langendorff system as detailed in **Section 3.3.5**. Atrioventricular (AV) nodal crush was performed, after which endocardial RV pacing was conducted at cycle lengths of 200 ms, 150 ms, 120 ms, 100 ms and 80 ms. At each cycle length, monophasic action potentials (MAPs) were recorded for one minute using epicardial electrodes on springs placed on the left and right ventricular free walls.

Analysis

For blinded analyses, for each mouse, raw data of voltage versus time was exported for each paced cycle length for left ventricular traces (IsoHeart software, Harvard Biosciences). I wrote a custom script in MATLAB (MathWorks) to measure APD. Briefly, the script detects the peaks in voltage throughout the recording and after pacing artefact removal, generates a mean MAP for that cycle length. The quality of peak detection and artefact removal was assessed by manual review of the superimposition of all traces contributing to the averaged MAP on a single plot prior to generation. APDs at 20%, 30%, 50%, 70%, 80% and 90% of total repolarisation were then calculated and exported (**Figure 4.1**).

Figure 4.1 – Action potential duration measurements from monophasic action potential

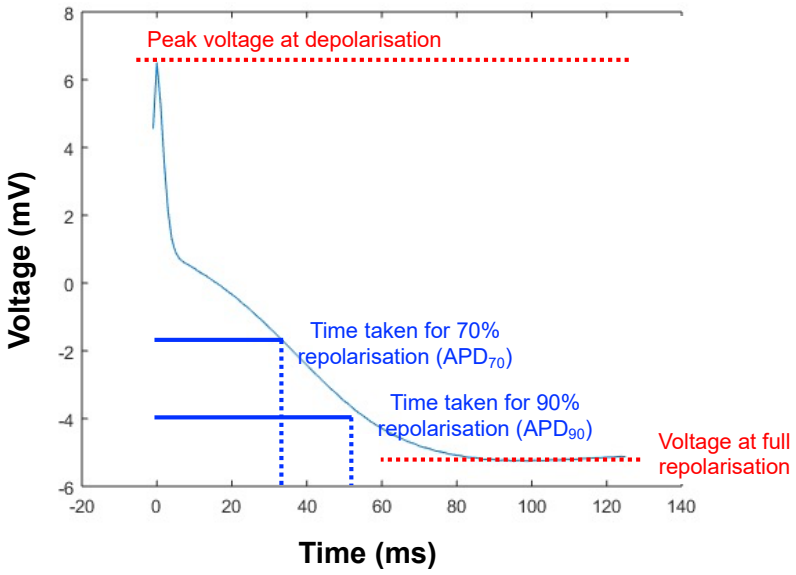


Figure 4.1: Example of averaged monophasic action potential generated by custom MATLAB script (light blue trace). After detection of peak and minimum voltages at full depolarisation and full repolarisation to calculate voltage change during total repolarisation, action potential duration (APD) measurements at varying percentages of total repolarisation were calculated.

4.2.3 Calcium transient measurements

Measurements

Left ventricular myocytes were isolated as described in **Section 2.3**. Myocytes were introduced to calcium (0.5 mmol/L Ca^{2+} in Tyrode) and then loaded with the ratiometric Ca^{2+} sensitive fluorescent dye, Fura-2-AM (5 µmol/L; ThermoFisher Scientific) and 3 µL pluronic to aid cell permeabilisation. Following a 8-10 minute loading period (room temperature in low-light conditions) the solution was then replaced with Tyrode solution containing 500 µmol/L Ca^{2+} to wash out any unloaded dye. This wash out process was repeated twice and then cells were used within 2 hours.

Aliquots of myocytes were transferred to a perfusion-controlled recording chamber maintained at a temperature of 35 °C. Myocytes were perfused with Tyrode solution and visualised using an inverted microscope (Leica Microsystems). Myocytes were electrically field stimulated at a frequency of 3 Hz. Fura-2 fluorescence was excited by light from a Xenon arc lamp, which was

passed through a filter (alternately at 365 nm and 380 nm) and reflected to the cells via an oil-immersion lens. Light collected was restricted to a specific myocyte by using adjustable aperture shutters (IonOptix Corporation). Recordings were continuously displayed by a data acquisition software program (IonWizard). Background fluorescence measurements in the absence of cells were obtained for each experiment and subtracted from the fluorescence signal before analysis.

Analysis

The Fura-2 fluorescence ratio (e.g., the ratio of the photon count detected by excitation at 365 nm compared with that at 380 nm) is proportional to $[Ca^{2+}]_i$. After averaging at least 15 seconds of transients for each cell studied, the amplitude of the $[Ca^{2+}]_i$ transient was calculated by subtracting the baseline (diastolic) $[Ca^{2+}]_i$ from the peak (systolic) $[Ca^{2+}]_i$. The time constant (tau, τ) was calculated by fitting a second order exponential curve to the transient using specialist software (Axon Clampfit version 8.2.0.233).

4.2.4 Conduction velocity measurements using optical mapping

Measurements

After cervical dislocation, murine hearts were rapidly excised from the chest and the aorta cannulated. Using published methods [185], the hearts were then perfused with oxygenated Krebs-Henseleit (K-H) solution (flow rate 10 ml/min; NaCl 120.3 mM, KCl 4 mM, $MgSO_4*7H_20$ 1.3 mM, NaH_2PO_4 1.2 mM, $CaCl_2$ 1.2 mM, $NaHCO_3$ 25.2 mM, glucose 11 mM). Blebbistatin (200 µl of 6 µM) was used to stabilise the heart and prevent motion artifacts during imaging and pluronic (100 µl per 200 ml of K-H solution) was used to aid dye loading. After the heart stopped moving, a thin plastic tube was inserted to the left ventricle via the left atrial appendage and mitral valve to prevent perfusate pressure build-up. RH-237 dye was used for voltage mapping (injected through a gel membrane into the plastic tube above the perfusion cannula; 50 µl of 1 mg/ml over 5 minutes and 20 µl of 5 mg/ml over 1 minute respectively).

The imaging system was based on a previously described design [186], but here two Photometrics Evolve 128 cameras attached to a dual emission image splitter (Cairn Research TwinCam) were used. Light was collected using a 50 mm f0.95 lens (Navitar), and directed to the cameras after

passing through a dichroic mirror with a cut-off of 630 nm. Fluorescence light below 630 nm passed through a 585 ± 20 nm interference filter and the fluorescence light above 630 nm was passed through a 715 nm high pass filter before being imaged by the cameras. Two green LEDs (530 nm Cairn Research OptoLED) were used to illuminate the heart after being passed through bandpass filters (530 ± 20 nm) to minimise stray excitation light reaching the sensors. Custom written software was used to capture images from both cameras and control the stimulator (Model DS2A, Digitimer Ltd.). The software interfaced with a micro-controller (Arduino Uno) to synchronize excitation lights, both cameras and the stimulator to minimise phototoxicity (excitation lights were switched on for 1 s at the end of a stimulation protocol to capture the results from S1 and S2 stimuli). The hearts were suspended in a way that the field of view encompassed the free wall of the left ventricle and epicardial pacing was performed from the left ventricle at 120 ms. After dye loading, the Langendorff apparatus was set to recycle perfused Krebs-Henseleit solution. The effective refractory period (ERP) was determined by a sequence of S2 stimuli at decreasing coupling intervals. Dr Jillian Simon and I performed the experiments and were blinded to genotype, performing the experiments in a randomised manner. An example of the optical mapping setup and data collection is shown in **Figure 4.2**.

Figure 4.2 – Optical mapping setup

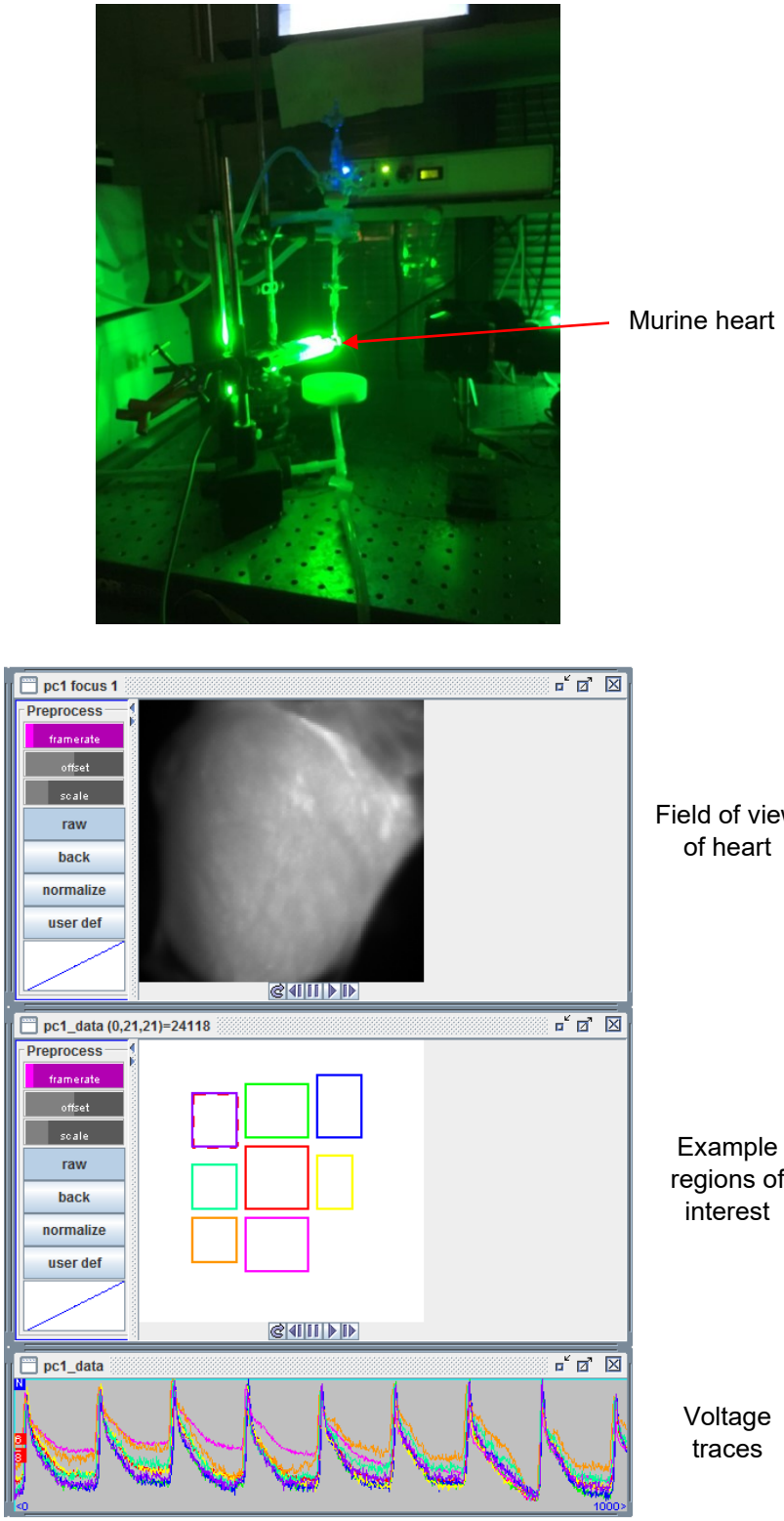


Figure 4.2: Optical mapping setup. **Top panel** shows retrograde perfusion and murine heart (arrowed) hung up with pacing electrodes and green light illuminating field of view. **Bottom panel** shows the camera field of view of the same murine heart with multiple regions of interest drawn within and voltage waveforms being recorded, with colours of the waveforms corresponding to the regions of interest.

Analysis

Raw data were analysed by Dr Jakub Tomek in an entirely blinded fashion using custom-written software for optical mapping analysis known as COSMAS [187]. Briefly, firstly, the software identifies peaks in the voltage signal recording and then applies a standardised clock to these peaks to allow an absolute time reference for any signal. Subsequently, every pixel has its voltage trace extracted and is then processed, removing any noise or filtering baseline drift. Signal diastoles (points of least activation) are extracted via a comb algorithm and this then allows individual activations to be extracted. A set point is used to determine local activation and this is converted to global time co-ordinates and synchronised. A summary scheme is shown in **Figure 4.3 A-D**.

Thus, activation maps showing the spread of a wavefront of electrical depolarisation are generated once analysis is completed for all pixels from which conduction velocities are estimated. Global conduction velocity was measured by drawing a line parallel to the wavefront activation from near the pacing site running along the direction of propagation, measuring the difference in activation time at the end versus start, and dividing it by the distance to get the conduction velocity (**Figure 4.3 E**). This was repeated over 10 measurements and the average reported.

Action potential durations were measured at 80% maximal repolarisation. ERP was defined as the longest coupling interval that failed to capture the myocardium. The ventricular excitation wavelength (λ), is the theoretical distance that a depolarisation wave travels during the refractory period and was calculated (λ = conduction velocity × ERP) at a paced cycle length of 120 ms [188]. For arrhythmias with re-entrant mechanisms, an excitation wavelength below a minimum based on chamber size allows for more re-entrant circuits to form and may be a marker of arrhythmogenicity [189,190].

Figure 4.3 – Example analysis of optical mapping data

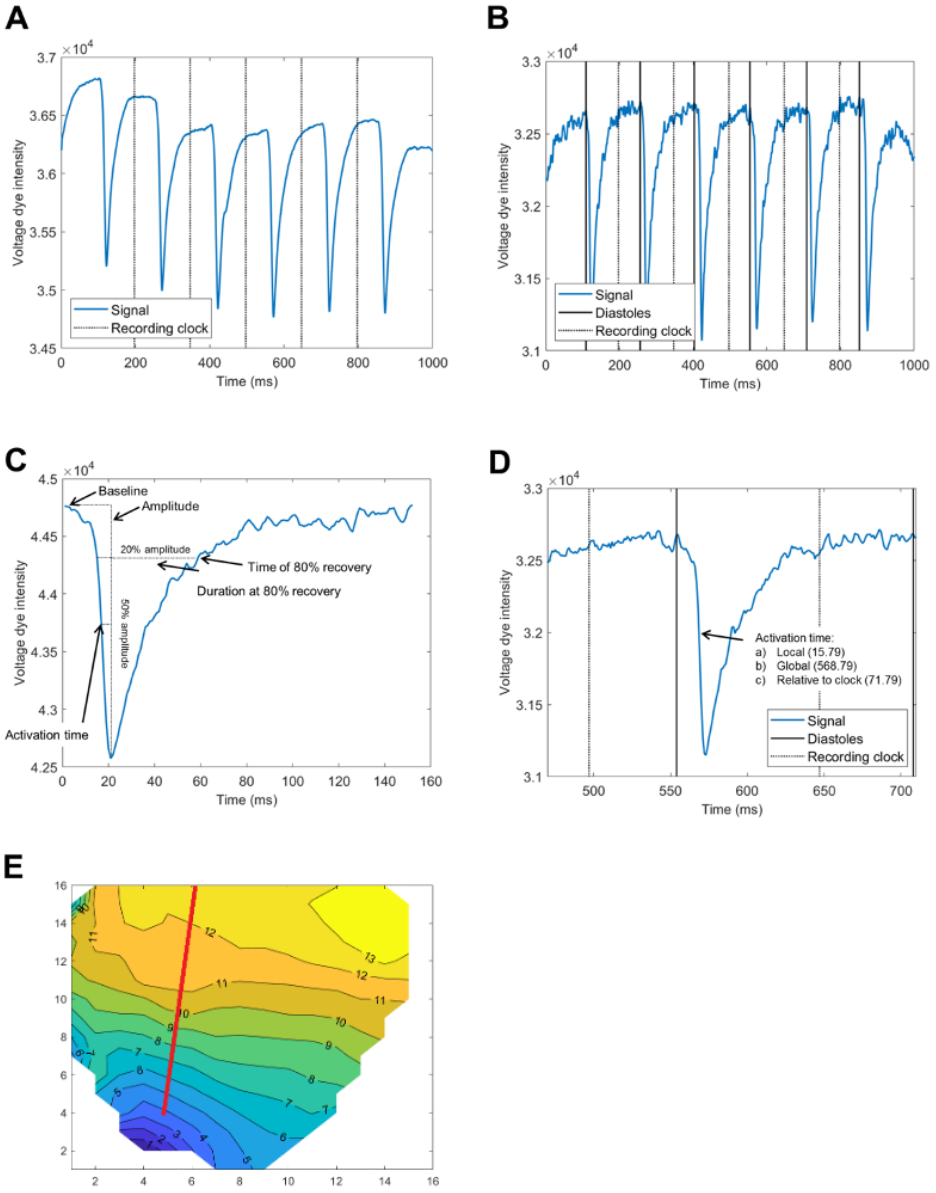


Figure 4.3: Illustration of stimulus segmentation and feature extraction. (**A**) Average trace of a voltage mapping recording at 130 ms basic cycle length (the lower the intensity, the higher the membrane potential), showing the recording clock. (**B**) Single-pixel trace from the recording used in **A**, also showing the points corresponding to the points of smallest activation ("diastoles", solid black lines), as well as the global clock (dotted black lines). (**C**) Illustrations of features extracted from a single action potential. The difference in intensity from baseline to peak activation is defined as the amplitude of the action potential. Activation time is defined as the time from initial baseline to reaching 50% of the maximal amplitude. Action potential duration at 80% recovery is defined as the time taken for the intensity of peak activation to reduce by 80% from maximum (or equivalently at 20% of the maximal amplitude). (**D**) Illustration of how activation times are treated with extraction of the local clock time and synchronization to the global time (within the whole recording) of 568.79 ms. From this, the time of the preceding clock boundary is subtracted, and COSMAS records that the activation came 71.79 ms after the preceding clock. In this way, even though each pixel's trace may have diastoles detected at different times, all pixels are synchronized to the same global clock. (**E**) Isochronal map of epicardial left ventricle conduction velocity with red line representing direction of measurement of conduction velocity. [Figure courtesy of Dr Jakub Tomek]

4.2.5 Assessment of gene expression

Gene expression was assessed using quantitative real-time PCR using TaqMan gene expression probes as described in **Section 2.1**. The specific probes used were Mm01208059_m1 for murine *Nos1* and Mm02342430_g1 for murine *Ppia* (all probes from ThermoFisher Scientific).

For quantification of transgenic gene expression relative to wild-type, the mean △Ct for wild-type was subtracted from the mean △Ct for a corresponding transgenic sample and relative gene expression of transgenic genes to wild-type expressed as $2^{-\triangle\triangle Ct}$.

4.2.6 Assessment of protein expression

Protein expression was assessed using Western blotting as described in **Section 2.2**. Specifically, protein homogenates from tissues were separated on 3-8% Tris-Acetate for NOS1 blots or 10% Bis-Tris NuPage gels for connexin blots (ThermoFisher Scientific) and separated using gel electrophoresis at 180 V for ~90 minutes at room temperature. Samples were then transferred onto nitrocellulose membranes in transfer buffer with 15% methanol for NOS1 blots or 10% methanol for connexin blots at 250 mA for 120 min at 4°C. After cutting membranes at appropriate molecular weights, blocking of non-specific binding was performed using 5% bovine serum albumin for NOS1 blots or 5% skimmed milk for connexin blots in phosphate buffered saline with 0.1% Tween-20 (ThermoFisher Scientific). This was followed by incubation with the primary antibodies (mouse monoclonal anti-NOS1 A-11 sc-5302, Santa Cruz Biotechnology, at 1:1000 dilution; rabbit polyclonal anti-connexin 43 C6219, Merck, at 1:1000 dilution and rabbit polyclonal anti-GAPDH PA1-987, ThermoFisher Scientific, at 1:50000) overnight at 4°C. After washing, appropriate species-specific secondary antibodies at 1:25000 for anti-mouse and 1:50000 for anti-rabbit were added for one hour and then washed off. Membranes were developed using Prime for NOS1 blots or Dura extended duration substrate for connexin blots (ThermoFisher Scientific) and band intensities quantified.

4.2.7 NOS activity assay

Measurements

Left ventricular NOS activity was assessed indirectly by measuring conversion of [^{14}C] radiolabeled L-arginine to citrulline using high-performance liquid chromatography (HPLC) in the presence of an arginase inhibitor *N*ω-hydroxy-nor-arginine (nor-NOHA). Measurements were performed on homogenates from each sample, with and without the NOS inhibitor L-NAME, and results expressed as the L-NAME inhibitable fraction of citrulline detected.

More specifically, murine left ventricles were homogenized using pre-cooled metal beads in 400 µl Krebs-HEPES buffer with 5 µM nor-NOHA and 1µM Dithioerythritol (DTE) and protease inhibitor. After centrifugation, the supernatant's protein concentration was determined using a BCA assay. A basal sample, and one with L-NAME were individually prepared by the addition of 1 mg of sample protein in 200 µl of Krebs-HEPES buffer to each tube along with co-factors flavin adenine dinucleotide (FAD; 10 µM), flavin mononucleotide (FMN; 10 µM), nicotinamide adenine dinucleotide phosphate (NADPH; 1 mM) and tetrahydrobiopterin (BH_4; 10 µM), with or without 1 mM L-NAME.

With Dr Ricardo Carnicer's assistance, 1.5 µl of [^{14}C] L-arginine (1.85 MBq/ml, Amersham Biosciences UK Ltd.) was added into every reaction tube. Tubes were then incubated for 4 hours at 37°C. After the incubation, the proteins were precipitated by adding 60 µl of 10% trichloroacetic acid (TCA) and samples centrifuged. The supernatant was transferred to HPLC vials with 100 µl of 10% TCA and 450 µl of H_2O. The vials were placed in an autosampler rack and 700 µl of the solution was injected into the HPLC column. The HPLC separation of the arginine metabolism products was obtained by ion-exchange chromatography using a Supelcosil LC-SCX column (Sigma). Separated products were detected using a continuous flow liquid scintillation detector (Lablogic β- RAM Model 3).

Analysis

Various peaks of separation products were identified and the area under the curve (AUC) for these calculated using the specialist software Laura (v 6, LabLogic; **Figure 4.4**). The difference between

the AUC of citrulline with or without L-NAME was taken as the NOS-inhibitable fraction and a measure of NOS activity.

Figure 4.4 – Example traces from NOS activity assay

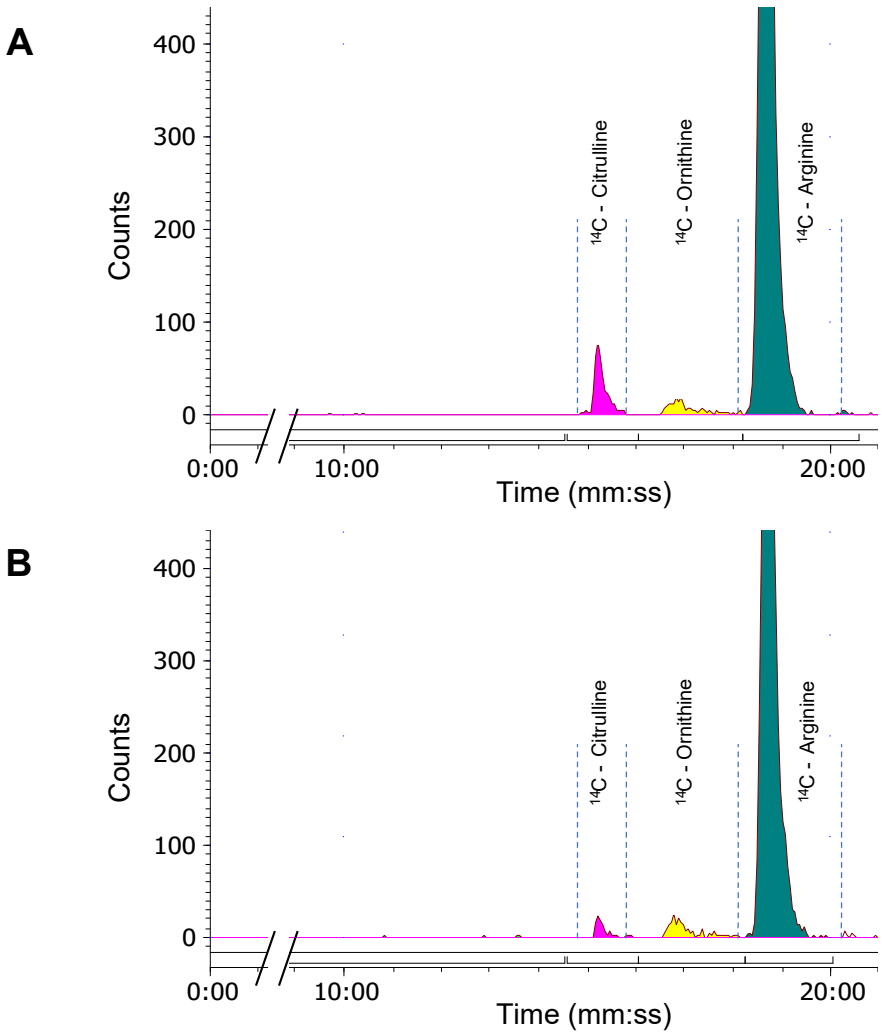


Figure 4.4: Representative example high performance liquid chromatography (HPLC) traces to assess conversion of radiolabeled arginine to citrulline in the absence (**A**) or presence (**B**) of the NOS inhibitor, L-NAME. The difference in the area under the curve for the ^{14}C – Citrulline trace is taken to be the L-NAME-inhibitable fraction and used as a measure of NOS activity.

4.2.8 Immunofluorescence

General Methods

Left ventricular myocytes were isolated as described in **Section 2.3**. After isolation, cells were plated on laminin coated coverslips and left to adhere for 3 hours before fixing and staining. This was to help increase the health of the cells as cytospinning can sometimes damage the cells and

reduce staining quality. Cells were fixed for 7 minutes at 4°C using a 1:1 acetone: methanol solution or 15 minutes using 4% paraformeldahyde. For the later fixation method, samples were subsequently permeabilised for 4 mins using 0.5% Triton in phosphate buffered saline (PBS). After rinsing in PBS, non-specific binding was blocked for 1 hour at room temperature. Antibodies to the protein of interest, made up in the same blocking solution, were added and incubated overnight at 4°C. After further washing with PBS, secondary antibodies were made up and incubated with the slides for 3 hours. Full details are described in **Table 4.1**. After further washing, the cells were mounted with mounting media. Images were obtained using a Leica TCS SP5 confocal scanning microscope (Leica Microsystems Wetzlar) with the aid of Dr Jillian Simon.

Table 4.1 – Conditions for immunofluorescence staining

Protein of interest	Fixation	Blocking solution	Primary Antibody	Secondary Antibody
NOS1	Acetone Methanol	5% donkey serum with 0.1% Triton	Rabbit polyclonal anti-NOS1 (PA3-032A, ThermoFisher) 1:100	AF488-conjugated anti-Rabbit (ThermoFisher) 1:500
NOS1AP	Acetone Methanol	5% donkey serum with 0.1% Triton	Mouse monoclonal anti-NOS1AP (C-9 sc-374504, Santa Cruz Biotechnology) 1:100	AF568-conjugated anti-Mouse (ThermoFisher) 1:500
Connexin-43	4% PFA	5% BSA with 0.1% Triton	Mouse monoclonal anti-Cx43 (Invitrogen Clone 3B9, #33-3900) 1:500	AF594-conjugated anti-Rabbit (ThermoFisher) 1:500
N-Cadherin	4% PFA	5% BSA with 0.1% Triton	Rabbit monoclonal anti- N-Cadherin (Sigma C6219) 1:300	AF488-conjugated anti-Mouse (ThermoFisher) 1:500

Table 4.1: Details of conditions for staining.

Connexin-43 quantification

This was performed by Dr Tomek in a blinded manner using Image J software (v1.51, NIH). Simple thresholding was used to segment intercalated discs in images of N-cadherin staining and to segment gap junctions in images of Cx43 staining. Morphological dilation (with a diamond-shaped structural element of radius 1) was subsequently applied to the obtained segmentation masks to

improve coverage of intercalated discs and gap junctions. The resulting segmentation masks (and their overlay) allowed quantification of total amount of pixels belonging to N-cadherin or Cx43 staining, as well as computation of indices of their co-localisation (e.g. the fraction of Cx43 present at N-cadherin pixels).

4.2.9 Single-cell I_{Na} current measurements

These experiments were performed by Dr Xing Liu in a blinded manner. The methods used are reproduced below for completeness but have important limitations which are discussed further in **Section 4.3.7** of the results.

Left ventricular myocytes were isolated as described in **Section 2.3**. Whole cell voltage-clamp recordings were carried out at physiological temperature 35-37°C using an Axopatch 200B amplifier and a Digidata 1440A data-acquisition system (Axon Instruments). The electrode resistance ranged from 2-5 MΩ. After rupture of the membrane, cell capacitance (Cm) was measured. Series resistance and cell membrane capacitance were compensated for 80%. To measure I_{Na}, depolarising pulses were evoked by 5 mV increment steps in the range of –130 to +30 mV with a cycle length of 5 s for 500 ms from a holding potential of –120 mV. I_{Na} *density* was measured as steady-state current subtracted from peak outward current at the beginning of the depolarising step and normalised to the cell capacitance. Steady-state currents were measured at the end of the depolarising steps. Voltage dependence of activation and inactivation curves were fitted with Boltzmann function $\left(y = \left[1 + e^{\frac{V - V_{1/2}}{k}}\right]^{-1}\right)$, where $V1/2$ is the half -maximal voltage of (in)activation and k, the slope factor. I_{Na} inactivation was obtained by measuring the decay of sodium current under a maintained depolarisation with peak sodium current plotted as a function of pre-pulse potential. Current amplitudes for activation and inactivation curves were normalized to the maximum current. The potentials at which 50% inactivation occurs were denoted EC50.

The pipette solution contained (in mmol/L): 3.0 NaCl, 133.0 CsCl, 2.0 $MgCl_2$, 2.0 Na_2ATP, 2.0 TEACl, 10.0 EGTA, 5.0 HEPES; pH 7.2 (CsOH). The bath solution contained (in mmol/L): 7.0 NaCl, 133.0 CsCl, 1.4 $CaCl_2$, 1.2 $MgCl_2$, 11.0 glucose, 5.0 HEPES. 0.05 $CdCl_2$; pH 7.4 (CsOH). Where

appropriate, myocytes were incubated with SMTC for at least one hour prior to experiments and SMTC was also in the patch pipette.

4.2.10 Statistical methods

Sample size calculations

Sample sizes for experiments were based on power calculations, determined using GPower 3.1 (Universitat Dusseldorf, Germany) using a power of 90% and 5% significance level ($\alpha = 0.05$). For the experiment measuring action potential duration, a 15% difference in APD_{90} between genotypes at a paced cycle length of 120 ms was chosen as the main outcome, reflecting the ~15% shorter QT interval on surface ECG at a mean heart rate of ~500 bpm (**Figure 3.11**). A minimum sample size of 11 per group was needed to detect a 15% difference in the main outcome between groups with wild-type epicardial APD_{90} estimated at 50 ms with a standard deviation of 5 ms based on published data [191].

For the experiment measuring conduction velocity, a minimum sample size of 8 per group was needed to detect a 20% difference in conduction velocity between genotypes as the main outcome, with wild-type optical mapping-measured conduction velocity estimated at 45 cm/s with a standard deviation of 5 cm/s based on published data [149,192,193].

For sodium current experiments, a minimum sample size of 32 cells per group was needed to detect a 15% difference in the main outcome of peak sodium current at -35 mV, using pilot data to estimate $I_{Na,P}$ at -30 pA/pF with a standard deviation of 7 pA/pF.

For the experiment measuring NOS activity, a minimum sample size of 23 per group was needed to detect a 20% difference between genotypes as the main outcome, with the wild-type ventricular L-NAME inhibitable fraction of citrulline estimated at 1% with a standard deviation of 0.2% based on pilot and published data [126].

Statistical testing

Data were analysed using GraphPad Prism 7 (GraphPad Software Inc.). Normality of data was assessed using the D'Agostino Pearson test. Comparisons between two groups were performed by

two-tailed unpaired *t*-tests for normally distributed data with Welch's correction for unequal variance between groups as needed, or Mann-Whitney tests for non-normally distributed data. Two-way analysis of variation (ANOVA) was used to comparing genotype effects across different APDs and paced cycle lengths and for investigating genotype effects on sodium current parameters with NOS inhibition or to investigate sex differences in outcomes across genotypes.

The effects of genotype on calcium transient measurements were analysed using hierarchical cluster modeling as previously published [194]. Briefly, this method allows for cellular replicates from independent hearts to be accounted for appropriately without either considering all cells as independent datapoints and artificially reducing the variance, or having to consider a mean for each heart and significantly reducing the power to detect differences.

Normally distributed data are expressed as mean and standard deviation with non-normally distributed data expressed as median and interquartile range. Measurements of APD, conduction velocity, sodium current and Cx43 quantification were performed and analysed in a blinded fashion with respect to genotype, with unblinding only occurring after the analysis dataset had been completed.

4.3 Results

4.3.1 Differences in left ventricular collagen content do not explain arrhythmogenic phenotype

As reported in **Figure 3.11**, transgenic mice had significantly prolonged ECG parameters representing both atrial and ventricular depolarisation (P-wave duration and QRS interval) compared with wild-type. Significant cardiac fibrosis may reduce the speed of depolarisation by disrupting normal cardiomyocyte electrical coupling [195]. This could therefore lead to prolonged P-wave and QRS durations as well as being associated with increased arrhythmogenicity, independent of any other changes.

To investigate this, I measured total collagen content in left ventricular homogenates from 8 wild-type (5 male and 3 female) and 8 transgenic mice (4 male and 4 female) aged 16 – 20 weeks old. I found no differences in total collagen content between wild-type mice and their transgenic littermates (mean 2.9 ± 0.5 µg/mg vs 2.5 ± 1.2 µg/mg, *P*=0.44; **Figure 4.5**) suggesting that ventricular collagen deposition as a marker of fibrosis was not a significant feature of the phenotype explaining differences in the electrical substrate.

Figure 4.5 – Left ventricular collagen content for Tg(*Myh6-hNOS1AP*) colony

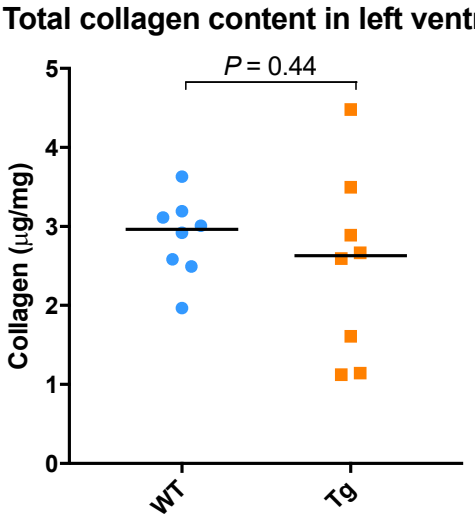


Figure 4.5: Total collagen content in the left ventricles of wild-type (WT, n=8) mice and their transgenic (Tg, n=8) littermates. Horizontal lines represent mean values; unpaired *t*-test for comparisons.

4.3.2 Left ventricular monophasic action potential durations are shorter in transgenic mice at slower, but not physiological heart rates

With the limitations of measuring and interpreting a shorter surface ECG QT interval in transgenic mice, I wanted to assess whether this was associated with changes in cardiac repolarisation as reflected by changes in APD. I used *ex-vivo* methods to measure epicardial left ventricular monophasic action potential (MAP) durations in intact hearts across a variety of pacing cycle lengths in 19 wild-type mice (6 males and 13 females) and 23 transgenic mice (8 males and 15 females) aged 16 – 20 weeks old. The main outcome of APD_{90} at 120 ms pacing cycle length (similar to intrinsic heart rates during QT measurement) was not significantly different between transgenic and wild-type littermates (mean 36 ± 7 ms vs 39 ± 8 ms, $P = 0.30$). Further, univariate testing suggested a shorter APD_{90} in transgenic mice at longer pacing cycle lengths (**Table 4.2**).

Table 4.2 – Left ventricular action potential durations at 90% repolarisation (APD_{90})

Cycle length (ms)	Wild-type APD_{90}	Transgenic APD_{90}	Unadjusted *P* for difference*	Bonferroni adjusted *P* for difference†	Sidak adjusted *P* for difference**
80	27 ± 6	27 ± 6	0.90	0.99	0.99
100	34 ± 8	33 ± 6	0.48	0.99	0.96
120	39 ± 8	36 ± 7	0.30	0.99	0.84
150	48 ± 8	43 ± 7	0.04	0.12	0.12
200	54 ± 10	49 ± 7	0.09	0.20	0.19

Table 4.2: *Ex-vivo* measured left ventricular epicardial action potential durations at 90% total repolarisation (APD_{90}) across different paced cycle lengths for wild-type (n=19) and transgenic (n=23) littermates with mean ± standard deviation reported. *Unadjusted *P* values calculated using *t*-test for comparison. †Adjusted *P* values calculated using two-way analysis of variance (ANOVA) and Bonferroni correction for multiple testing. **Adjusted *P* values calculated using ANOVA and Sidak's correction for multiple testing.

To test for genotype differences across cycle lengths, two-way ANOVAs were conducted for each APD at different percentages of repolarisation, examining the effect of genotype and cycle length on APD. Genotype was significant for $APD_{50\text{-}90}$ (**Figure 4.6**) with no effect seen at shorter APD percentages. As expected, shortening cycle lengths was significantly associated with shorter APDs at 50% to 90% of repolarisation ($P = 0.02$ for APD_{50} and $P < 1 \times 10^{-4}$ for $APD_{70\text{-}90}$) in both genotypes. Across all APD measurements, there was no significant interaction between genotype and cycle length on APD (**Figure 4.6**). Post-hoc comparisons for genotype at different cycle

lengths for any APD percentage were not statistically significant after adjustment for multiple testing.

Figure 4.6 – Left ventricular monophasic action potential duration (APD) comparisons

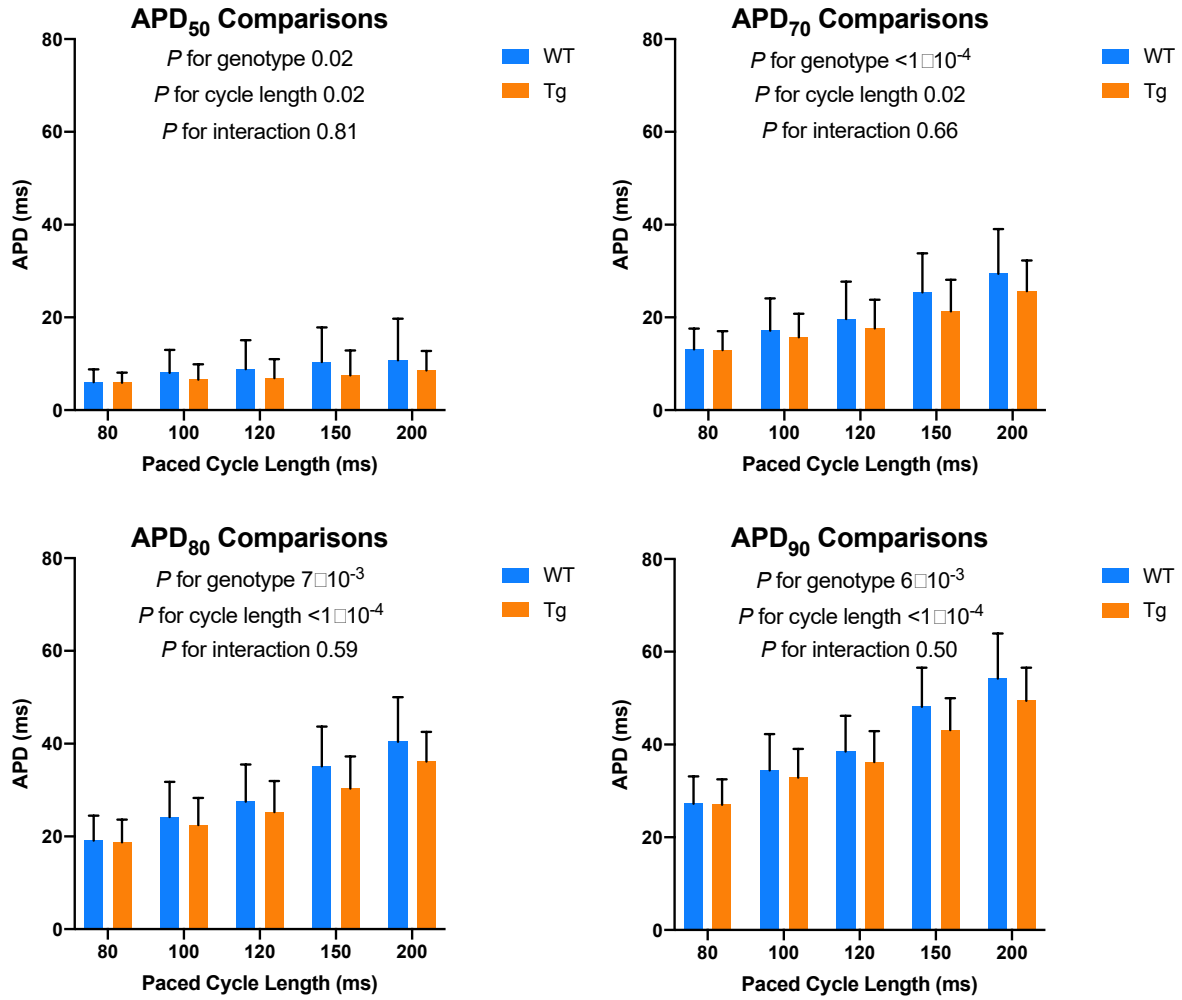


Figure 4.6: Left ventricular epicardial e*x-vivo* monophasic action potential durations (APDs) measured at 50, 70, 80 and 90% of total repolarisation in wild-type mice (WT; n=19) and transgenic littermates (Tg; n=23) at a variety of cycle lengths with bars representing mean values and error bars representing standard deviation. Differences between genotypes were compared using a two-way ANOVA for each APD percentage with terms for genotype and cycle length and *P* values adjusted using Sidak's correction for multiple testing. Post-hoc, after correction for multiple testing, no statistically significant differences were observed between genotypes at each cycle length for any APD percentage.

Typically, as cycle length shortens, the APD at later percentages of repolarisation does so as well (hence the need for heart rate correction of the QT interval). Across our range of paced cycle lengths, this relationship (also known as APD restitution) is shown in **Figure 4.7**.

Figure 4.7 – Left ventricular *ex-vivo* monophasic action potential durations

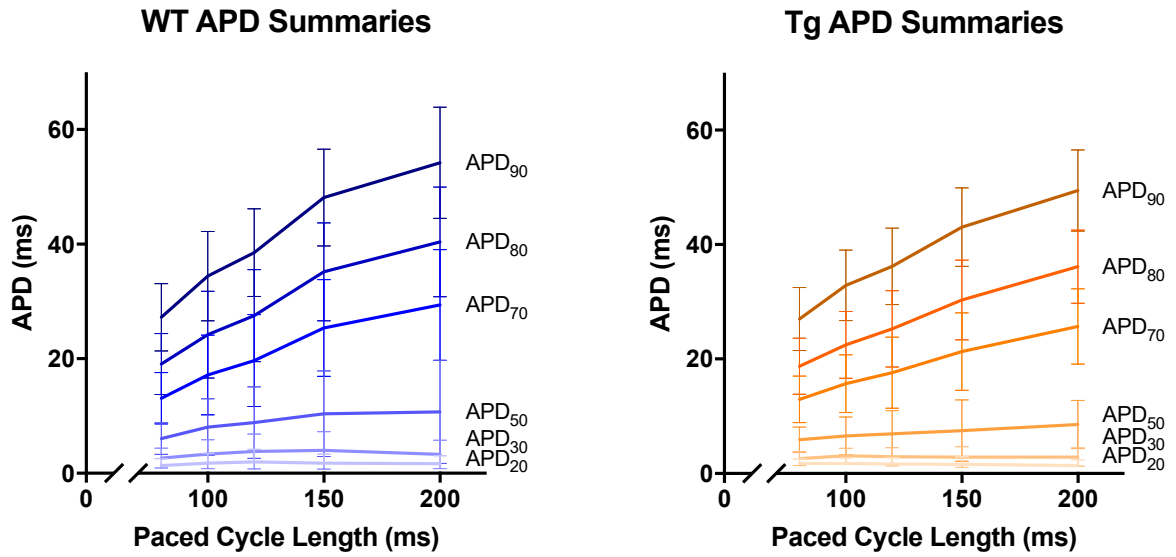


Figure 4.7: Action potential durations (APDs) measured in wild-type mice (WT; n=19) and transgenic littermates (Tg; n=23) at a variety of percentages of total repolarisation and steady state paced cycle lengths. Lines represent mean values with error bars representing standard deviation.

By treating the paced cycle length as a continuous variable and performing linear regression across the later range of APDs where we would expect to see restitution differences ($APD_{70\text{-}90}$), I was able to calculate the slope coefficient (effectively, the rate of change of APD per unit cycle length) for each genotype (**Table 4.3**). Comparing slope coefficients between genotypes revealed no significant differences, although a trend towards a flatter slope in NOSIAP-Tg (i.e. less change in APD for heart rate). Fitting a non-linear exponential curve did not improve the goodness of fit (R^2 = 0.59 for both wild-type and transgenic data) over a linear model (R^2 = 0.58 for both wild-type and transgenic data).

Table 4.3 – Slope coefficients for cycle length vs action potential duration

$APD_{\%}$ of repolarisation	Wild-type slope coefficient	Goodness of fit (R^2)	Transgenic slope coefficient	Goodness of fit (R^2)	*P* for difference
APD_{70}	0.14 (0.10 – 0.17)	0.36	0.11 (0.08 – 0.13)	0.37	0.17
APD_{80}	0.18 (0.14 – 0.22)	0.48	0.14 (0.12 – 0.17)	0.48	0.15
APD_{90}	0.22 (0.19 – 0.26)	0.58	0.18 (0.15 – 0.21)	0.58	0.10

Table 4.3: Slope coefficients from wild-type (n=19) and transgenic (n=23) mice for change in action potential duration (APD) at varying cycle lengths using linear regression. Mean and 95% confidence intervals reported as well as goodness of fit (R^2). *P* for difference represents differences in slope coefficients between genotypes calculated from linear regression.

With female mice having shorter QT intervals on surface ECG (**Figure 3.12**), I investigated if there was a genotype interaction with sex for the main outcome of APD_{90} across the paced cycle lengths. Using two-way ANOVA, sex was not significant across any of the cycle lengths, but as seen in **Figure 4.8**, at a paced cycle length of 200 ms there was a borderline statistically significant interaction between genotype and sex ($P = 0.05$) with post-hoc analysis showing a longer APD_{90} in the 6 wild-type males (mean 61 ± 8 ms) versus the 8 transgenic males (mean 48 ± 10 ms, $P = 0.04$). No other interactions or significant findings at other paced cycle lengths were found.

Overall, these data suggest that left ventricular epicardial APD_{90} may be shorter in male transgenic mice compared with wild-type, but only at *ex-vivo* paced cycle lengths corresponding to heart rates slower than 300 bpm. There were no other sex differences detected. This suggests that the *in-vivo* shorter QT interval in transgenic mice detected on surface ECG at intrinsic heart rates of 500 bpm may involve mechanisms beyond changes in local repolarisation. It also suggests that that differences in rate-related repolarisation are unlikely to fully explain the pro-arrhythmic phenotype induced by rapid burst pacing.

Figure 4.8 – Left ventricular APD_{90} values by sex

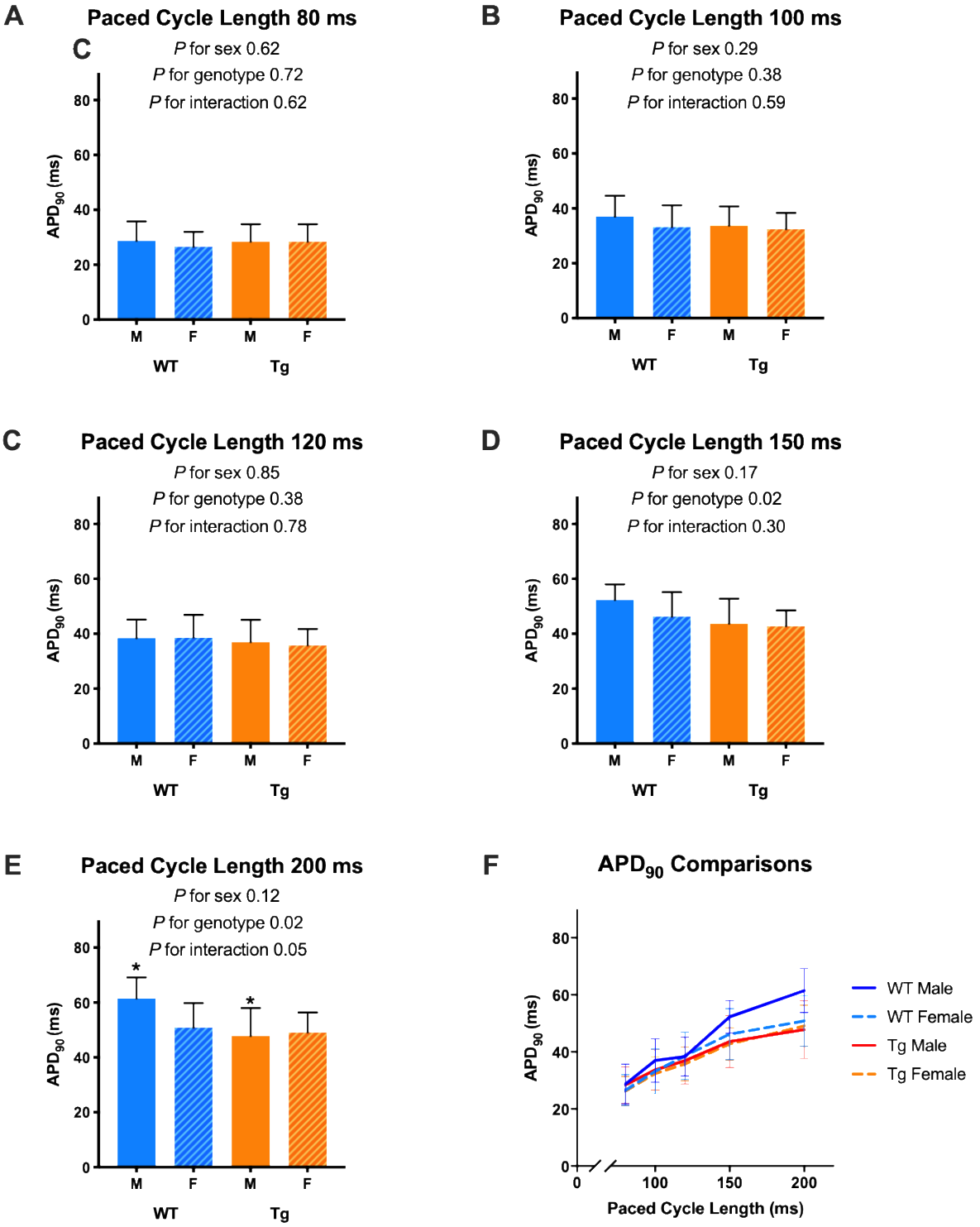


Figure 4.8: (**A**) to (**E**): Left ventricular epicardial action potential durations at 90% repolarisation (APD_{90}) at varying paced cycle lengths in 6 wild-type (WT) males and 13 WT females as well as 8 transgenic (Tg) males and 15 Tg females. *P* for interaction using two-way analysis of variance with terms for genotype and sex. **P*-value of 0.04 (WT male vs Tg male) for post-hoc differences for APD_{90} at 200 ms cycle length using Tukey's adjustment for multiple comparisons. (**F**): Graphical representation of panels **A** to **E** on a single plot.

4.3.3 Calcium handling in ventricular cardiomyocytes is not affected by myocardial overexpression of *NOS1AP*

I investigated whether alterations in myocyte calcium handling may contribute to the propensity to arrhythmias in NOSIAP overexpressing mice. I measured left ventricular myocyte calcium transients $[Ca^{2+}]_i$ in 5 wild-type (114 cells total; 37 cells from 2 males and 77 cells from 3 females) and 8 transgenic mice (174 cells total; 111 cells from 5 males and 63 cells from 3 females) aged 16-20 weeks old. I found no differences in diastolic calcium, transient amplitude or transient decay time constant (tau) as shown in **Figure 4.9** and **Table 4.4**. This suggests that major genotype differences in calcium handling were unlikely to contribute to the phenotypic differences seen between transgenic and wild-type mice.

Figure 4.9 – Example calcium transient traces

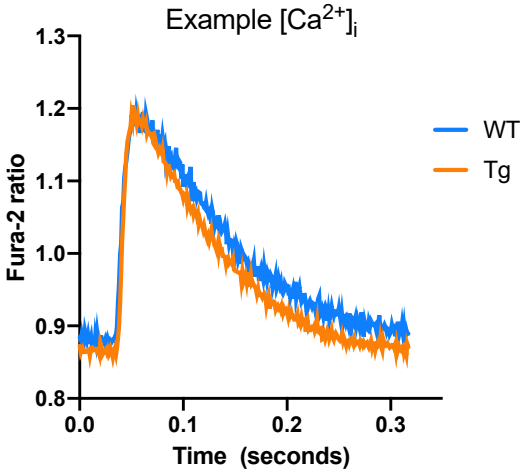


Figure 4.9: Averaged tracings from single cells showing Fura-2-ratio versus time for wild-type (WT; blue) and transgenic (Tg; orange) left ventricular myocytes.

Table 4.4 – Calcium transient parameters in Tg(*Myh6-hNOS1AP*) colony

Parameter	Wild-type	Transgenic	*P* for difference
Number	114 cells from 5 mice	174 cells from 8 mice	
Diastolic Ca^{2+}	0.86 ± 0.04	0.85 ± 0.03	0.83
Transient amplitude	0.24 ± 0.04	0.20 ± 0.03	0.32
Tau (ms)	103 ± 9	105 ± 7	0.87

Table 4.4: Mean ± standard deviation of parameters reflecting calcium handling in wild-type and transgenic mice. *P* for difference calculated using hierarchical clustering as described in statistical methods and elsewhere [194].

4.3.4 Transgenic mice have slower left ventricular epicardial conduction as measured by optical mapping

Noting the prolongation of ECG parameters representing atrial and ventricular depolarisation (P-wave and QRS duration) in transgenic mice, I hypothesised that there may be differences in conduction velocity between genotypes. Further, changes in ventricular conduction velocity increasing the heterogeneity of ventricular depolarisation would also increase the spatiotemporal heterogeneity of subsequent repolarisation, a key factor in ventricular arrhythmogenicity [196,197]. This heterogeneity of either de- or subsequent repolarisation may also be reflected by changes in the QT interval on the surface ECG, similar to the 'depolarisation' and 'repolarisation' models proposed to explain the altered ECG changes seen in Brugada syndrome [175,179,180].

I assessed left ventricular epicardial conduction velocity using high-resolution optical mapping techniques in an *ex-vivo* setting with a pacing rate of 120 ms, again, similar to the intrinsic heart rate at which the surface ECG parameters were measured. In 7 wild-type hearts (from 6 males and 1 female) and 10 transgenic hearts (from 7 males and 3 females, aged 16 – 20 weeks old), transgenic hearts had significantly slower left ventricular epicardial conduction velocity compared with their wild-type littermates (mean 64 ± 4 cm/s versus 91 ± 21 cm/s, $P = 0.01$; **Figure 4.10 A-C**). Notably, the transgenic hearts also had a significantly smaller variance.

The experiments were powered to detect differences in mean conduction velocity but not in other end-points. Within the same experiments and with that in mind, we did not find any significant differences between genotypes in APD_{80} measurements at 120 ms paced cycle length (41 ± 9 ms for Tg versus mean 47 ± 10 ms for WT, $P = 0.27$; **Figure 4.10 D**) nor in measured effective refractory periods (34 ± 6 ms for Tg versus mean 44 ± 17 ms for WT, $P = 0.15$ for difference; **Figure 4.10 E**) even though, as observed previously, APD tended to be shorter in transgenic mice. However, we did find a significant difference in the ventricular excitation wavelength λ, with transgenic mice having a shorter λ (2.1 ± 0.4 cm versus 3.9 ± 1.4 cm, $P = 0.02$; **Figure 4.10 F**) compared with WT, supporting a more susceptible substrate to re-entrant arrhythmias.

Figure 4.10 – Data from left ventricular optical mapping experiments

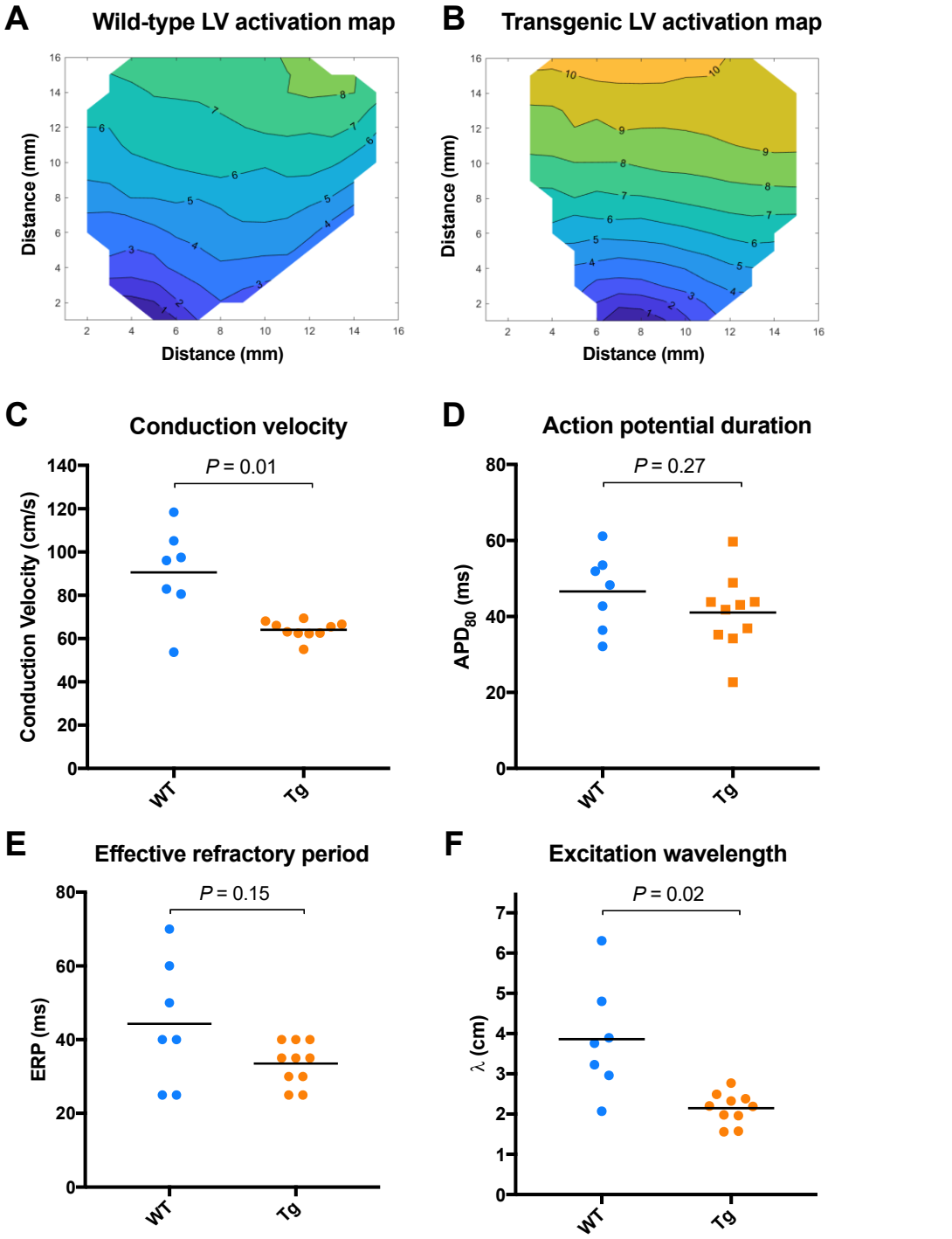


Figure 4.10: Representative isochronal maps showing optical mapping measured conduction velocity (cm/s) in (**A**) wild-type (WT) and (**B**) transgenic (Tg) left ventricles [courtesy Dr Jakub Tomek]. (**C**) Conduction velocity and (**D**) action potential duration at 80% repolarisation (APD_{80}) at 120 ms pacing cycle length measured in WT mice (n=7) and Tg littermates (n=10). (**E**) Effective refractory period (ERP) and (**F**) excitation wavelength (λ) measurements in the same groups. Horizontal lines represent mean values. Comparisons between groups for conduction velocity made using unpaired *t*-test with Welch's correction for unequal variances ($P = 0.01$ if Mann-Whitney test used). Comparisons between groups for APD_{80} made using unpaired *t*-test. Comparisons between groups for ERP and λ made using unpaired *t*-test with Welch's correction for unequal variances ($P = 0.18$ for ERP and $P = 0.003$ for λ if Mann-Whitney test used).

Determinants of conduction velocity between cardiac myocytes have classically been thought of in the form of the cable equation, modelling a current flowing along a linear cell structure from one depolarising myocyte to the next, connected by gap junctions [198]. This theory identifies the rate of depolarisation, governed by the fast inward depolarising sodium current (I_{Na}) as well as resistance to local current flow between cells (affected by gap junction function or due to fibrosis) as key determinants of conduction velocity [198]. I thus sought to see whether factors affecting these parameters might be altered as a consequence of *NOSIAP* overexpression.

4.3.5 Myocardial overexpression of *NOS1AP* is associated with a reduction in connexin-43

Without markers of myocardial fibrosis explaining the slower conduction velocity seen in transgenic mice, I next sought to investigate whether *NOSIAP* overexpression may affect electrical conduction through gap junctions. Inter-cellular gap junctions are comprised of two hemichannels (one on each cell) with each hemichannel being formed of six connexin molecules [199]. For electrical conduction in the myocardium, gap junctions act as gated ion channels, localised predominantly to the intercalated disc at the end of each myocyte, with the major constituent of ventricular inter-cellular gap junctions being connexin-43 (Cx43) [199].

I investigated if there were differences in left ventricular gene expression, protein expression, or localisation of Cx43 between wild-type and transgenic animals.

Gene expression

Connexin-43 has rapid turnover in cardiac tissues, with some studies showing a half-life in the heart of ~1.5 hours [200]. Accordingly, I investigated if gene expression levels were altered in the transgenic animals that may reflect changes in downstream protein. As expected, expression of *Gja1* (gap junction alpha-1; the gene encoding connexin-43) mRNA was higher in cardiac tissues (**Figure 4.11**) than in skeletal muscle or brain homogenates. Interestingly, left ventricular *Gja1* expression was higher in transgenic versus wild-type mice (*P* for difference 0.04; **Figure 4.11**), with a similar pattern for right ventricular tissue which did not reach statistical significance (*P* for difference 0.12) but no significant differences noted for atrial tissue (*P* for difference 0.93).

Figure 4.11 – Gene expression profile of *Gja1* in Tg(*Myh6-hNOS1AP*) colony

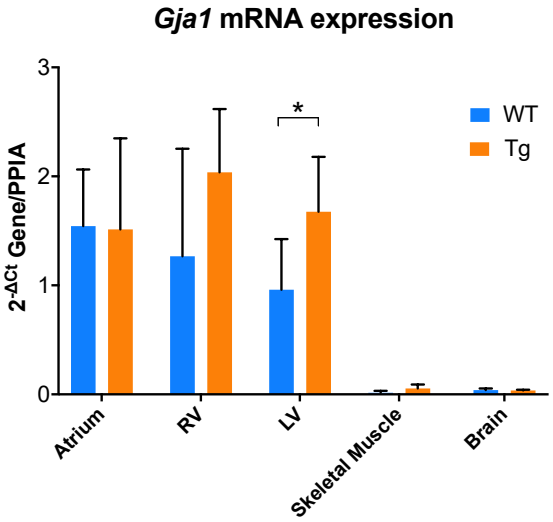


Figure 4.11: *Gja1* gene expression (mean and standard deviation) in wild-type (WT; n=8) and transgenic (Tg; n=6) mice as measured by RT-QPCR. For the left ventricle (LV), there was an increase in *Gja1* mRNA expression in the Tg mice versus WT littermates (*P*=0.04) with no other significant differences noted (unpaired *t*-tests).

Protein expression

As seen in **Figure 4.12**, transgenic mice appeared to have lower levels of total connexin-43 protein in left ventricular homogenates. Connexin-43 can be phosphorylated and this increases the apparent molecular weight of the protein. Although the phosphorylated/non-phosphorylated bands were not sufficiently distinct from each other for robust quantification, the transgenic mice consistently appeared to have a lower of amount of the phosphorylated form of Cx43 on western blots. Increased gene expression, but reduced total Cx43 protein may be consistent with faster connexin protein degradation associated with dephosphorylation [200,201], with a subsequent compensatory increase in gene expression.

Figure 4.12 – Connexin-43 protein expression

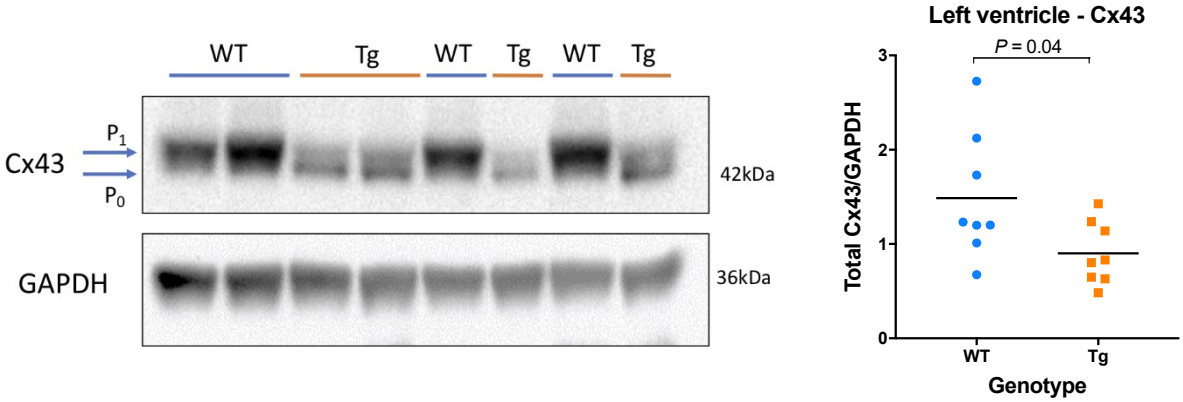


Figure 4.12: Connexin-43 (Cx43) protein expression in left ventricular homogenates from wild-type mice (WT) and transgenic (Tg) littermates. **Left panel**: representative Western blot with P_0 and P_1 denoting likely unphosphorylated and phosphorylated isoforms of protein. Only total Cx43 was quantifiable. **Right panel**: quantification of total Cx43 normalised to GAPDH in WT (n=8) and transgenic (n=8) mice. Horizontal lines represent means, unpaired *t*-test for difference.

Localisation

Cx43 is predominantly localised to the intercalated disc; however, under conditions of stress, dephosphorylation and subsequent lateralisation of Cx43 have been reported as being associated with myocyte electrical decoupling [201]. Given my findings suggestive of a reduced amount of total and phosphorylated Cx43 in the hearts of transgenic mice, we investigated if changes in localisation of Cx43 may also contribute the slower conduction velocity seen in transgenic mice. Using immunofluorescence and co-staining of N-cadherin, a key structural component of the intercalated disc, OCT embedded left ventricular sections were stained, preserving the myocardial architecture.

Total Cx43 intensity was lower in transgenic compared with wild-type mice (*P* for difference $< 1 \times 10^{-4}$) with no change in N-cadherin (*P* for difference 0.64; **Figure 4.13**). The fluorescence of Cx43 at the intercalated disc was reduced in transgenic compared with wild-type mice (*P* for difference 0.02), but proportionally, Cx43 remained predominantly localised at the intercalated disc (*P* for difference 0.03). This suggests that whilst total Cx43 at the intercalated disc was reduced, this was not accompanied by lateralisation. Overall, a reduction in ventricular Cx43 protein may contribute to reduced electrical coupling and slower conduction velocity in transgenic mice.

Figure 4.13 – Cx43 and N-cadherin in left ventricular myocytes

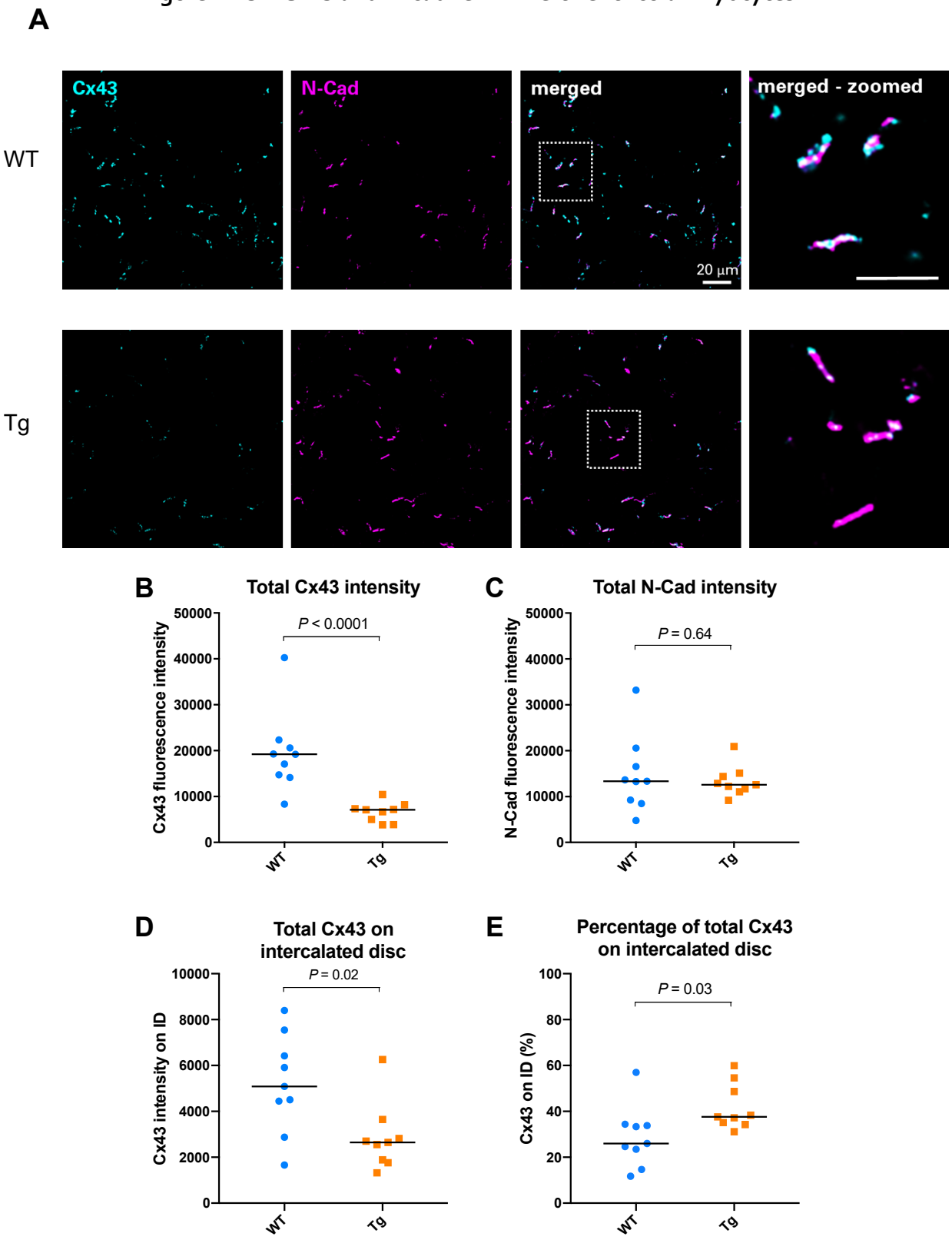


Figure 4.13: Connexin-43 (Cx43) and N-Cadherin (N-Cad) intensities assessed by immunofluorescence focusing on the intercalated disc (ID) in three replicates from three wild-type (WT) and three transgenic (Tg) mice. Horizontal lines represent median values, Mann-Whitney tests for comparisons. (**A**) Representative images from staining in WT and Tg. (**B**) Total Cx43 intensity. (**C**) Total N-Cad intensity. (**D**) Total Cx43 on ID (i.e. co-localising with N-Cad). (**E**) Percentage of total Cx43 on ID.

4.3.6 Myocardial overexpression of *NOS1AP* is not associated with changes in NOS1 gene or protein expression or alterations in NOS1 activity

Given interactions between NOSIAP and NOSI, it is possible that some of the phenotypic changes observed in transgenic mice may be NOSI-mediated. I therefore specifically investigated whether there were differences in NOSI gene and protein expression, NOS activity and NOSI localisation between genotypes.

Gene expression

There were no differences in endogenous *Nosl* mRNA expression between wild-type mice and their transgenic littermates across a variety of tissues (**Figure 4.14**).

Figure 4.14 – Gene expression profile of *Nos1* in Tg(*Myh6-hNOS1AP*) colony

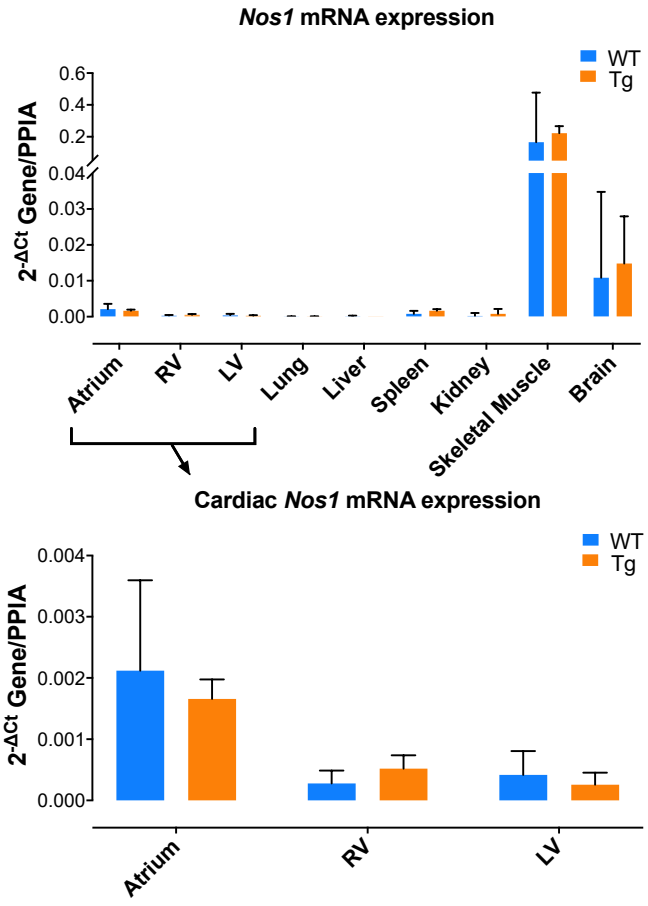


Figure 4.14: *Nos1* gene expression (median and interquartile ranges) in wild-type (WT; n=8) and transgenic (Tg; n=6) mice as measured by RT-QPCR. There were no significant changes in gene expression between WT and Tg mice for *Nos1* in all tissue types (Mann-Whitney tests).

Protein expression

The level of NOS1 protein expression detectable using Western blotting was low and variable in left ventricular homogenates from both genotypes. Broadly speaking, in keeping with gene expression data from the same tissues, there were no significant differences in NOS1 protein levels between wild-type mice and their transgenic littermates (**Figure 4.15**) although the large variability and relative low sample size would have precluded detection of moderate differences. With this limitation, a robust functional representation of NOS1 activity was important to obtain.

Figure 4.15 – NOS1 protein expression

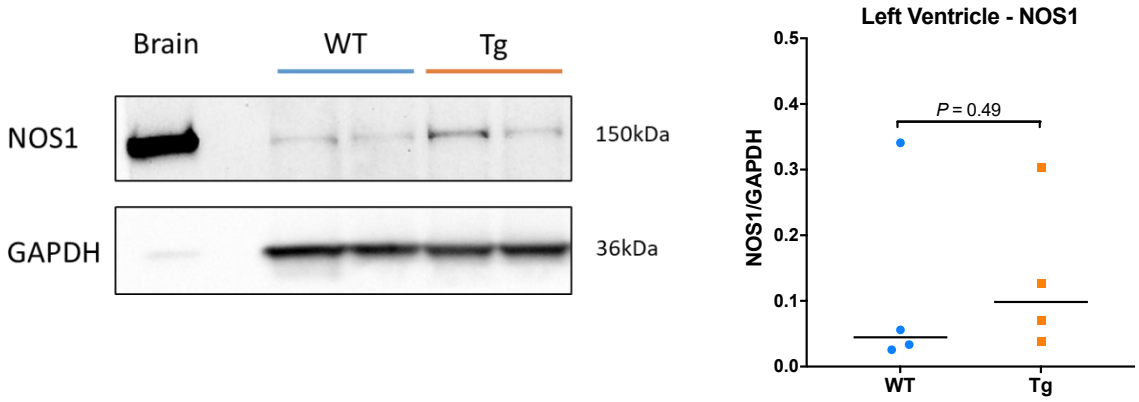


Figure 4.15: NOS1 protein expression in left ventricular homogenates from wild-type mice (WT) and transgenic (Tg) littermates. **Left panel**: representative Western blot with positive control as brain homogenate. **Right panel**: quantification of NOS1 normalised to GAPDH in WT (n=4) and transgenic (n=4) mice with horizontal line at median value, Mann-Whitney test for difference.

NOS activity in left ventricular tissue homogenates

With earlier studies suggesting that NOS1AP had effects on NOS activity [105,107], I used the conversion of radiolabeled arginine to citrulline to quantitatively measure NOS activity defined as the % inhibited by the non-isoform specific NOS inhibitor L-NAME in left ventricular homogenates from 24 transgenic mice (10 male and 14 female) and 24 wild-type littermates (15 male and 9 female). As is seen in **Figure 4.16 A**, there were no differences in NOS activity between genotypes. Using a two-way ANOVA with terms for genotype and sex revealed no significant sex specific differences (**Figure 4.16 B**).

Figure 4.16 – NOS activity (L-NAME inhibitable fraction) in the left ventricle

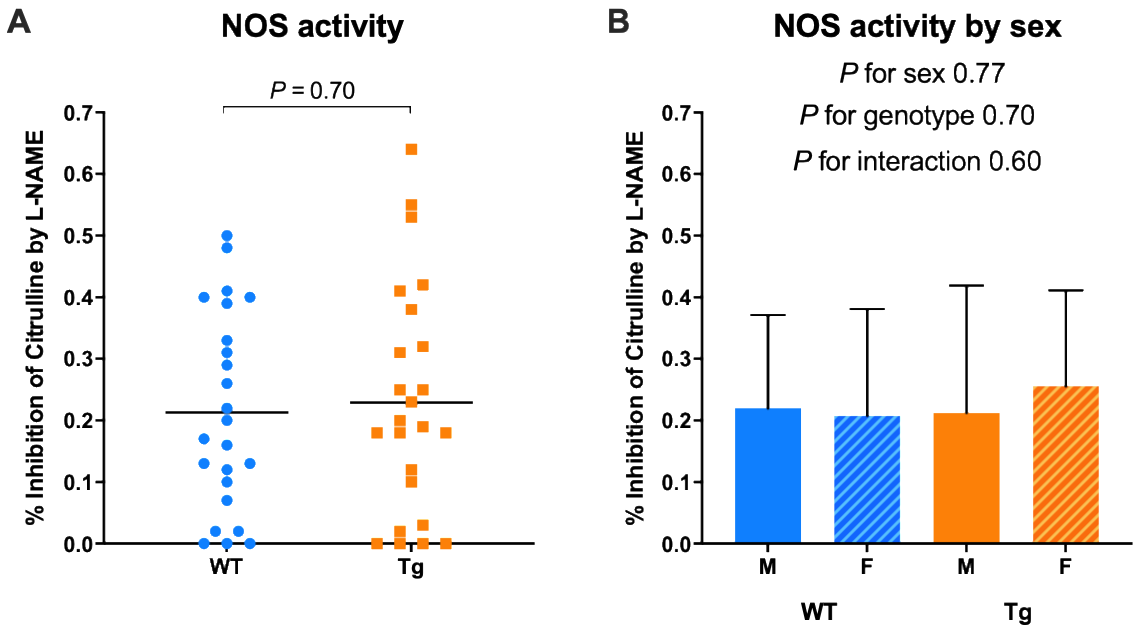


Figure 4.16: (**A**) Nitric Oxide Synthase (NOS) activity shown as the L-NAME attributable inhibition of the conversion of L-arginine to citrulline measured by high-performance liquid chromatography in left ventricular homogenates in wild-type mice (WT, n=24; 10 male and 14 female) and their transgenic littermates (Tg, n=24; 15 male and 9 female). Horizontal lines represent mean values, unpaired *t*-test for comparisons. (**B**) Same data in panel **A** grouped by sex with two-way analysis of variance; bars represent mean values and error bars represent standard deviation.

Immunofluorescence

To investigate if overexpression of NOSIAP altered NOSI intracellular localisation, we performed isolated cell imaging in the first instance using confocal microscopy. Qualitatively, the striated pattern of NOSI staining did not appear different in wild-type versus transgenic left ventricular myocytes (**Figure 4.17**). In the transgenic myocytes, NOSIAP overexpression was associated with sarcolemmal membrane and nuclear immunofluorescence (**Figure 4.17**). There was no obvious change in NOSI localisation in the transgenic myocytes, but this was at a gross scale within the limitations of confocal microscopy.

Figure 4.17 – NOS1AP and NOS1 in left ventricular myocytes

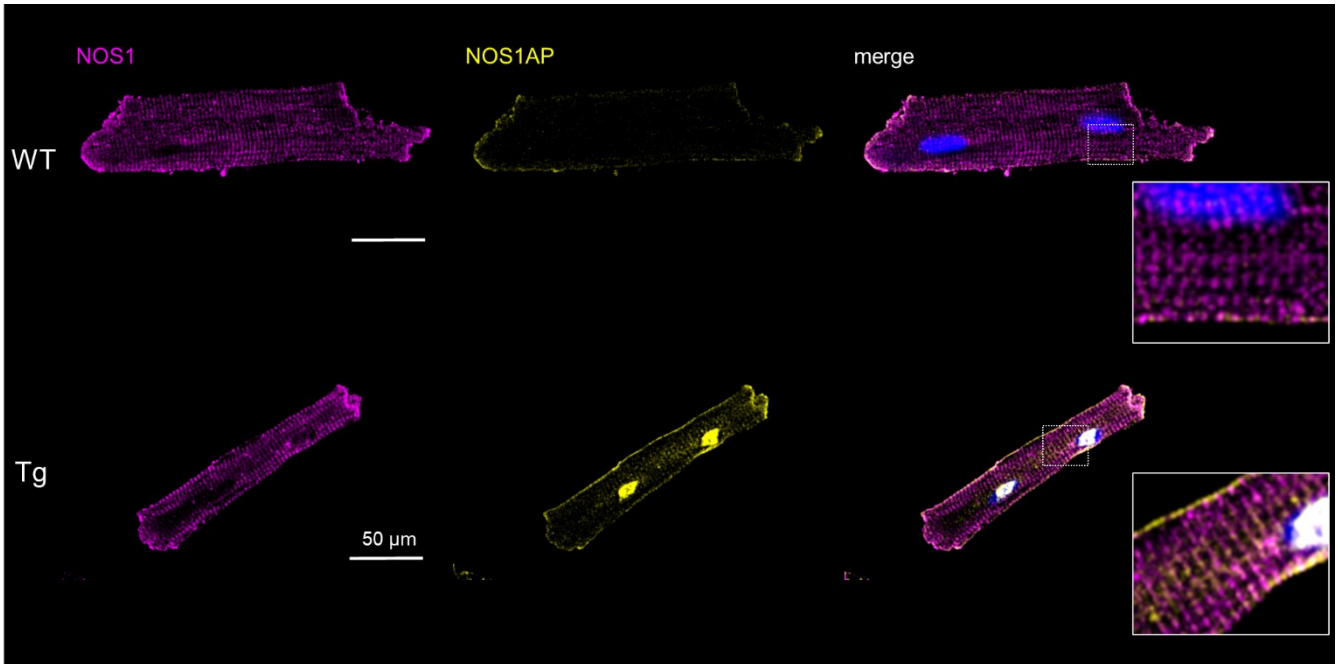


Figure 4.17: Confocal imaging of isolated left ventricular myocytes from wild-type (WT) and transgenic (Tg) littermates showing immunofluorescence imaging of NOS1AP and NOS1.

4.3.7 Exploratory sodium current data

Given the slowed conduction velocity seen, Dr Xing Liu performed experiments to try to measure I_{Na} characteristics in the NOS1AP-Tg colony. As mentioned in **Section 4.2.9**, a physiological temperature of 35-37°C was chosen to allow us to test whether any differences between genotypes may be NOS dependent (as NOS activity as well as NOS-mediated signalling are temperature-sensitive). The experiments proved difficult from a technical point of view, and subsequent data suggested that the current density readings obtained and the slope values of the activation curves were lower than would be expected across both genotypes. Consequently, the results presented can only be viewed as exploratory, although they did not support significant differences in peak I_{Na} between genotypes.

Measurements of I_{Na} were taken using single-cell patch clamping of left ventricular myocytes isolated from 14 wild-type (24 cells total; 14 cells from 8 males and 10 cells from 6 females) and 14

transgenic mice (29 cells total; 13 cells from 5 males and 16 cells from 9 females) aged 16-20 weeks old. Example raw tracings are shown in **Figure 4.18**.

Figure 4.18 – Example raw tracings for sodium current measurements

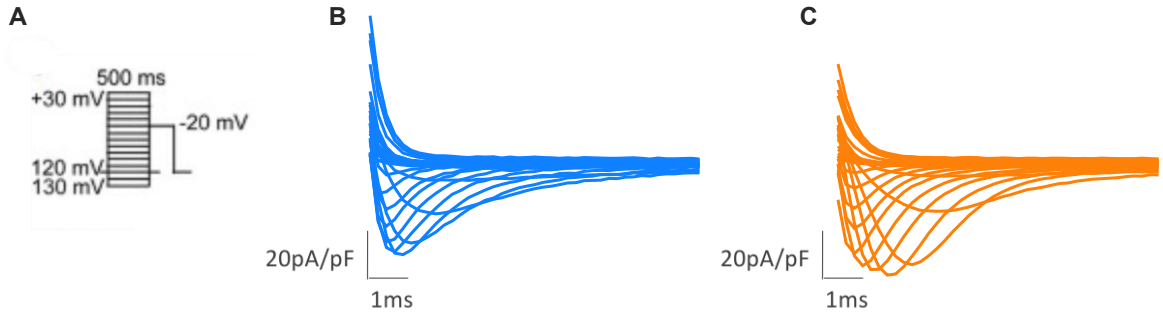


Figure 4.18: (**A**) Voltage step protocol for I_{Na} measurement as described in **Section 4.2.9**. (**B**) Representative current vs time trace for a cardiomyocyte from a wild-type mouse. (**C**) Representative current vs time trace for a cardiomyocyte from a transgenic mouse.

The peak I_{Na} was not significantly different in transgenic mice compared to their wild-type littermates (median: -30.0 pA/pF; interquartile range [IQR] -44.0 to -24.3 versus -31.3 pA/pF; IQR -41.7 to -24.3, P = 0.84; **Figure 4.19 A** and **B**). There were no significant differences between transgenic and wild-type mice with regard to I_{Na} activation characteristics (**Figure 4.19 C** to **E**). Although there were no differences in the voltage sensitivity of the channel (i.e. the inactivation slope of the current-voltage relationship; **Figure 4.19 H**), I_{Na} reached 50% of maximal inactivation at a more positive voltage in the transgenic mice compared with wild-type littermates (mean of -69.5 ± 4.4 mV versus -76.9 ± 5.5 mV, P for difference 0.003, **Figure 4.19 F** and **G**). In isolation, this shift in the voltage of inactivation would theoretically suggest that after activation, more sodium channels are available at any given voltage (i.e. fewer sodium channels have been inactivated) in NOS1AP-Tg mice, potentially meaning Tg mice may show higher excitability at hyperpolarised voltages. This positive shift of I_{Na} inactivation may arise from incomplete voltage-dependent Na channel inactivation thus leaving some channels in a conductive state - although we did not measure the late sodium current.

NOS1 has been reported to regulate I_{Na} with increased nitrosation of the sodium channel encoded by *SCN5A* associated with a persistent sodium current leading to a long QT syndrome [129,202].

To investigate if any of the differences seen in the NOSIAP-Tg mice were NOS1 dependent, the experiments were repeated using the NOS1 inhibitor SMTC in 10 wild-type (20 cells total; 11 cells from 6 males and 9 cells from 4 females) and 9 transgenic mice (22 cells total; 7 cells from 3 males and 15 cells from 6 females) aged 16-20 weeks old. These data were analysed along with data from the non-SMTC experiments described earlier using a two-way ANOVA with terms for presence of SMTC and genotype. **Figure 4.20** shows these results alongside data from **Figure 4.19** displayed for ease of comparison. There was no interaction between genotype and SMTC and post-hoc analyses did not reveal an effect of SMTC on any of the measured parameters. For the voltage at 50% I_{Na} inactivation, post-hoc analyses showed no significant effect of SMTC on either wild-type or transgenic groups, but there was no significant genotype difference in this parameter in the presence of SMTC (mean -69.6 ± 5.7 mV for Tg + SMTC versus -72.2 ± 6.3 mV for WT + SMTC, *P* for difference 0.21).

Figure 4.19 – Sodium current characteristics

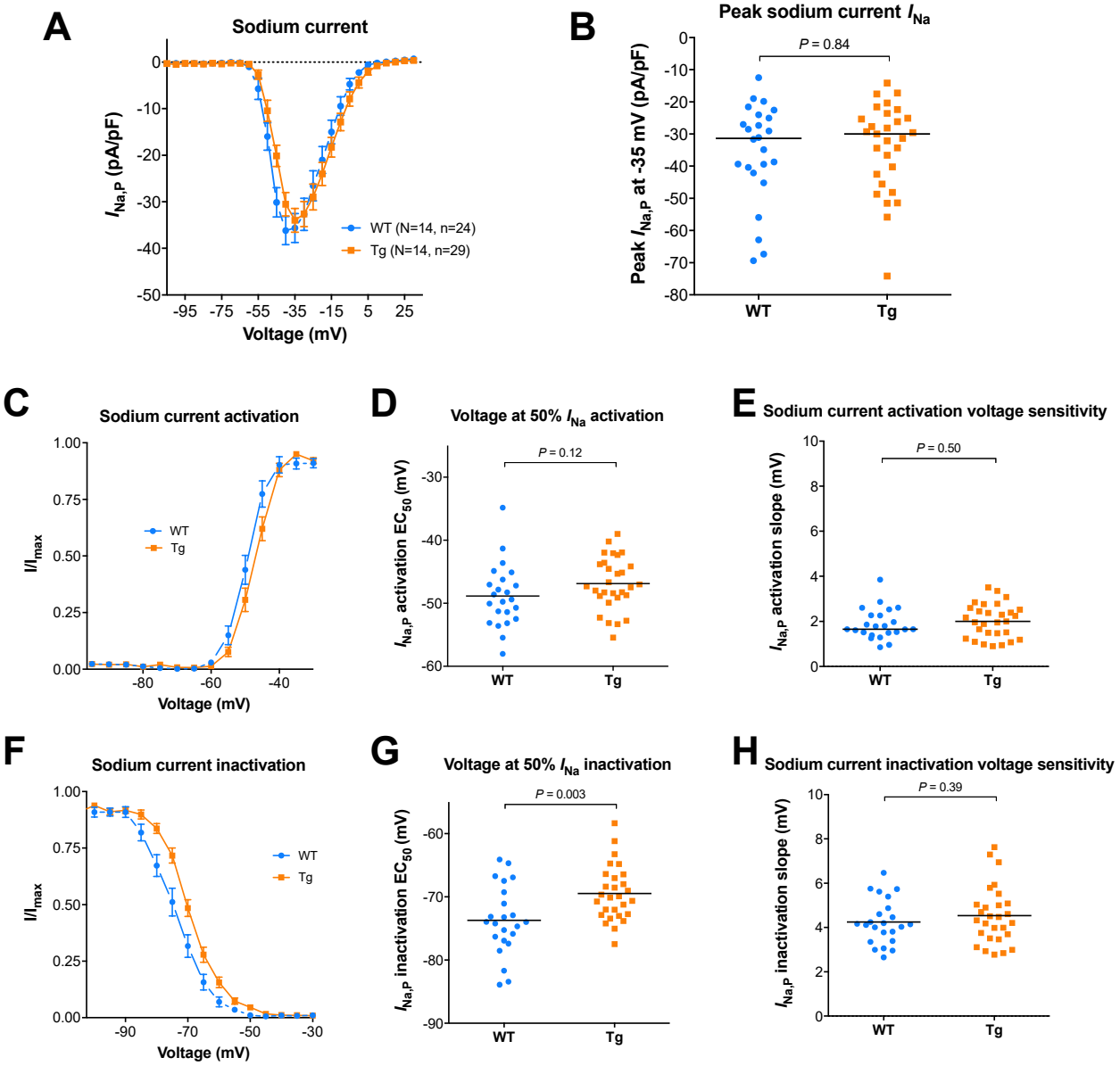


Figure 4.19: Details of measurements of large depolarising sodium current I_{Na} in left ventricular myocytes. (**A**) Voltage versus peak sodium current ($I_{Na,P}$) density in 24 cells from 12 wild-type (WT) mice and 29 cells from 13 transgenic (Tg) littermates. (**B**) Peak sodium current density at -35mV for WT and Tg groups. Horizontal lines represent median values; Mann-Whitney test for comparisons. (**C**) Voltage versus sodium current (I) relationships normalised to the maximal sodium current (I_{max}) during the activation phase measured for WT and Tg. (**D**) Voltage at which 50% of maximal sodium activation current was achieved for WT and Tg. Horizontal lines represent mean values; unpaired t-test for comparisons. (**E**) Voltage sensitivity of the sodium current during the activation phase, or the slope of the relationship depicted in panel **C** for WT and Tg. Horizontal lines represent median values; Mann-Whitney test for comparisons. (**F**) Voltage versus sodium current (I) relationships normalised to the maximal sodium current (I_{max}) during the inactivation phase measured for WT and Tg. (**G**) Voltage at which 50% of peak sodium current was achieved for WT and Tg during inactivation phase. Horizontal lines represent mean values; unpaired t-test for comparisons. (**H**) Voltage sensitivity of the sodium current during the inactivation phase, or the slope of the relationship depicted in panel **F** for WT and Tg. Horizontal lines represent mean values; unpaired *t*-test for comparisons.

Figure 4.20 – Effects of SMTC on the sodium current

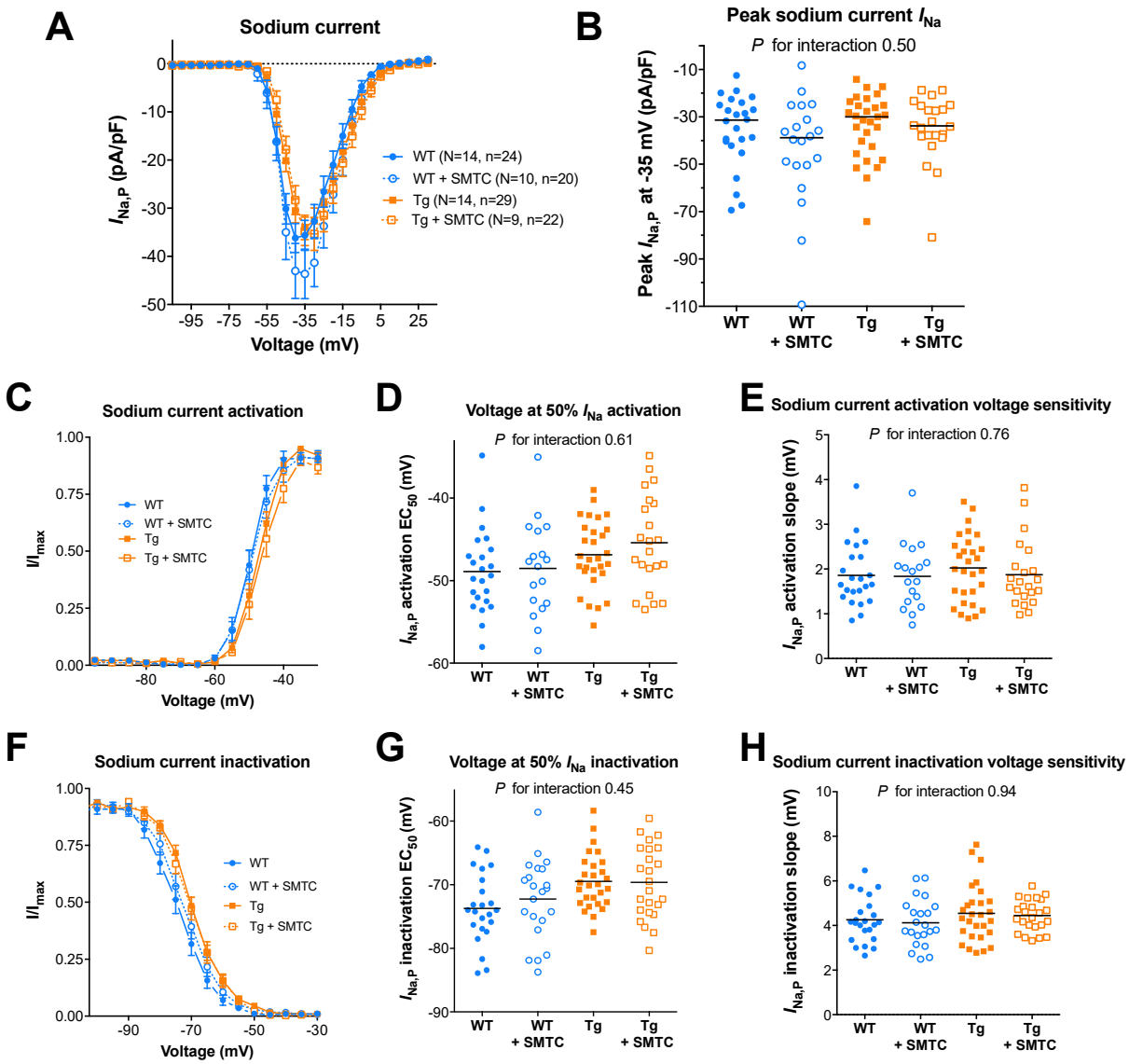


Figure 4.20: Effects of S-Methyl-L-thiocitrulline acetate (SMTC; a NOS1 inhibitor) on measurements of large depolarising sodium current I_{Na} from 20 cells in 11 wild-type (WT) and 22 cells from 9 transgenic (Tg) littermates. Non-SMTC data replicated from **Figure 4.19** across all panels. *P* for interaction after Sidak's adjustment for multiple tests calculated using two-way analysis of variance with terms for genotype and SMTC after transformation of data if not normally distributed. (**A**) Effects of SMTC on voltage versus peak sodium current ($I_{Na,P}$) density. (**B**) Effect of SMTC on peak sodium current density at -35mV for WT and Tg. Horizontal lines represent median values. (**C**) Effect of SMTC on voltage versus sodium current (*I*) relationships normalised to the maximal sodium current (I_{max}) during the activation phase measured for WT and Tg. (**D**) Effect of SMTC on the voltage at which 50% of peak sodium activation current was achieved for WT and Tg. Horizontal lines represent mean values. (**E**) Effect of SMTC on voltage sensitivity of the sodium current during the activation phase, or the slope of the relationship depicted in panel **C** for WT and Tg. Horizontal lines represent median values; comparisons made using log transformed data. (**F**) Effects of SMTC on voltage versus sodium current (*I*) relationships normalised to the maximal sodium current (I_{max}) during the inactivation phase measured for WT and Tg. (**G**) Effects of SMTC on voltage at which 50% of peak sodium current was achieved for WT and Tg during inactivation phase. Horizontal lines represent mean values. (**H**) Effects of SMTC on voltage sensitivity of the sodium current during the inactivation phase, or the slope of the relationship depicted in panel **F** for WT and Tg. Horizontal lines represent mean values.

4.4 Discussion

Interpreting the potential effect of molecular changes on arrhythmogenesis is difficult as the electrophysiological properties of a tissue in which an arrhythmia initiates and is sustained are not always directly controlled by single molecules. Instead, a number of molecular interactions at a cellular level must first come together to define the electrophysiological properties of the cell such as the action potential, calcium handling dynamics and the individual cell's excitability and refractory thresholds. Individual cellular electrical properties then combine to generate the tissue and organ's electrophysiological properties. Meanwhile, as Coumel described [172], other organ systems (e.g. autonomic and endocrine) are dynamically modulating these factors at molecular, cellular and whole organ levels.

4.4.1 Action potential duration

Despite the shorter measured QT interval seen on surface ECGs in transgenic mice, I found no significant differences in *ex-vivo* left ventricular epicardial action potential duration between mice overexpressing *NOSIAP* and their wild-type littermates at physiological pacing rates; however, APD_{90} tended to be shorter in transgenic mice at slower heart rates, particularly in male mice. Both shortening [86,107] and lengthening [108] of APD in response to changes in *NOSIAP* gene expression have been reported. A number of factors may explain these findings.

Specifics of APD measurements

In my experiments, measurements of APD were conducted in intact hearts – either using epicardial electrodes or optical mapping. Whilst single-cell transmembrane action potential duration recording may remain the 'gold-standard', there is sufficient evidence that contact (i.e. non injury based) monophasic action potentials (MAPs), such as those measured in these experiments, mirror intracellular recordings well [203]. Additionally, similar results were obtained using a different technique (optical mapping), suggesting that epicardial APDs may only partially explain the differences in QT interval between genotypes.

Across many mammalian species, including humans and mice, action potentials on the epicardium are shorter than endocardial action potentials, leading to a heterogeneous gradient of

repolarisation within the ventricle, thought to be driven by transmural differences in the transient outward potassium current I_{to} [204-207]. Experiments comparing APDs measured in single cardiomyocytes versus electrically coupled myocytes have shown significant differences as a result of electrical coupling between cells [208]. Isolation of cardiomyocytes from smaller hearts can also give rise to unrepresentative mixtures of epicardial, endocardial and transitional cells [209]. If NOS1AP preferentially affects APD in certain cell types, this may also contribute to explaining the differing effects noted between single cell and whole heart epicardial APD measurements. It is also known that different tissue types within the specialised cardiac conduction system have differing action potential and electrophysiological properties [48].

Chang *et al.* [107] suggested *Nos1ap* overexpression resulted in a shortening of APDs all the way from 10% to 90% of maximal repolarisation (APD_{10} – APD_{90}) in isolated guinea pig ventricular myocytes paced at 1 Hz, although they did not quantify the degree of protein overexpression. They found no differences in I_{Na} or total I_{K1}, I_{Kr} or I_{Ks} currents, which was surprising given that APD shortening was observed across all percentages of repolarisation; however, they found a reduction in $I_{Ca,L}$ to which they attributed most of the changes seen. Kapoor *et al.* overexpressed human *NOS1AP* (again, without any quantification of degree of protein expression) in a neonatal rat ventricular myocyte monolayer and found, using optical mapping, that APD_{80} at 2 Hz stimulation was shorter in monolayers with overexpression of *NOS1AP*. By contrast, Milan *et al.* [108] used zebrafish morpholino based *nos1ap* knockdown and found, using optical mapping in whole hearts, that this resulted in shortening of APD_{90} at 1 Hz stimulation.

Increases in heart rates shorten action potential durations in a non-linear fashion, a phenomenon known as electrical restitution [210]. All three existing published papers used stimulation frequencies of 1 to 2 Hz or 60 to 120 bpm, considerably below the physiological heart rates for the species (guinea-pig, rats, zebrafish) from which the cells or tissue came from. My measurements for MAP based APDs were from intact murine hearts paced between 5 to 12.5 Hz or 300 to 750 bpm, broadly in keeping with the species' spontaneous heart rate. Similarly, measurements from optical mapping were taken at a stimulation frequency of 8.3 Hz or 500 bpm.

I chose a variety of stimulation frequencies to measure APDs to account for any potential effects of NOSIAP on rate-dependent adaptation. My data suggested that at 300 bpm (200 ms cycle length), male wild-type mice have a longer APD_{90} compared with transgenic male and female mice, but no other sex-specific differences were detected. Compared to the published data, it is however possible that as APD shortened at faster heart rates, I was unable to detect small differences in APD that would have been detectable at the lower heart rates used in previously published work. Importantly though for the transgenic mice, the shorter measured QT interval on surface ECG was measured at an average heart rate of ~500bpm.

Species-specific differences

One could debate whether taking APD measurements of a non-human model at human heart rates or at the organism's own natural heart rate better approximates to the human phenotype. Ultimately, all non-human models have limitations and do not accurately replicate all aspects of human physiology. For example, although guinea-pigs ventricular myocytes have a similar shaped action potential to human ventricular myocytes, when paced at a non-physiological rates (e.g. 1 Hz), they show markedly altered action potential shapes due to specific alterations in the activation state of I_{Ks} [211]. Chang *et al*. used guinea-pig *Nos1ap* for adenoviral overexpression in their model. However, the NOSIAP protein in the guinea-pig has only 83% sequence homology (UniProt.org) to human NOSIAP. In particular, the N-terminal segment of guinea pig NOSIAP is very different to the human protein, which has as its characteristic feature a phosphotyrosine-binding (PTB) domain, known to be important in mediating subcellular localisation through interactions with structural proteins [88]. It is therefore possible that guinea-pig NOSIAP protein may not exert its effects in the same way as human NOSIAP.

Focusing on the mouse model, repolarisation is dependent on different inward delayed rectifier potassium currents when compared with humans [212]. It is therefore possible that if NOSIAP's effects on the human QT interval were a result of APD prolongation due to specific interactions with human potassium channels, then these may not be reflected in a murine system. However, whilst the currents between mice and humans may be different, the molecular subunits of

potassium channels have a significant homology and multiple mouse models with disruption of potassium channel subunits do show long QT changes on surface electrocardiography and at a cellular level [213]. As discussed previously, the human NOS1AP protein overexpressed in the NOS1AP-Tg mice has a 94% sequence homology to the murine form, with similar N- and C-terminals and so a lack of interaction with endogenous ion channel proteins would be less likely to be the cause of not detecting an effect on APD.

Repolarisation reserve

The term 'repolarisation reserve' refers to a concept advanced by Dan Roden, which initially sought to explain the seemingly variable nature of QT prolongation in humans due to drugs or genetic mutations inhibiting the I_{Kr} repolarising current [21,22]. Evidence suggests that repolarisation is not solely accomplished by a single current and that a multitude of currents contribute to this complex phenomenon, such that some accommodation for impaired repolarisation might be possible if other mechanisms were intact [22,23]. It may therefore be possible that the effects of NOS1AP on APD were not detected due to other mechanisms compensating.

There is also genetic evidence supporting the concept of repolarisation reserve. Lahrouchi *et al.* [29] found that patients with long QT syndrome without a recognised pathogenic mutation (so called 'genotype negative') had a significantly increased burden of 'common' variants associated with QT prolongation when compared with patients with long QT syndrome with a defined pathogenic variant and healthy controls. This suggests that genotype negative long QT syndrome may be a polygenic condition, with accumulation of numerous smaller factors ultimately reducing the repolarisation reserve and prolonging the QT interval. They also found that in a case-control genome wide association study using a mixed population of patients with long QT syndrome, the same *NOS1AP* allele (rs12143842) identified in the general population was significantly associated with the risk of long QT syndrome. This again lends weight to the theory that small genetic changes in repolarisation are accumulated but, more specifically, implies that the functional effects of *NOS1AP* on QT prolongation are relevant even in patients with pre-existing long QT syndrome.

Relevant to the NOSIAP-Tg mice, the fact that the QT prolonging effects of alleles of *NOSIAP* were seen in healthy people as well as in those with long QT interval with depleted repolarisation reserves suggests that the actions of NOSIAP may extend beyond factors affecting the APD and ion channels involved in individual cellular repolarisation.

4.4.2 Calcium handling

Although my experiments did not reveal any changes in $[Ca^{2+}]_i$ transients characteristics in the NOSIAP-Tg, a number of studies have suggested associations between NOSIAP and calcium handling in cardiomyocytes. The role of calcium in arrhythmogenesis is well described and multi-faceted [173,182]. Simplistically, increased intracellular Ca^{2+} (for a variety of reasons) can trigger delayed after-depolarisations (DAD) leading to the initiation of new spontaneous cellular depolarisation – i.e. triggered activity. From a substrate perspective, alterations in individual cells' calcium handling can lead to heterogeneity across the whole organ, with discordance in APD, refractoriness and subthreshold DAD altering excitability.

Chang *et al.* [107] suggested the main change driving their findings of a shortened APD secondary to viral overexpression of *NosIap* in guinea pig cardiomyocytes was reduced $I_{Ca,L}$. Similar findings were obtained in rat sympathetic neurons, with Lu *et al.* [105] showing a reduction in peak $I_{Ca,N}$ as well as $[Ca^{2+}]_i$ amplitude after viral overexpression of *NOSIAP*. Conversely, Treuer and Gonzalez [109] showed that *NOSIAP* gene silencing in neonatal rat ventricular myocytes was associated with a reduction in $[Ca^{2+}]_i$ amplitude. In sympathetic neurons with viral overexpression of *NOSIAP*, the NOSI inhibitor AAAN also normalised the reduced I_{Ca} observed. Ronchi *et al.* [111] reported that NOSI inhibition significantly increased $I_{Ca,L}$ in control guinea pig myocytes, something not observed by Chang *et al.* [107] in response to L-NAME, or seen in the experiments involving sympathetic neurons [105], suggesting variable responses based on experimental design.

As seen in **Figure 1.6**, data from eQTL databases suggests that human *NOSIAP* alleles prolonging the QT are associated with increased myocardial gene expression, so, the shortened APD and reduced $I_{Ca,L}$ associated with increased expression of *NOSIAP* observed in some studies suggest that these effects may not necessarily explain or significantly contribute to the human phenotype.

Overall, in our mouse model of cardiac limited *NOSIAP* overexpression, there was no convincing evidence of significant changes in cardiomyocyte calcium handling contributing to the phenotype observed.

4.4.3 Conduction velocity

Our experiments showed a marked reduction in epicardial conduction velocity across the left ventricle in NOSIAP overexpressing mice compared with their wild-type littermates, something that has not been described previously. Kapoor *et al*. found that lentiviral mediated *NOSIAP* overexpression resulted in a shorter APD and an increased conduction velocity in cultured plates of neonatal rat ventricular myocytes [86]. Somewhat strikingly in our experiments, the variance in conduction velocity measured in the NOSIAP-Tg mice was much smaller than that seen in wild-type littermates. This may suggest the presence of a mechanism with a large effect size over-riding other causes of variability.

A number of factors can affect conduction velocity in cardiac tissues. These have classically been conceptualised via the cable equation, modelling a current flowing along a linear cell from one depolarising myocyte to the next, connected by gap junctions [198]. Here, conduction velocity is related to the maximum rate of action potential depolarisation, predominantly governed by the fast inward depolarising sodium current (I_{Na}); resistance to local current flow between cells; their membrane capacitances; and in 3-dimensions, the relationship or coupling between adjoining myocytes in cardiac tissue [198].

Tissue architecture

Disruption of closely coupled myocytes by insulating connective tissue such as that seen due to cardiac fibrosis would be expected to slow conduction velocities in cardiac tissue. Specifically, this could alter both the resistance to current flow between cells as well as potential membrane capacitances. Given the prolonged P-wave duration, PR and QRS intervals on ECG in the NOSIAP-Tg mice, an altered tissue structure was important to exclude. Areas of fibrosis would also mean current propagating from adjacent myocytes in alternative directions, and the resultant slowing of conduction would increase the potential for re-entrant arrhythmia development.

In the NOS1AP-Tg model, left ventricular collagen content was no different between transgenic mice and their wild-type littermates suggesting that fibrosis was not a key factor explaining the slowed conduction velocity seen in the NOS1AP-Tg mice, although further histological examination may prove useful.

Myocyte coupling via gap junctions

In human heart sections, NOS1AP has been found to localise to the intercalated disc, co-localising with connexin-43 (marker of gap junctions), N-cadherin (fascia adherens) and plakoglobin (desmosomes) [86]. Broadly speaking, intercalated discs between cardiomyocytes are made up of the fascia adherens, a structure important for anchoring actin and transmitting contractile forces; desmosomes, a structure important to stop cell separation under mechanical load, and finally gap junctions, which connect adjacent myocytes electrically and allow for the spread of the action potential. Relevant to the spread of the electrical impulse and conduction velocity, the main component of gap junctions between cardiomyocytes are hexamers of connexin proteins forming a connexon or hemichannel, which, when connected with another hemichannel on a neighbouring cell forms a gap junction, allow the spread of electrical activity between cardiomyocytes [199].

Cardiac connexins are mainly composed of three types – connexin-40 (Cx40), connexin-43 (Cx43) and connexin 45 (Cx45). There are regional differences in the expression of the connexins. Cx43 is found throughout the heart but is the only connexin within the ventricles, Cx40 is expressed in the atrium and Cx45 seems to be localised to specialised cardiac conducting tissue such as nodal tissues and possibly the Purkinje network [199]. Given the changes in conduction velocity noted on optical mapping of the wall of the left ventricle and the widespread distribution of Cx43, I focused on this protein for investigation.

Firstly, protein expression of Cx43 was markedly reduced in left ventricular homogenates from NOS1AP-Tg mice and this was also associated with a reduction in the phosphorylated form. Gap junctions are dynamic structures and have high turnover rates [214,215]. Cx43 can be phosphorylated at many sites with very different effects on protein and gap junction stability [214,215] so whilst suggestive, it is not clear whether the reduced Cx43 found in transgenic hearts is

caused by the protein dephosphorylation and increased degradation. In the NOS1AP-Tg, the decreased amount of Cx43 was accompanied by a small but significant increase in gene expression in the left ventricle. With the rapid turnover of Cx43, this provides some suggestive evidence that there may be enhanced post-translational degradation of Cx43 in NOS1AP-Tg with a "compensatory" increase in gene expression.

Immunofluorescence in heart sections showed that NOS1AP overexpression was associated with lower global Cx43 intensity, with no change in other components of the intercalated disc, such as N-cadherin. In keeping with the lack of increased collagen and structurally normal hearts seen in the NOS1AP-Tg, this suggests a specific process affecting gap junctions rather than the intercalated discs and tissue architecture as a whole. Myocardial disease has been associated with lateralisation of Cx43 away from the intercalated disc leading to slowed conduction velocities [199]. This is unlikely to be the case in the NOS1AP-Tg mice who had a lower intensity of Cx43 on the intercalated disc, but a higher fraction of total Cx43 still present in that location. However, in my experimental setup, conduction velocity was measured globally and epicardially, parallel to the main spread of depolarisation and it was not possible to separate it into longitudinal and transverse components.

From my results, the specific mechanism by which NOS1AP may affect Cx43 levels is unclear. After translation in the endoplasmic reticulum, connexins may pass through the Golgi network and then to the plasma membrane followed by internal trafficking for degradation, with turnover highly dependent on their phosphorylation status [215]. The C-terminus PDZ domain of the NOS1AP protein has been thought to be important for its interaction with NOS1, whilst the N-terminus phosphotyrosine binding domain has been thought to bind to 'structural' proteins, including actin (in neurons and in human kidneys) [57,95,216]. However, PDZ domains are well recognised across many protein interactions and indeed, have also been found in the zonula occludens-1 protein (ZO-1), which appears to have a specific separate site for Cx43 binding in a configuration to allow phosphorylation/dephosphorylation [217], and which also contributes to gap junction stability [218].

Thus far, the work by Kapoor *et al.* [86] is the only published study localising NOS1AP to the intercalated disc in human hearts, and indeed in any whole heart sections. Of note however, the authors used a custom rabbit polyclonal antibody generated using a peptide mapping to amino acids 486-503 of human NOS1AP which is not commercially available. The commercial antibody I used was generated as a mouse monoclonal using peptides mapping to amino acids 304-503 for rat NOS1AP, but which shares a 94% sequence homology to human NOS1AP. By contrast, in isolated neonatal rat ventricular myocytes, endogenous NOS1AP did not co-localise with Cx43 (measured using immunofluorescence and light microscopy) when a commercial antibody was used [109].

There have been variable results reported in the literature about the effects of Cx43 knockdown on conduction velocity and ECG parameters in a variety of mouse models [157]. The variability is likely explained by a combination of the nature of the Cx43 deficiency induced (germ-line or inducible) and the extent to which other connexin isoforms 'compensate'. Additionally, the various models focused on measuring total Cx43 levels and not specifically on the effects of phosphorylation.

Nademanee *et al.* [219] reported a series of human autopsy cases comparing the hearts of patients who died suddenly with a family history of Brugada syndrome (typified by a coved form of ST elevation and QT changes in specific ECG leads) to a random set of controls dying unnaturally (e.g. accidents). Careful histological study of the hearts showed variable degrees of epicardial infiltration by collagen localised to the right ventricular outflow tract (RVOT) in patients with presumed Brugada syndrome. Interestingly, immunofluorescence of the RVOT in these same hearts showed a significant reduction in Cx43 localised to the intercalated disc without lateralisation, when compared with control hearts. This remained significant even after correction for the increased collagen content. Further studies have suggested that autoantibodies to Cx43 may be a feature of Brugada syndrome, describing aggregates of sodium channel subunits and Cx43 in the cytoplasm of cells of the RVOT [220]. The authors suggested that the mis-aggregated proteins underwent disposal and generated an autoantibody response.

Beyond its role in coupling adjacent cardiomyocytes, novel work by Hulsmans *et al.* [221] suggests that Cx43 may be key in facilitating cardiomyocyte interactions with cardiac macrophages which

appear to modulate conduction velocity. Absence of Cx43 from cardiac macrophages in fact led to a prolonged AV delay.

Whilst the specific mechanisms by which Cx43 levels and phosphorylation state were altered in the NOS1AP-Tg model need further investigation (e.g. by investigating how NOS1AP might interact with Cx43), it is likely that a reduced amount of Cx43 at the intercalated disc at least partially explains the slowed conduction velocities observed in transgenic mice.

Depolarising sodium current I_{Na}

Changes in the rapid depolarising sodium current affect the rate of spread of depolarisation [198]. Within the exploratory analyses, NOS1AP-Tg overexpressing mice did not show changes in peak sodium current compared to their wild-type littermates. Some mutations in the *SCN5A* gene encoding sodium channel subunits have been described as having an overlap Brugada - long QT syndrome, showing longer QT intervals but also ECG evidence of conduction abnormalities in other cardiac chambers – namely prolonged PR and QRS intervals [222]. In these individuals, the QT interval was of normal duration at higher heart rates, but was only found to be prolonged when heart rates were slowed. Expressing the same mutation in *Xenopus* oocytes revealed a significantly lower peak sodium current compared to wild-type channels.

Our findings are however in keeping with results from Chang *et al.* [107] where adenoviral mediated overexpression of *Nos1ap* had no effect on peak sodium current. In the NOS1AP-Tg mice, we saw no changes in the activation characteristics of I_{Na} but found that I_{Na} reached 50% of maximal inactivation at a more positive voltage in the transgenic mice compared with wild-type littermates. In isolation, this finding may lead to a higher proportion of sodium channels remaining activated and would not explain the slowing of conduction velocity seen. However, further investigation of I_{Na} activation/inactivation characteristics as well as investigation of the late sodium current is needed.

4.4.4 NOS1AP and NOS1

In the NOS1AP-Tg mice, I detected no change in myocardial NOS1 gene expression, protein content or total NOS activity, but I was not able to convincingly exclude potential changes in NOS1 sub-cellular localisation. By contrast, Chang *et al.* [107] suggested that NOS1AP stabilised NOS1 protein levels and led to enhanced intracellular NO production in cultured ventricular myocytes. They also suggested that the observed reduction in APD was mediated by NO. Similarly, in cultured rat sympathetic neurons, Lu *et al.* [105] found an increase in NOS1 activity after NOS1AP overexpression. Using guinea-pig cardiomyocytes and human induced pluripotent stem-cell derived cardiomyocytes, Ronchi *et al.* [111] claimed that QT prolonging alleles of *NOS1AP* were associated with loss of NOS1 function. A number of reasons may explain these apparent discrepancies.

NOS1AP-NOS1 interaction

NOS1AP was originally described as a binding protein for NOS1 [57]. Subsequent evidence from co-immunoprecipitation in myocardial tissue has indirectly confirmed that the two proteins interact [107,112]. This doesn't necessarily imply that NOS1AP's effects are mediated exclusively via NOS1. In fact, in the original description, Jaffrey *et al.* [57] provided evidence that NOS1AP may compete with other proteins to bind to NOS1 via its PDZ domain.

Chang *et al.* [107] suggested that the APD_{90} shortening they found after viral mediated *Nos1ap* overexpression in guinea pig cardiomyocytes normalised to control values (i.e. increased) after treatment with the non-specific NOS inhibitor L-NAME. On the other hand, also in guinea pig cardiomyocytes, Ronchi *et al.* [111] reported that the NOS1-specific inhibitor SMTC prolonged APD_{90} even in control cells, something not observed in Chang *et al.*'s [107] experiments. By contrast, in human and murine atrial cardiomyocytes, NOS1 inhibition using SMTC shortened APD_{90} [126]. Similarly, in *Nos1*$^{-/-}$ mice, APD_{90} in atrial myocytes was significantly shortened compared to wild-type littermates [126].

It is difficult to reconcile and explain all the incongruous and contrasting effects, even in the same species. This suggests that experimental setup, choice of NOS inhibitors or species-specific factors

may play a role in determining the 'output' of such experiments and that caution must be exercised in attributing the effects of NOS1AP to NOS1 mediated outcomes based on the use of NOS1 inhibitors.

NOS1 protein levels

Chang *et al*. [107] inferred that NOS1AP stabilised NOS1 protein based on the lack of decline of detectable NOS1 protein after prolonged culture in guinea-pig cardiomyocytes after viral *Nos1ap* overexpression. Interestingly, the viral transduction efficiency was 100% when GFP alone was used but dropped to 50% (measured by number of GFP positive cells) when *Nos1ap* was introduced into the viral vector. This somewhat complicates claims about NOS1AP stabilising NOS1 as it represents a mixed population including non-transduced cells. Importantly, NOS1 protein levels between groups were unchanged at baseline and only differed after ~40 hours of culture. It is unclear what the physiological relevance or correlate of this might be.

By contrast, Lu *et al*. [105] found no difference in NOS1 protein levels in rat sympathetic neurons that had viral mediated *NOS1AP* overexpression, despite a ~5-fold increase in NOS1AP protein.

In our model, NOS1 protein was variably and modestly expressed in the ventricle, implying that differences in NOS1 between genotypes may have been missed. However, no studies have convincingly demonstrated differences in NOS1 protein under baseline conditions as a result of changes in NOS1AP.

NOS1 activity

In cardiomyocytes, both NOS1 and NOS3 (endothelial NOS) are thought to be responsible for the constitutive production of NO [223]. Thus, extrapolation about 'NOS1' activity must be carefully scrutinized based on the experimental protocols used.

Chang *et al*. [107] used DAR-4M AM, a rhodamine-based chromophore that fluoresces in response to NO. They claimed that whilst there were no differences in DAR-4M AM fluorescence intensity at baseline between guinea-pig ventricular myocytes, in response to L-arginine (the substrate for all NOS), cells with viral overexpression of *Nos1ap* fluoresced more compared to 'control' myocytes

and concluded that NOSIAP increased intracellular NO production. On closer scrutiny, a number of limitations become apparent. Firstly, DAR-4M AM has rapid time dependent non-linear fluorescence kinetics in response to NO, best fit by an exponential curve [224]. It is unclear whether cells from both groups were assessed within a very short time window which may mean that fluorescence intensity could have been affected. Secondly, the choice of control myocytes is unusual. In other experiments in their study, Chang *et al.* [107] use myocytes transfected with GFP only expressing adenovirus as their control but in this case, they chose non-transfected myocytes. One cannot therefore rule out that some effect of viral transfection alone may have led to the differences seen. Finally, there are some statistical considerations with the data presented. At baseline, 30 *Nos1ap* overexpressing myocytes and 90 controls were included, and after L-arginine, 43 *Nos1ap* overexpressing myocytes with 166 controls suggesting that the measurements were not repeated in the same cells. At baseline, there were no statistical differences between the groups, as measured using a Student's *t*-test. The increased fluorescence between the groups after L-arginine was however statistically significant, again after the use of a *t*-test. The baseline values were not taken into account by the use of an ANOVA test. This may have given somewhat different results, especially as at baseline, there was a 4% difference in the mean fluorescence intensity between groups (higher in the *Nos1ap* overexpressing cells), and only a 7% difference after the addition of L-arginine. The higher number of myocytes included in the L-arginine groups may have increased the power to detect a 'statistically significant' result when considered separately to the baseline conditions.

Similar to the method I used, Lu *et al.* [105] used the radiolabeled conversion of arginine to citrulline (partially due to NOS) to quantify NOS activity in cultured rat sympathetic neurons with viral overexpression of *NOSIAP*. Specifically, they used the % of arginine to citrulline conversion as their end-point of NOS activity and found that neurons overexpressing *NOSIAP* had a higher percentage of conversion (and thus presumed NOS activity) compared to neurons transfected with the empty viral vector. However, the L-arginine to citrulline conversion is not entirely specific to NOS and it is known that NOS-independent citrulline formation occurs [225]. Whilst some

measures can be taken to mitigate this using arginase inhibitors (as both myself and Lu *et al.* [105] did), the specificity of the conversion is better assessed by the change in citrulline peak formed with and without a NOS inhibitor. Due to the relatively low level of NOS in the left ventricle, I used the non-specific NOS inhibitor L-NAME and found no differences between genotypes in total NOS activity although I cannot rule out that small differences in NOS1 activity were compensated for by NOS3 (eNOS). In a tissue with higher NOS1 activity such as neurons, Lu *et al.* [105] used AAAN, a specific NOS1 inhibitor and found a higher percentage of L-arginine to citrulline conversion in cells with NOS1AP overexpression compared with controls. Whilst the AAAN inhibitable fraction was not quantified, there was no difference between groups in L-arginine to citrulline conversion after addition of AAAN, suggesting it was likely that the increase in basal conversion was NOS1 specific.

Even in neuronal tissues however, the increase in NOS1 activity was modest, approximating a 25% increase associated with a 500% increase in NOS1AP protein overexpression. Whilst I did not detect any differences in NOS activity between genotypes in ventricular homogenates, the relatively low NOS activity levels in the ventricle and the ~2.5 fold increase in NOS1AP protein in myocardial NOS1AP-Tg tissue may have meant that in tissues with a higher endogenous NOS activity or higher NOS1AP expression, differences may have been detectable. However, on balance, it seems unlikely that significant changes in NOS activity, in the myocardium at least, are the main mechanism by which NOS1AP exerts its electrophysiological effects.

NOS1AP-NOS1 localisation

The effector molecule of NOS1, NO has a limited diffusion distance intra-cellularly. In cardiomyocytes, it is thought that NOS1 mostly localises to the sarcoplasmic reticulum and to a lesser extent at the sarcolemmal membrane, and that subcellular targeting of NOS1 plays a key role in understanding its diverse effects on excitation-contraction coupling [184].

Using immunoprecipitation, Beigi *et al.* [112] found co-localisation of NOS1AP with NOS1 in the sarcoplasmic reticulum membrane subfraction of murine ventricular cardiomyocytes. However, using conventional confocal microscopy and immunofluorescence with caveolin-3 co-staining,

they suggested that NOS1AP did not localise to the sarcolemmal membrane. In a murine myocardial infarction model, they found no reduction in total NOS1AP but found redistribution of NOS1AP to the sarcolemmal membrane, paralleling that of NOS1, which was not observed in NOS1 knockout mice. Of note though, the authors used confocal microscopy and immunofluorescence at baseline, but, post-infarct used dual immuno-gold electron microscopy to confirm NOS1AP localisation to the sarcolemmal membrane without concomitantly using confocal microscopy and immunofluorescence. The spatial resolution and sensitivity of these techniques are naturally very different and so we cannot be sure that there was an absence of NOS1AP at the sarcolemmal membrane at baseline. Additionally, Beigi *et al.* [112] were unable to detect any NOS1AP immunofluorescence signal in *Nos1*$^{-/-}$ mice despite detecting no significant changes in NOS1AP protein via Western blotting compared to wild-type mice. This may suggest that antibody binding to specific epitopes may be dependent on conformational changes dependent on the formation of a NOS1AP-NOS1 complex.

In my experiments, I was not able to reliably quantify immunofluorescence staining for NOS1 or NOS1AP in isolated cardiomyocytes. This may have been due to a combination of the low protein expression level, the antibody specificity and the staining protocols. Accordingly, whilst no quantitative measurements of co-localisation with NOS1 were possible, the NOS1AP-Tg had an increased abundance of NOS1AP which appeared to be distributed at the sarcolemmal membrane and in the nucleus.

Overall, further investigation of whether distribution of NOS1 is altered consequent to NOS1AP is needed, preferably using higher resolution imaging techniques.

4.4.5 Sex-specific differences

As seen in **Figure 3.12**, female mice had a shorter QT interval than their male littermates, which was seen in both wild-type and transgenic mice. This was not accompanied by a significant difference in VT induction probabilities. We did not observe any changes in APD parameters explaining this in these experiments, nor did we see changes in I_{Na} or NOS activity. The differences in humans between sexes are heart rate specific, with females specifically having a longer QT

interval at slower heart rates. Electrophysiological sex-specific differences in mice have not yielded consistent results across a variety of measured parameters, with most explanations for this relating to strain specific differences as well as possible heart rate specific measurements [68].

I did not have sufficient numbers of mice from both sexes to draw conclusions regarding differences in conduction velocity or Cx43 protein levels between genders. Having said that, the very small variation in conduction velocity measurements seen in the transgenic mice (across both sexes) suggest that potential sex differences in these parameters may not explain the differences between sexes in the ECG parameters seen. Once again, it is unclear whether the shorter QT intervals measured on surface ECG in female mice (both wild-type and transgenic) truly represent accelerated repolarisation or are a murine ECG specific measurement quirk.

Whilst I have investigated the mechanisms underlying some of the differences in ECG parameters seen in the NOSlAP-Tg in the ventricle, the mice also notably had a prolonged P-wave duration and PR interval on ECG. In **Chapter 5**, I investigate whether these surface ECG changes in NOSlAP-Tg mice are a reflection of an altered atrial electrical substrate predisposing to atrial arrhythmogenesis with further discussion about how NOSlAP may affect the electrical substrate and predispose to arrhythmogenesis in the discussion in **Chapter 7**.

5

Atrial arrhythmias in Tg(*Myh6-hNOS1AP*)

Summary

Genetic variants that have been associated with increased ventricular *NOS1AP* gene expression, have not, as yet, been directly implicated in GWAS of other ECG parameters such as P-wave duration, PR interval or associated with an increased risk of AF. Nevertheless, along with altered ventricular ECG parameters, NOS1AP-Tg mice also had a prolonged P-wave duration and PR interval and a much higher propensity to develop atrial arrhythmias in response to burst pacing *in-vivo*. Overall, this suggests that NOS1AP overexpression affected not only the ventricular, but also the atrial electrical substrate and facilitated arrhythmia induction in both chambers. The relevance of these findings in humans is at present unclear.

5.1 Introduction

As shown in **Figure 3.13**, NOS1AP overexpression was associated with an increased propensity to pacing-induced ventricular arrhythmias *ex-vivo*. However, I also found that atrial ECG parameters – specifically P-wave duration and PR interval were prolonged in transgenic mice compared to wild-type littermates. I therefore wondered whether the changes in atrial ECG parameters may reflect further alterations in the underlying substrate that may affect atrial arrhythmogenesis.

5.1.1 ECG parameters in murine models of atrial arrhythmias

Atrial fibrillation (AF) is the main atrial arrhythmia in humans and is thought to dependent on an interplay between a complex atrial electrical substrate and triggers, prominently from the pulmonary veins [226]. In mice, modelling changes in the atrial electrical substrate can lead to an increased propensity to AF, albeit typically requiring induction rather than occurring spontaneously [227,228]. A wide range of murine models have been developed to investigate different aspects of the arrhythmia [227,228].

In the NOS1AP-Tg, atrial mRNA levels of *GJA1* were not different to wild-type (**Figure 4.15**). However, the main atrial-specific connexin is connexin-40 (encoded by *GJA5*) [157]. Mice with connexin-40 deficiencies have been described as having prolonged P-wave duration and PR intervals, conduction slowing, and an increased propensity to atrial arrhythmias [160,161,229]. Relevant to the ECG findings in the NOS1AP-Tg mice, knock-in mice models using different *SCN5A* mutants from human families have also showed prolonged PR intervals on surface ECG and an increased tendency to burst pacing induced atrial arrhythmias [230,231]. This suggests that the 'end-point' of an altered electrical substrate represented by the surface ECG parameters may encompass multiple pro-arrhythmic molecular mechanisms.

5.1.2 NOS1AP, QT interval and AF in humans

Beyond the QT interval, genetic variants in *NOSIAP* have not, as yet, been directly implicated in GWAS of other ECG parameters such as P-wave duration, PR interval or for genetic risk of AF. This may be related to not having a direct effect on the ECG parameters but equally, stringent GWAS

statistical discovery thresholds do mean that smaller effects may not be detected, especially in GWAS with a relatively small sample size such as those for P-wave duration, which identified only 15 'significant' variants [152].

In GWAS of normal individuals, genetic variants in *SCN5A* have been reported as being relevant to P-wave duration [152], the PR interval [154] and genetic risk of AF [232]. Genetic variants in both *GJA1* and *GJA5* have recently been shown to be associated with the PR interval [233], but only variants in *GJA5* (expressing connexin-40) have been shown to be associated with a genetic risk of AF [232]. In human patients with long QT syndromes (LQTS1 – 3), associations with an increased incidence of atrial arrhythmias have been described, presumed to be due to shared associations between atrial and ventricular substrates [44-46]. Thus, there is evidence of a mechanistic link between altered ECG parameters reflecting an underlying electrical substrate and both ventricular and atrial arrhythmogenesis in humans.

Overall, I hypothesised that the mechanisms reflecting the altered ventricular substrate in the NOS1AP-Tg mice outlined in **Chapter 4** may be reflected by the altered atrial ECG parameters on surface ECG and that this may be linked to an increased risk of atrial arrhythmias in the transgenic mice.

5.2 Chapter specific methods

5.2.1 Atrial fibrillation induction *in-vivo*

After ECG measurements as described in **Section 3.3.4**, anaesthetised mice had an octapolar catheter (CIBer mouse EP catheter, NuMed Inc.) inserted directly into the oesophagus. The catheter was positioned at the location of the maximal amplitude of the measured atrial signal. The minimum pacing threshold was determined (defined as minimum output at which a pacing stimulus captured the atrium and generated a P-wave) and output programmed to be twice this value at 1 ms duration. Using a custom script, the burst pacing protocol consisted of 40 individual stimuli delivered initially at 60 ms intervals, with each burst decrementing by 2 ms until a minimum coupling interval of 10 ms was reached. In between each burst, the ECG response of the atria was observed and the protocol paused if atrial fibrillation (absence of P-waves, irregular R-R intervals) was induced and not recommenced until sinus rhythm was restored spontaneously. This protocol was repeated three times for each mouse.

For subsequent analysis, the ECG data for each mouse was reviewed. A minimum duration of AF of 2 seconds was needed for a pacing train to have deemed to have induced AF, although further sensitivity analyses were performed with minimum durations of 5 and 10 seconds. The proportion of wild-type or transgenic mice developing any episode of AF was calculated, as well as the probability of any given pacing train to induce AF in any mouse (number of episodes of AF/total pacing trains expressed as a percentage). The duration of each episode of AF was measured (from the end of the final pacing stimulus and ending with the first sinus P-wave) and thus the cumulative duration of arrhythmias (sum of all AF episodes) as well as the mean duration of any arrhythmia (sum of all AF episodes / number of episodes) calculated for each mouse.

5.2.2 Assessment of protein expression

Protein expression was assessed using Western blotting as described in **Section 2.2**. Specifically, protein homogenates from left and right atrial tissues were separated on 10% Bis-Tris NuPage gels (ThermoFisher Scientific) and separated using gel electrophoresis at 180 V for ~100 minutes at room temperature. Samples were then transferred onto nitrocellulose membranes in transfer

buffer with 10% methanol for connexin blots at 250 mA for 120 min at 4°C. After cutting membranes at appropriate molecular weights, blocking of non-specific binding was performed using 5% skimmed milk in phosphate buffered saline with 0.1% Tween-20 (ThermoFisher Scientific). This was followed by incubation with the primary antibodies (rabbit monoclonal anti-connexin 40 36-4900, ThermoFisher Scientific, at 1:1000 dilution; and rabbit monoclonal anti-β tubulin, BT7R MA5-16308 ThermoFisher Scientific, at 1:2000) overnight at 4°C. After washing, appropriate species-specific secondary antibodies at 1:25000 for anti-mouse and 1:50000 for anti-rabbit were added for one hour and then washed off. Membranes were developed using Dura extended duration substrate for connexin blots (ThermoFisher Scientific).

5.2.3 Statistical methods

Sample sizes for experiments were based on power calculations for determined using GPower 3.1 (Universitat Dusseldorf, Germany) using a power of 90% power and 5% significance level ($\alpha = 0.05$). For these experiments, a 10% difference between genotypes of probability of AF induction was chosen as the main outcome, reflecting the ~15-20% difference in P-wave duration and QT interval on surface ECG in transgenic mice. A minimum sample size of 19 per group was needed to detect a 10% difference in the main outcome between groups with wild-type AF induction probability estimated at 10% with a standard deviation of 10%.

Data were analysed using GraphPad Prism 7 (GraphPad Software Inc.). Normality of data was assessed using the D'Agostino Pearson test. Statistical testing between groups was performed by two-tailed unpaired *t*-tests for normally distributed data, Mann-Whitney tests for non-parametric data, or chi-squared tests for proportions. Data was expressed as mean and standard deviation for normally distributed data and median and interquartile ranges for non-normally distributed data.

AF induction was performed by me in a blinded manner to genotype with unblinding only occurring after the analysis dataset was completed.

5.3 Results

5.3.1 The probability of *in-vivo* pacing induced atrial arrhythmias is increased in transgenic mice

The *in-vivo* atrial arrhythmia induction protocol was performed in 21 wild-type mice (13 males and 8 females) and 19 transgenic mice (8 males and 11 females) aged 16 – 20 weeks. As shown in **Figure 5.1**, some mice developed atrial arrhythmias, mainly atrial fibrillation, but occasionally atrial flutter after rapid burst pacing of the left atrium via a transoesophageal catheter under general anaesthesia. It was not always possible to be certain of the specific nature of the arrhythmia based on the ECG (fibrillation vs flutter) so they were grouped together.

Figure 5.1 – Representative ECG trace showing burst pacing induced atrial arrhythmia

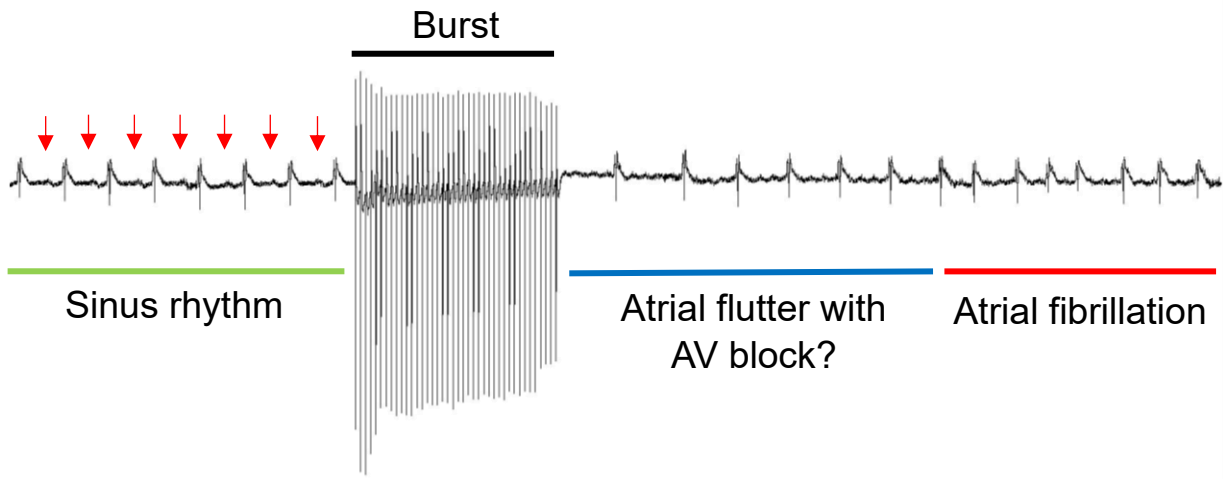


Figure 5.1: Surface ECG recording from mouse under general anaesthesia showing P-waves (red arrows) and sinus rhythm before a transoesophageal burst of atrial pacing. This is followed initially by what may represent atrial flutter with variable atrio-ventricular nodal block and then by an irregular rhythm with no discernable P-waves – i.e. atrial fibrillation (AF).

The probability of developing an atrial arrhythmia of >2 seconds duration after any given burst of pacing (i.e. number of bursts inducing arrhythmia out of total of 78 bursts) was significantly higher in transgenic mice (median 13%, interquartile range [IQR]: 2.6 – 22) compared to their wild-type littermates (median 0%, IQR: 0 – 3.2; *P* for difference $< 1 \times 10^{-4}$; **Figure 5.2 A**). As discussed in **Section 5.2.1**, the atrial arrhythmia had to be sustained for a minimum duration of 2 seconds after pacing termination for it to count as an episode. To test the sensitivity of this time cut-off, I

investigated if similar results were obtained using sustained arrhythmia minimum durations of 5 and 10 seconds and found a similar pattern (**Figure 5.2 C** and **E**).

Furthermore, a higher proportion of transgenic mice had at least one episode of atrial arrhythmia lasting more than 2 seconds as compared to their wild-type littermates (84% vs 43%, $P = 0.01$; **Figure 5.2 B**). Using minimum arrhythmia durations of 5 and 10 seconds, a similar pattern was observed (**Figure 5.2 D** and **F**), with more transgenic mice having atrial arrhythmias (84% vs 38%, $P = 0.004$ for both time cut-offs).

Delving deeper, the cumulative duration of all atrial arrhythmias induced per mouse was also higher in transgenic mice compared to their wild-type littermates, again robust to different time cut-offs used to define sustained arrhythmia (**Figure 5.3 A, C** and **E**). This is perhaps unsurprising given the transgenic mice had more episodes of atrial arrhythmia. To clarify whether there were any differences in the 'sustainability' of atrial arrhythmias, I evaluated the median duration per episode of atrial arrhythmias, excluding mice who had no arrhythmias. This showed no differences between genotypes (**Figure 5.3 B, D** and **F**), suggesting that the transgenic mice overall had a higher propensity to atrial arrhythmia induction but not to arrhythmia sustainability. There were no sex-specific differences noted in the main end-points (**Figure 5.4**).

Figure 5.2 – Probabilities of atrial arrhythmia induction for Tg(*Myh6-hNOS1AP*) colony

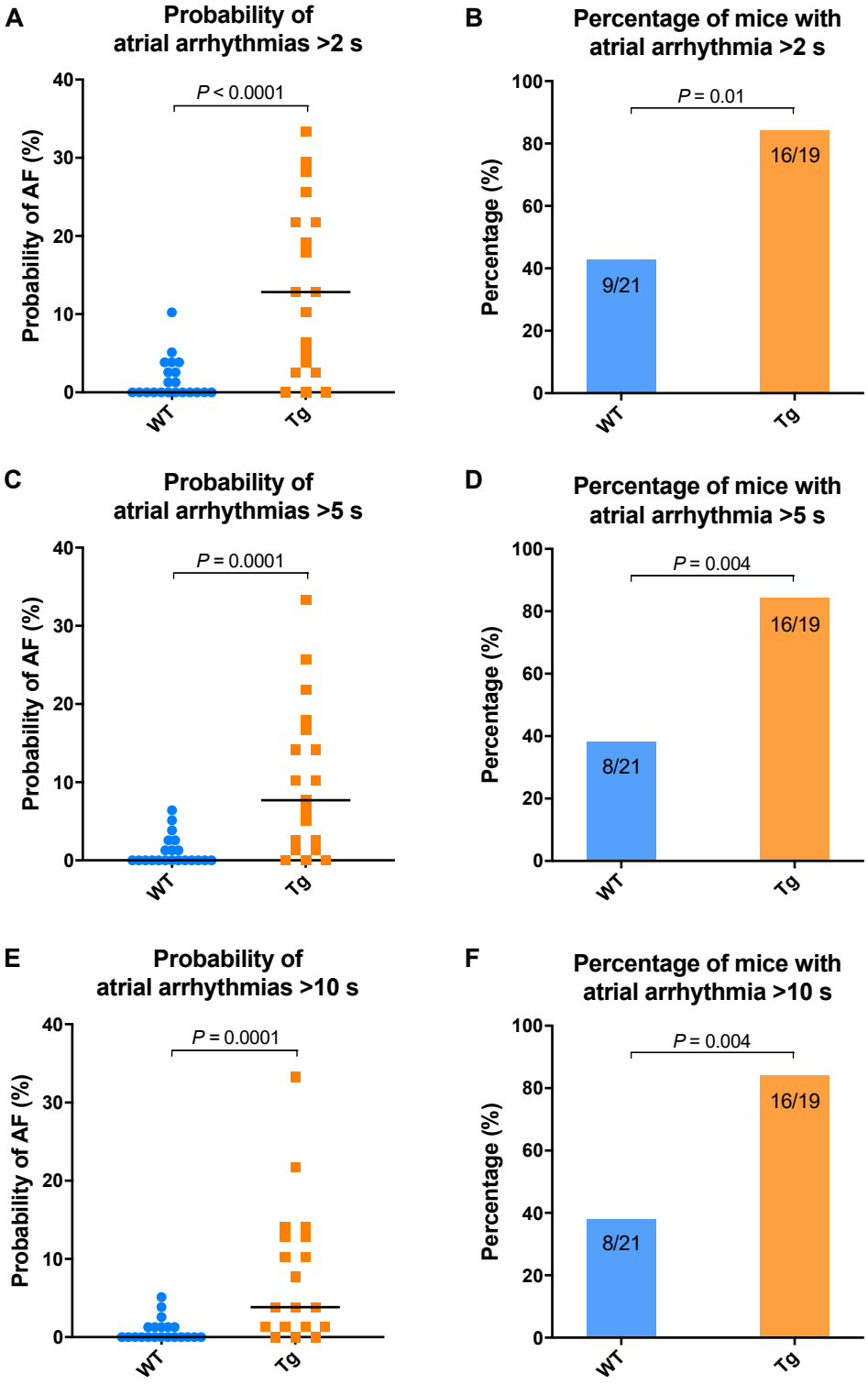


Figure 5.2: Left-hand panels show the probability of any given burst pacing stimulus inducing an atrial arrhythmia of a minimum of (**A**) 2, (**C**) 5 or (**E**) 10 second durations (number of episodes of arrhythmia/total pacing trains); horizontal lines represent median values with Mann-Whitney test for comparisons. Right-hand panels show proportions of wild-type (WT, n=21) or transgenic (Tg, n=19) mice developing any episode of atrial arrhythmia of (**B**) 2, (**D**) 5 or (**F**) 10 second duration in response to burst pacing; Fisher's exact test for comparisons.

Figure 5.3 – Duration of induced atrial arrhythmias for Tg(*Myh6-hNOS1AP*) colony

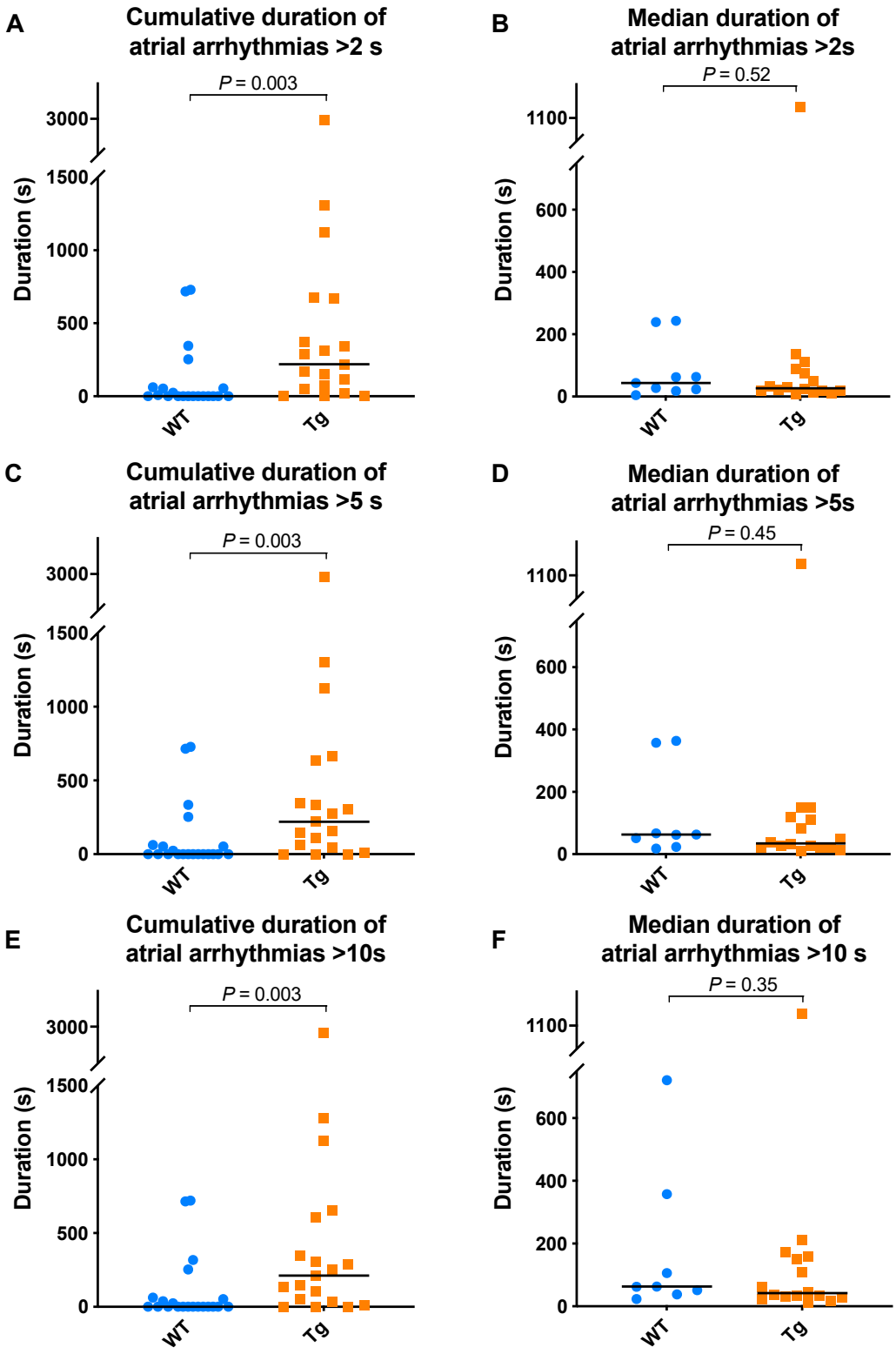


Figure 5.3: Left-hand panels show total cumulative duration of all atrial arrhythmias in wild-type (WT, total n=21) or transgenic (Tg, total n=19) mice induced by burst pacing with minimum lengths of (**A**) 2, (**C**) 5 or (**E**) 10 seconds. Right-hand panels show the median duration of any arrhythmia with minimum lengths of (**B**) 2, (**D**) 5 or (**F**) 10 seconds, excluding animals with no arrhythmia documented. Across all panels, horizontal lines represent median values with Mann-Whitney tests for comparisons.

Figure 5.4 – Probability of atrial arrhythmia induction for Tg(*Myh6-hNOS1AP*) colony by sex

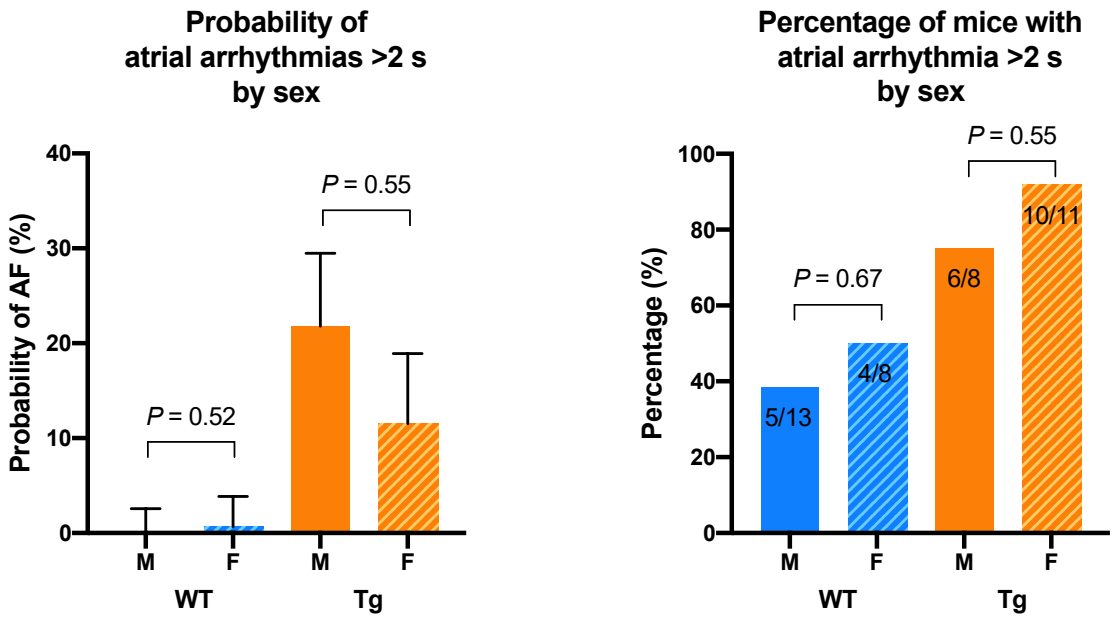


Figure 5.4: The left-hand panel shows the probability of any given burst pacing stimulus inducing an atrial arrhythmia of a minimum of 2 seconds durations (number of episodes of arrhythmia/total pacing trains) with bars representing median values and interquartile ranges with Mann-Whitney test for comparisons between sex within genotype (wild-type; WT, n=13 males; M and 8 females; F and transgenic; Tg, n=8 M and 11 F). The right-hand panel shows proportions of wild-type (WT, n=21) or transgenic (Tg, n=19) mice developing any episode of atrial arrhythmia of 2 second duration in response to burst pacing; Fisher's exact test for comparison between sex within genotype only.

5.3.2 Exploratory data on atrial connexin-40 protein levels

Exploratory investigation of left and right atrial protein levels of connexin-40 (the main atrial form of connexin) suggested possible reductions in transgenic mice (**Figure 5.5**).

Figure 5.5 – Exploratory atrial connexin-40 protein expression

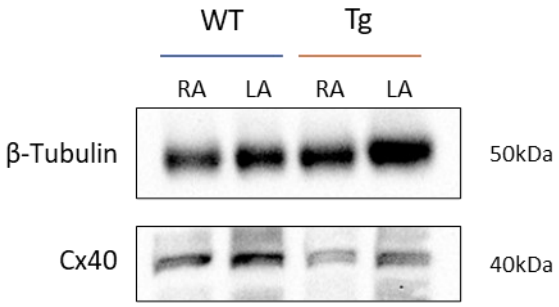


Figure 5.5: Connexin-40 (Cx40) protein expression in right and left atrial (RA, LA) homogenates from a wild-type (WT) and transgenic (Tg) mouse.

5.4 Discussion

5.4.1 Atrial Arrhythmogenesis in NOS1AP-Tg

The NOS1AP-Tg mice developed more *in-vivo* atrial arrhythmias in response to burst pacing compared to their wild-type littermates as assessed by different measures, but the mean arrhythmia duration was not different between genotypes. In conjunction with the prolonged P-wave duration, this suggests that NOS1AP overexpression leads to a significantly altered atrial electrical substrate with a propensity to arrhythmogenesis in response to triggers.

Drawing major conclusions about arrhythmia sustainability in murine models is challenging. Previous theories relying on macroscopic concepts of mechanisms of AF held that a critical size of atrium would be required for a fibrillatory wave to propagate and therefore, that the murine atrium might not be able to do so [149]. Whilst no longer felt to be accurate, it is clear that transgenic murine models that do develop arrhythmia have some other abnormality to allow the arrhythmia to sustain. For example, mice with TGF-β overexpression display an increased propensity to AF induction due to atrial fibrosis without changes in gross atrial structure, but, with abnormalities in atrial conduction in the absence of changes in action potential properties or surface ECG parameters [234].

The NOS1AP-Tg did have changes in atrial surface ECG parameters, and while I explored in more depth in **Chapter 4** the mechanistic changes in the ventricular electrical substrate, I did not have a chance to extend this to the atria. There are important electrophysiological differences between the atria and ventricles in mice, relevant to the work presented earlier. Murine atrial APDs are shorter than those in the ventricle [235]. In the atrium, both connexin-40 as well as connexin-43 are expressed [199]. A variety of connexin-40 knockout mouse models showing atrial arrhythmogenesis have shown prolonged P-wave duration, PR intervals and QRS intervals, similar to those seen in the NOS1AP-Tg mice [160,161,229]. However, the models have shown either significantly prolonged QT [160,161] or a slightly shorter QT interval [229], probably highlighting the difficulty of measuring murine QT intervals.

Overall, the evidence suggests that in the transgenic mice, NOS1AP overexpression likely leads to a global change in electrical substrate across the atria and ventricles which predisposes to arrhythmogenesis. Further work would be needed to explore whether the mechanisms underlying the arrhythmic substrate in the atria are similar to those seen in the ventricles of NOS1AP-Tg mice.

5.4.2 Implications for human atrial arrhythmogenesis

Whilst ventricular arrhythmias may be considered to be more 'serious', atrial arrhythmias and AF in particular are far commoner and are associated with significant morbidity and mortality [236]. Arrhythmias in humans are multifactorial in origin and investigating mechanistic changes in the myocardial electrical substrate that may affect these arrhythmias is more challenging on a population level. Genetic variants in *NOS1AP* have not yet been implicated in GWAS for AF, but stringent thresholds for significance mean that it might take larger sample sizes to detect smaller effects, especially in 'normal' individuals.

Looking at the extremes, Kirchhof *et al*. [44] investigated atrial electrophysiology invasively in patients with genetically proven long QT syndrome and found a longer APD and increased incidence of spontaneous atrial arrhythmias with an undulating P-wave axis compared to controls. They suggested that these episodes of 'atrial torsades' may degenerate to AF. In a larger single-centre dataset, patients with long QT syndrome were found to have a 17.5-fold increased risk of AF compared with age-matched controls, with the mean age of diagnosis of AF being 24 years old [45]. Equally, Hong *et al*. [237] reported a gain of function mutation in *KCNQ1*, a gene encoding potassium channel subunits which was associated with a short QT interval and AF, more in keeping with findings from human atrial tissue of patients with AF having shorter APDs, possibly due to enhanced delayed rectifier potassium currents due to a reduction in NOS1 [126].

In patients with Brugada syndrome, data across observational studies have suggested a high incidence of AF estimated at ~22% [238]. Some studies suggested patients with Brugada syndrome had a longer P-wave duration compared to controls over prolonged ECG monitoring with some data suggesting that this might be due to slowed inter-atrial (rather than intra-atrial) conduction

[238]. Other studies went as far as screening patients who developed AF below the age of 45 and found that approximately ~16% met criteria for a diagnosis of Brugada syndrome [239].

Overall, these findings suggest that variation in genes such as *NOSIAP* affecting ECG parameters, such as the QT interval, may reflect common changes in electrical parameters across both atria and ventricles also predisposing to atrial arrhythmogenesis. Non-invasive markers of the electrical substrate in the form of the P-wave duration, PR interval and QT interval on surface ECG have all been associated with increased incidences of AF in large observational studies [48,240,241].

Chapter 6 describes this further and reports work I undertook to investigate the causal nature of the association between ECG parameters and AF in large human datasets.

6

Causal relevance of ECG parameters and atrial arrhythmias in humans

Summary

Prolonged atrial ECG parameters but a shorter QT interval in the NOSIAP-Tg mouse are associated with an increased incidence of atrial arrhythmias. In humans, a variety of ECG parameters have been associated with risks of development of atrial fibrillation (AF) in observational studies. However, these are subject to limitations such as confounding and reverse causality so the causal relevance is unclear. We used Mendelian randomisation to avoid some of these limitations by using weighted genetic scores for P-wave duration, PR interval and QT interval to represent lifelong differences in cardiac electrical parameters. Here, we showed novel evidence supporting causal relationships between lifelong differences in cardiac electrical parameters and risks of developing both AF and non-AF supraventricular tachycardias in large human population datasets. Unexpectedly, results supported a causal association between lifelong differences in ECG parameters representing longer atrial conduction times within the normal range, and a lower risk of AF. In particular, genetically predicted differences in PR interval showed robust associations across a broad range of analyses and mechanistic pathways.

The work presented in this chapter formed the basis of a publication [242].

6.1 Introduction

Having observed a relationship between altered ECG intervals and risk of atrial arrhythmias in the NOS1AP-Tg mice as discussed in **Chapter 5**, I wished to ascertain whether this relationship was applicable in humans. Specifically, I wished to investigate whether differences in ECG parameters (as a reflection of an altered electrical substrate) predisposed to atrial fibrillation (AF), or, whether they were predominantly biomarkers of disease related to other conditions such as ischaemic heart disease or hypertension that might also affect the risk of AF.

6.1.1 Historical perspective of ECG parameters and atrial fibrillation

After spending time in Einthoven's laboratory, a young British physician, Thomas Lewis, returned to London in 1908 with an ECG machine. In conjunction with a general practitioner, James Mackenzie, he became interested in atrial, or auricular fibrillation. After modifying the techniques used to record the ECG, he realized that the rhythm that Mackenzie had thought to originate from the atrio-ventricular node actually arose from fibrillation of the atria as the R waves were relatively normal and that the 'f-waves' seemed to be present regardless [243]. In 1930 came the first reports from Wolff, Parkinson and White of a series of patients with paroxysms of atrial fibrillation (AF) and short PR intervals with no structural heart disease [244], but attributing the short PR interval to vagally mediated alterations. Early debate surrounded the mechanism of AF being either related to a re-entrant mechanism [245-247] or being as a result of an ectopic focus [248,249].

With more routine use of the ECG as a diagnostic tool, AF was being recognized and diagnosed more commonly, with a case series of 500 patients in 1955 with AF describing dyspnoea and systemic embolism as adverse consequences [250]. As the incidence of AF increased and digital ECG technology progressed, by the late 70s and early 80s came small studies suggesting that a prolonged P-wave on an ECG represented inter-atrial conduction block and was associated with atrial arrhythmias [251,252]. However, it remained unclear whether this was simply a biomarker (postulated to be due to an underlying fibrotic processes) or specifically causal in the pathogenesis of AF.

6.1.2 Contemporary perspective of mechanisms of atrial fibrillation and ECG parameters

Despite extensive research, our understanding of the specific mechanisms of AF remains incomplete. Broadly speaking, two electrophysiological mechanisms of importance in AF have been proposed over the years: ectopic activity and re-entry. These factors likely interact to initiate and sustain AF and their importance may vary between individuals, and indeed, within individuals over time. Early in the disease process, triggers appear to be of more importance and episodes of AF are paroxysmal. As the disease progresses, the underlying substrate which sustains AF starts to play more of a role in the disease becoming persistent.

Triggers for atrial fibrillation

The importance of ectopic foci was conclusively demonstrated in 1998. In a landmark paper, Haïssaguerre *et al.* [253] observed that pulmonary vein ectopy (demonstrated as frequent atrial ectopics on longer ECG recordings) in particular was an important trigger for paroxysmal AF and that catheter ablation could reduce the occurrences of AF. These observations in particular have led to the development of electrical isolation of the pulmonary veins as a mainstream therapeutic procedure and being given a Class I indication for rhythm control after failure of drug therapy for AF in the latest European Society of Cardiology guidelines [236].

Substrate for sustaining atrial fibrillation

In a number of people, AF is persistent and sinus rhythm is not easily restored. Typically, this occurs after initial paroxysms of AF. The phrase 'atrial fibrillation begets atrial fibrillation' was coined after Allessie's experiments in goats, where pacing electrodes inducing AF in awake goats caused longer paroxysms of AF until they were sustained [254]. This was accompanied by 'electrical remodelling' where atrial effective refractory periods markedly shortened over time and likely contributed to sustaining AF.

For a sustained arrhythmia like AF, the substrate on which the arrhythmia persists is a very important part of the mechanism. Beyond changes in ion channel function, it is clear that changes in atrial structure – fibrosis, loss of cell-cell integrity and possibly inflammation all contribute to

changes in conduction velocity, alterations in homogeneity of refractoriness and increases in spontaneous electrical activity that seem to generate a substrate conducive for AF to persist [255]. These changes also seem to have a positive feedback loop with further structural remodeling continuing, both as a result of AF itself but also the other underlying conditions (e.g. hypertension, diabetes, atrial stretch) that continue to progress.

The ECG in atrial fibrillation

The complexities of AF can be detected on a macroscopic electrophysiological level by the ECG. This is in the form of increasingly sophisticated analysis of the atrial 'f-waves' seen. In persistent AF in particular, f-wave amplitude and dominant frequency have been shown to correlate with recurrence of AF after electrical cardioversion [256,257] or catheter ablation [258,259], although the results are by no means conclusive [260]. Whilst interesting, these detailed ECG analytics have not translated into widespread clinical use, predominantly because they require sophisticated hardware and signal post-processing, suggesting that there is still a need for simpler methods to assess the electrical substrate.

6.1.3 Observational data linking ECG parameters and AF

In contrast to the specialist electrophysiological measurements taken from individuals whilst in AF, the widespread utilisation of the conventional 12-lead ECG has made it possible more recently for large population-based observational studies to investigate the associations between non-invasively derived and routinely measured ECG parameters (P-wave duration, PR interval and QT interval) and risk of incident AF.

P-wave duration and AF

A number of large studies have shown associations between P-wave duration measured on ECG and incidence of AF [240,261,262]. Magnani *et al.* [261] showed in 1,550 participants from the Framingham Heart Study (FHS) who were aged 60 and above at baseline that maximal P-wave durations >95th percentile (>110 ms) were associated with a higher risk of AF over a median follow-up of around 16 years. Magnani *et al.* [262] subsequently combined data from the FHS cohort as well as the Atherosclerosis Risk In Communities (ARIC) study and showed that in over 11,000

patients with a mean age of 62 years at baseline, that a maximal P-wave duration of >120 ms was associated with a higher incidence of AF compared to P-wave durations of ≤120 ms.

To date, the largest study examining the relationship between P-wave duration and risk of AF was reported by Nielsen *et al*. [240] and came from the Copenhagen ECG study. Here, in ~290,000 individuals, both short (<89 ms) and longer (> 110 ms) P-wave durations on the ECG were associated with an increased incidence of developing AF when compared to the 'reference' group of P-wave durations of 100-105 ms. As this study involved all participants routinely referred for an ECG for clinical reasons, further analysis showed that those with shorter P-wave durations were younger and had fewer cardiovascular risk factors at baseline compared with those with longer P-wave durations who tended to be older and having a higher prevalence of cardiovascular risk factors. However, the findings persisted after extensive multivariable adjustment for common cardiovascular risk factors as well as various medications that might affect the P-wave. Interestingly, in a subset of people who had cardiac CT, there was only a weak association between P-wave duration on ECG and left atrial end-diastolic volume suggesting that atrial conduction velocity (rather than atrial size) was a more important determinant of P-wave duration on ECG. The authors hypothesised that the associations seen outside of the normal ranges between longer P-wave duration and a higher risk of AF may be explained by prolonged atrial remodeling whilst the shorter P-wave duration and higher risk of AF may be more related to electrical re-entry.

PR interval and risk of AF

PR interval measurements are more clinically used and easier to measure on ECGs and have been associated with incidence of AF as well [241,263,264]. In a study of ~7,500 individuals from the FHS with a mean age of 47 years at baseline, Cheng *et al*. [263] reported PR interval prolongation particularly >200 ms (the clinical definition of 'abnormal') was associated with a 4-fold higher risk of developing AF compared to those with PR intervals of ≤200 ms. After multivariable adjustment for cardiovascular risk factors, these findings remained significant with a 2-fold higher risk of AF if the baseline PR interval was >200 ms, which was similar to the risk reported by Perez *et al*. [265]. In the ARIC study, Smith *et al.* [264] reported similar findings of an increased risk of AF in those

with baseline PR intervals >200 ms but additionally suggested that differing components of the PR interval may be associated with different risks of AF.

The Copenhagen ECG study is largest observational dataset showing associations between the PR interval and incidence of AF, from which Nielsen *et al.* [241] reported that PR intervals >200 ms were associated with an higher incidence of AF among ~290,000 individuals. Again, as with P-wave duration, those with longer PR intervals appeared to have a higher burden of cardiovascular risk factors and the authors acknowledged that they did not have data on blood pressure, body mass index and smoking status for use in their multivariable analyses which may lead to some residual confounding. They did find evidence that very short PR intervals (<123 ms) were also associated with a higher incidence of AF. Overall, similar to P-wave duration, the observational data suggest abnormally long and possibly abnormally short PR intervals are associated with a higher incidence of AF.

QT interval and risk of AF

The first reports linking the QT interval with an increased risk of AF came from observations in patients with Mendelian long QT syndromes as discussed in **Section 5.4.2**. In these patients, AF was noted to develop at a younger age than might be expected [45,46] and invasive electrophysiological testing suggested that these patients had electrophysiological abnormalities within the atria as well, suggesting a shared electrical substrate with the ventricle [44].

Whether the QT interval is associated with AF in otherwise healthy individuals has been investigated through a variety of observational studies in large populations [47-50]. Nielsen *et al.* [48] reported again from the Copenhagen ECG study and suggested that an extremely short QT_c (below 1st percentile, <370 ms) and also longer QT_c intervals (>430 ms) all were associated with an increased incidence of AF. Mandyam *et al.* [49] found that a prolonged QT_c (>450 ms) was associated with a higher risk of AF, with similar findings in a more ethnically diverse study reported by O'Neal *et al.* [50] from the Multi-Ethnic Study of Atherosclerosis cohort.

6.1.4 Limitations of observational data

Across the ECG parameters in the large observational datasets an increased risk of AF was associated with either short or long values outside of 'normal' reference ranges. However, observational studies are potentially subject to confounding, in particular by age and co-morbid cardiac conditions affecting both ECG parameters and the risk of developing AF. For example, P-wave or PR interval duration has been associated with hypertension [266], ischemic heart disease and heart failure [267], and the QT interval lengthens with age [268], all of which are established risk factors for AF. Whilst the observational studies attempted to adjust for these confounders, not all 'known' confounders were available within the datasets and of course 'unknown' confounders cannot be adjusted for. Furthermore, the association between ECG parameters and AF may be subject to reverse causality, since having a history of AF or being treated with rate or rhythm control drugs may alter ECG parameters. These potential biases limit the value of observational studies for making causal inferences.

6.1.5 Mendelian randomisation

Mendelian randomisation (MR) can limit some of these potential biases by using genetic variants as proxies for a trait and then assessing their association with an outcome of interest [269]. As the genetic variants are randomly allocated at conception, this produces a 'naturally randomised' experiment by which groups with different genetically determined levels of a trait should be balanced on all potential confounders (**Figure 6.1**).

To improve our understanding of the causal mechanisms for AF, I used genetic variants conferring lifelong differences in cardiac electrical parameters (P-wave duration, PR interval and QT interval separately), and examined their associations with AF among ~300,000 individuals in UK Biobank. Additionally, I was interested in investigating relationships between ECG parameters and other atrial arrhythmias, specifically non-AF supraventricular tachycardias (SVT) which are generally perceived as being mechanistically different from AF.

Figure 6.1 – Example overview of Mendelian randomisation

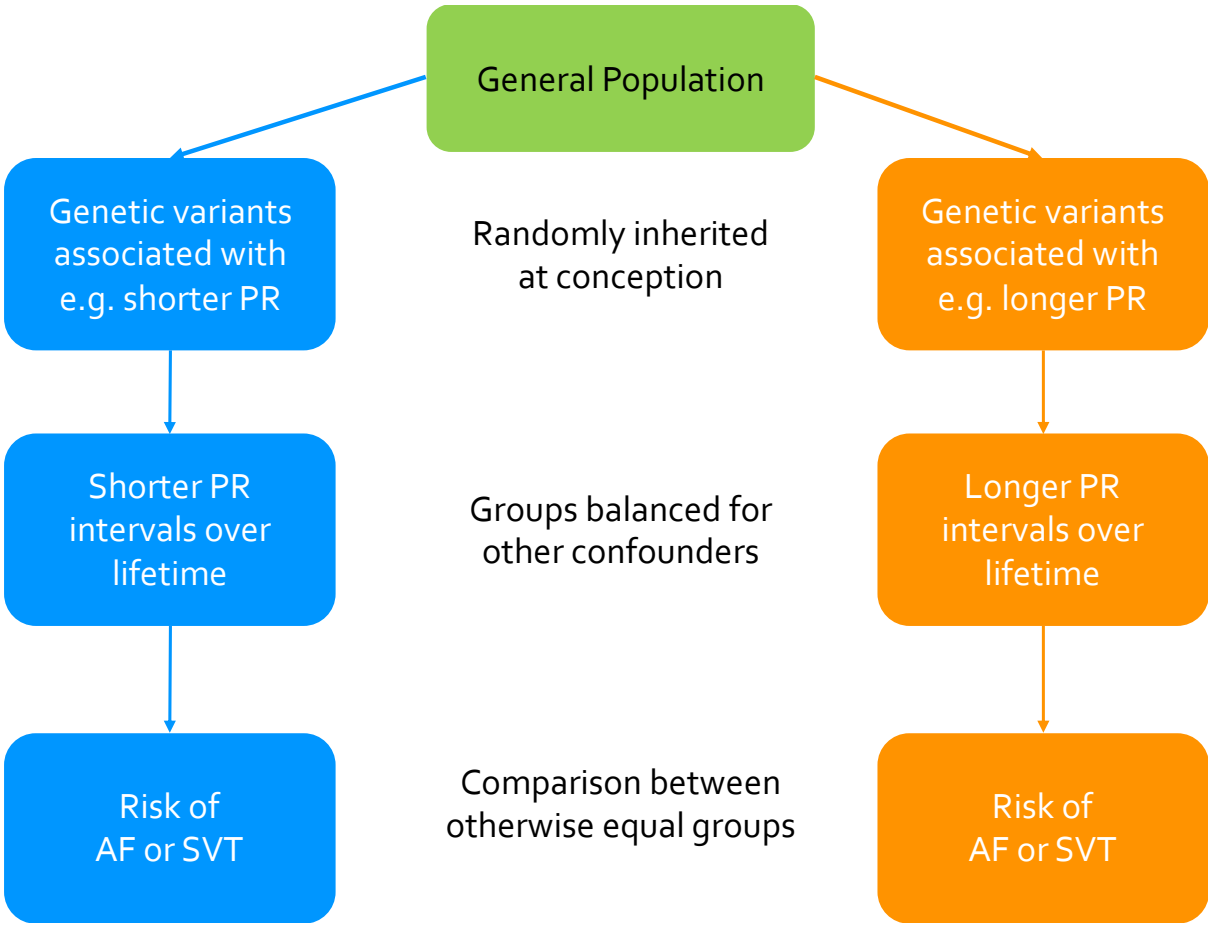


Figure 6.1: Example of concept of Mendelian randomisation as applied to ECG parameters and risk of atrial fibrillation (AF) and other supra-ventricular tachycardias (SVT).

6.2 Methods

The work presented adheres to the key principles of STROBE-MR [270].

6.2.1 Study populations and outcome definitions

UK Biobank

Primary analyses were conducted using individual level data in UK Biobank, a population-based study including ~500,000 individuals from the United Kingdom, who were 40 to 69 years old at the time of recruitment (2006-2010). UK Biobank includes extensive baseline data including medical history as well as prospective linkage to electronic healthcare records. Further information regarding the UK Biobank data as well as detailed genotyping procedures have been reported elsewhere [271,272]. In the present study, a total of 278,792 participants were included in the primary analyses, after exclusion of samples failing bioinformatic quality control (extreme heterozygosity, missing rate on autosomes of >0.02 and sex mismatch between reported and genetically inferred), those of non-white British ancestry and related participants. Resting 12-lead ECGs and interval measurements (using Cardiosoft v6 program, GE Healthcare, Chicago, USA) were available in 15,365 of these participants, and in 13,314 of those after excluding anyone who had AF on ECG, or AF identified from self-reports at baseline or electronic healthcare records. Cardiac magnetic resonance imaging (MRI) data on left atrial volumes indexed to body surface area were available in 2,581 participants after excluding 415 participants with either poor quality images, or AF identified from self-reports or electronic healthcare records. Details of the cardiac MRI protocol have been reported elsewhere [273]. A flow diagram detailing how the different datasets were generated is shown in **Figure 6.2**.

Figure 6.2 – Generation of main analyses datasets

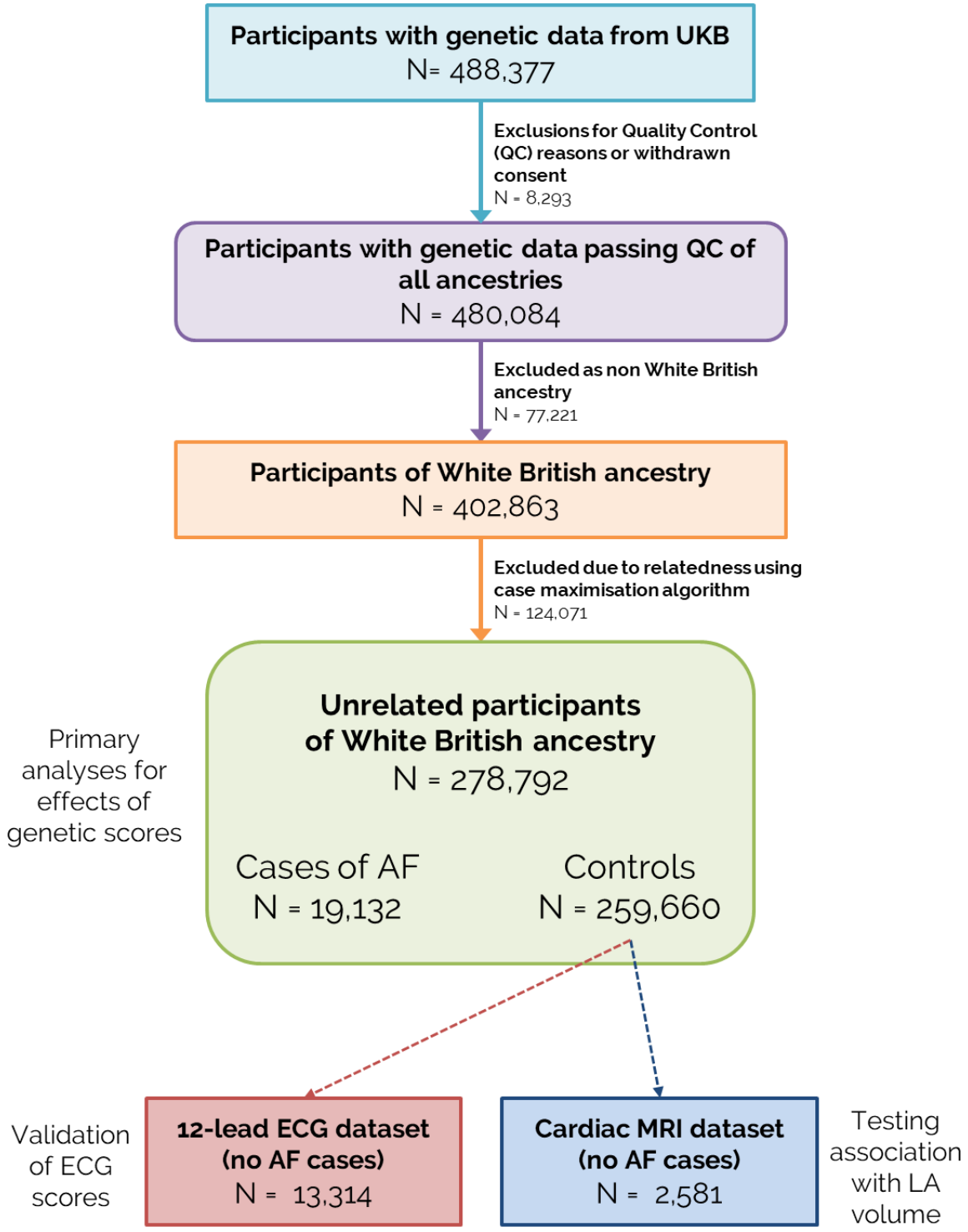


Figure 6.2: Flow chart depicting how main analyses datasets were generated using data from UK Biobank (UKB). AF: atrial fibrillation; MRI: magnetic resonance imaging; LA: left atrial.

Defining AF, SVT, and other outcomes in UK Biobank

We identified 19,132 cases of AF or flutter from electronic healthcare records (97% of cases) or self-reported at nurse-led interviews at baseline (3% of cases). Cases defined using healthcare records had at least one diagnostic code from: national in-patient hospital data statistics (International Statistical Classification of Diseases 10th revision [ICD-10] codes), procedure codes (national classification of interventions and procedure [OPCS-4]), or national death records.

For participants in England, data from in-patient hospital admissions was obtained from Hospital Episode Statistics for England (NHS digital) from 1996 – 31st March 2017, with information on cause of death from NHS Digital from April 2006 – 31st January 2018. For participants in Wales, data from in-patient hospital admissions was obtained from the Patient Episode Database for Wales (Secure Anonymised Information Linkage, Wales) from 1999 – 29th February 2016, with information on cause of death from NHS Digital from April 2006 – 31st January 2018. For participants in Scotland, data from in-patient hospital admissions was obtained from the Scottish Morbidity Record (Information and Statistics Division, Scotland) from 1996 – 31st October 2016 with information on cause of death provided by the same organisation from April 2006 -30th November 2016. See http://biobank.ctsu.ox.ac.uk/crystal/exinfo.cgi?src=Data_providers_and_dates for further details.

4,805 participants were identified as having 'lone' AF, defined as AF without known coronary heart disease, heart failure, hypertension or diabetes (based on self-reported medical conditions or electronic healthcare records available at baseline, as well as electronic healthcare record diagnoses up to one year after the first recorded AF diagnosis). Furthermore, 2,884 cases of non-AF SVT were identified using diagnostic codes that excluded AF or flutter and that had been previously validated in an external cohort [274]. Details of definitions of codes used for outcomes are listed in **Table 6.1** and **Table 6.2**.

Table 6.1 – Phenotype codes for definition of atrial fibrillation

Field	Description	Algorithm Elements
20002	Non-cancer illness code, self-reported	Atrial Fibrillation – 1471, Atrial Flutter – 1483
20004	Operation code	Cardiac Ablation – 1553, Cardioversion – 1524
41202	Diagnoses – main ICD10	Atrial Fibrillation or Flutter – I48*
41204	Diagnoses – secondary ICD10	Atrial Fibrillation or Flutter – I48*
41200	Operative procedures – main OPCS	K22.3 Exclusion of left atrial appendage, K57.1 Percutaneous transluminal ablation of atrioventricular node, K57.5 Percutaneous transluminal ablation of atrial wall, K62.1 Percutaneous transluminal ablation of pulmonary vein to left atrium conducting system, K62.2 Percutaneous transluminal ablation of atrial wall for atrial flutter, K62.3 Percutaneous transluminal ablation of conducting system of heart for atrial flutter, K62.4 Percutaneous transluminal internal cardioversion, K62.5 Percutaneous transluminal occlusion of left atrial appendage, X50.1 Direct current cardioversion, X50.2 External cardioversion
41210	Operative procedures – secondary OPCS	K22.3 Exclusion of left atrial appendage, K57.1 Percutaneous transluminal ablation of atrioventricular node, K57.5 Percutaneous transluminal ablation of atrial wall, K62.1 Percutaneous transluminal ablation of pulmonary vein to left atrium conducting system, K62.2 Percutaneous transluminal ablation of atrial wall for atrial flutter, K62.3 Percutaneous transluminal ablation of conducting system of heart for atrial flutter, K62.4 Percutaneous transluminal internal cardioversion, K62.5 Percutaneous transluminal occlusion of left atrial appendage, X50.1 Direct current cardioversion, X50.2 External cardioversion
40001	Underlying (primary) cause of death: ICD10	Atrial Fibrillation or Flutter – I48*
40002	Contributory (secondary) causes of death: ICD10	Atrial Fibrillation or Flutter – I48*

Table 6.1: Field codes refer to UK Biobank specific codes. ICD10: International classification of diseases, 10th edition; OPCS: OPCS Classification of Interventions and Procedures version 4; *Indicates all ICD10 sub-codes under main heading included.

Table 6.2 – Phenotype codes for other definitions

Disease	Code Type	Codes and Description
Supraventricular tachycardia	ICD10	Preexcitation syndrome – I45.6
		Supraventricular tachycardia – I47.1
		Atrial premature depolarisation – I49.1
	OPCS	Open division of accessory pathway within heart – K52.4
		Percutaneous transluminal ablation of conducting system of heart NEC – K57.2
		Percutaneous transluminal ablation of accessory pathway – K57.4
	Self-reported	Illness codes – 1484, 1487
Coronary Heart Disease	ICD10	Angina – I20*
		Acute Myocardial Infarction – I21*
		Subsequent Myocardial Infarction – I22*
		Certain current complications following acute myocardial infarction – I23*
		Other acute ischaemic heart diseases – I24*
		Chronic ischaemic heart disease – I25*
	OPCS	Transluminal balloon angioplasty of coronary artery – K49*
		Other therapeutic transluminal operations on coronary artery – K50*
		Percutaneous transluminal balloon angioplasty and insertion of stent into coronary artery – K75*
		Saphenous vein graft replacement of coronary artery – K40*
		Other autograft replacement of coronary artery – K41*
		Allograft replacement of coronary artery – K42*
		Prosthetic replacement of coronary artery – K43*
		Other replacement of coronary artery – K44*
		Connection of thoracic artery to coronary artery – K45*
		Other bypass of coronary artery – K46*
	Self-reported	Illness codes - 1074, 1075
		Operation codes – 1070, 1071, 1095
Heart failure	ICD10	Heart Failure – I50*
		Hypertensive heart disease – I11.0
		Hypertensive heart and renal disease – I13.0, I13.2
	Self-reported	Illness code – 1076
Hypertension	ICD10	Essential (primary) hypertension – I10*
		Hypertensive heart disease – I11*
		Hypertensive heart and renal disease – I13*
		Secondary hypertension – I15*
	Self-reported	Illness codes – 1065, 1072
Diabetes	ICD10	Insulin-dependent diabetes mellitus – E10*
		Non-insulin-dependent diabetes mellitus – E11*
		Other specified diabetes mellitus – E13*
		Unspecified diabetes mellitus – E14*
	Self-reported	Probable Type 1 and Type 2 Diabetes used from algorithm validated in UK Biobank data from Eastwood et. al, 2016 [275]

Table 6.2: Self-reported codes refer to UK Biobank specific codes. ICD10: International classification of diseases, 10th edition; OPCS: OPCS Classification of Interventions and Procedures version 4; *Indicates all ICD10 sub-codes under main heading included.

6.2.2 Selection of genetic variants

For each individual ECG parameter in turn, independent genetic variants with genome-wide significant associations ($P < 5 \times 10^{-8}$) were selected from published studies [55,152,154,276], none of which included UK Biobank participants. The coded allele was defined as being associated with a longer ECG interval. The P-wave duration score comprised 8 variants, the PR interval score comprised 52 variants and the QT interval score comprised 54 variants. An overview of the process is presented in **Figure 6.3**. To examine the specificity of any findings to electrical pathways, for each ECG parameter, we identified a subset of variants that were annotated to gene loci for known ion channels (e.g. *SCN5A, SCN10A, KCNQ1, KCNJ2)*.

Figure 6.3 – Details of genetic variant selection

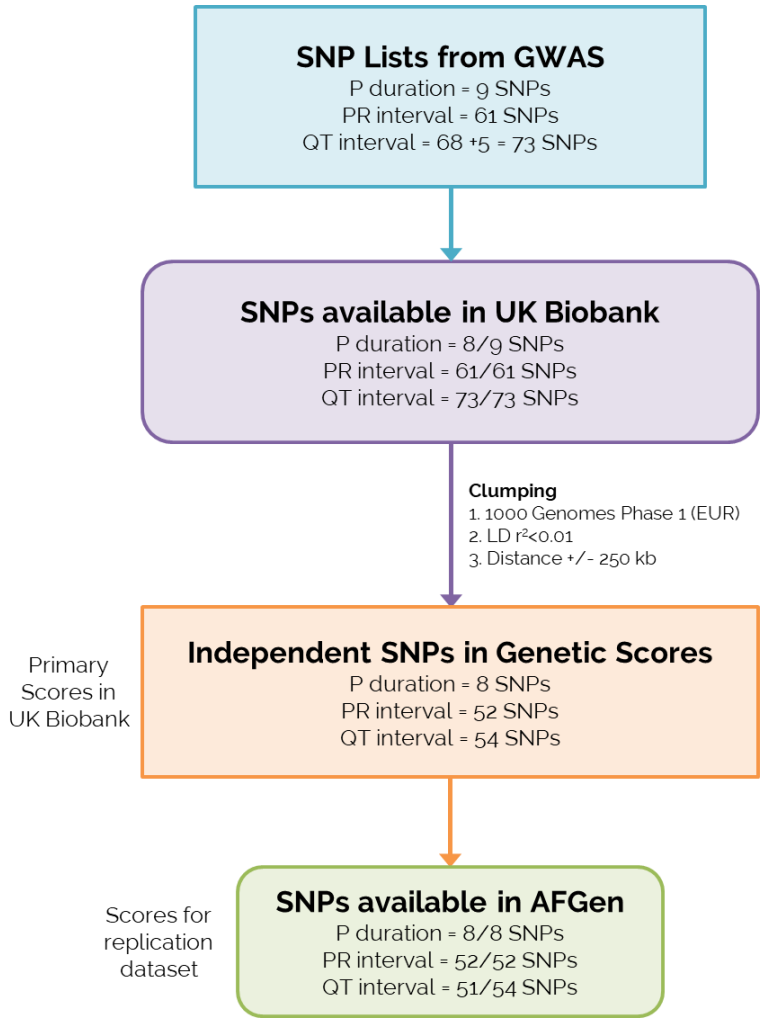


Figure 6.3: Overview of genetic variant selection for ECG genetic scores. AF: Atrial fibrillation; GWAS: Genome wide association study; LD: Linkage disequilibrium; SNP: Single nucleotide polymorphism.

Selection of genetic variants for P-wave duration score

A large-scale genome-wide association study (GWAS) meta-analysis for P-wave duration identified 9 individual single nucleotide polymorphisms (SNPs) that met genome-wide significance in nearly 38,000 individuals of European ancestry from a variety of studies, but not including UK Biobank [152]. Briefly, all studies used in the GWAS meta-analysis excluded participants with AF, an implanted pacemaker, Wolff-Parkinson-White syndrome, complete heart block and those who received medications altering atrioventricular nodal conduction (β-blockers, dihydropyridine calcium channel blockers, Vaughan-Williams class I and III anti-arrhythmic medications and digoxin) as well as those in whom the P-wave duration could not be determined. In each cohort, P-wave duration was adjusted in a linear model for age, sex, RR interval and principal components of ancestry.

Taking the summary data from the meta-analysis, further clumping of SNPs was performed to identify independent variants based on linkage disequilibrium (LD) r^2<0.01 within a ±250kb window using 1000 Genomes Phase 1 (EUR) reference data. One of the variants identified (rs148020424) was flagged as an insertion-deletion and was excluded from our score leaving 8 SNPs (**Table 6.3**) that were included in our P-wave duration score.

Selection of genetic variants for PR interval duration score

The latest large-scale GWAS meta-analysis for PR interval duration identified 61 individual SNPs that met genome-wide significance based on analyses of over 92,000 individuals of European ancestry from a variety of studies, but not including UK Biobank [154]. Briefly, all studies used in the GWAS meta-analysis excluded participants with AF, history of myocardial infarction or heart failure, extreme PR interval values (≤80ms or ≥320ms), Wolff-Parkinson-White syndrome, pacemaker implantation and use of β-blockers, Vaughan-Williams class I and III anti-arrhythmic medications or digoxin. In each cohort, age, sex, height, body mass index and principal components of genetic ancestry were included as covariates.

Clumping of GWAS significant SNPs was undertaken as for P-wave duration which yielded 52 SNPs (**Table 6.4**) that were included in our PR interval score.

Selection of genetic variants for QT interval score

A large-scale GWAS meta-analysis for QT interval included ~103,000 individuals of European ancestry from a variety of studies, but not including UK Biobank [55]. Additionally, an exome-chip sequencing GWAS was published including 95,626 individuals [276]. All studies used in both of the meta-analyses excluded participants with AF, QRS duration >120ms, bundle branch block, and, when available, electronic pacemaker use or QT-altering medication use. In each cohort, QT interval duration was adjusted for age, sex, RR interval and principal components of genetic ancestry and tested for association with 2.5million directly genotyped or imputed SNPs.

Clumping of GWAS significant SNPs was undertaken as previously which yielded 54 SNPs (**Table 6.5**) that were included in our QT interval score.

Selection of genetic variants for ion channel scores

To test biological plausibility of the ECG scores, scores with genetic variants mapping to specific biological pathways involving electrical ion channels only were generated. To identify these in an unbiased way, the SNPnexus tool [277] was used to annotate the variants to known gene regions. Each variant in the main analysis was annotated to the closest gene within 25kb. Biological pathways were investigated using the Gene Ontology (GO) tool [278,279]. Variants that were annotated to genes involved in known biological pathways affecting action potential duration were included in the ion channel scores for each ECG parameter and are highlighted separately in each table.

Table 6.3 – SNPs included in P-wave duration score

SNP (rsID)	Chromosome	Nearest gene locus	Coded Allele	Non-coded Allele	Weighting for score (ms)
rs562408	1	*SSBP3*	G	A	0.53
rs11689011	2	*EPAS1*	T	C	0.60
rs41312411*	3	*SCN5A*	G	C	1.91
rs6790396*†	3	*SCN10A*	C	G	1.22
rs2285703	4	*CAMK2D*	G	A	0.56
rs4276421	5	*HCN1*	C	T	0.61
rs13242816†	7	*CAV1/CAV2*	T	C	1.21
rs452036†	14	*MYH6*	A	G	0.59

Table 6.3: Genetic variants included in P-wave duration score. Weighting for score is per coded allele and reported unaltered from the GWAS. SNP: Single nucleotide polymorphism. *SNPs included in Ion Channel Score; †SNPs excluded by MR-PRESSO method.

Table 6.4 – SNPs included in PR interval score

SNP (rsID)	Chromosome	Nearest gene locus	Coded Allele	Non-coded Allele	Weighting for score (ms)
rs11264339	1	*KRTCAP2*	C	T	0.709
rs12127701	1	*MYBPHL*	G	A	1.668
rs397637	1	*OBSCN*	T	G	0.769
rs4648819	1	*SKI*	A	G	1.735
rs7538988	1	*EPS15*	T	C	2.129
rs13018106	2	*FIGN*	G	C	0.776
rs1873164	2	*CCDC141*	A	G	0.723
rs2732860	2	*TMEM182*	A	G	0.893
rs3856447	2	*ID2*	A	G	1.218
rs4430933	2	*MEIS1*	A	G	1.299
rs922984	2	*TTN*	T	C	1.518
rs11708996*	3	*SCN5A*	C	G	3.089
rs13087058	3	*PDZRN3*	T	C	0.982
rs16858828	3	*PHLDB2*	C	A	0.853
rs6441111	3	*CCNL1*	C	T	0.817
rs6599234*	3	*SCN10A*	T	A	2.000
rs6599250*	3	*SCN10A*	T	C	3.765
rs7638853	3	*SENP2*	G	A	0.685
rs900669	3	*FRMD4B*	A	T	0.770
rs9826413	3	*EOMES*	T	A	2.024
rs17446418	4	*CAMK2D*	G	T	0.781
rs343849	4	*ARHGAP24*	T	A	2.074
rs3733409	4	*FAT1*	T	C	0.949
rs255292	5	*BNIP1 / NKX2-5*	A	C	1.083
rs7729395	5	*PAM*	T	C	2.361
rs11763856	7	*HERPUD2*	T	C	3.062
rs12673438	7	*TBX20*	G	T	1.360
rs2129561	7	*MKLN1*	G	A	0.973

SNP (rsID)	Chromosome	Nearest gene locus	Coded Allele	Non-coded Allele	Weighting for score (ms)
rs3807989†	7	*CAV1*	A	G	2.035
rs12678719	8	*ZFPM2*	G	C	0.799
rs881301	8	*FGFR1*	C	T	0.757
rs12257568	10	*SH3PXD2A*	T	C	1.036
rs12359272	10	*ALDH18A1*	A	G	1.019
rs12575413	11	*NAV2*	A	G	0.743
rs1372797	11	*NAV2*	G	T	1.067
rs652673	11	*WNT11*	T	C	0.827
rs11067104	12	*TBX5*	G	C	1.381
rs11067773	12	*MED13L*	T	C	1.297
rs17287293†	12	*C12orf67*	A	G	2.179
rs1896312	12	*TBX3*	C	T	1.604
rs35471	12	*TBX3*	G	A	0.686
rs6489953†	12	*TBX5*	C	T	1.227
rs6489974	12	*TBX3*	A	G	0.973
rs2585897	13	*XPO4*	A	G	1.222
rs718426	13	*EFHA1*	A	G	1.158
rs9590974	13	*LRCH1*	C	A	1.097
rs11465506	14	*IL25*	G	A	6.433
rs17767398	14	*SNORD56B*	G	C	0.951
rs365990†	14	*MYH6*	A	G	0.705
rs4901308	14	*FERMT2*	C	T	0.835
rs904974	15	*TLE3*	T	C	1.062
rs1984481	17	*MYOCD*	G	C	0.810

Table 6.4: Genetic variants included in PR interval score. Weighting for score is per coded allele and reported unaltered from the GWAS. SNP: Single nucleotide polymorphism. *SNPs included in Ion Channel Score; †SNPs excluded by MR-PRESSO method.

Table 6.5 – SNPs included in QT interval score

SNP (rsID)	Chromosome	Nearest gene locus	Coded Allele	Non-coded Allele	Weighting for score (ms)
rs10919070	1	*ATP1B1*	A	C	1.68
rs12061601	1	*ATP1B1*	T	C	1.41
rs12143842	1	*NOS1AP*	T	C	3.50
rs1361754	1	*PM20D1*	G	A	0.47
rs17457880	1	*NOS1AP*	G	A	1.90
rs17460657	1	*NOS1AP*	A	C	4.60
rs1983546	1	*ATP1B1*	A	G	0.81
rs2298632	1	*TCEA3*	T	C	0.70
rs347272	1	*NOS1AP*	A	G	1.80
rs4657172	1	*NOS1AP*	G	C	0.81
rs545833	1	*ATP1B1*	T	C	0.90
rs846111	1	*RNF207*	C	G	1.73
rs12997023	2	*SLC8A1*	T	C	1.69
rs295140†	2	*SPATS2L*	T	C	0.61
rs6544311	2	*SLC8A1*	A	C	0.65

SNP (rsID)	Chromosome	Nearest gene locus	Coded Allele	Non-coded Allele	Weighting for score (ms)
rs7561149	2	*TTN-CCDC141*	T	C	0.52
rs938291	2	*SP3*	G	C	0.53
rs11710077*	3	*SCN5A-SCN10A*	T	A	0.92
rs17784882	3	*C3ORF75*	C	A	0.54
rs1801725	3	*CASR*	G	T	0.58
rs6599234*	3	*SCN5A-SCN10A*	A	T	0.70
rs6793245*	3	*SCN5A-SCN10A*	G	A	1.12
rs2363719	4	*SLC4A4*	A	G	0.97
rs3857067	4	*SMARCAD1*	T	A	0.51
rs10040989†	5	*GFRA3*	G	A	0.85
rs11153730	6	*SLC35F1-PLN*	C	T	1.65
rs3902035	6	*SLC35F1-PLN*	T	C	0.85
rs7765828	6	*GMPR*	G	C	0.55
rs2072413*	7	*KCNH2*	C	T	1.68
rs3807375*	7	*KCNH2*	T	C	1.22
rs9920†	7	*CAV1*	C	T	0.79
rs11779860	8	*LAPTM4B*	T	C	0.61
rs16936870	8	*NCOA2*	A	T	0.99
rs1961102	8	*AZIN1*	T	C	0.57
rs2485376†	10	*GBF1*	G	A	0.56
rs3189030	10	*NRAP*	G	A	0.48
rs4934956	10	*ZNF37A*	T	C	0.58
rs174583	11	*FADS2*	C	T	0.57
rs2301696*	11	*KCNQ1*	C	G	1.14
rs7122937*	11	*KCNQ1*	T	C	1.93
rs3026445	12	*ATP2A2*	C	T	0.62
rs728926	13	*KLF12*	T	C	0.57
rs2273905	14	*ANKRD9*	T	C	0.61
rs3105593	15	*USP50-TRPM7*	T	C	0.66
rs1296720	16	*CREBBP*	C	A	0.83
rs246185	16	*MKL2*	C	T	0.72
rs246196	16	*CNOT1*	T	C	1.73
rs4784934	16	*CNOT1*	A	G	0.67
rs735951	16	*LITAF*	G	A	1.15
rs1052536	17	*LIG3*	C	T	0.98
rs1396515*	17	*KCNJ2*	G	C	0.98
rs17608766	17	*GOSR2*	C	T	0.72
rs9892651	17	*PRKCA*	T	C	0.74
rs1805128*	21	*KCNE1*	T	C	7.42

Table 6.5: Genetic variants included in QT interval score. Weighting for score is per coded allele and reported unaltered from the GWAS. SNP: Single nucleotide polymorphism. *SNPs included in Ion Channel Score; †SNPs excluded by MR-PRESSO method.

6.2.3 Statistical analysis

UK Biobank

In UK Biobank, separate genetic scores for P-wave duration, PR interval and QT interval were calculated for each participant by summing the number of coded alleles of each variant, weighted by their published per-allele effect size on the ECG parameter (in milliseconds; ms). The distributions of the different ECG genetic scores are shown in **Figure 6.4**. Associations between the genetic scores and 12-lead ECG parameters were estimated using linear regression and associations between genetic scores and risk of AF and SVT using logistic regression. All analyses involving the genetic scores were adjusted for sex, genotyping array and 40 principal components of ancestry (as provided by UK Biobank) [280]. Effects of the ECG genetic scores on risk of AF and SVT are reported per 5 ms difference in ECG score. Confidence intervals based on floated variances are presented in figures for variables with more than two levels in order to allow direct comparisons between different groups (avoiding restriction to a single arbitrary reference group). Estimates and standard confidence intervals are given for direct two-way comparisons. To allow for multiple testing, two tailed *P* values < 0.01 were considered significant and *P* values < 0.05 were considered suggestive.

Power calculations

The strength of the genetic variants used was assessed by calculation of the explained variance (R^2) of the trait using the following formula described elsewhere [281].

$$R^2 = \sum R_i^2 = \frac{\beta_i^2 \times var(SNP_i)}{var(X)}$$

where

$$var(SNP_i) = 2 \times MAF_{SNP_i} \times (1 - MAF_{SNP_i})$$

The total variance explained by the score is the sum of the individual variances explained by *i* SNPs within the score. β_i is the estimated effect of the i^{th} SNP on the ECG parameter; $var(SNP_i)$ is calculated using the minor allele frequencies (MAF) of each SNP and $var(X)$ is the variance of the ECG parameter. In this case $var(X)$ was set as 1 standard deviation (SD) unit, from the reported SDs

of the original population phenotypes in the GWAS. The variance explained by each genetic score for each ECG parameter was estimated (P-wave duration: 1.8%; PR interval: 5.0%; QT interval: 5.0%), and used to inform power calculations.

To assess the potential for weak instrument bias, *F*-statistics for each SNP were calculated [282] as β^2/SE^2 and all were well above the F>10 threshold typically recommended to avoid weak instrument bias in MR analyses [283]. I used the online tool https://sb452.shinyapps.io/power/ for power calculations for Mendelian Randomisation analyses. The different ECG scores had between 80-99% power to detect a 15% effect on risk of AF in UK Biobank per standard deviation unit of the ECG parameter (**Table 6.6**).

Figure 6.4 – Distribution of genetic scores in UK Biobank Population

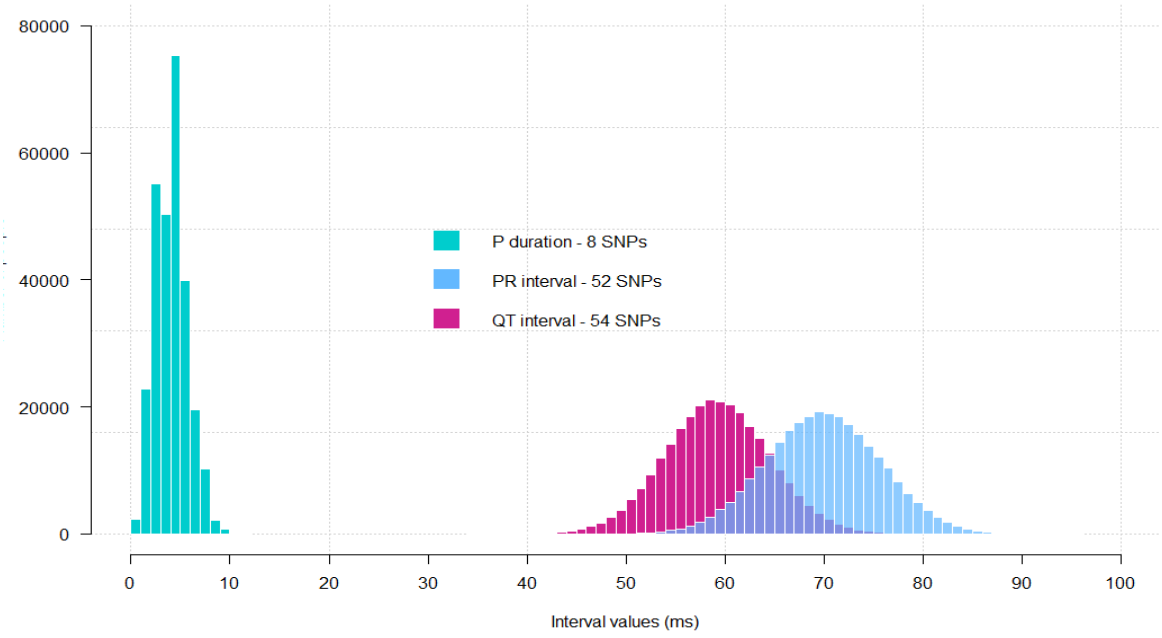


Figure 6.4: Weighted genetically predicted ECG score values. Total number of people in each score is 278,792. Mean ± standard deviation of genetic scores: P-wave duration: 4.1 ± 1.6 ms; PR interval: 69.9 ± 5.8 ms; QT interval: 59.3 ± 5.3 ms.

Table 6.6 – Power calculations for genetic ECG scores

ECG score	Number of SNPs	SD of ECG parameter*	% Variance explained† – R^2	*F*-statistic per SNP‡ – Median (Range)	Calculated Power
P-wave duration	8	12 ms	1.8	43 (35 – 184)	79.6%
PR interval	52	26 ms	5.0	40 (20 – 1110)	99.6%
QT interval	54	23 ms	5.0	47 (24 – 1012)	99.6%

Table 6.6: Power calculated using online tool (https://sb452.shinyapps.io/power/) for a binary outcome, with sample size 278,792; ratio of cases : controls of 1:15; causal detection effect of 0.85 per SD unit and significance of $P = 0.05$. *Standard deviation (SD) estimates from genome wide association studies; †Refers to % variance in measured ECG parameter explained by genetic variants in the score; ‡Refers to *F*-statistic per single nucleotide polymorphism (SNP) included in each score. Calculated using ($Beta^2/SE^2$).

External replication dataset

Replication analyses were performed using publicly available summary data from the AFGen Consortium genome-wide meta-analysis [284] accessed via the Cardiovascular Disease Knowledge Portal (2017 AFGen genome-wide association study [285]). Details of the contributing studies, phenotyping and genotyping processes have been published previously and did not include any UK Biobank participants [284]. Estimates of the log odds of AF (per-allele) for individual genetic variants among a total of 17,931 AF cases and 115,142 controls of primarily (~90%) European ancestry were available. Based on these data, we estimated causal effects for each ECG score on risk of AF using the fixed-effects inverse variance weighted method for summarised data. Meta-analyses of the AFGen and UK Biobank estimates were performed using fixed-effects methods.

Sensitivity analyses in UK Biobank

Causal inferences from MR studies are subject to instrumental variable assumptions [286]. In particular, MR can be sensitive to pleiotropy, which can occur when genetic variants potentially affect independent biological pathways for risk factors associated with the outcome. In the primary analysis method, based on an individual level genetic risk score, all genetic variants were assumed to be valid instruments. Therefore, we conducted sensitivity analyses to establish the robustness of the MR results including: the inverse variance weighted method combining individual causal estimates across the selected genetic variants (using a summary data approach although also

assuming all instruments valid), using the weighted median approach (in which 50% of the genetic variants are permitted to be invalid instrumental variables), the weighted mode approach (which allows the majority of variants to be invalid provided the most common causal effect estimate is a consistent estimate of the true causal effect) and MR-Egger (in which all genetic variants are permitted to be invalid instrumental variables, provided that the pleiotropic and risk factor effects of the variants are independently distributed) [286,287]. Further analyses of each genetic ECG score were also undertaken after exclusion of outlier variants identified using the MR-PRESSO outlier detection method [288].

In addition, to further explore potential pleiotropic associations, the Phenoscanner [289] search tool was used to identify published associations with the each of the genetic variants selected (and those in close linkage disequilibrium) for the ECG parameter scores. For variants contained in each score, we used PhenoScanner (http://www.phenoscanner.medschl.cam.ac.uk/information.html) to extract phenotypes with a screening *P*-value < 0.001 and using proxies for any of the variants in the scores with $r^2 > 0.8$ in 1000 Genomes Phase 3 data. We then limited our analysis to reports of GWAS significant *P*-values ($< 5 \times 10^{-8}$) only. We selected the proxy with the highest r^2 with the variant in the score for each individual trait described. In the case of multiple reports of the same trait, we selected the study with the strongest association described to report (i.e. smallest P-value). We examined these for consistent associations with known confounders.

Finally, in order to investigate whether being at higher risk of AF may have causal effects on ECG parameters, bi-directional MR analyses were conducted using a genetic score for risk of AF to ascertain the direction of effect. To generate an AF genetic risk score for the bi-directional analysis, we used the latest large-scale GWAS for AF including 60,620 cases of AF and 970,216 controls of predominantly European ancestry from a variety of studies [232]. As the discovery GWAS included UK Biobank as a constituent study, we used weights for the individual SNPs published in the GWAS for the SNPs derived from studies with UK Biobank excluded to avoid bias. Data with UK Biobank excluded weights was available for 142 SNPs reaching GWAS significance ($P < 5 \times 10^{-8}$) [232].

Clumping of SNPs as described previously yielded 133 SNPs (**Table 6.7**) that were included in the AF risk score. In UK Biobank, genetic scores were calculated for each participant by summing the number of AF risk increasing alleles of each SNP weighted by their effect size on the AF risk (unit log-odds). Effects of the AF risk score on 12-lead ECG parameters were estimated using linear regression adjusted for sex, genotyping array and forty principal components of ancestry (as provided by UK Biobank), with effects reported per unit log-odds (~2.7 OR increase).

Table 6.7 – SNPs included in AF score

SNP (rsID)	Chromosome	Nearest gene locus	Coded Allele	Non-coded Allele	Weighting for score (log-odds)
rs284277	1	*CASZ1*	C	T	0.0357
rs1545300	1	*KCND3*	G	C	0.0822
rs4073778	1	*CASQ2*	G	A	0.0551
rs79187193	1	*intergenic*	A	G	0.0425
rs6689306	1	*IL6R*	T	C	0.0679
rs11264280	1	*intergenic*	A	G	0.0800
rs72700114	1	*intergenic*	T	C	0.0533
rs72700118	1	*intergenic*	T	G	0.0529
rs577676	1	*intergenic*	C	A	0.0649
rs10753933	1	*PPFIA4*	A	G	0.0507
rs4951258	1	*NUCKS1*	A	C	0.0768
rs7529220	1	*intergenic*	C	T	0.0295
rs2885697	1	*SCMH1*	C	T	0.0322
rs11590635	1	*AGBL4*	C	T	0.0677
rs146518726	1	*intergenic*	T	C	0.1258
rs28387148	2	*GYPC*	G	A	0.0526
rs67969609	2	*ncRNA_TEX41*	A	G	0.1731
rs56181519	2	*intergenic*	G	A	0.1498
rs2288327	2	*TTN*	C	T	0.0327
rs3820888	2	*SPATS2L*	T	C	0.0410
rs35544454	2	*ERBB4*	A	C	0.0924
rs7578393	2	*KIF3C*	T	G	0.1064
rs11125871	2	*USP34*	G	T	0.1784
rs2540949	2	*CEP68*	A	G	0.0784
rs6747542	2	*GMCL1*	C	A	0.0376
rs72926475	2	*intergenic*	C	T	0.0309
rs10804493	3	*PHLDB2*	T	C	0.0369
rs7650482	3	*CAND2*	T	C	0.0995
rs1278493	3	*PPP2R3A*	G	A	0.0327
rs7612445	3	*GNB4*	C	T	0.0553
rs60902112	3	*XXYLT1*	G	T	0.0931
rs73041705	3	*THRB*	G	A	0.0696
rs7373065	3	*intergenic*	G	A	0.0637
rs6790396	3	*SCN10A*	T	C	0.0478
rs34080181	3	*LRIG1*	C	T	0.1196
rs17005647	3	*FRMD4B*	A	G	0.1439
rs6771054	3	*EPHA3*	T	C	0.0406

SNP (rsID)	Chromosome	Nearest gene locus	Coded Allele	Non-coded Allele	Weighting for score (log-odds)
rs10006327	4	*SLC9B1*	A	G	0.1709
rs244017	4	*intergenic*	C	A	0.3406
rs67249485	4	*intergenic*	G	A	0.0357
rs79399769	4	*intergenic*	C	T	0.0500
rs1532170	4	*intergenic*	T	C	0.0669
rs138311480	4	*intergenic*	T	C	0.0342
rs114904067	4	*intergenic*	C	T	0.0439
rs7687819	4	*ALPK1*	C	T	0.0489
rs6829664	4	*CAMK2D*	G	A	0.0500
rs10213171	4	*ARHGAP10*	A	G	0.0441
rs10520260	4	*HAND2-AS1*	T	C	0.1025
rs12648245	4	*intergenic*	G	A	0.0825
rs1458038	4	*intergenic*	A	T	0.1577
rs6596717	5	*intergenic*	T	G	0.0189
rs337705	5	*KCNN2*	A	T	0.0625
rs2012809	5	*intergenic*	A	G	0.0704
rs2040862	5	*WNT8A*	A	G	0.0420
rs6580277	5	*NR3C1*	T	G	0.1010
rs12188351	5	*SLIT3*	T	C	0.0872
rs6891790	5	*intergenic*	C	A	0.0432
rs28439930	5	*intergenic*	T	G	0.0745
rs3951016	6	*SLC35F1*	G	C	0.0409
rs9401451	6	*intergenic*	A	C	0.0476
rs13195459	6	*intergenic*	G	T	0.0403
rs117984853	6	*UST*	G	A	0.0680
rs73366713	6	*ATXN1*	G	T	0.0583
rs34969716	6	*KDM1B*	G	A	0.0371
rs3176326	6	*CDKN1A*	A	G	0.0651
rs2031522	6	*intergenic*	C	T	0.0695
rs11773845	7	*CAV1*	C	T	0.0546
rs55985730	7	*OPN1SW*	A	T	0.1281
rs55734480	7	*DGKB*	A	T	0.0633
rs7789146	7	*KCNH2*	C	A	0.0510
rs6462079	7	*CREB5*	C	T	0.0599
rs35005436	7	*GTF2I*	A	T	0.0723
rs56201652	7	*CDK6*	A	C	0.0493
rs35620480	8	*intergenic*	C	T	0.0246
rs62521286	8	*FBXO32*	T	C	0.0418
rs4871397	8	*intergenic*	G	C	0.0829
rs6994744	8	*PTK2*	T	A	0.0362
rs7508	8	*UTR3/ASAH1*	A	G	0.0344
rs7834729	8	*XPO7*	C	G	0.0397
rs2274115	9	*LHX3*	T	C	0.0446
rs10821415	9	*C9orf3*	A	G	0.0419
rs55693294	10	*NEURL1*	G	T	0.0782
rs11598047	10	*NEURL1*	C	T	0.0576
rs35176054	10	*SH3PXD2A*	G	A	0.0563
rs10749053	10	*RBM20*	C	T	0.0977
rs12245149	10	*REEP3*	A	C	0.0270
rs7096385	10	*SIRT1*	T	C	0.0388
rs60212594	10	*SYNPO2L*	G	A	0.1131

SNP (rsID)	Chromosome	Nearest gene locus	Coded Allele	Non-coded Allele	Weighting for score (log-odds)
rs10458660	10	*C10orf11*	A	G	0.0519
rs4935786	11	*intergenic*	C	T	0.0510
rs76097649	11	*KCNJ5*	G	A	0.0759
rs10741807	11	*NAV2*	C	A	0.0356
rs883079	12	*UTR3/TBX5*	T	C	0.0788
rs10773657	12	*HIP1R*	A	G	0.1536
rs6560886	12	*FBRSL1*	A	G	0.0440
rs4963776	12	*intergenic*	T	C	0.1531
rs17380837	12	*SSPN*	T	A	0.3422
rs12809354	12	*PKP2*	T	C	0.0602
rs11614818	12	*intergenic*	G	C	0.0604
rs2860482	12	*NACA*	G	C	0.0764
rs71454237	12	*intergenic*	G	A	0.0638
rs775498	12	*BEST3*	G	T	0.0716
rs12426679	12	*intergenic*	C	A	0.0330
rs35569628	13	*CUL4A*	T	C	0.0680
rs9506925	13	*intergenic*	G	A	0.0613
rs422068	14	*MYH6*	A	G	0.0389
rs1957021	14	*AKAP6*	G	A	0.0744
rs11156751	14	*AKAP6*	C	G	0.1698
rs73241997	14	*intergenic*	A	C	0.1162
rs2738413	14	*SYNE2*	G	C	0.0658
rs74884082	14	*DPF3*	G	A	0.0548
rs10873298	14	*intergenic*	T	C	0.0465
rs147301839	15	*GCOM1*	G	A	0.0923
rs7170477	15	*HERC1*	T	C	0.1813
rs74022964	15	*intergenic*	T	C	0.1079
rs12908004	15	*intergenic*	C	T	0.0461
rs2759301	15	*ABHD17C*	A	G	0.0711
rs4965430	15	*IGF1R*	C	T	0.0686
rs118159104	16	*CRAMP1*	T	C	0.0615
rs140185678	16	*RPL3L*	A	G	0.0988
rs77316573	16	*PGP*	T	G	0.0428
rs2359171	16	*ZFHX3*	G	A	0.0668
rs72811294	17	*MYOCD*	A	G	0.0200
rs7225165	17	*intergenic*	T	C	0.0383
rs11658278	17	*ZPBP2*	G	A	0.0362
rs1563304	17	*WNT3*	G	A	0.0568
rs9899183	17	*TNFSF12*	G	T	0.0587
rs12604076	17	*CYTH1*	G	A	0.1136
rs9953366	18	*SMAD7*	A	C	0.0388
rs8088085	18	*MEX3C*	T	C	0.0872
rs2834618	21	*ncRNA_LINC01426*	G	A	0.0703
rs464901	22	*TUBA8*	T	C	0.0365
rs133902	22	*MYO18B*	T	C	0.0432

Table 6.7: Genetic variants included in AF risk score. Weighting for score is per coded allele and reported unaltered from the GWAS. SNP: Single nucleotide polymorphism; AF: atrial fibrillation.

All analyses were performed using SAS (v 9.4, SAS Institute, Cary, USA) and R (v3.5.2, The R Foundation for Statistical Computing, Vienna, Austria, https://www.r-project.org). We used the R package Mendelian Randomization (v0.4.0 - https://cran.r-project.org/web/packages/MendelianRandomization/index.html) to generate inverse variance weighted estimates, weighted median estimates and MR-Egger estimates. The weighted mode-based estimate function was obtained from GitHub (https://github.com/MRCIEU/mbe). The MR-PRESSO R package (https://github.com/rondolab/MR-PRESSO) was used to exclude outlying genetic variants as described previously [288]. The R package metafor (v2.0.0 - http://www.metafor-project.org/doku.php) was used for meta-analysis.

6.2.4 Standard protocol approvals, registration and patient consent

All procedure and data collection in UK Biobank were approved by the UK Biobank Research Ethics Committee (reference number 11/NW/0274). This research was conducted using the UK Biobank Resource under Application Number 14568.

6.3 Results

6.3.1 UK Biobank participant characteristics

In UK Biobank, participants with AF were older, more likely to be male and had a higher prevalence of cardiovascular risk factors than those without AF (**Table 6.8**). Of the 259,660 control subjects without a history of AF, 13,314 participants had a 12-lead ECG. Within this cohort, the mean and standard deviation of P-wave duration was 97 ± 16 ms (95% of measured P-wave durations between 65 and 129 ms); for PR interval 163 ± 27 ms (95% of measured PR intervals between 109 and 217 ms) and for Bazett corrected QT_c 420 ± 26 ms (95% of measured QT_c between 368 and 472 ms).

Table 6.8 – Baseline characteristics of participants in UK Biobank

Characteristic	No atrial fibrillation	Atrial fibrillation
Number of participants	259660	19132
Age at recruitment (yr)	56.6 ± 8.0	62.2 ± 5.9
Male sex	118596 (45.7)	12662 (66.2)
Body-mass index (kg/m^2)	27.3 ± 4.7	29.0 ± 5.3
Coronary Heart Disease	19297 (7.4)	7332 (38.3)
Heart Failure	2840 (1.1)	3826 (20.0)
Hypertension	80806 (31.1)	15862 (66.5)
Diabetes	16056 (6.2)	3270 (17.1)
'Lone' atrial fibrillation	0 (0)	4805 (25.1)
Other supraventricular tachycardias	1164 (0.4)	1720 (9.0)

Table 6.8: Population restricted to unrelated white British ancestry (see **Section 6.2.1** for full details). Continuous variables are presented as mean ± standard deviation and categorical variables as number (%). 'Lone' atrial fibrillation defined as atrial fibrillation without known coronary heart disease, heart failure, hypertension or diabetes (see **Section 6.2.1** for full definition).

6.3.2 Genetic scores associated with measured 12-lead ECG parameters

To illustrate the association between each genetic score and corresponding ECG parameter, which is a required assumption of MR analyses, we used the subset of 13,314 UK Biobank participants with a 12-lead ECG and no history of AF (to reduce potential for reverse causality). Each genetic score was strongly and positively associated with the corresponding measured 12-lead ECG parameter ($5\times10^{-140} < P < 2\times10^{-13}$), predicting these within normal reference ranges (**Figure 6.5**).

Figure 6.5 – Associations between genetic scores and 12-lead ECG parameters in UK Biobank

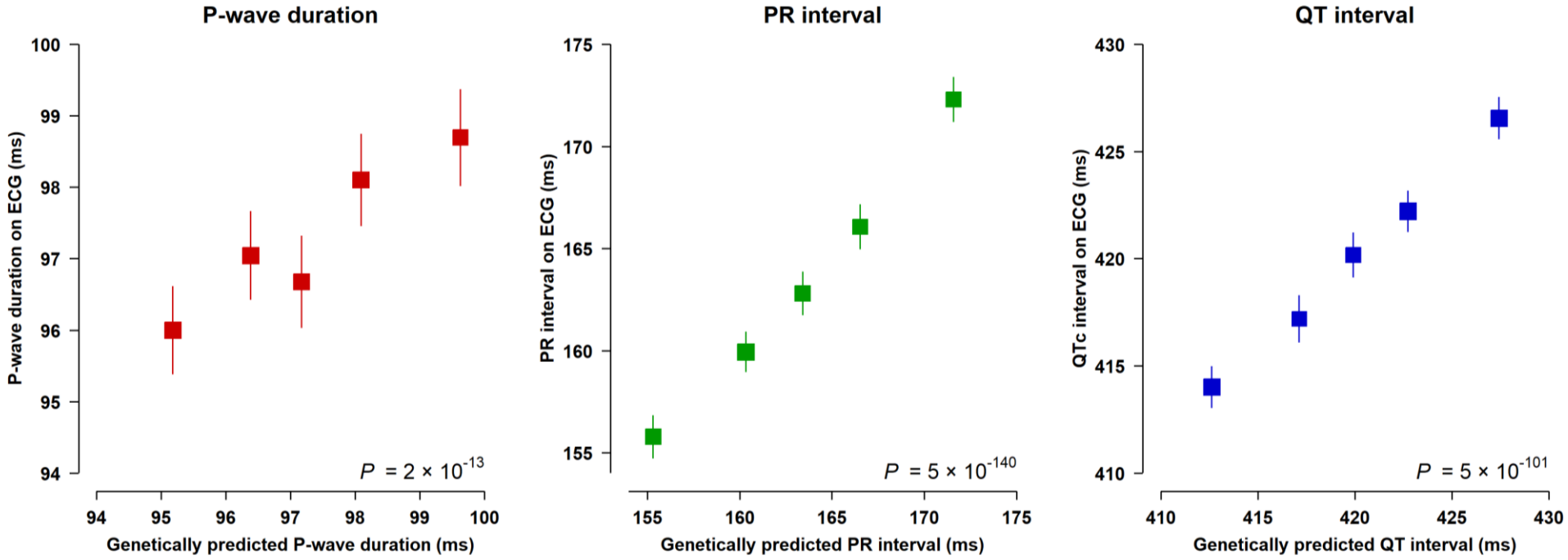


Figure 6.5: Association between quintiles of genetic scores for ECG parameters (defined in non-AF cases) and 12-lead ECG parameters in in 13,314 participants in UK Biobank. Boxes represent mean values with their size inversely proportional to variance, and lines represent 95% confidence intervals. A constant representing the population mean non-genetically predicted ECG interval was added to all genetic score values (the population mean of measured 12-lead ECG parameter excluding the genetic contribution; 93.2 ms for P-wave duration, 93.5 ms for PR interval and 360.7 ms for QT interval) for display purposes. *P* calculated across the genetic score using linear regression adjusting for sex, genotyping array and forty principal components of ancestry.

6.3.3 Genetically predicted differences in ECG parameters and risk of AF

In UK Biobank, a genetically predicted longer P-wave duration was associated with a lower risk of AF, with a 6% lower risk of AF in the top versus bottom quintile of the P-wave genetic score (Odds ratio [OR] 0.94; 95% confidence interval [CI]: 0.89-0.98, $P = 5\times10^{-3}$; **Figure 6.6**), and 9% lower risk of AF per 5 ms longer P-wave duration (OR 0.91; 95% CI: 0.87-0.96, $P = 2\times10^{-4}$). Genetically predicted differences in PR interval were strongly associated with AF, with a 17% lower risk of AF in the top versus bottom quintile of the PR interval genetic score (OR 0.83; 95% CI: 0.79-0.87, $P = 9\times10^{-15}$; **Figure 6.6**) resulting in a 6% lower risk of AF per 5 ms longer PR interval (OR 0.94; 95% CI: 0.93-0.96, $P = 2\times10^{-19}$). To explore the independent effect of PR interval after consideration of genetically predicted P-wave duration, we repeated the regression analyses after adjusting for the P-wave duration score; the effect of PR interval was unchanged and remained significantly associated with AF (OR 0.94 per 5 ms longer PR interval, 95% CI: 0.93-0.96, $P = 3\times10^{-16}$). Differences in QT interval were not associated with statistically significant differences in risk of AF (OR 0.96 for top versus bottom quintile; 95% CI: 0.91-1.00, $P = 0.08$; **Figure 6.6**), albeit a statistically suggestive 2% lower risk of AF per 5 ms longer QT interval was observed (OR 0.98; 95% CI: 0.97-1.00, $P = 0.02$). The effects seen for all ECG parameters were similar in both males and females.

Figure 6.6 – Effects of genetically predicted ECG parameters on risk of atrial fibrillation in UK Biobank

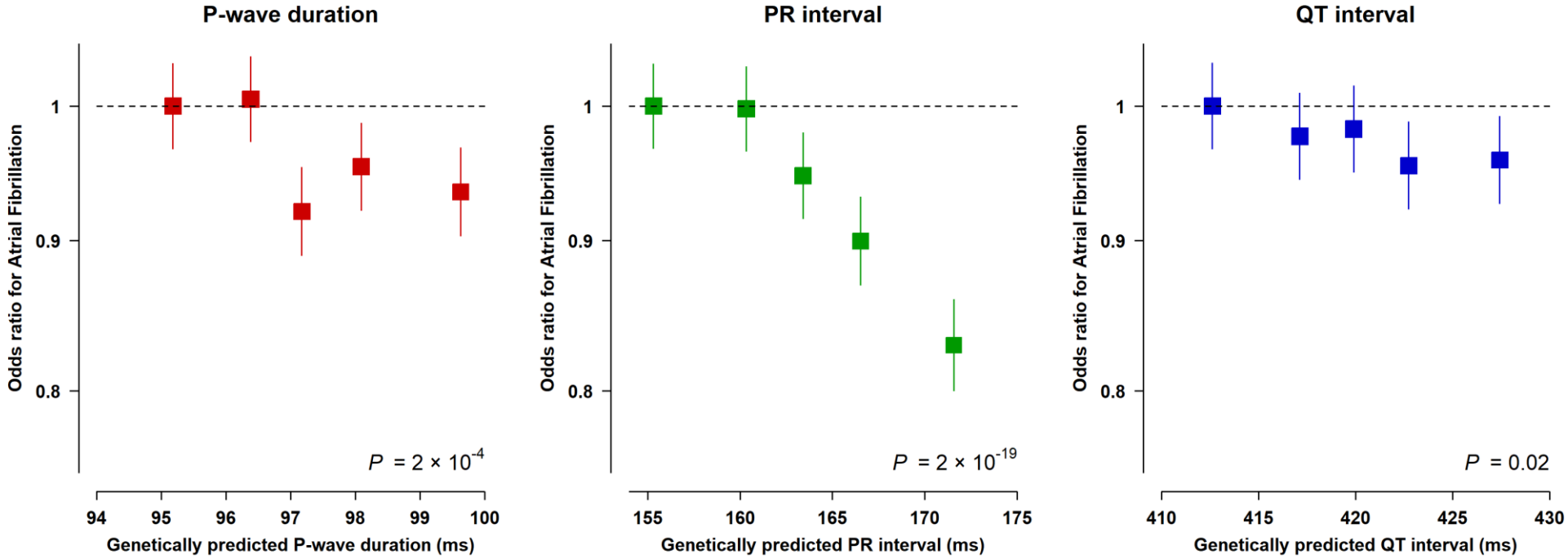


Figure 6.6: Odds ratios (OR) for atrial fibrillation (AF) per quintile of genetic score (defined in non-AF cases) in 278,792 participants in UK Biobank. Boxes represent effect estimates with their size inversely proportional to variance. Solid lines represent 95% confidence intervals (CI) calculated using floating absolute risks. ORs are adjusted for genotyping array, sex and forty principal components of ancestry. *P* calculated across continuous genetic score values adjusting for sex, genotyping array and forty principal components of ancestry.

To explore whether the association between ECG scores and AF was affected by underlying cardiovascular comorbidities, we also examined associations with 'lone' AF (as defined in **Section 6.2.1**), for which comparable effect sizes were observed. A longer genetically predicted P-wave duration was associated with an 8% lower risk of lone AF in the top versus the bottom quintile of the P-wave genetic score of borderline statistical significance (OR 0.92; 95% CI: 0.84-1.00, P = 0.06; **Figure 6.7**) and a 11% lower risk of lone AF per 5 ms longer P-wave duration: OR 0.89; 95% CI: 0.82-0.98, P = 0.01; **Figure 6.8**. Genetically predicted differences in PR interval were strongly associated with lone AF, with a 22% lower risk of lone AF in the top versus bottom quintile of the PR interval genetic score (OR 0.78; 95% CI: 0.71-0.85, $P = 1\times10^{-7}$; **Figure 6.7**) and an 8% lower risk of lone AF per 5 ms longer PR interval: OR 0.92; 95% CI: 0.90-0.95, $P = 5\times10^{-10}$; **Figure 6.8**. Differences in QT interval were not associated with statistically significant differences in risk of lone AF (OR 0.92 for top versus bottom quintile; 95% CI: 0.84-1.01, P = 0.08; **Figure 6.7**) and OR 0.98 per 5 ms longer QT genetic score; 95% CI: 0.95-1.00, P = 0.11; **Figure 6.8**). Taken together, these findings suggest that longer P-wave duration and PR intervals (within normal ranges) are causally associated with a lower risk of AF.

Figure 6.7 – Effects of genetically predicted ECG parameters on risk of 'lone' atrial fibrillation in UK Biobank

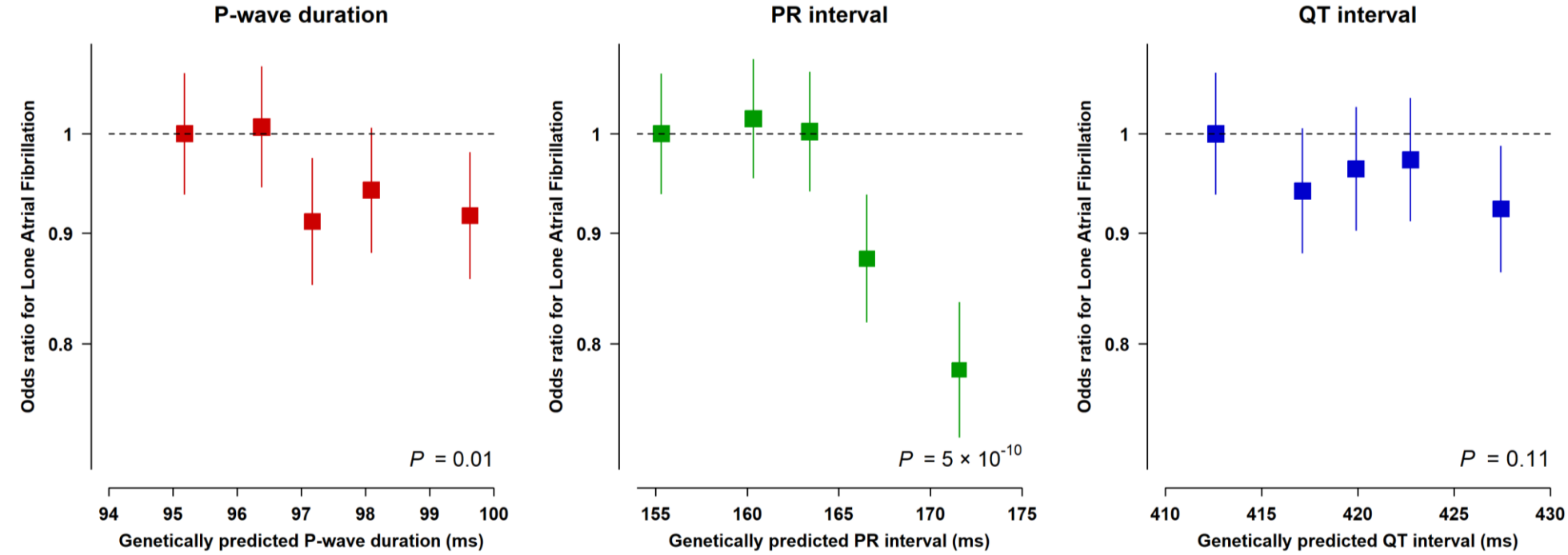


Figure 6.7: Odds ratios (OR) for 'lone' atrial fibrillation per quintile of genetic score (defined in non-AF cases) in 278,792 participants in UK Biobank. Boxes represent effect estimates with their size inversely proportional to variance. Solid lines represent 95% confidence intervals (CI) calculated using floating absolute risks. ORs are adjusted for genotyping array, sex and forty principal components of ancestry. *P* calculated across continuous genetic score values adjusting for sex, genotyping array and forty principal components of ancestry.

Figure 6.8 – Effects of genetically predicted ECG parameters on risk of 'lone' atrial fibrillation in UK Biobank

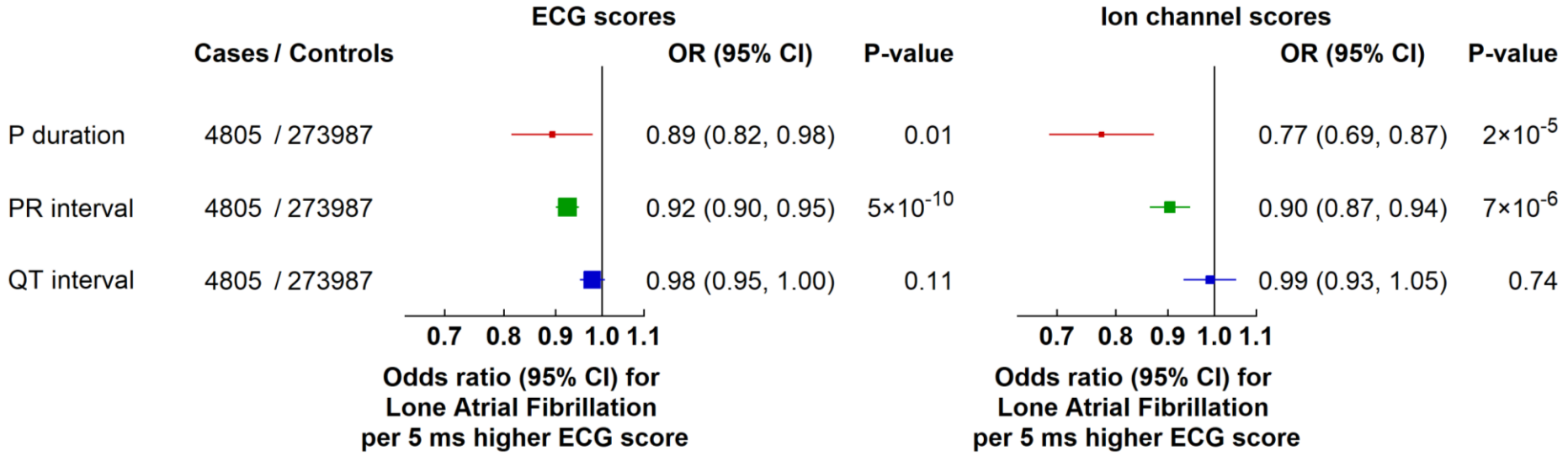


Figure 6.8: Effects of genetically predicted ECG parameters on risk of 'lone' atrial fibrillation in UK Biobank. Ion channel scores for each ECG parameter include only genetic variants annotated to known ion channel genes. Boxes represent point estimates of effect per 5 ms higher ECG score with sizes inversely proportional to their variance, and lines represent 95% confidence intervals (CI). Odds Ratios (OR) are adjusted for genotyping array, sex and forty principal components of ancestry.

6.3.4 Genetically predicted differences in ECG parameters and risk of SVT

To explore if our findings also applied to supraventricular tachyarrhythmia (SVT) phenotypes, which are conventionally perceived as being mechanistically different to AF [290], we investigated the relationship between the ECG genetic scores and risk of (non-AF) SVT among 2,884 SVT and 275,908 non-SVT cases. Compared to those with AF, participants with other SVTs were younger, less likely to be male and had fewer cardiovascular co-morbidities (**Table 6.9**).

Table 6.9 – Baseline characteristics of participants with SVT in UK Biobank

Characteristic	No supraventricular tachycardias	Supraventricular tachycardias
Number of participants	275908	2884
Age at recruitment (yr)	56.9 ± 8.0	59.6 ± 7.3
Male sex	129751 (47.0)	1507 (52.3)
Body-mass index (kg/m^2)	27.4 ± 4.8	27.8 ± 5.0
Coronary Heart Disease	25673 (9.3)	956 (33.2)
Heart Failure	6211 (2.3)	455 (15.8)
Hypertension	91964 (33.2)	1566 (54.3)
Diabetes	18940 (6.9)	386 (13.4)
Atrial fibrillation	17412 (6.3)	1720 (59.6)
'Lone' atrial fibrillation	4203 (1.5)	602 (20.9)

Table 6.9: Population restricted to unrelated white British ancestry (see **Section 6.2.1** for full details). Continuous variables are presented as mean ± standard deviation and categorical variables as number (%). 'Lone' atrial fibrillation defined as atrial fibrillation without known coronary heart disease, heart failure, hypertension or diabetes (see **Section 6.2.1** for full definition).

Surprisingly, as for AF, genetic scores explaining 5 ms longer P-wave duration and PR interval were also associated with a lower risk of SVT (OR 0.86; 95% CI: 0.76-0.96, P = 0.01 and OR 0.92; 95% CI: 0.89-0.95, $P = 3\times10^{-7}$, respectively). Furthermore, the association of PR interval with risk of SVT was unchanged after adjusting for the P-wave duration score (OR 0.92; 95% CI: 0.89-0.96, $P = 9\times10^{-6}$ per 5 ms longer score). In contrast, and consistent with the lack of relationship between QT interval and AF, there was no significant association of QT interval with SVT (OR 1.00; 95% CI: 0.97-1.04, P = 0.86; **Figure 6.9**). Comparable associations were observed after exclusion of participants with any AF diagnosis.

Figure 6.9 – Effects of genetically predicted ECG parameters on risk of supraventricular tachycardias in UK Biobank

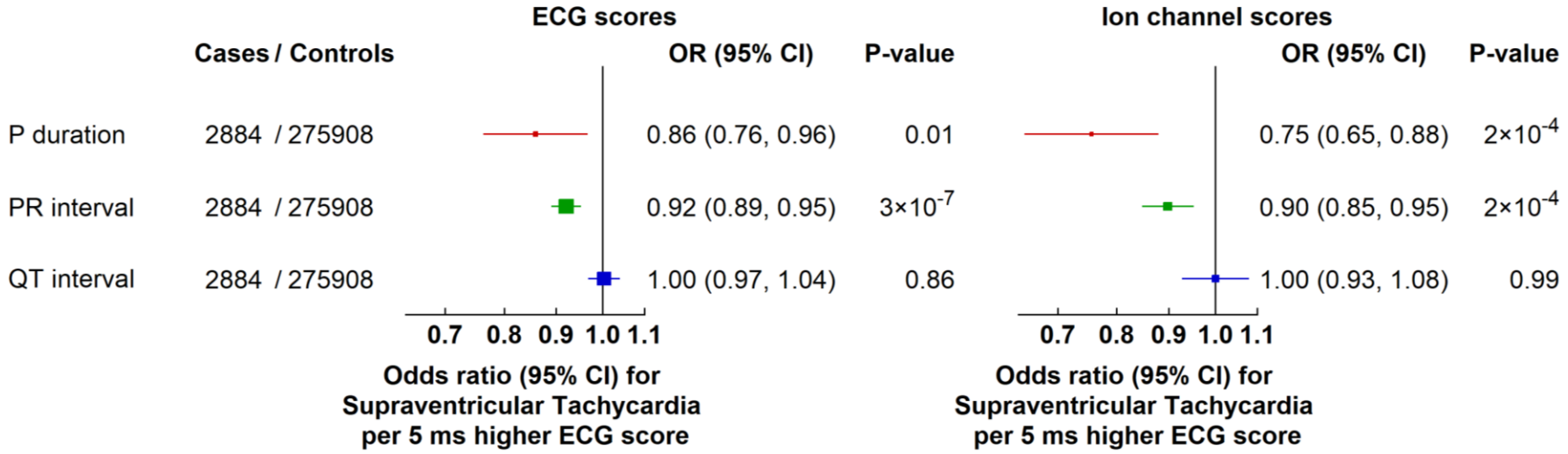


Figure 6.9: Effects of genetically predicted ECG parameters on risk of supraventricular tachycardias in UK Biobank. Ion channel scores for each ECG parameter include only genetic variants annotated to known ion channel genes. Boxes represent point estimates of effect per 5 ms higher ECG score with sizes inversely proportional to their variance, and lines represent 95% confidence intervals (CI). Odds Ratios (OR) are adjusted for genotyping array, sex and forty principal components of ancestry.

6.3.5 Genetically predicted ECG parameter score associations with left atrial size on cardiac MRI

ECG parameters may be affected by atrial chamber size, which could also alter the risk of AF. To investigate whether differences in atrial chamber size may have contributed to our findings, we tested the associations of our ECG genetic scores with indexed biplanar left atrial volumes in 2,581 participants with cardiac MRI data and no history of AF. The scores were not associated with differences in left atrial volumes (-0.37 ml/m^2 per 5 ms longer P-wave duration; 95% CI: -0.84-1.60, P = 0.54; 0.04 ml/m^2 per 5 ms longer PR interval; 95% CI: -0.28-0.38, P = 0.79 and 0.18 ml/m^2 per 5 ms longer QT interval; 95% CI: -0.18-0.53, P = 0.34), suggesting the effects of the genetically predicted differences in atrial ECG parameters on risk of AF and SVT were not associated with left atrial size.

6.3.6 Genetically predicted ECG parameters, via ion channel pathways, and risk of AF, lone AF and SVT

To investigate the relevance of specific electrical mechanisms for AF or SVT, we examined the effects of genetic scores for the different ECG parameters restricted to variants annotated to known ion channel genes (defined using independent databases – see **Section 6.2.2**). Variants associated with longer P-wave duration and PR interval were similarly associated with lower risks of AF (**Figure 6.10**), lone AF (**Figure 6.8**), and SVT (**Figure 6.9**), with no association with atrial arrhythmia seen for variants in ion channel genes associated with QT interval, and directionally consistent with estimates from the genetic scores that included all variants (**Figure 6.8**, **Figure 6.9** and **Figure 6.10**).

Overall, these results suggest that changes in ion channel pathways (along with other pathways), contribute to the effects of the atrial ECG parameters on risk of AF and SVT.

6.3.7 Independent replication and meta-analysis

The results for the effects of genetic ECG parameter scores on risk of AF were independently replicated in data from the AFGen Consortium [284], with estimates similar to those seen in UK Biobank for the overall scores as well as the ion channel scores (**Figure 6.10**). Overall, a meta-

analysis of a total of 37,063 cases of AF and 374,802 controls showed that a 5 ms longer genetically predicted P wave duration, PR interval and QT interval were each associated with a lower risk of AF (OR 0.91; 95% CI: 0.88-0.94, $P = 8\times10^{-8}$; OR 0.95; 95% CI: 0.94-0.95, $P = 2\times10^{-29}$ and OR 0.98; 95% CI: 0.97-1.00, $P = 8\times10^{-3}$ respectively; **Figure 6.10**).

Figure 6.10 – Effects of genetically predicted ECG parameters on risk of atrial fibrillation in UK Biobank and AFGen

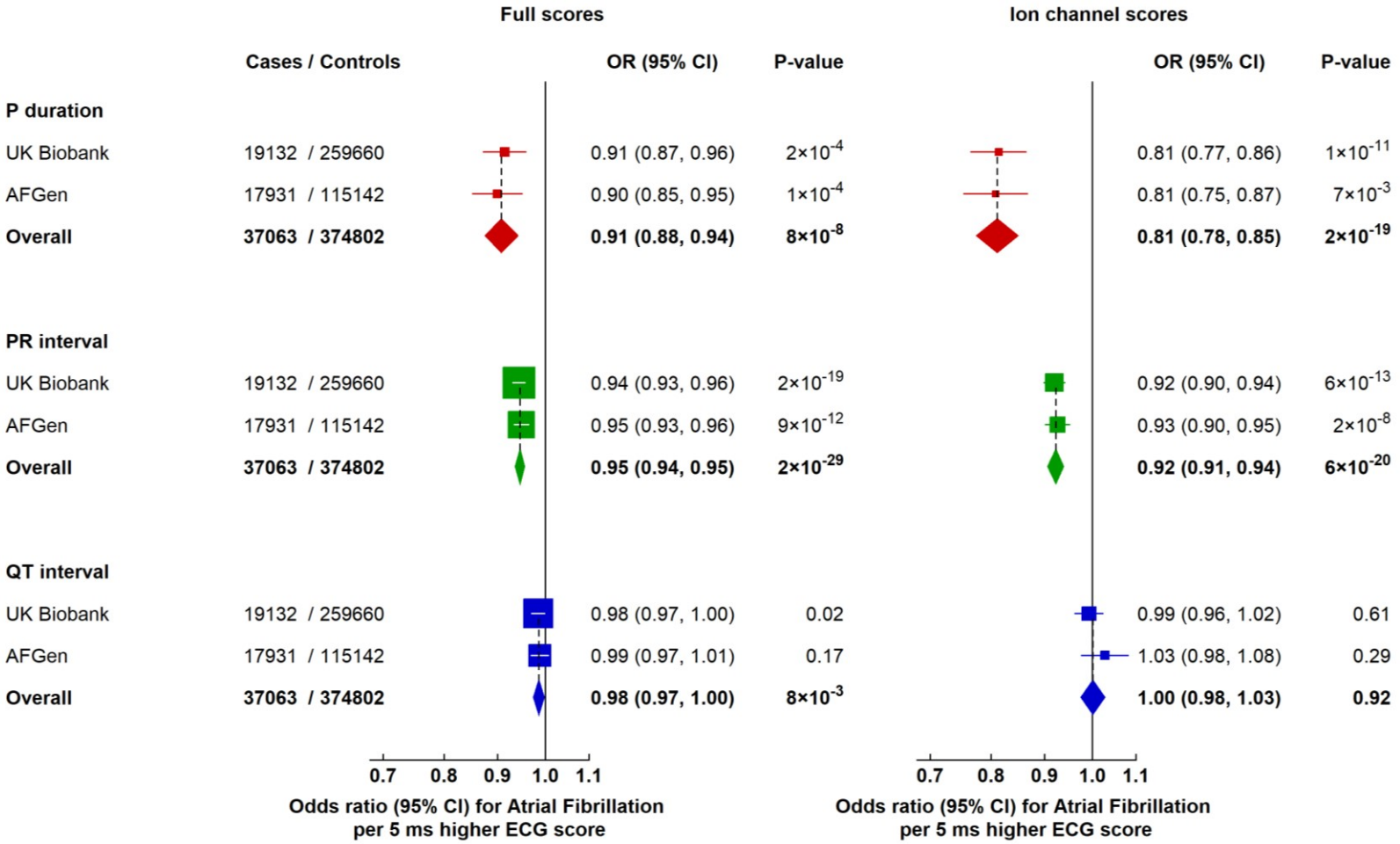


Figure 6.10: Ion channel scores for each ECG parameter include only genetic variants annotated to known ion channel genes. Boxes represent point estimates of effect per 5 ms higher ECG score, diamonds represent meta-analysis estimates, with sizes inversely proportional to their variance, and lines represent 95% confidence intervals (CI). UK Biobank derived odds ratios (OR) are adjusted for sex, genotyping array and forty principal components of ancestry. ORs for AFGen were calculated using inverse-variance weighted fixed-effects methods from published summary data.

6.3.8 Sensitivity analyses

Genetically predicted risk of AF and effect on 12-lead ECG parameters

To assess if a higher genetic risk of AF was associated with differences in measured ECG parameters, (potential bi-directional effect), the effects of a genetic AF risk score (generated as described in **Section 6.2.3**) on 12-lead ECG parameters were examined in 13,314 individuals in UK Biobank with ECG data and no history of AF. Overall, there were no significant associations between genetically predicted AF risk and PR interval or QTc interval, but higher genetically predicted risk of AF was associated with a shorter P-wave duration ($P = 4\times10^{-4}$; **Table 6.10**). However, the effect size was very small, with a ~10% change in AF risk accounting for a 0.1 ms change in P-wave duration, explaining only 1/50th of the causal effect estimate observed for P-wave duration on AF risk described previously (~9% change in AF risk per 5 ms change in P-wave duration).

Table 6.10 – Effect of genetic risk score for atrial fibrillation on 12-lead ECG parameters

ECG parameter	Change in parameter (ms) (95% CI) *per unit log odds*	*P*-value
UK Biobank – 13,314 participants		
P-wave duration	-1.1 (-1.7 to -0.5)	4×10^{-4}
PR interval	-0.4 (-1.4 to 0.5)	0.40
QT_c (Bazett)	-1.1 (-2.0 to -0.2)	0.02

Table 6.10: Sensitivity analyses for bi-directional Mendelian randomisation analyses – i.e. effect of genetic risk score for atrial fibrillation (AF) on 12-lead ECG parameters in 13,314 participants with ECG data and no history of AF in UK Biobank. Effect on 12-lead ECG parameter in milliseconds (ms) and 95% Confidence Intervals (CI) presented per unit log odds (~2.7 OR) increase. *P* calculated using linear regression adjusting for sex, genotyping array and first forty principal components of ancestry.

Sensitivity analyses for pleiotropy and other assumption violations

Other statistical sensitivity analyses were carried out in UK Biobank to further investigate potential pleiotropic effects of the genetic variants in the ECG scores (**Table 6.11**). The inverse variance weighted approach (random effects), combining individual causal estimates across the selected genetic variants, gave comparable estimates to the genetic score as anticipated. However, the effects of P-wave duration and QT interval on risk of AF were not statistically significant. The

weighted median and weighted mode MR methods gave comparable results to the primary analyses. MR-Egger analyses provided no evidence of directional pleiotropy within either the PR interval or QT interval scores (Egger-intercept $P = 0.69$ and $P = 0.99$ respectively), and also showed comparable causal effect estimates for AF to the primary results for both PR interval and QT interval, albeit non-significant. For P-wave duration, MR-Egger analyses indicated possible bias (Egger-intercept $P = 0.02$), which may be a result of directional pleiotropy, but the bias-adjusted causal effect estimate showed a significant association between P-wave duration and AF (OR: 0.64; 95% CI: 0.45-0.89, $P = 0.009$). The results after excluding outlying genetic variants based on the MR-PRESSO method were comparable to the primary results for both PR interval and QT interval. In contrast, after 3 of the 8 genetic variants comprising the P-wave duration score were excluded by the MR-PRESSO method, the association between P-wave duration and AF risk was attenuated and no longer statistically significant. Information from the PhenoScanner database suggested that there were no meaningful effects of the genetic variants contributing to the scores on other cardiovascular phenotypes (**Table 6.12**). Funnel plots to visualise the causal estimates for each variant within each ECG genetic score are shown in **Figure 6.11**, **Figure 6.12** and **Figure 6.13**.

Table 6.11 – Sensitivity analyses for estimate of ECG score effects on atrial fibrillation in UK Biobank

	P-wave duration per 5 ms		PR interval per 5 ms		QT interval per 5 ms	
	OR* (95% CI)	***P***	**OR* (95% CI)**	***P***	**OR* (95% CI)**	***P***
UK Biobank – 19,132 cases of AF						
Primary genetic score	0.91 (0.87-0.96)	2×10^{-4}	0.94 (0.93-0.96)	2×10^{-19}	0.98 (0.97-1.00)	0.02
IVW estimate (fixed-effects)	0.92 (0.88-0.96)	3×10^{-4}	0.94 (0.93-0.96)	3×10^{-19}	0.98 (0.97-0.99)	0.02
IVW estimate (random-effects)	0.92 (0.75-1.12)	0.40	0.94 (0.91-0.98)	1×10^{-3}	0.98 (0.95-1.01)	0.32
Weighted Median MR estimate	0.87 (0.81-0.94)	4×10^{-4}	0.93 (0.91-0.95)	4×10^{-9}	0.99 (0.97-1.01)	0.38
Weighted Mode MR estimate	0.86 (0.79-0.93)	0.006	0.93 (0.91-0.96)	4×10^{-7}	0.98 (0.96-1.00)	0.11
MR-Egger estimate	0.64 (0.45-0.89)	0.009	0.93 (0.86-1.00)	0.06	0.98 (0.92-1.05)	0.57
Egger-intercept test	-	*0.02*	-	*0.69*	-	*0.99*
MR-PRESSO corrected estimate	0.98 (0.86-1.12)	0.79	0.95 (0.93-0.98)	8×10^{-4}	0.99 (0.96-1.02)	0.38

Table 6.11: Sensitivity analyses for main ECG score effects on atrial fibrillation (AF) in UK Biobank. Odds ratios (OR) and 95% Confidence Intervals (CI) presented per 5ms higher genetic ECG score but (*) not applicable to Egger pleiotropic bias estimate. IVW: Inverse variance weighted; MR: Mendelian Randomisation; MR-PRESSO: Mendelian Randomisation Pleiotropy Residual Sum and Outlier

Table 6.12 – Phenoscanner derived details for non-ECG parameter associated traits for SNPs in ECG scores

SNP in score	Reported SNP	r^2 with sentinel	Trait	First author	PMID	*P*-value
P-wave duration score						
rs11689011	rs11894252	0.979	Renal cell carcinoma	Purdue MP	21131975	9.11E-09
rs13242816	rs7801950	0.911	Maternal transmission distortion	Meyer	22377632	6.21E-19
PR interval score						
rs12127701	rs12127701	1	LDL	GLGC	24097068	4.54E-36
	rs12127701	1	Total cholesterol	GLGC	24097068	3.87E-26
rs11264339	rs11264339	1	Serum magnesium	Meyer TE	20700443	2.50E-17
rs7638853	rs7638853	1	Expression of SENP2 in brain cortex	Heinzen	19222302	1.83E-09
rs12678719	rs12678719	1	Serum VEGF	Debette S	21757650	1.95E-10
rs4901308	rs8008270	0.964	Prostate cancer	Eeles RA	23535732	2.00E-14
QT interval score						
rs12061601	rs12061601	1	Normalized agkistrodon contortrix venom ratio in venous thrombosis	Oudot Mellakh T	22443383	4.53E-16
rs1361754	rs1361754	1	Chromosome Methylation levels in Neural Tissues	Gibbs J	20485568	2.44E-30
	rs1361754	1	Differential expression of PM20D1 probe 2452744 in brain cortex	Heinzen	19222302	2.92E-10
rs1801725	rs1801725	1	Calcium levels	OSeaghdha CM	24068962	9.00E-86
rs7765828	rs6459467	0.996	Blood metabolite levels	Shin SY	24816252	2.00E-16
rs3807375	rs3807375	1	Height	GIANT	25282103	7.20E-11
rs2485376	rs2485376	1	Years of educational attainment	SSGAC	27225129	4.63E-10
rs7122937	rs7122937	1	Chromosome Methylation levels in Neural Tissues	Gibbs J	20485568	2.57E-24
rs174583	rs174583	1	Serum LAPUFA	Kettunen J	22286219	1.33E-267
	rs174583	1	Plasma docosapentaenoic acid levels	Lemaitre RN	21829377	4.17E-147
	rs174583	1	PC aa C363, PC aa C364	Illig T	20037589	6.40E-91
	rs174583	1	Serum ratio of 1- PE (20:4/0:0)/ CHEBI:85670	Suhre K	21886157	3.10E-68
	rs174583	1	LDL	GLGC	24097068	7.00E-41
	rs174583	1	Total cholesterol	GLGC	24097068	6.05E-38
	rs174583	1	Triglycerides	GLGC	24097068	8.38E-35
	rs174583	1	HDL	GLGC	24097068	1.19E-26
	rs174583	1	Plasma stearic acid	Wu JH	23362303	9.91E-19

SNP in score	Reported SNP	r^2 with sentinel	Trait	First author	PMID	*P*-value
	rs174583	1	Fasting glucose	MAGIC	20081858	1.17E-08
	rs174576	0.979	Differential expression of FADS2 in peripheral blood mononuclear cells	Heinzen	19222302	6.51E-15
	rs174577	0.966	Iron status biomarkers transferrin levels	Benyamin B	25352340	2.00E-17
rs246185	rs246185	1	Height	GIANT	25282103	2.00E-18
	rs246185	1	Age at menarche	ReproGen	25231870	6.80E-16
rs17608766	rs17608766	1	Gene expression of GOSR2 in liver	ICBP	21909115	3.00E-24
	rs17608766	1	Blood pressure	Wain LV	21909110	6.00E-15
	rs17608766	1	Coronary artery disease	Howson JMM	28530674	4.14E-08

Table 6.12: Shown are the association results for all single nucleotide polymorphisms (SNPs) in the ECG genetic scores with $r^2>0.8$ (1000 Genomes Phase 3 data) to one of the associated SNPs that achieved genome-wide significance of $P<5\times10^{-8}$ for any biomedical trait (excluding other ECG parameters – P-duration, PR interval, QRS duration, QT duration) as reported in catalogues of associations for European ancestry. Data retrieved via phenoscanner (http://www.phenoscanner.medschl.cam.ac.uk/phenoscanner).

Figure 6.11 – Funnel plot for SNPs in P-wave duration score

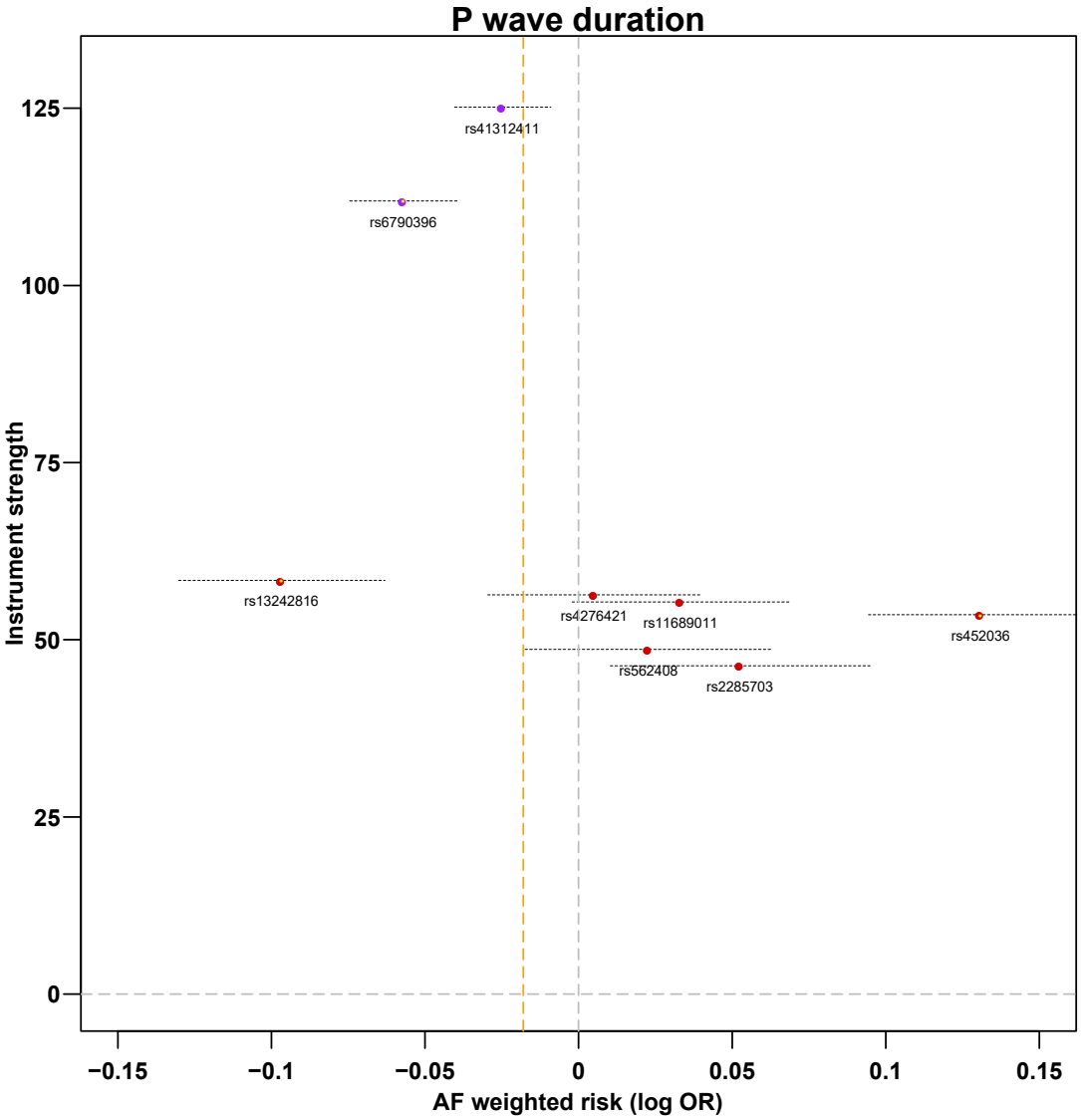


Figure 6.11: Funnel plot showing individual single nucleotide polymorphism (SNP) effects on atrial fibrillation (AF) expressed as log odds ratio (OR) estimate from UK Biobank data vs. strength of SNP in genetic P-wave duration score (effect on P-wave duration / standard error of estimate of effect on AF). Orange dotted line is the overall effect estimate for the score, red circles represent SNPs in P-wave duration score, purple circles represent SNPs in ion channel sub-score, inner white circles represent a SNP excluded by MR-PRESSO method.

Figure 6.12 – Funnel plot for SNPs in PR interval score

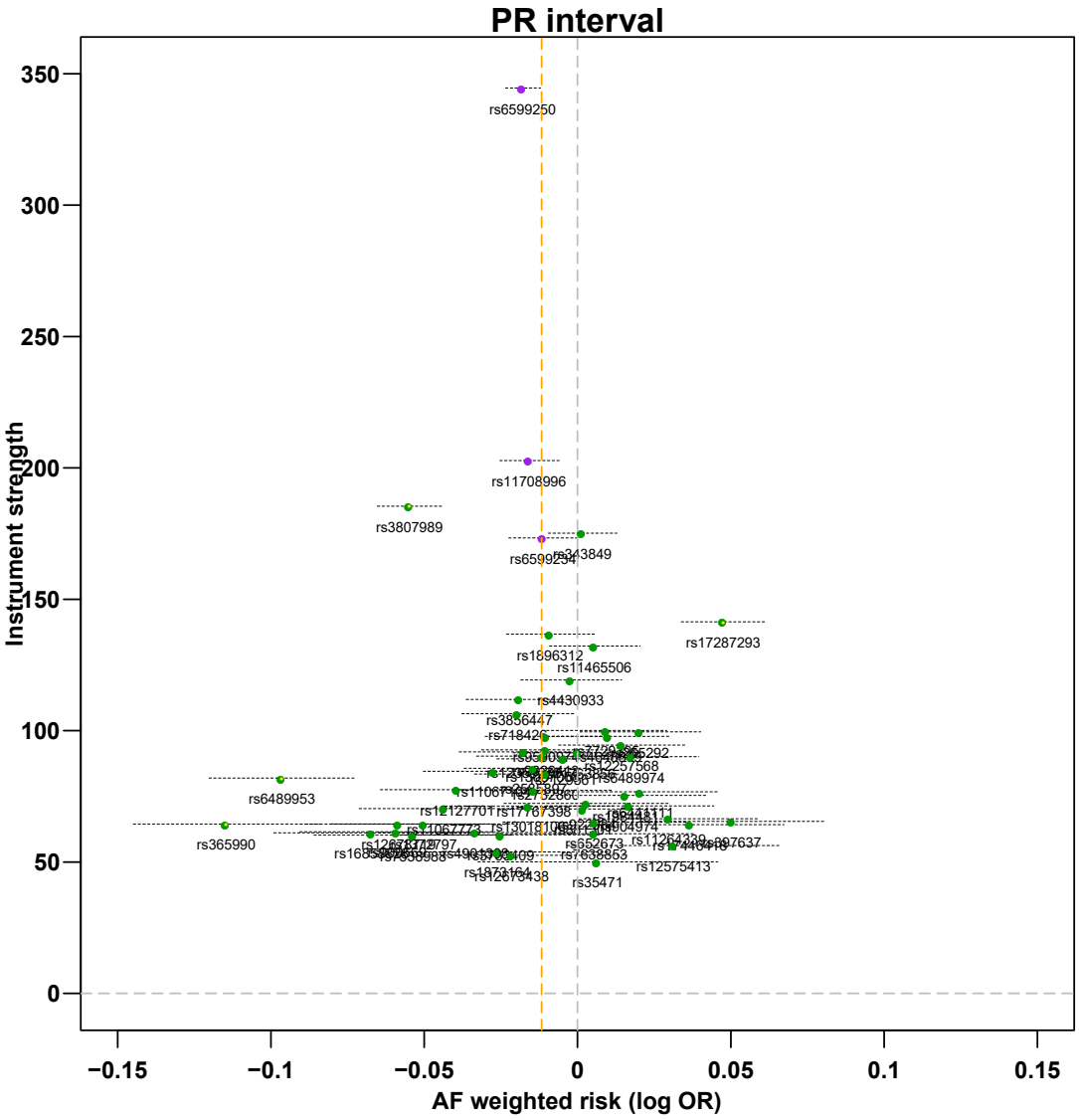


Figure 6.12: Funnel plot showing individual single nucleotide polymorphism (SNP) effects on atrial fibrillation (AF) expressed as log odds ratio (OR) estimate from UK Biobank data vs. strength of SNP in genetic PR interval score (effect on PR interval / standard error of estimate of effect on AF). Orange dotted line is the overall effect estimate for the score, green circles represent SNPs in PR interval score, purple circles represent SNPs in ion channel sub-score, inner yellow circles represent a SNP excluded by MR-PRESSO method.

Figure 6.13 – Funnel plot for SNPs in QT interval score

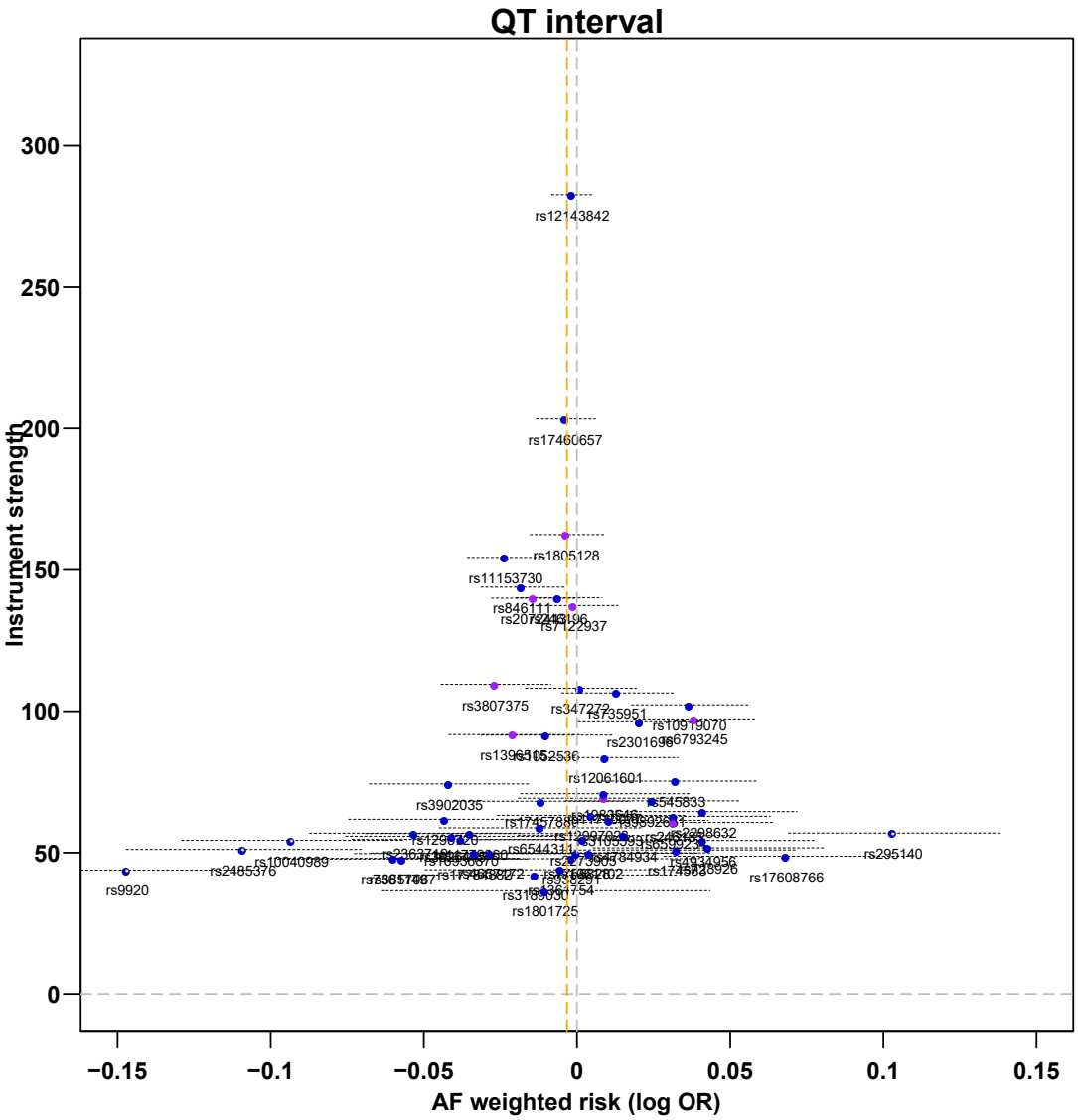


Figure 6.13: Funnel plot showing individual single nucleotide polymorphism (SNP) effects on atrial fibrillation (AF) expressed as log odds ratio (OR) estimate from UK Biobank data vs. strength of SNP in genetic QT interval score (effect on QT interval / standard error of estimate of effect on AF). Orange dotted line is the overall effect estimate for the score, blue circles represent SNPs in QT interval score, purple circles represent SNPs in ion channel sub-score, inner yellow circles represent a SNP excluded by MR-PRESSO method.

6.4 Discussion

AF is characterised by a disruption in coordinated atrial electrical activity. Following on from the NOS1AP-Tg mouse model with altered ECG parameters and an increased risk of arrhythmogenesis, I used Mendelian randomisation methods to provide novel evidence supporting causal relationships between genetically predicted lifelong differences in cardiac electrical parameters and risks of developing both AF and non-AF SVT. Unexpectedly, I found evidence supporting a causal association between lifelong differences in ECG parameters representing longer atrial conduction times within the normal range, and a lower risk of AF. In particular, genetically predicted differences in PR interval showed robust associations across a broad range of analyses and mechanistic pathways.

6.4.1 ECG parameters as predictors of AF

ECG parameters reflecting the propagation of the electric impulse through the atria to the ventricular myocardium have been associated with incident AF in a number of large observational studies [240,241,261-264,291]. However, risk factors for AF, such as age and heart failure, a history of AF and use of anti-arrhythmic or rate-controlling medications also influence ECG parameters, limiting any causal inferences from observational data. In the largest observational study to examine associations between atrial ECG parameters and AF [240,241], investigators observed the highest risk of AF in those with abnormally long PR intervals (> 200 ms), but these observations were made in patients who had been referred for ECGs by their general practitioner, who therefore may have been at higher risk of cardiovascular disease than the general population. Indeed, risk scores for predicting incident AF use an abnormal PR interval as a component of the score [291,292], again implying that longer atrial conduction time in older patients with cardiovascular disease is a risk indicator for, but not necessarily a causal determinant of, AF.

In UK Biobank, in the subgroup of participants who had measured 12-lead ECG parameters, these mainly fell within normal reference ranges. Assuming similar characteristics across the whole cohort, a longer genetically predicted P-wave duration was associated with a lower risk of AF, consistent with data from observational studies over the same range of values [240,262]. A longer

PR interval was also associated with a lower risk of AF but over a range of values (~155 to 175 ms) that had previously been associated with a higher risk of AF in observational studies [241]. The consistent effects of the ECG genetic scores on risk of so-called 'lone' AF further support the conclusion that the potential causal associations were independent of any shared links with major AF risk factors. Furthermore, being at higher genetic risk of AF was not associated with altered ECG parameters to a meaningful extent, suggesting that bidirectional relationships do not explain the observed effects of ECG parameters on risk of AF.

In UK Biobank, the association between QT interval and AF was not strong, but after meta-analysis, showed association between a longer QT_c interval within the normal range (~410 to 430 ms) and a lower risk of AF. Observational studies have typically showed the largest size of associations with AF once the QT interval was abnormal (i.e. QT_c > 450ms) [49,50]. The QT interval prolongs with age, concomitant cardiovascular disease or as a result of anti-arrhythmic medication for AF [268,293]. Mechanistically, it is difficult to link ventricular repolarisation directly to AF, although it is plausible that atrial and ventricular depolarisation (the QRS interval, a small part of the QT) would share similar electrophysiological properties. Overall, an altered QT interval may be more likely to reflect a similarly altered atrial electrical substrate than being directly causal itself.

Previous GWAS for the PR interval reported that some individual genetic variants that affected the PR interval were associated with risk of AF [294,295]. Here, the different variants' effects on AF were not consistent with their effects on PR interval and were not quantified. The strengths of a formal Mendelian randomisation analysis are that all the genetic variants are included as appropriately weighted surrogates for the exposure of interest, with estimation of the effect of lifelong exposure on the outcome and subsequent consideration of pleiotropy.

6.4.2 Mechanistic insights into pathophysiology of arrhythmias

The relationship between abnormal prolongation of the P-wave and PR interval and a higher risk of AF has been interpreted as reflecting prolonged atrial conduction times, secondary to structural

remodelling and fibrosis, promoting re-entry circuits and favouring the maintenance of AF [296]. I found that within their normal range, longer P-wave duration and PR interval were associated with lower risks of both AF and SVT, implying that shorter atrial electrical conduction times may directly increase the risk of both arrhythmias. The mechanism underpinning the causal link between findings I observed may seem less intuitive, but has some supporting evidence in the literature. For example, consistent with what I observed, commonly used anti-arrhythmic drugs for AF such as flecainide, propafenone and amiodarone are known to prolong the PR interval, and yet reduce risk of AF and SVT [297]. Within the ion channel scores, variants in the *SCN5A* gene that lengthened P-wave duration and PR interval were associated with a lower risk of AF and SVT, in keeping with the antiarrhythmic action of flecainide, which, by blocking $Na_v1.5$ (the sodium channel encoded by *SCN5A*), prolongs the PR interval and prevents AF and SVT recurrence. Furthermore, consistent with the overall scores, ion channel scores for atrial conduction parameters affected risk of AF and SVT, whereas ion channel scores for ventricular repolarisation did not, suggesting that chamber specific drug targets may have therapeutic potential. Whilst familial studies investigating 'lone' AF due to *SCN5A* have yielded conflicting results regarding pathogenicity [298,299], more recent data suggest that genetic variation in the nearby *SCN10A* regulates *SCN5A* expression [300], with alleles associated with prolonged PR interval reducing *SCN5A* mRNA levels in a dose dependent manner, which is directionally consistent with my findings.

Both P-wave duration and PR interval are affected by atrial volume and tissue characteristics (e.g., fibrosis, muscle fibre orientation, etc.). I did not find the ECG scores to be associated with differences in left atrial volume, suggesting the genetic scores did not alter the risk of AF through this well-established mechanism.

Large-scale epidemiological studies have reported a 'U-shaped relationship' between ECG parameters and AF, with individuals with both short and long intervals at higher risk [48,241,292]. Interestingly, individuals with shorter intervals were much younger and had a very low prevalence of cardiovascular co-morbidities compared to those with longer intervals, although both groups

had similarly increased risks of AF. In other studies, individuals with a short PR interval but no other signs of pre-excitation have been reported to have an increased incidence of supraventricular arrhythmia, including SVT, AF and atrial flutter [301,302]. Overall, this suggests distinct mechanisms of arrhythmogenicity in the presence or absence of altered atrial structure.

There is limited large-scale epidemiological evidence regarding SVT. Similarly, the heritability of non-AF SVT is not well understood, with most cases thought to be sporadic, although there is some evidence that Wolff-Parkinson-White (WPW) syndrome has a hereditary basis [303]. Patients with WPW (comprising ~10% of SVT cases in the UKB dataset) have a shortened PR interval on ECG and a higher risk of AF that persists despite successful accessory pathway ablation, suggesting the presence of an additional atrial pro-arrhythmic substrate beyond the accessory pathway [304]. More recently, an increased risk of AF has been reported in patients who have undergone ablation for atrioventricular nodal re-entrant tachycardia [305], which is the commonest non-AF form of SVT, comprising ~60% of cases and typically due to re-entry within dual 'slow' and 'fast' pathways. Similarly, patients with short PR interval and normal QRS duration, as originally described by Lown, Ganong and Levine [302] present with a variety of atrial arrhythmias in the absence of a defined accessory pathway, suggesting that fast impulse transmission through the atria and to the ventricles may be arrhythmogenic *per se*.

Overall, my findings provide evidence supporting the concept that AF may be a common arrhythmia representing different mechanisms and atrial substrates. Interestingly, these specific findings seem to be also applicable to non-AF SVT, which conventionally has not been thought to be similar to AF mechanistically [290]. This suggests that more individualised ascertainment and therapeutic targeting of specific mechanisms of arrhythmia is warranted.

6.4.3 Limitations

The genome-wide association studies for ECG parameters that were used for genetic variant selection were conducted in participants with European ancestry, and UK Biobank chiefly includes White British individuals, consequently my analyses were restricted to this population. Further

studies are needed to assess the generalisability of our results across ethnicities. Furthermore, whilst UK Biobank includes comprehensive phenotyping data, information from AF diagnoses recorded in primary care were not included in the present study due to limited availability.

P-wave duration is part of the PR interval and it is therefore difficult to robustly assess its relevance alone. Further, the P-wave duration genetic risk score was comprised of 8 variants with the most heterogeneity in terms of effects of individual SNPs and greater variability across results from the sensitivity analyses when compared with the PR interval genetic risk score. Limited analyses suggest that the effects of PR interval are unaffected by P-wave duration, and so it is likely that components of both atrial depolarisation and atrio-ventricular nodal conduction time affect the risk of AF and SVT. Consequently, I refer to atrial electrical conduction times to encompass the underlying biological mechanism behind both P-wave duration and PR interval. It is also not clear whether the weaker effects of QT interval on AF reflect a small but genuine impact of ventricular characteristics on AF or some common heritability between atrial and ventricular electrical traits.

A potential limitation of any MR study is pleiotropy – where the genetic variants affect the outcome (i.e. AF) by a biological pathway not mediated by the risk factor of interest (i.e. the ECG parameters). Multiple sensitivity analyses provided similar effect estimates as the primary analyses, with particularly robust results for PR interval, making it unlikely that pleiotropy had a meaningful impact on the results. The consistent associations of the ECG scores with AF and 'lone' AF, and the similar results obtained from the ion channel scores, provide additional evidence of the robustness of the reported associations.

The effect sizes on AF and SVT observed in this study represent a lifelong cumulative effect of differences in ECG parameters and are not necessarily directly comparable to those derived from observational or clinical studies. Additionally, the study results may be limited to the normal reference ranges of the ECG measurements, as only these ranges were observed in a subgroup of UK Biobank participants. As with any large middle-aged cohort, UK Biobank includes participants with a wide range of medical conditions who may receive various medications that affect measured ECG parameters and thus influence the range of values represented in this study. Most

importantly, these findings do not rule out different relationships between the ECG parameters and AF outside of the ranges studied, and thus further studies exploring wider ECG ranges and non-linear relationships with AF are warranted.

6.4.4 Conclusion

We have provided evidence that supports, within the normal range of ECG parameters, a causal relationship between lifelong differences that reflect longer atrial electrical conduction and lower risks of AF and SVT. Our study also provides mechanistic insight into the underlying pathophysiology of these arrhythmias, and shows that the effects of ECG parameters on AF appear to be driven partly by differences in atrial electrical substrate, and not atrial size or major cardiovascular co-morbidities. This emphasises that substantial variation in the mechanisms underpinning AF exists, and warrants the consideration of more individualised treatment strategies.

6.4.5 Implications for NOS1AP-Tg

Superficially, these findings in humans are contradictory to those seen in the NOS1AP-Tg mice where a longer P-wave and PR interval were the main atrial ECG findings seen with an increase in atrial arrhythmogenesis. As discussed previously, my findings in humans related predominantly to ECG parameters within normal reference ranges and did not rule out different mechanisms of arrhythmia which might be the case with the NOS1AP-Tg mice. Further overall consideration of the findings from all the results chapters as a whole will follow in **Chapter 7**.

7

Conclusions

Summary

Based on evidence from the transgenic mouse model, *NOSIAP* appears to predominantly affect the electrical substrate by altering conduction velocity, with alterations in connexin-43 likely playing an important role. Mechanistic translation of this finding to understand how whole organ ECG parameters might be altered will likely require further investigation of specific interactions between NOSIAP and proteins at the intercalated disc and more complex and representative computational modeling of human ECG parameters integrating cellular, tissue and organ specific variables. The complex nature of such parameters might also require a more fundamental shift away from how we have historically conceptualised specific ECG parameters in isolation to more unbiased approaches using integrated modelling.

7.1 Discussion of key findings

7.1.1 Summary

As described in **Chapter 1**, genetic variants in *NOSIAP* associated with increased gene expression are strongly associated with longer QT intervals and presumed ventricular arrhythmias, manifesting as the phenotype of sudden unexplained death.

To investigate this, we generated a transgenic mouse overexpressing human *NOSIAP* in the myocardium (NOSIAP-Tg) as described in **Chapter 3**. Cardiac overexpression of *NOSIAP* resulted in the NOSIAP-Tg mice having a shortened measured QT interval on surface ECG but an increased propensity to the induction of *ex-vivo* ventricular arrhythmias in the absence of echocardiographic changes in left ventricular structure or function. Further investigation of the cardiac electrical substrate in **Chapter 4** surprisingly revealed no differences in action potential duration at physiological pacing rates between genotypes, but showed a significant reduction in conduction velocity in the left ventricles of transgenic mice without an increase in cardiac fibrosis. The slowing of conduction velocity was accompanied by reductions in ventricular connexin-43 content, particularly localised to the intercalated discs. No differences in calcium handling or NOS activity were detected. There were no obvious changes in the rapid sodium current $I_{Na.}$ The NOSIAP-Tg mice also had a prolonged P-wave duration and PR interval in transgenic mice and, as described in **Chapter 5**, a higher propensity to develop *in-vivo* atrial arrhythmias, suggesting that NOSIAP overexpression affected not only the ventricular, but also the atrial electrical substrate.

Following on from this, in human populations, ECG parameters have been observed to be associated with risks of development of atrial fibrillation but these observational studies are subject to limitations so the causal relevance is unclear. As discussed in **Chapter 6**, I used Mendelian randomisation to overcome this and using weighted genetic scores for P-wave duration, PR interval and QT interval showed novel evidence supporting causal relationships between lifelong differences in cardiac electrical parameters and risks of developing AF in large human population datasets. Unexpectedly, I found evidence supporting a causal association between

lifelong differences in ECG parameters representing longer atrial conduction times within the normal range, and a lower risk of AF.

7.1.2 NOS1AP and the electrical substrate

The main change in electrical substrate that I found in the NOS1AP-Tg mice was a reduction in conduction velocity across the left ventricle which was associated with lower levels of Cx43 compared to wild-type. Localised changes in conduction velocity are a key feature of changes in substrate that can pre-dispose to the development of re-entrant arrhythmias [198]. A number of murine models of connexin deficiency show an increase in ventricular arrhythmias [157], and in humans, genetic variants associated with the *GJA5* (the gene encoding connexin 40, predominantly found in the atrium) have been associated with AF, initially in familial cases of 'idiopathic' AF [306] and then subsequently also in the wider population via GWAS [232]. This provides evidence of a mechanistic link between altered connexin biology, conduction velocity and arrhythmogenesis.

Conduction velocity and depolarisation

Could the reduced conduction velocity contribute to the altered ECG parameters seen in the transgenic mice? Simplistically, a slower conduction velocity would be expected to increase the time taken for electrical depolarisation to transit through the atria, resulting in a longer P-wave as shown in **Figure 3.11**. As also noted in the earlier results, the prolongation of the PR interval in the NOS1AP-Tg mice was due to the longer P-wave duration and not due to a significantly prolonged isoelectric component. I had also observed a longer QRS duration in the transgenic mice and again, simplistically, this may be explained by a slower conduction velocity and slower depolarisation through the ventricles.

As discussed briefly in **Section 4.4.3**, Hulsmans *et al*. [221] provided novel evidence suggesting that macrophages actively modulated the electrical properties of cardiomyocytes via connexin-43 (Cx43). Providing detailed evidence, they found that macrophages with a Cx43 deletion were unable to couple to murine cardiomyocytes and that this led to a prolonged PR interval, although they did not report on other ECG parameters. The role of macrophages in other areas of the

myocardium remains to be determined but this provides direct evidence that Cx43 may be relevant beyond linking adjacent cardiomyocytes electrically.

In humans, genetic variation in *NOSIAP* has not previously been described in GWAS as being a significant contributor to atrial ECG parameters or for AF. However, as has been noted over the years, GWAS have stringent thresholds for statistical significance and for the atrial parameters are relatively underpowered at present, explaining only approximately 2 – 5 % of the total variance [242]. It is therefore possible that smaller effects of *NOSIAP* on other electrical parameters may not yet be appreciated.

Conduction velocity and repolarisation

The relationship between changes in conduction velocity and repolarisation on a tissue level is more complicated. As discussed in **Section 3.5.3**, the murine QT interval has been well described as not being entirely representative of repolarisation (for instance due to the absence of a defined T-wave for measurement and simultaneous de- and repolarisation occurring within the murine heart [307]). Accordingly, by measuring APD, I investigated another marker of repolarisation, but this was unchanged between wild-type and transgenic mice, at least at physiological heart rates. It is possible that in our model, the shorter QT interval did not accurately represent repolarisation but equally it is possible that the type of APD measurements alone were unable to detect changes in repolarisation parameters, perhaps not being sensitive enough.

Whether changes in conduction velocity might affect the QT interval without affecting APD is more complicated. Simple modelling of myocytes as linear cables suggests no effect of isolated changes in intercellular resistance on APD despite marked effects on conduction velocity [198]. However, the QT interval is a representation of the total electrical activity across both right and left ventricles. It is well known that in humans and mice there exist heterogeneities in repolarisation at an organ level that may not be detected by measuring APD in single cells or at single points of the organ. As discussed earlier, studies have shown changes in APD measurements between single cells and coupled cells [208], so whilst gap junctions affect conduction velocity, it is

possible they may also play other roles in modulating repolarisation. In this regard, there may be insights to be gained from more complex methods of electrical mapping.

Mapping repolarisation in humans

In humans, specialist technology using an external high density electrode mapping jacket (ECGI) can image de- and repolarisation across the surface of the human heart non-invasively [308]. Using the ECGI vest in patients with Brugada syndrome, Zhang *et al.* [309] showed localised changes in electrical substrate localised to the RVOT. They showed that local activation time, a marker of the depolarisation wavefront, was significantly prolonged in the RVOT when compared with control subjects and other areas of the heart. Interestingly, the recovery time (a marker of repolarisation) as well as the local activation recovery time (correlating to local APD) were also significantly prolonged in the RVOT in patients with Brugada syndrome when compared to other areas of the heart and healthy controls. This suggests that, at least in Brugada syndrome, localised morphological changes in the QT interval on ECG may be related to both de- and repolarisation abnormalities. As described earlier, in autopsy specimens, a localised reduction in Cx43 at the intercalated disc was seen in the RVOT of patients with presumed Brugada syndrome [219,220]. Separately, radiofrequency ablation of areas of slow conduction in the epicardial RVOT in patients with Brugada syndrome has been described as leading to normalisation of the typical Brugada ECG [310], even after subsequent flecainide or ajmaline challenge (which typically block I_{Na} and slow conduction and reveal the ECG pattern) [219]. Overall, this suggests that morphological changes in the QT interval may be associated with changes in conduction velocity and that Cx43 may play a role in altering QT parameters in some diseases.

Vijayakumar *et al.* [311] used the ECGI technology in patients with a variety of long QT syndromes and showed global activation time was not significantly longer compared to control subjects. As expected, global recovery time (a marker of repolarisation), and the activation recovery interval (correlating to local APD) were both significantly increased. However, compared to controls, in patients with long QT syndromes, there were significant gradients of repolarisation heterogeneity on the epicardium. Specifically, patients with long QT syndrome showed regions of delayed

ventricular recovery on the epicardium, leading to significant 'gradients' of repolarisation across the heart's surface. Additionally, the local electrograms from these areas showed a predominantly negative T-wave polarity when compared to other areas with a more conventional positive T-wave. Even more interestingly, the length of the QT_c interval on surface ECG from patients with long QT syndrome did not correlate with any of the global repolarisation indices measured, although the repolarisation indices were able to reliably differentiate patients with previous arrhythmic symptoms from those without. This suggests that whilst the QT interval is a useful marker of repolarisation, it is not comprehensive. It also suggests that more refined whole organ approaches to measuring repolarisation are required for mouse models, where the QT interval even under 'normal' conditions may not reflect the true extent of repolarisation.

Intercalated disc and QT interval

It is possible that alterations in gap junctions at the intercalated disc may affect both conduction velocity as well as repolarisation, independently of changes in conduction velocity. The sodium channel $Na_v1.5$ is also reported to be found in high levels at the intercalated disc [312].

Kapoor *et al*. [86] investigated the possible contribution of the intercalated disc to the QT interval using human genetic variants with protein products localised to the intercalated disc. They found that a set of these variants (27,000 variants from 170 genes including *GJA1* for Cx43) were more likely to be found to be significant in GWAS for the QT interval when compared with a 'control' set of genetic variants expressing cardiac proteins not in the intercalated disc (11,000 variants from 166 genes). This suggests a role for genetic variants thought to affect the intercalated disc in the complex variation surrounding generation of the human QT interval.

Referring back to Hulsmans *et al*.'s work [221], the authors also noted that Cx43 mediated coupling of macrophages to cardiomyocytes in murine cells accelerated repolarisation. Although not a focus of their work, they also noted that in mice with selective macrophage Cx43 deficiency, ventricular effective refractory periods were prolonged. One might speculate that a global loss of Cx43, in keeping with what was seen in NOS1AP-Tg might not only slow conduction but additionally decouple macrophages that modulate cardiomyocyte electrophysiology.

Overall, this suggests there are further insights to be gleaned beyond the conventional view of Cx43 and the intercalated disc's involvement in conduction of electrical activity.

7.1.3 Mechanisms of arrhythmogenesis

Conceptualising arrhythmogenesis like Coumel [172], consideration could be made of the effect of NOS1AP overexpression on arrhythmia triggers, the electrical substrate, and broader factors modulating arrhythmogenesis such as the autonomic nervous system. In our model, having seen evidence of changes in the electrical substrate in the form of altered ECG parameters, the main positive findings from the experiments conducted were a significant slowing of conduction velocity in the ventricles of transgenic mice, associated with reduced Cx43 at the intercalated disc and some isolated changes in I_{Na} inactivation characteristics as well.

NOS1AP and arrhythmia triggers

As discussed in **Chapter 3** and **Chapter 5**, the NOS1AP-Tg model developed arrhythmias secondary to burst pacing triggers but these did not develop spontaneously. A study by Sugiyama *et al*. [110] described the generation of a mouse model ostensibly with global murine *Nos1ap* knockout (*Nos1ap*$^{-/-}$). They found no baseline changes in ECG parameters, cardiac function, calcium handling, conduction velocity or spontaneous arrhythmias when the knockout mice were compared to wild-types, again confirming no effect of NOS1AP on spontaneous arrhythmogenesis.

Sugiyama *et al*. [110] subsequently administered the cytotoxic agent doxorubicin (25mg/kg body weight) intraperitoneally, and found a marked increase in spontaneous lethal ventricular arrhythmias in *Nos1ap*$^{-/-}$ mice when compared to wild-type mice which were less severely affected. Additionally, after doxorubicin injection and when compared to wild-type mice, *Nos1ap*$^{-/-}$ had a longer QRS and QT_c on ECG, a longer APD_{90}, a reduction in peak $[Ca^{2+}]_i$, a higher B-type natriuretic peptide level indicating cardiac dysfunction, but no changes in conduction velocity or histological fibrosis. Pre-treatment of mice with N-acetyl-cysteine (NAC) before the doxorubicin injection ameliorated the majority of the changes observed. However, as the model was generated (although not confirmed) to be a global *Nos1ap* knockout and non-specific stress was used, it is difficult to draw inferences about the specific role of myocardial NOS1AP other than concluding

that NOS1AP may play a role in maintaining electrical stability under conditions of doxorubicin induced cardiotoxicity as a trigger.

NOS1AP and the autonomic system

As our NOS1AP-Tg mouse model was that of cardiac limited *NOS1AP* overexpression, Coumel's [172] 'modulating factors' for arrhythmogenesis involving the autonomic nervous system may not necessarily be relevant to the arrhythmogenesis we observed, which was seen both *in-vivo* and *ex-vivo*. However, in humans, it is possible that part of the effect of *NOS1AP* is mediated via the cardiac autonomic system, as of course the alleles are expressed throughout all tissues and gene expression of *NOS1AP* is high within the nervous system. In this scenario, the findings of Lu *et al.* [105] would suggest that overexpression of *NOS1AP* in cardiac sympathetic neurons is associated with a small but significantly reduced amount of calcium triggered noradrenaline release. Sympathetic stimulation is thought to shorten APD and has been implicated in both atrial and ventricular arrhythmogenesis [313]. Therefore, reduced sympathetic noradrenaline consequent to NOS1AP overexpression may be conceptualized as contributing to a longer APD. However, whether this subtle change to the sympathetic nervous system might have a significant contribution to the resting QT interval in humans (as the original GWAS studies noted) is unclear.

From the evidence thus far from both humans and in our transgenic model, it is likely that the main reason for the increased arrhythmogenesis was due to changes in the electrical substrate.

7.1.4 ECG parameters and arrhythmias

The underlying rationale for much of the work in **Chapter 6** was that on a population level, conventionally defined ECG parameters could prove useful markers of the underlying electrical substrate and therefore could give us insight into mechanisms of arrhythmogenesis. Data from observational studies suggested that excessively prolonged atrial and ventricular ECG parameters were associated with an increased risk of AF and indeed the NOS1AP-Tg mice had prolonged P-wave duration and PR intervals and an increased risk of inducible AF. It might therefore seem contrary that the genetic scores representing lifelong differences in ECG parameters suggested that prolonged atrial ECG parameters were in fact associated with a lower risk of AF.

It is important to be clear what the genetic scores and their results represent. They are a representation of differences in ECG parameters over a lifetime and the associations with AF similarly represent the effects of these over a lifetime and across a large population. Any individual's genetic score represents a small proportion of their own ECG variability and could be be dwarfed by other factors. Thus, two individuals with very different genetic scores may well have the same measured ECG parameters. An individual person's ECG remains the correct representation of that individual's cardiac electrical substrate at that point in time. As has been stressed previously, the genetic scores were representative of ECG parameters within the normal range, and so the numerous observational studies in humans suggesting associations between e.g. extremely prolonged PR interval and AF are not incompatible with our findings. Again, it is important to differentiate between a potentially causal relationship and one where a prolonged PR interval may be a biomarker of other alterations in the atrial substrate predisposing someone to AF.

AF is a heterogenous condition and going back to the NOS1AP-Tg mice, it may well be that the specific mechanism by which the mice developed AF were different to those represented by the genetic scores in our population study. In the larger observational studies [240,241], there was a 'U' shaped relationship between P-wave duration or PR interval and AF. Typically, those with longer P-wave durations or PR intervals were older with more co-morbidities, whilst those with shorter durations were younger and without co-morbidities. It may well be that our genetic scores, representing differences in ECG parameters free from confounding by other co-morbidities more closely represent the mechanisms by which younger, otherwise healthy individuals develop AF. Those older individuals with more cardiovascular co-morbidities may develop AF due to different mechanisms with their electrical substrate being represented by more prolonged atrial ECG parameter durations. Indeed, there is evidence suggesting that most ECG intervals prolong as people age even in the absence of 'overt' confounding co-morbidities [314].

It is therefore likely that multiple mechanisms lead to AF and that our population results reflect one aspect of changes in electrical substrate that lead to AF.

7.2 Limitations

7.2.1 Transgenic mouse model

Rationale for generation

Generation of the Tg(*Myh6-hNOSIAP*) mouse model was based on evidence that the *NOSIAP* alleles associated with a longer QT in human populations were associated with increases in gene expression. The model assumed that overexpression in cardiac tissues only of *NOSIAP* would be relevant to the human phenotype. Firstly, it is possible that the non-coding genetic variants associated with the QT interval did not act solely on *NOSIAP* gene expression and may have had 'trans' effects on other genes that are as yet unknown. Secondly, we knowingly limited over-expression of *NOSIAP* to cardiac tissues to investigate these effects but of course the presumed overexpression of *NOSIAP* would occur in all tissues, in particular tissues within the nervous system which are well known to affect electrophysiology. It is likely that the effects of *NOSIAP* on electrophysiology result from a mixture of effects, primarily within the heart but also within the autonomic nervous system which we did not investigate using the transgenic model. As discussed in **Chapter 3**, we chose overexpression of a human *NOSIAP* gene and protein with extremely close homology to the murine form. However, it is possible that key secondary modifications may be different in mouse and human and that these may have led to different protein-protein interactions.

Generation of model

As discussed in **Chapter 3**, a key limitation of the work presented is the fact that we were unable to generate transgenic mice with different degrees of *NOSIAP* expression. This may have allowed for more quantitative measurements showing different levels of *NOSIAP* expression correlating with different degrees of variation in the phenotypic parameters studied.

Fundamental use of murine model

The use of a mouse model particularly for electrophysiological investigation of human characteristics is inherently the biggest limitation of the work presented. We tried to mitigate this by the use of human *NOSIAP* gene and protein expression but it is possible that some of our

findings are limited to the murine model and not applicable to humans. In particular, at face value, the NOSIAP-Tg had a shorter QT interval than their wild-type littermates. The differences between murine versus human cardiac electrophysiology are well described [149,315,316]. Beyond the difficulties in measuring murine ECG parameters representing repolarisation [307], of relevance to the work presented here are the differences in repolarisation currents in the ventricles. Specifically, although mice are reliant on potassium currents for repolarisation (I_{to} in particular), these are different to those described in humans (I_{Kr} and I_{Ks}). It is possible that the specific effects of *NOSIAP* are mediated differently in humans and mice as a result.

7.2.2 Population science work

Beyond the limitations described in **Section 6.4.3**, I was unable to specifically use a genetic instrument for *NOSIAP* or *GJA1* to investigate the associations of the gene with arrhythmias. It did not prove possible to select non-coding genetic variants for inclusion into a putative instrument without some knowledge of their biological functions beyond associations with the QT interval. As a result, it was not possible to test the effects seen in the NOSIAP-Tg mice in a human population directly.

Separately, although it proved possible to generate a population phenotype representing atrial fibrillation and supraventricular tachycardias separately, it was not possible to develop an accurate phenotype of ventricular arrhythmias or ventricular fibrillation using the UK Biobank data. As was discussed in **Section 1.2.2**, these events are rare and accurate curation of such a phenotype usually requires individual case review which was not possible. A recent GWAS using definitions of sudden cardiac death did not find any significant SNPs at GWAS significance thresholds, with the authors suggesting that without detailed phenotyping post-mortem, the heterogenous nature of the cohort may dilute genetic associations [317].

7.3 Future work

The NOSIAP-Tg mice have a complex electrical substrate and further investigation of specific interactions between NOSIAP and intercalated disc proteins, including both Cx43 and $Na_v1.5$ may

prove useful. It would also be interesting to reproduce some of the NOS1 experiments in the atrium, where NOS1 levels are typically higher.

Going forward, it is likely that more complex and representative computational modeling of human ECG parameters integrating cellular, tissue and organ specific variables would be needed to understand such a multi-faceted system. This may be in the form of incremental improvements in modelling of ECG parameters as described by Tomek *et al.* [318], but might also require a more fundamental shift in how we conveniently classify ECG parameters from their earliest descriptions.

Verweij *et al.* [319] conceptualised the ECG as a continuous representation of electrical activity and selected 500 time points across a single averaged heart beat in a large data sample. They then performed a GWAS looking for what they termed 'genetic ECG signatures'. For individual genetic variants, they plotted the *P*-value for association with each of these time points across a representative ECG trace, available in a freely searchable online database (www.ecgenetics.org). For instance, for the *NOSIAP* allele with the strongest association with QT interval, rs12143842, this is plotted in **Figure 7.1 A**. The red line is the plot of the *P*-values for association, with a positive value representing a positive association (i.e. that the allele increases the value of that datapoint). It is clear that the QT prolonging allele of *NOSIAP* is positively associated with a higher amplitude at end of the T-wave but a lower amplitude in the earlier part of the T-wave – i.e. a more prolonged T-wave. There is also a suggestion that this allele of *NOSIAP* may be associated with a lower amplitude of the QRS interval in the early part and a higher amplitude later on – again, leading to a more prolonged QRS interval. Using polygenic scores, Verweij *et al.* [319] also showed the polygenic score for QT interval was associated with a subtle increase in the amplitude of the P-wave as well (**Figure 7.1 B**). The polygenic PR interval score and the polygenic AF score (**Figure 7.1 C** and **D**) showed opposite associations across the PR interval, in keeping with the findings from **Chapter 6** suggesting that a longer PR interval was associated with a lower risk of AF.

Future investigation of the electrical substrate using an integrative combination of fundamental molecular knowledge, genetics and electrophysiology may yield novel insights and new therapeutic options.

Figure 7.1 – Genetic associations across ECG timepoints

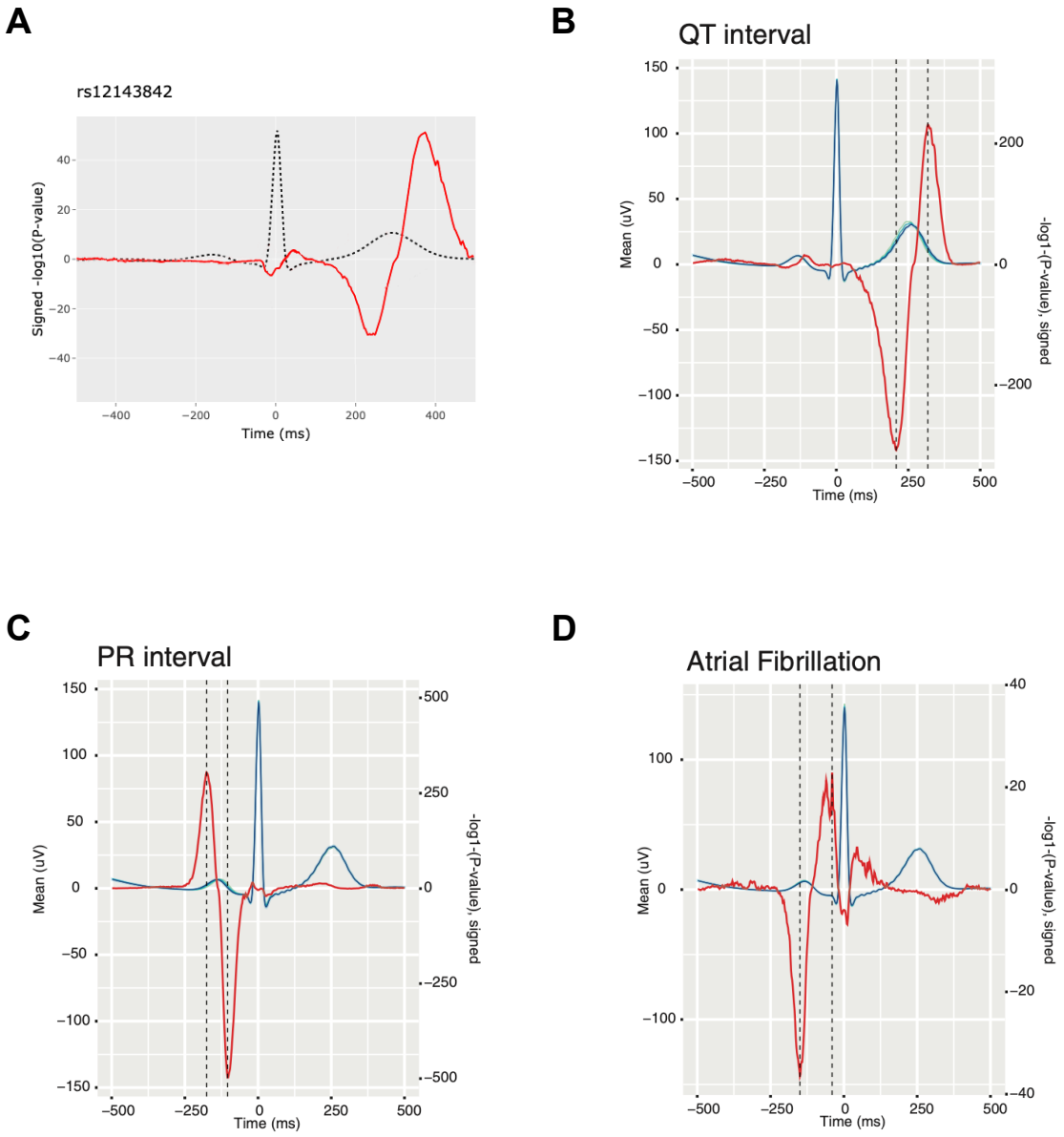


Figure 7.1: For all panels, the red lines represent strength of association (as *P*-value) with amplitude of the ECG (average trace in blue) for a variety of genetic scores. A positive *P*-value implies that the genetic score is associated with a higher amplitude of the ECG at that time point, with a negative *P*-value implying association with a lower amplitude. (**A**) Associations with ECG amplitudes for genetic variant rs12143842 in *NOS1AP* taken from www.ecgenetics.org. (**B**) Associations with ECG amplitudes for a polygenic QT score. (**C**) Associations with ECG amplitudes for a polygenic PR interval score. (**D**) Associations with ECG amplitudes for a polygenic score for risk of atrial fibrillation. Panels **B** to **D** adapted from Verweij *et al.* [319].

References

1. Henson JR. Descartes and the ECG lettering series. J Hist Med Allied Sci. 1971;26(2):181-6. doi: 10.1093/jhmas/xxvi.2.181. PMID: 4930789.

2. Einthoven W. Ueber die form des menschlichen electrocardiogramms. Archiv für die gesamte Physiologie des Menschen und der Tiere. 1895;60(3):101-23. doi: 10.1007/BF01662582.

3. Herring N, Paterson DJ. ECG diagnosis of acute ischaemia and infarction: Past, present and future. QJM. 2006;99(4):219-30. doi: 10.1093/qjmed/hcl025. PMID: 16495300.

4. Wilson FN, Kossmann CE, Burch GE, Goldberger E, Graybiel A, Hecht HH, et al. Recommendations for standardization of electrocardiographic and vectorcardiographic leads. Circulation. 1954;10(4):564-73. doi: doi:10.1161/01.CIR.10.4.564.

5. Hayashi M, Shimizu W, Albert CM. The spectrum of epidemiology underlying sudden cardiac death. Circ Res. 2015;116(12):1887-906. doi: 10.1161/CIRCRESAHA.116.304521. PMID: 26044246.

6. Priori SG, Blomstrom-Lundqvist C, Mazzanti A, Blom N, Borggrefe M, Camm J, et al. 2015 ESC guidelines for the management of patients with ventricular arrhythmias and the prevention of sudden cardiac death: The Task Force for the management of patients with ventricular arrhythmias and the prevention of sudden cardiac death of the European Society of Cardiology (ESC) endorsed by: Association for European Paediatric and Congenital cardiology (AEPC). Europace. 2015;17(11):1601-87. doi: 10.1093/europace/euv319. PMID: 26318695.

7. Al-Khatib SM, Stevenson WG, Ackerman MJ, Bryant WJ, Callans DJ, Curtis AB, et al. 2017 AHA/ACC/HRS guideline for management of patients with ventricular arrhythmias and the prevention of sudden cardiac death: Executive summary: A report of the American College of Cardiology/American Heart Association Task Force on clinical practice guidelines and the Heart Rhythm Society. Heart Rhythm. 2018;15(10):e190-e252. doi: 10.1016/j.hrthm.2017.10.035. PMID: 29097320.

8. Jervell A, Lange-Nielsen F. Congenital deaf-mutism, functional heart disease with prolongation of the Q-T interval, and sudden death. Am Heart J. 1957;54(1):59-68. doi: https://doi.org/10.1016/0002-8703(57)90079-0.

9. Smirk FH, Palmer DG. A myocardial syndrome. With particular reference to the occurrence of sudden death and of premature systoles interrupting antecedent T waves. Am J Cardiol. 1960;6:620-9. doi: 10.1016/0002-9149(60)90265-4. PMID: 13831826.

10. Selzer A, Wray HW. Quinidine syncope. Paroxysmal ventricular fibrillation occurring during treatment of chronic atrial arrhythmias. Circulation. 1964;30:17-26. doi: 10.1161/01.cir.30.1.17. PMID: 14197832.

11. Dessertenne F. Ventricular tachycardia with 2 variable opposing foci. Arch Mal Coeur Vaiss. 1966;59(2):263-72. PMID: 4956181.

12. Krikler DM, Curry PV. Torsade de pointes, an atypical ventricular tachycardia. Br Heart J. 1976;38(2):117-20. doi: 10.1136/hrt.38.2.117. PMID: 1259825.

13. Keating M, Atkinson D, Dunn C, Timothy K, Vincent GM, Leppert M. Linkage of a cardiac arrhythmia, the long QT syndrome, and the Harvey ras-1 gene. Science. 1991;252(5006):704-6. doi: 10.1126/science.1673802. PMID: 1673802.

14. Curran M, Atkinson D, Timothy K, Vincent GM, Moss AJ, Leppert M, et al. Locus heterogeneity of autosomal dominant long QT syndrome. J Clin Invest. 1993;92(2):799-803. doi: 10.1172/JCI116653. PMID: 8102381.

15. Wang Q, Curran ME, Splawski I, Burn TC, Millholland JM, VanRaay TJ, et al. Positional cloning of a novel potassium channel gene: KVLQT1 mutations cause cardiac arrhythmias. Nat Genet. 1996;12(1):17-23. doi: 10.1038/ng0196-17. PMID: 8528244.

16. Jackman WM, Friday KJ, Anderson JL, Aliot EM, Clark M, Lazzara R. The long QT syndromes: A critical review, new clinical observations and a unifying hypothesis. Prog Cardiovasc Dis. 1988;31(2):115-72. doi: 10.1016/0033-0620(88)90014-x. PMID: 3047813.

17. Haverkamp W, Breithardt G, Camm AJ, Janse MJ, Rosen MR, Antzelevitch C, et al. The potential for QT prolongation and pro-arrhythmia by non-anti-arrhythmic drugs: Clinical and regulatory implications. Report on a policy conference of the European Society of Cardiology. Cardiovasc Res. 2000;47(2):219-33. doi: 10.1016/s0008-6363(00)00119-x. PMID: 10947683.

18. Fenichel RR, Malik M, Antzelevitch C, Sanguinetti M, Roden DM, Priori SG, et al. Drug-induced torsades de pointes and implications for drug development. J Cardiovasc Electrophysiol. 2004;15(4):475-95. doi: 10.1046/j.1540-8167.2004.03534.x. PMID: 15090000.

19. Sanguinetti MC, Jiang C, Curran ME, Keating MT. A mechanistic link between an inherited and an acquired cardiac arrhythmia: HERG encodes the IKr potassium channel. Cell. 1995;81(2):299-307. doi: 10.1016/0092-8674(95)90340-2. PMID: 7736582.

20. Kannankeril P, Roden DM, Darbar D. Drug-induced long QT syndrome. Pharmacol Rev. 2010;62(4):760-81. doi: 10.1124/pr.110.003723. PMID: 21079043.

21. Roden DM. Taking the "idio" out of "idiosyncratic": Predicting torsades de pointes. Pacing Clin Electrophysiol. 1998;21(5):1029-34. doi: 10.1111/j.1540-8159.1998.tb00148.x. PMID: 9604234.

22. Roden DM, Abraham RL. Refining repolarization reserve. Heart Rhythm. 2011;8(11):1756-7. doi: 10.1016/j.hrthm.2011.06.024. PMID: 21708111.

23. Sarkar AX, Sobie EA. Quantification of repolarization reserve to understand interpatient variability in the response to proarrhythmic drugs: A computational analysis. Heart Rhythm. 2011;8(11):1749-55. doi: 10.1016/j.hrthm.2011.05.023. PMID: 21699863.

24. Strauss DG, Vicente J, Johannesen L, Blinova K, Mason JW, Weeke P, et al. Common genetic variant risk score is associated with drug-induced QT prolongation and torsade de pointes risk: A pilot study. Circulation. 2017;135(14):1300-10. doi: 10.1161/CIRCULATIONAHA.116.023980. PMID: 28213480.

25. Schwartz PJ, Crotti L, Insolia R. Long-QT syndrome: From genetics to management. Circ Arrhythm Electrophysiol. 2012;5(4):868-77. doi: 10.1161/CIRCEP.111.962019. PMID: 22895603.

26. Bezzina CR, Lahrouchi N, Priori SG. Genetics of sudden cardiac death. Circ Res. 2015;116(12):1919-36. doi: 10.1161/CIRCRESAHA.116.304030. PMID: 26044248.

27. Wilde AAM, Amin AS, Postema PG. Diagnosis, management and therapeutic strategies for congenital long QT syndrome. Heart. 2021. doi: 10.1136/heartjnl-2020-318259. PMID: 34039680.

28. Adler A, Novelli V, Amin AS, Abiusi E, Care M, Nannenberg EA, et al. An international, multicentered, evidence-based reappraisal of genes reported to cause congenital long QT syndrome. Circulation. 2020;141(6):418-28. doi: 10.1161/CIRCULATIONAHA.119.043132. PMID: 31983240.

29. Lahrouchi N, Tadros R, Crotti L, Mizusawa Y, Postema PG, Beekman L, et al. Transethnic genome-wide association study provides insights in the genetic architecture and heritability of long QT syndrome. Circulation. 2020. doi: 10.1161/CIRCULATIONAHA.120.045956. PMID: 32429735.

30. Antzelevitch C. Sympathetic modulation of the long QT syndrome. Eur Heart J. 2002;23(16):1246-52. doi: 10.1053/euhj.2002.3287. PMID: 12175662.

31. Moss AJ, Goldenberg I. Importance of knowing the genotype and the specific mutation when managing patients with long QT syndrome. Circ Arrhythm Electrophysiol. 2008;1(3):213-26; discussion 26. doi: 10.1161/CIRCEP.108.796599. PMID: 19701491.

32. Schwartz PJ, Priori SG, Cerrone M, Spazzolini C, Odero A, Napolitano C, et al. Left cardiac sympathetic denervation in the management of high-risk patients affected by the long-QT syndrome. Circulation. 2004;109(15):1826-33. doi: 10.1161/01.CIR.0000125523.14403.1E. PMID: 15051644.

33. Schwartz PJ, Wolf S. QT interval prolongation as predictor of sudden death in patients with myocardial infarction. Circulation. 1978;57(6):1074-7. doi: 10.1161/01.cir.57.6.1074. PMID: 639227.

34. Algra A, Tijssen JG, Roelandt JR, Pool J, Lubsen J. QTc prolongation measured by standard 12-lead electrocardiography is an independent risk factor for sudden death due to cardiac arrest. Circulation. 1991;83(6):1888-94. doi: 10.1161/01.cir.83.6.1888. PMID: 2040041.

35. Goldberg RJ, Bengtson J, Chen ZY, Anderson KM, Locati E, Levy D. Duration of the QT interval and total and cardiovascular mortality in healthy persons (The Framingham Heart Study experience). Am J Cardiol. 1991;67(1):55-8. doi: 10.1016/0002-9149(91)90099-7. PMID: 1986505.

36. Robbins J, Nelson JC, Rautaharju PM, Gottdiener JS. The association between the length of the QT interval and mortality in the Cardiovascular Health Study. Am J Med. 2003;115(9):689-94. doi: 10.1016/j.amjmed.2003.07.014. PMID: 14693320.

37. Montanez A, Ruskin JN, Hebert PR, Lamas GA, Hennekens CH. Prolonged QTc interval and risks of total and cardiovascular mortality and sudden death in the general population: A review and qualitative overview of the prospective cohort studies. Arch Intern Med. 2004;164(9):943-8. doi: 10.1001/archinte.164.9.943. PMID: 15136301.

38. Straus SM, Kors JA, De Bruin ML, van der Hooft CS, Hofman A, Heeringa J, et al. Prolonged QTc interval and risk of sudden cardiac death in a population of older adults. J Am Coll Cardiol. 2006;47(2):362-7. doi: 10.1016/j.jacc.2005.08.067. PMID: 16412861.

39. Zhang Y, Post WS, Blasco-Colmenares E, Dalal D, Tomaselli GF, Guallar E. Electrocardiographic QT interval and mortality: A meta-analysis. Epidemiology. 2011;22(5):660-70. doi: 10.1097/EDE.0b013e318225768b. PMID: 21709561.

40. Ahlqvist E, Storm P, Karajamaki A, Martinell M, Dorkhan M, Carlsson A, et al. Novel subgroups of adult-onset diabetes and their association with outcomes: A data-driven cluster analysis of six variables. Lancet Diabetes Endocrinol. 2018;6(5):361-9. doi: 10.1016/S2213-8587(18)30051-2. PMID: 29503172.

41. Extramiana F, Leenhardt A. Prolonged QRS duration and sudden cardiac death risk stratification: Not yet ready for prime time. Heart Rhythm. 2011;8(10):1568-9. doi: 10.1016/j.hrthm.2011.07.007. PMID: 21740878.

42. Kurl S, Makikallio TH, Rautaharju P, Kiviniemi V, Laukkanen JA. Duration of QRS complex in resting electrocardiogram is a predictor of sudden cardiac death in men. Circulation. 2012;125(21):2588-94. doi: 10.1161/CIRCULATIONAHA.111.025577. PMID: 22615341.

43. Chen X, Hansson PO, Thunstrom E, Mandalenakis Z, Caidahl K, Fu M. Incremental changes in QRS duration as predictor for cardiovascular disease: A 21-year follow-up of a randomly selected general population. Sci Rep. 2021;11(1):13652. doi: 10.1038/s41598-021-93024-y. PMID: 34211015.

44. Kirchhof P, Eckardt L, Franz MR, Monnig G, Loh P, Wedekind H, et al. Prolonged atrial action potential durations and polymorphic atrial tachyarrhythmias in patients with long QT syndrome. J Cardiovasc Electrophysiol. 2003;14(10):1027-33. PMID: 14521653.

45. Johnson JN, Tester DJ, Perry J, Salisbury BA, Reed CR, Ackerman MJ. Prevalence of early-onset atrial fibrillation in congenital long QT syndrome. Heart Rhythm. 2008;5(5):704-9. doi: 10.1016/j.hrthm.2008.02.007. PMID: 18452873.

46. Zellerhoff S, Pistulli R, Monnig G, Hinterseer M, Beckmann BM, Kobe J, et al. Atrial arrhythmias in long-QT syndrome under daily life conditions: A nested case control study. J Cardiovasc Electrophysiol. 2009;20(4):401-7. doi: 10.1111/j.1540-8167.2008.01339.x. PMID: 19017345.

47. Miyamoto A, Hayashi H, Yoshino T, Kawaguchi T, Taniguchi A, Itoh H, et al. Clinical and electrocardiographic characteristics of patients with short QT interval in a large hospital-based population. Heart Rhythm. 2012;9(1):66-74. doi: 10.1016/j.hrthm.2011.08.016. PMID: 21855519.

48. Nielsen JB, Graff C, Pietersen A, Lind B, Struijk JJ, Olesen MS, et al. J-shaped association between QTc interval duration and the risk of atrial fibrillation: Results from the Copenhagen ECG study. J Am Coll Cardiol. 2013;61(25):2557-64. doi: 10.1016/j.jacc.2013.03.032. PMID: 23583581.

49. Mandyam MC, Soliman EZ, Alonso A, Dewland TA, Heckbert SR, Vittinghoff E, et al. The QT interval and risk of incident atrial fibrillation. Heart Rhythm. 2013;10(10):1562-8. doi: 10.1016/j.hrthm.2013.07.023. PMID: 23872693.

50. O'Neal WT, Efird JT, Kamel H, Nazarian S, Alonso A, Heckbert SR, et al. The association of the QT interval with atrial fibrillation and stroke: The Multi-Ethnic Study of Atherosclerosis. Clin Res Cardiol. 2015;104(9):743-50. doi: 10.1007/s00392-015-0838-z. PMID: 25752461.

51. Newton-Cheh C, Larson MG, Corey DC, Benjamin EJ, Herbert AG, Levy D, et al. QT interval is a heritable quantitative trait with evidence of linkage to chromosome 3 in a genome-wide linkage analysis: The Framingham Heart Study. Heart Rhythm. 2005;2(3):277-84. doi: 10.1016/j.hrthm.2004.11.009. PMID: 15851319.

52. Pfeufer A, Jalilzadeh S, Perz S, Mueller JC, Hinterseer M, Illig T, et al. Common variants in myocardial ion channel genes modify the QT interval in the general population: Results from The KORA study. Circ Res. 2005;96(6):693-701. doi: 10.1161/01.RES.0000161077.53751.e6. PMID: 15746444.

53. Ackerman MJ, Priori SG, Willems S, Berul C, Brugada R, Calkins H, et al. HRS/EHRA expert consensus statement on the state of genetic testing for the channelopathies and cardiomyopathies: This document was developed as a partnership between the Heart Rhythm Society (HRS) and the European Heart Rhythm Association (EHRA). Europace. 2011;13(8):1077-109. doi: 10.1093/europace/eur245. PMID: 21810866.

54. Arking DE, Pfeufer A, Post W, Kao WH, Newton-Cheh C, Ikeda M, et al. A common genetic variant in the NOS1 regulator NOS1AP modulates cardiac repolarization. Nat Genet. 2006;38(6):644-51. doi: 10.1038/ng1790. PMID: 16648850.

55. Arking DE, Pulit SL, Crotti L, van der Harst P, Munroe PB, Koopmann TT, et al. Genetic association study of QT interval highlights role for calcium signaling pathways in myocardial repolarization. Nat Genet. 2014;46(8):826-36. doi: 10.1038/ng.3014. PMID: 24952745.

56. Young WJ, Lahrouchi N, Isaacs A, Duong T, Foco L, Ahmed F, et al. Genetic analyses of the QT interval and its components in over 250k individuals identifies new loci and pathways affecting ventricular depolarization and repolarization. medRxiv. 2021. doi: 10.1101/2021.11.04.21265866.

57. Jaffrey SR, Snowman AM, Eliasson MJL, Cohen NA, Snyder SH. CAPON: A protein associated with neuronal nitric oxide synthase that regulates its interactions with PSD95. Neuron. 1998;20(1):115-24. doi: Doi 10.1016/S0896-6273(00)80439-0. PMID: WOS:000071719700014.

58. Eijgelsheim M, Aarnoudse AL, Rivadeneira F, Kors JA, Witteman JC, Hofman A, et al. Identification of a common variant at the NOS1AP locus strongly associated to QT-interval duration. Hum Mol Genet. 2009;18(2):347-57. doi: 10.1093/hmg/ddn341. PMID: 18927126.

59. Aarnoudse AJ, Newton-Cheh C, de Bakker PI, Straus SM, Kors JA, Hofman A, et al. Common NOS1AP variants are associated with a prolonged QTc interval in the Rotterdam study. Circulation. 2007;116(1):10-6. doi: 10.1161/CIRCULATIONAHA.106.676783. PMID: 17576865.

60. Post W, Shen H, Damcott C, Arking DE, Kao WH, Sack PA, et al. Associations between genetic variants in the NOS1AP (CAPON) gene and cardiac repolarization in the old order Amish. Hum Hered. 2007;64(4):214-9. doi: 10.1159/000103630. PMID: 17565224.

61. Lehtinen AB, Newton-Cheh C, Ziegler JT, Langefeld CD, Freedman BI, Daniel KR, et al. Association of NOS1AP genetic variants with QT interval duration in families from the Diabetes Heart Study. Diabetes. 2008;57(4):1108-14. doi: 10.2337/db07-1365. PMID: 18235038.

62. Lu J, Hu C, Hu W, Zhang R, Wang C, Qin W, et al. A common variant of NOS1AP is associated with QT interval duration in a Chinese population with type 2 diabetes. Diabet Med. 2010;27(9):1074-9. doi: 10.1111/j.1464-5491.2010.03072.x. PMID: 20722683.

63. Shah SA, Herrington DM, Howard TD, Divers J, Arnett DK, Burke GL, et al. Associations between NOS1AP single nucleotide polymorphisms (SNPs) and QT interval duration in four racial/ethnic groups in the Multi-Ethnic Study of Atherosclerosis (MESA). Ann Noninvasive Electrocardiol. 2013;18(1):29-40. doi: 10.1111/anec.12028. PMID: 23347024.

64. Arking DE, Khera A, Xing C, Kao WH, Post W, Boerwinkle E, et al. Multiple independent genetic factors at NOS1AP modulate the QT interval in a multi-ethnic population. PLoS ONE. 2009;4(1):e4333. doi: 10.1371/journal.pone.0004333. PMID: 19180230.

65. Avery CL, Sethupathy P, Buyske S, He Q, Lin DY, Arking DE, et al. Fine-mapping and initial characterization of QT interval loci in African Americans. PLoS Genet. 2012;8(8):e1002870. doi: 10.1371/journal.pgen.1002870. PMID: 22912591.

66. Avery CL, Wassel CL, Richard MA, Highland HM, Bien S, Zubair N, et al. Fine mapping of QT interval regions in global populations refines previously identified QT interval loci and identifies signals unique to African and Hispanic descent populations. Heart Rhythm. 2017;14(4):572-80. doi: 10.1016/j.hrthm.2016.12.021. PMID: 27988371.

67. Sedlak T, Shufelt C, Iribarren C, Merz CN. Sex hormones and the QT interval: A review. J Womens Health (Larchmt). 2012;21(9):933-41. doi: 10.1089/jwh.2011.3444. PMID: 22663191.

68. Salama G, Bett GC. Sex differences in the mechanisms underlying long QT syndrome. Am J Physiol Heart Circ Physiol. 2014;307(5):H640-8. doi: 10.1152/ajpheart.00864.2013. PMID: 24973386.

69. Locati EH, Zareba W, Moss AJ, Schwartz PJ, Vincent GM, Lehmann MH, et al. Age- and sex-related differences in clinical manifestations in patients with congenital long-QT syndrome: Findings from the International LQTS Registry. Circulation. 1998;97(22):2237-44. doi: papers3://publication/doi/10.1161/01.CIR.97.22.2237. PMID: 9631873.

70. Tobin MD, Kahonen M, Braund P, Nieminen T, Hajat C, Tomaszewski M, et al. Gender and effects of a common genetic variant in the NOS1 regulator NOS1AP on cardiac repolarization in 3761 individuals from two independent populations. Int J Epidemiol. 2008;37(5):1132-41. doi: 10.1093/ije/dyn091. PMID: 18511491.

71. Winbo A, Stattin EL, Westin IM, Norberg A, Persson J, Jensen SM, et al. Sex is a moderator of the association between NOS1AP sequence variants and QTc in two long QT syndrome founder populations: A pedigree-based measured genotype association analysis. BMC Med Genet. 2017;18(1):74. doi: 10.1186/s12881-017-0435-2. PMID: 28720088.

72. Eijgelsheim M, Newton-Cheh C, Aarnoudse AL, van Noord C, Witteman JC, Hofman A, et al. Genetic variation in NOS1AP is associated with sudden cardiac death: Evidence from the Rotterdam study. Hum Mol Genet. 2009;18(21):4213-8. doi: 10.1093/hmg/ddp356. PMID: 19643915.

73. Kao WH, Arking DE, Post W, Rea TD, Sotoodehnia N, Prineas RJ, et al. Genetic variations in nitric oxide synthase 1 adaptor protein are associated with sudden cardiac death in US white community-based populations. Circulation. 2009;119(7):940-51. doi: 10.1161/CIRCULATIONAHA.108.791723. PMID: 19204306.

74. Huang L, Yu Y, Chen Y, Tester DJ, Tang S, Ackerman MJ, et al. Association of common variants in NOS1AP gene with sudden unexplained nocturnal death syndrome in the southern Chinese Han population. Int J Legal Med. 2014;128(6):933-8. doi: 10.1007/s00414-014-0973-5. PMID: 24504561.

75. Liu X, Pei J, Hou C, Liu N, Chu J, Pu J, et al. A common NOS1AP genetic polymorphism, rs12567209 G>A, is associated with sudden cardiac death in patients with chronic heart failure in the Chinese Han population. J Card Fail. 2014;20(4):244-51. doi: 10.1016/j.cardfail.2014.01.006. PMID: 24418727.

76. Zhang R, Chen F, Yu H, Gao L, Yin X, Dong Y, et al. The genetic variation rs12143842 in NOS1AP increases idiopathic ventricular tachycardia risk in Chinese Han populations. Sci Rep. 2017;7(1):8356. doi: 10.1038/s41598-017-08548-z. PMID: 28827735.

77. Noseworthy PA, Havulinna AS, Porthan K, Lahtinen AM, Jula A, Karhunen PJ, et al. Common genetic variants, QT interval, and sudden cardiac death in a Finnish population-based study. Circ Cardiovasc Genet. 2011;4(3):305-11. doi: 10.1161/CIRCGENETICS.110.959049. PMID: 21511878.

78. van Noord C, Aarnoudse AJ, Eijgelsheim M, Sturkenboom MC, Straus SM, Hofman A, et al. Calcium channel blockers, NOS1AP, and heart-rate-corrected QT prolongation. Pharmacogenet Genomics. 2009;19(4):260-6. doi: 10.1097/FPC.0b013e328324e556. PMID: 19247217.

79. Jamshidi Y, Nolte IM, Dalageorgou C, Zheng D, Johnson T, Bastiaenen R, et al. Common variation in the NOS1AP gene is associated with drug-induced QT prolongation and ventricular arrhythmia. J Am Coll Cardiol. 2012;60(9):841-50. doi: 10.1016/j.jacc.2012.03.031. PMID: 22682551.

80. Crotti L, Monti MC, Insolia R, Peljto A, Goosen A, Brink PA, et al. NOS1AP is a genetic modifier of the long-QT syndrome. Circulation. 2009;120(17):1657-63. doi: 10.1161/CIRCULATIONAHA.109.879643. PMID: 19822806.

81. Tomas M, Napolitano C, De Giuli L, Bloise R, Subirana I, Malovini A, et al. Polymorphisms in the NOS1AP gene modulate QT interval duration and risk of arrhythmias in the long QT syndrome. J Am Coll Cardiol. 2010;55(24):2745-52. doi: 10.1016/j.jacc.2009.12.065. PMID: 20538168.

82. Earle N, Yeo Han D, Pilbrow A, Crawford J, Smith W, Shelling AN, et al. Single nucleotide polymorphisms in arrhythmia genes modify the risk of cardiac events and sudden death in long QT syndrome. Heart Rhythm. 2014;11(1):76-82. doi: 10.1016/j.hrthm.2013.10.005. PMID: 24096169.

83. Kolder I, Tanck MWT, Postema PG, Barc J, Sinner MF, Zumhagen S, et al. Analysis for genetic modifiers of disease severity in patients with long-QT syndrome type 2. Circ Cardiovasc Genet. 2015;8(3):447-56. doi: 10.1161/CIRCGENETICS.114.000785. PMID: 25737393.

84. Bezzina CR. Unpublished data from eQTL in human hearts database; personal communication.

85. Koopmann TT, Adriaens ME, Moerland PD, Marsman RF, Westerveld ML, Lal S, et al. Genome-wide identification of expression quantitative trait loci (eQTLs) in human heart. PLoS ONE. 2014;9(5):e97380. doi: 10.1371/journal.pone.0097380. PMID: 24846176.

86. Kapoor A, Sekar RB, Hansen NF, Fox-Talbot K, Morley M, Pihur V, et al. An enhancer polymorphism at the cardiomyocyte intercalated disc protein NOS1AP locus is a major regulator of the QT interval. Am J Hum Genet. 2014;94(6):854-69. doi: 10.1016/j.ajhg.2014.05.001. PMID: 24857694.

87. Fang M, Jaffrey SR, Sawa A, Ye K, Luo X, Snyder SH. Dexras1: A G protein specifically coupled to neuronal nitric oxide synthase via CAPON. Neuron. 2000;28(1):183-93. PMID: 11086993.

88. Jaffrey SR, Benfenati F, Snowman AM, Czernik AJ, Snyder SH. Neuronal nitric-oxide synthase localization mediated by a ternary complex with synapsin and CAPON. Proc Natl Acad Sci USA. 2002;99(5):3199-204. doi: 10.1073/pnas.261705799. PMID: 11867766.

89. Brzustowicz LM, Simone J, Mohseni P, Hayter JE, Hodgkinson KA, Chow EW, et al. Linkage disequilibrium mapping of schizophrenia susceptibility to the CAPON region of chromosome 1q22. Am J Hum Genet. 2004;74(5):1057-63. doi: 10.1086/420774. PMID: 15065015.

90. Xu B, Wratten N, Charych EI, Buyske S, Firestein BL, Brzustowicz LM. Increased expression in dorsolateral prefrontal cortex of CAPON in schizophrenia and bipolar disorder. PLoS Med. 2005;2(10):e263. doi: 10.1371/journal.pmed.0020263. PMID: 16146415.

91. Gao S, Zhang T, Jin L, Liang D, Fan G, Song Y, et al. CAPON is a critical protein in synaptic molecular networks in the prefrontal cortex of mood disorder patients and contributes to depression-like behavior in a mouse model. Cereb Cortex. 2019;29(9):3752-65. doi: 10.1093/cercor/bhy254. PMID: 30307500.

92. Wratten NS, Memoli H, Huang Y, Dulencin AM, Matteson PG, Cornacchia MA, et al. Identification of a schizophrenia-associated functional noncoding variant in NOS1AP. Am J Psychiatry. 2009;166(4):434-41. doi: 10.1176/appi.ajp.2008.08081266. PMID: 19255043.

93. Carrel D, Hernandez K, Kwon M, Mau C, Trivedi MP, Brzustowicz LM, et al. Nitric oxide synthase 1 adaptor protein, a protein implicated in schizophrenia, controls radial migration of cortical neurons. Biol Psychiatry. 2015;77(11):969-78. doi: 10.1016/j.biopsych.2014.10.016. PMID: 25542305.

94. Candemir E, Kollert L, Weissflog L, Geis M, Muller A, Post AM, et al. Interaction of NOS1AP with the NOS-1 PDZ domain: Implications for schizophrenia-related alterations in dendritic morphology. Eur Neuropsychopharmacol. 2016;26(4):741-55. doi: 10.1016/j.euroneuro.2016.01.008. PMID: 26861996.

95. Hernandez K, Swiatkowski P, Patel MV, Liang C, Dudzinski NR, Brzustowicz LM, et al. Overexpression of isoforms of nitric oxide synthase 1 adaptor protein, encoded by a risk gene for schizophrenia, alters actin dynamics and synaptic function. Front Cell Neurosci. 2016;10:6. doi: 10.3389/fncel.2016.00006. PMID: 26869880.

96. Zhu LJ, Li TY, Luo CX, Jiang N, Chang L, Lin YH, et al. CAPON-nNOS coupling can serve as a target for developing new anxiolytics. Nat Med. 2014;20(9):1050-4. doi: 10.1038/nm.3644. PMID: 25129479.

97. Lee WH, Carey LM, Li LL, Xu Z, Lai YY, Courtney MJ, et al. ZLc002, a putative small-molecule inhibitor of nNOS interaction with NOS1AP, suppresses inflammatory nociception and chemotherapy-induced neuropathic pain and synergizes with paclitaxel to reduce tumor cell viability. Mol Pain. 2018;14:1744806918801224. doi: 10.1177/1744806918801224. PMID: 30157705.

98. Lee WH, Li LL, Chawla A, Hudmon A, Lai YY, Courtney MJ, et al. Disruption of nNOS-NOS1AP protein-protein interactions suppresses neuropathic pain in mice. Pain. 2018. doi: 10.1097/j.pain.0000000000001152. PMID: 29319606.

99. Zhu LJ, Chang L, Shi HJ, Li N. Systemic administration of ZLc-002 exerts anxiolytic-like effects by dissociation of nNOS from CAPON in adult mice. Biochem Biophys Res Commun. 2020;523(2):299-306. doi: 10.1016/j.bbrc.2019.12.037. PMID: 31864709.

100. Courtney MJ, Li LL, Lai YY. Mechanisms of NOS1AP action on NMDA receptor-nNOS signaling. Front Cell Neurosci. 2014;8:252. doi: 10.3389/fncel.2014.00252. PMID: 25221472.

101. Ni HY, Song YX, Lin YH, Cao B, Wang DL, Zhang Y, et al. Dissociating nNOS (Neuronal NO Synthase)-CAPON (Carboxy-terminal Postsynaptic Density-95/discs large/zona occludens-1 ligand of nNOS) interaction promotes functional recovery after stroke via enhanced structural neuroplasticity. Stroke. 2019;50(3):728-37. doi: 10.1161/STROKEAHA.118.022647. PMID: 30727847.

102. Li LL, Melero-Fernandez de Mera RM, Chen J, Ba W, Kasri NN, Zhang M, et al. Unexpected heterodivalent recruitment of NOS1AP to nNOS reveals multiple sites for pharmacological

intervention in neuronal disease models. J Neurosci. 2015;35(19):7349-64. doi: 10.1523/JNEUROSCI.0037-15.2015. PMID: 25972165.

103. Li LL, Cisek K, Courtney MJ. Efficient binding of the NOSIAP C-terminus to the nNOS PDZ pocket requires the concerted action of the PDZ ligand motif, the internal ExF site and structural integrity of an independent element. Front Mol Neurosci. 2017;10:58. doi: 10.3389/fnmol.2017.00058. PMID: 28360833.

104. Herring N, Paterson DJ. Letter by Herring and Paterson regarding article, "common NOSIAP variants are associated with a prolonged QTc interval in the Rotterdam study". Circulation. 2007;116(24):e564; Author Reply e5. doi: 10.1161/CIRCULATIONAHA.107.729426. PMID: 18071084.

105. Lu CJ, Hao G, Nikiforova N, Larsen HE, Liu K, Crabtree MJ, et al. CAPON modulates neuronal calcium handling and cardiac sympathetic neurotransmission during dysautonomia in hypertension. Hypertension. 2015;65(6):1288-97. doi: 10.1161/HYPERTENSIONAHA.115.05290. PMID: 25916729.

106. Jost N, Virag L, Bitay M, Takacs J, Lengyel C, Biliczki P, et al. Restricting excessive cardiac action potential and QT prolongation: A vital role for IKs in human ventricular muscle. Circulation. 2005;112(10):1392-9. doi: 10.1161/CIRCULATIONAHA.105.550111. PMID: 16129791.

107. Chang KC, Barth AS, Sasano T, Kizana E, Kashiwakura Y, Zhang Y, et al. CAPON modulates cardiac repolarization via neuronal nitric oxide synthase signaling in the heart. Proc Natl Acad Sci USA. 2008;105(11):4477-82. doi: 10.1073/pnas.0709118105. PMID: 18337493.

108. Milan DJ, Kim AM, Winterfield JR, Jones IL, Pfeufer A, Sanna S, et al. Drug-sensitized zebrafish screen identifies multiple genes, including GINS3, as regulators of myocardial repolarization. Circulation. 2009;120(7):553-9. doi: 10.1161/CIRCULATIONAHA.108.821082. PMID: 19652097.

109. Treuer AV, Gonzalez DR. NOSIAP modulates intracellular Ca(2+) in cardiac myocytes and is up-regulated in dystrophic cardiomyopathy. Int J Physiol Pathophysiol Pharmacol. 2014;6(1):37-46.

110. Sugiyama K, Sasano T, Kurokawa J, Takahashi K, Okamura T, Kato N, et al. Oxidative stress induced ventricular arrhythmia and impairment of cardiac function in Nos1ap deleted mice. Int Heart J. 2016;57(3):341-9. doi: 10.1536/ihj.15-471. PMID: 27170476.

111. Ronchi C, Bernardi J, Mura M, Stefanello M, Badone B, Rocchetti M, et al. NOSIAP polymorphisms reduce NOSI activity and interact with prolonged repolarization in arrhythmogenesis. Cardiovasc Res. 2020. doi: 10.1093/cvr/cvaa036. PMID: 32061134.

112. Beigi F, Oskouei BN, Zheng M, Cooke CA, Lamirault G, Hare JM. Cardiac nitric oxide synthase-1 localization within the cardiomyocyte is accompanied by the adaptor protein, CAPON. Nitric Oxide. 2009;21(3-4):226-33. doi: 10.1016/j.niox.2009.09.005. PMID: 19800018.

113. Jian Z, Han H, Zhang T, Puglisi J, Izu LT, Shaw JA, et al. Mechano-chemotransduction during cardiomyocyte contraction is mediated by localized nitric oxide signaling. Sci Signal. 2014;7(317):ra27. doi: 10.1126/scisignal.2005046. PMID: 24643800.

114. Xu KY, Huso DL, Dawson TM, Bredt DS, Becker LC. Nitric oxide synthase in cardiac sarcoplasmic reticulum. Proc Natl Acad Sci USA. 1999;96(2):657-62. PMID: 9892689.

115. Xu KY, Kuppusamy SP, Wang JQ, Li H, Cui H, Dawson TM, et al. Nitric oxide protects cardiac sarcolemmal membrane enzyme function and ion active transport against ischemia-induced inactivation. J Biol Chem. 2003;278(43):41798-803. doi: 10.1074/jbc.M306865200. PMID: 12904295.

116. Williams JC, Armesilla AL, Mohamed TM, Hagarty CL, McIntyre FH, Schomburg S, et al. The sarcolemmal calcium pump, alpha-1 syntrophin, and neuronal nitric-oxide synthase are parts of a macromolecular protein complex. J Biol Chem. 2006;281(33):23341-8. doi: 10.1074/jbc.M513341200. PMID: 16735509.

117. Sun J, Picht E, Ginsburg KS, Bers DM, Steenbergen C, Murphy E. Hypercontractile female hearts exhibit increased S-nitrosylation of the l-type Ca2+ channel alphal subunit and reduced ischemia/reperfusion injury. Circ Res. 2006;98(3):403-11. doi: 10.1161/01.RES.0000202707.79018.0a. PMID: 16397145.

118. Damy T, Ratajczak P, Robidel E, Bendall JK, Oliviero P, Boczkowski J, et al. Up-regulation of cardiac nitric oxide synthase 1-derived nitric oxide after myocardial infarction in senescent rats. FASEB J. 2003;17(13):1934-6. doi: 10.1096/fj.02-1208fje. PMID: 12897062.

119. Damy T, Ratajczak P, Shah AM, Camors E, Marty I, Hasenfuss G, et al. Increased neuronal nitric oxide synthase-derived NO production in the failing human heart. The Lancet. 2004;363(9418):1365-7. doi: 10.1016/s0140-6736(04)16048-0.

120. Venema VJ, Ju H, Zou R, Venema RC. Interaction of neuronal nitric-oxide synthase with caveolin-3 in skeletal muscle. Identification of a novel caveolin scaffolding/inhibitory domain. J Biol Chem. 1997;272(45):28187-90. PMID: 9353265.

121. Zhang YH, Casadei B. Sub-cellular targeting of constitutive NOS in health and disease. J Mol Cell Cardiol. 2012;52(2):341-50. doi: 10.1016/j.yjmcc.2011.09.006. PMID: 21945464.

122. Wang H, Kohr MJ, Traynham CJ, Wheeler DG, Janssen PM, Ziolo MT. Neuronal nitric oxide synthase signaling within cardiac myocytes targets phospholamban. Am J Physiol Cell Physiol. 2008;294(6):C1566-75. doi: 10.1152/ajpcell.00367.2007. PMID: 18400986.

123. Zhang YH, Zhang MH, Sears CE, Emanuel K, Redwood C, El-Armouche A, et al. Reduced phospholamban phosphorylation is associated with impaired relaxation in left ventricular myocytes from neuronal NO synthase-deficient mice. Circ Res. 2008;102(2):242-9. doi: 10.1161/CIRCRESAHA.107.164798. PMID: 18007024.

124. Sears CE, Bryant SM, Ashley EA, Lygate CA, Rakovic S, Wallis HL, et al. Cardiac neuronal nitric oxide synthase isoform regulates myocardial contraction and calcium handling. Circ Res. 2003;92(5):e52-9. doi: 10.1161/01.RES.0000064585.95749.6D. PMID: 12623875.

125. Carnicer R, Hale AB, Suffredini S, Liu X, Reilly S, Zhang MH, et al. Cardiomyocyte GTP cyclohydrolase 1 and tetrahydrobiopterin increase NOS1 activity and accelerate myocardial relaxation. Circ Res. 2012;111(6):718-27. doi: 10.1161/CIRCRESAHA.112.274464. PMID: 22798524.

126. Reilly SN, Liu X, Carnicer R, Recalde A, Muszkiewicz A, Jayaram R, et al. Up-regulation of mir-31 in human atrial fibrillation begets the arrhythmia by depleting dystrophin and neuronal nitric oxide synthase. Sci Transl Med. 2016;8(340):340ra74. doi: 10.1126/scitranslmed.aac4296. PMID: 27225184.

127. Wang H, Viatchenko-Karpinski S, Sun J, Gyorke I, Benkusky NA, Kohr MJ, et al. Regulation of myocyte contraction via neuronal nitric oxide synthase: Role of Ryanodine receptor S-nitrosylation. J Physiol. 2010;588(Pt 15):2905-17. doi: 10.1113/jphysiol.2010.192617. PMID: 20530114.

128. Blayney LM, Lai FA. Ryanodine receptor-mediated arrhythmias and sudden cardiac death. Pharmacol Ther. 2009;123(2):151-77. doi: 10.1016/j.pharmthera.2009.03.006. PMID: 19345240.

129. Ueda K, Valdivia C, Medeiros-Domingo A, Tester DJ, Vatta M, Farrugia G, et al. Syntrophin mutation associated with long QT syndrome through activation of the nNOS-SCN5A macromolecular complex. Proc Natl Acad Sci USA. 2008;105(27):9355-60. doi: 10.1073/pnas.0801294105. PMID: 18591664.

130. Auer DR, Sysa-Shah P, Bedja D, Simmers JL, Pak E, Dutra A, et al. Generation of a cre recombinase-conditional Noslap over-expression transgenic mouse. Biotechnol Lett. 2014;36(6):1179-85. doi: 10.1007/s10529-014-1473-x. PMID: 24563304.

131. Choate JK, Murphy SM, Feldman R, Anderson CR. Sympathetic control of heart rate in nNOS knockout mice. Am J Physiol Heart Circ Physiol. 2008;294(1):H354-61. doi: 10.1152/ajpheart.00898.2007. PMID: 17951372.

132. Truett GE, Heeger P, Mynatt RL, Truett AA, Walker JA, Warman ML. Preparation of PCR-quality mouse genomic DNA with hot sodium hydroxide and tris (HoTSHOT). Biotechniques. 2000;29(1):52, 4. doi: 10.2144/00291bm09. PMID: 10907076.

133. Gardin JM, Siri FM, Kitsis RN, Edwards JG, Leinwand LA. Echocardiographic assessment of left ventricular mass and systolic function in mice. Circ Res. 1995;76(5):907-14. doi: 10.1161/01.res.76.5.907. PMID: 7729009.

134. Boukens BJ, Hoogendijk MG, Verkerk AO, Linnenbank A, van Dam P, Remme CA, et al. Early repolarization in mice causes overestimation of ventricular activation time by the QRS duration. Cardiovasc Res. 2013;97(1):182-91. doi: 10.1093/cvr/cvs299. PMID: 22997159.

135. Mulla W, Gillis R, Murninkas M, Klapper-Goldstein H, Gabay H, Mor M, et al. Unanesthetized rodents demonstrate insensitivity of QT interval and ventricular refractory period to pacing cycle length. Front Physiol. 2018;9:897. doi: 10.3389/fphys.2018.00897. PMID: 30050462.

136. Mitchell GF, Jeron A, Koren G. Measurement of heart rate and QT interval in the conscious mouse. Am J Physiol. 1998;274(3 Pt 2):H747-51. doi: 10.1152/ajpheart.1998.274.3.H747. PMID: 9530184.

137. Kirchhof P, Fabritz L, Zwiener M, Witt H, Schafers M, Zellerhoff S, et al. Age- and training-dependent development of arrhythmogenic right ventricular cardiomyopathy in heterozygous plakoglobin-deficient mice. Circulation. 2006;114(17):1799-806. doi: 10.1161/CIRCULATIONAHA.106.624502. PMID: 17030684.

138. Kuhlmann MT, Kirchhof P, Klocke R, Hasib L, Stypmann J, Fabritz L, et al. G-CSF/SCF reduces inducible arrhythmias in the infarcted heart potentially via increased connexin43 expression and arteriogenesis. J Exp Med. 2006;203(1):87-97. doi: 10.1084/jem.20051151. PMID: 16401694.

139. London B, Jeron A, Zhou J, Buckett P, Han X, Mitchell GF, et al. Long QT and ventricular arrhythmias in transgenic mice expressing the N terminus and first transmembrane segment of a voltage-gated potassium channel. Proc Natl Acad Sci USA. 1998;95(6):2926-31. doi: 10.1073/pnas.95.6.2926. PMID: 9501192.

140. Kuo HC, Cheng CF, Clark RB, Lin JJ, Lin JL, Hoshijima M, et al. A defect in the Kv channel-interacting protein 2 (KChIP2) gene leads to a complete loss of I(to) and confers susceptibility to ventricular tachycardia. Cell. 2001;107(6):801-13. doi: 10.1016/s0092-8674(01)00588-8. PMID: 11747815.

141. Fabritz L, Kirchhof P, Franz MR, Nuyens D, Rossenbacker T, Ottenhof A, et al. Effect of pacing and mexiletine on dispersion of repolarisation and arrhythmias in DeltaKPQ SCN5A (long QT3) mice. Cardiovasc Res. 2003;57(4):1085-93. doi: 10.1016/s0008-6363(02)00839-8. PMID: 12650887.

142. Bellin M, Casini S, Davis RP, D'Aniello C, Haas J, Ward-van Oostwaard D, et al. Isogenic human pluripotent stem cell pairs reveal the role of a KCNH2 mutation in long-QT syndrome. EMBO J. 2013;32(24):3161-75. doi: 10.1038/emboj.2013.240. PMID: 24213244.

143. Subramaniam A, Jones WK, Gulick J, Wert S, Neumann J, Robbins J. Tissue-specific regulation of the alpha-myosin heavy chain gene promoter in transgenic mice. J Biol Chem. 1991;266(36):24613-20. PMID: 1722208.

144. Jones WK, Sanchez A, Robbins J. Murine pulmonary myocardium: Developmental analysis of cardiac gene expression. Dev Dyn. 1994;200(2):117-28. doi: 10.1002/aja.1002000204. PMID: 7919499.

145. Sanbe A, Gulick J, Hanks MC, Liang Q, Osinska H, Robbins J. Reengineering inducible cardiac-specific transgenesis with an attenuated myosin heavy chain promoter. Circ Res. 2003;92(6):609-16. doi: 10.1161/01.RES.0000065442.64694.9F. PMID: 12623879.

146. Edfors F, Danielsson F, Hallstrom BM, Kall L, Lundberg E, Ponten F, et al. Gene-specific correlation of RNA and protein levels in human cells and tissues. Mol Syst Biol. 2016;12(10):883. doi: 10.15252/msb.20167144. PMID: 27951527.

147. Liu Y, Beyer A, Aebersold R. On the dependency of cellular protein levels on mRNA abundance. Cell. 2016;165(3):535-50. doi: 10.1016/j.cell.2016.03.014. PMID: 27104977.

148. de Sousa Abreu R, Penalva LO, Marcotte EM, Vogel C. Global signatures of protein and mRNA expression levels. Mol Biosyst. 2009;5(12):1512-26. doi: 10.1039/b908315d. PMID: 20023718.

149. Kaese S, Verheule S. Cardiac electrophysiology in mice: A matter of size. Front Physiol. 2012;3:345. doi: 10.3389/fphys.2012.00345. PMID: 22973235.

150. Salama G, London B. Mouse models of long QT syndrome. J Physiol. 2007;578(Pt 1):43-53. doi: 10.1113/jphysiol.2006.118745. PMID: 17038432.

151. Zhang Y, Wu J, King JH, Huang CL, Fraser JA. Measurement and interpretation of electrocardiographic QT intervals in murine hearts. Am J Physiol Heart Circ Physiol. 2014;306(11):H1553-7. doi: 10.1152/ajpheart.00459.2013. PMID: 24705556.

152. Christophersen IE, Magnani JW, Yin X, Barnard J, Weng LC, Arking DE, et al. Fifteen genetic loci associated with the electrocardiographic P wave. Circ Cardiovasc Genet. 2017;10(4):e001667. doi: 10.1161/CIRCGENETICS.116.001667. PMID: 28794112.

153. Sotoodehnia N, Isaacs A, de Bakker PI, Dorr M, Newton-Cheh C, Nolte IM, et al. Common variants in 22 loci are associated with QRS duration and cardiac ventricular conduction. Nat Genet. 2010;42(12):1068-76. doi: 10.1038/ng.716. PMID: 21076409.

154. van Setten J, Brody JA, Jamshidi Y, Swenson BR, Butler AM, Campbell H, et al. PR interval genome-wide association meta-analysis identifies 50 loci associated with atrial and atrioventricular electrical activity. Nat Commun. 2018;9(1):2904. doi: 10.1038/s41467-018-04766-9. PMID: 30046033.

155. Manolio TA, Collins FS, Cox NJ, Goldstein DB, Hindorff LA, Hunter DJ, et al. Finding the missing heritability of complex diseases. Nature. 2009;461(7265):747-53. doi: 10.1038/nature08494. PMID: 19812666.

156. Huang CL. Murine electrophysiological models of cardiac arrhythmogenesis. Physiol Rev. 2017;97(1):283-409. doi: 10.1152/physrev.00007.2016. PMID: 27974512.

157. Verheule S, Kaese S. Connexin diversity in the heart: Insights from transgenic mouse models. Front Pharmacol. 2013;4:81. doi: 10.3389/fphar.2013.00081. PMID: 23818881.

158. Remme CA, Verkerk AO, Nuyens D, van Ginneken AC, van Brunschot S, Belterman CN, et al. Overlap syndrome of cardiac sodium channel disease in mice carrying the equivalent mutation of human SCN5A-1795insD. Circulation. 2006;114(24):2584-94. doi: 10.1161/CIRCULATIONAHA.106.653949. PMID: 17145985.

159. Martin CA, Zhang Y, Grace AA, Huang CL. In vivo studies of SCN5A+/- mice modeling Brugada syndrome demonstrate both conduction and repolarization abnormalities. J Electrocardiol. 2010;43(5):433-9. doi: 10.1016/j.jelectrocard.2010.05.015. PMID: 20638671.

160. Kirchhoff S, Nelles E, Hagendorff A, Kruger O, Traub O, Willecke K. Reduced cardiac conduction velocity and predisposition to arrhythmias in connexin40-deficient mice. Curr Biol. 1998;8(5):299-302. doi: 10.1016/s0960-9822(98)70114-9. PMID: 9501070.

161. Hagendorff A, Schumacher B, Kirchhoff S, Luderitz B, Willecke K. Conduction disturbances and increased atrial vulnerability in connexin40-deficient mice analyzed by transesophageal stimulation. Circulation. 1999;99(11):1508-15. doi: 10.1161/01.cir.99.11.1508. PMID: 10086977.

162. Morley GE, Vaidya D, Samie FH, Lo C, Delmar M, Jalife J. Characterization of conduction in the ventricles of normal and heterozygous Cx43 knockout mice using optical mapping. J Cardiovasc Electrophysiol. 1999;10(10):1361-75. doi: 10.1111/j.1540-8167.1999.tb00192.x. PMID: 10515561.

163. Gutstein DE, Morley GE, Tamaddon H, Vaidya D, Schneider MD, Chen J, et al. Conduction slowing and sudden arrhythmic death in mice with cardiac-restricted inactivation of connexin43. Circ Res. 2001;88(3):333-9. doi: 10.1161/01.res.88.3.333. PMID: 11179202.

164. Eckardt D, Theis M, Degen J, Ott T, van Rijen HV, Kirchhoff S, et al. Functional role of connexin43 gap junction channels in adult mouse heart assessed by inducible gene deletion. J Mol Cell Cardiol. 2004;36(1):101-10. doi: 10.1016/j.yjmcc.2003.10.006. PMID: 14734052.

165. Eckardt D, Kirchhoff S, Kim JS, Degen J, Theis M, Ott T, et al. Cardiomyocyte-restricted deletion of connexin43 during mouse development. J Mol Cell Cardiol. 2006;41(6):963-71. doi: 10.1016/j.yjmcc.2006.07.017. PMID: 16963078.

166. Vaidya D, Morley GE, Samie FH, Jalife J. Reentry and fibrillation in the mouse heart. A challenge to the critical mass hypothesis. Circ Res. 1999;85(2):174-81. doi: 10.1161/01.res.85.2.174. PMID: 10417399.

167. Sabir IN, Killeen MJ, Grace AA, Huang CL. Ventricular arrhythmogenesis: Insights from murine models. Prog Biophys Mol Biol. 2008;98(2-3):208-18. doi: 10.1016/j.pbiomolbio.2008.10.011. PMID: 19041335.

168. Jeron A, Mitchell GF, Zhou J, Murata M, London B, Buckett P, et al. Inducible polymorphic ventricular tachyarrhythmias in a transgenic mouse model with a long QT phenotype. Am J Physiol Heart Circ Physiol. 2000;278(6):H1891-8. doi: 10.1152/ajpheart.2000.278.6.H1891. PMID: 10843886.

169. Guo W, Li H, London B, Nerbonne JM. Functional consequences of elimination of I(to,f) and I(to,s): Early afterdepolarizations, atrioventricular block, and ventricular arrhythmias in mice lacking Kv1.4 and expressing a dominant-negative Kv4 alpha subunit. Circ Res. 2000;87(1):73-9. doi: 10.1161/01.res.87.1.73. PMID: 10884375.

170. Burke JH, Ehlert FA, Kruse JT, Parker MA, Goldberger JJ, Kadish AH. Gender-specific differences in the QT interval and the effect of autonomic tone and menstrual cycle in healthy adults. Am J Cardiol. 1997;79(2):178-81. doi: 10.1016/s0002-9149(96)00707-2. PMID: 9193019.

171. Earle N, Ingles J, Bagnall RD, Gray B, Crawford J, Smith W, et al. NOS1AP polymorphisms modify QTc interval duration but not cardiac arrest risk in hypertrophic cardiomyopathy. J Cardiovasc Electrophysiol. 2015;26(12):1346-51. doi: 10.1111/jce.12827. PMID: 26332198.

172. Coumel P. The management of clinical arrhythmias. An overview on invasive versus non-invasive electrophysiology. Eur Heart J. 1987;8(2):92-9. doi: 10.1093/oxfordjournals.eurheartj.a062259. PMID: 2436917.

173. Tse G. Mechanisms of cardiac arrhythmias. J Arrhythm. 2016;32(2):75-81. doi: 10.1016/j.joa.2015.11.003. PMID: 27092186.

174. Katz LN. The genesis of the electrocardiogram. Physiol Rev. 1947;27(3):398-435. doi: 10.1152/physrev.1947.27.3.398. PMID: 20262019.

175. Hlaing T, DiMino T, Kowey PR, Yan GX. ECG repolarization waves: Their genesis and clinical implications. Ann Noninvasive Electrocardiol. 2005;10(2):211-23. doi: 10.1111/j.1542-474X.2005.05588.x. PMID: 15842434.

176. Meijborg VM, Conrath CE, Opthof T, Belterman CN, de Bakker JM, Coronel R. Electrocardiographic T wave and its relation with ventricular repolarization along major

anatomical axes. Circ Arrhythm Electrophysiol. 2014;7(3):524-31. doi: 10.1161/CIRCEP.113.001622. PMID: 24837645.

177. Antzelevitch C. Ionic, molecular, and cellular bases of QT-interval prolongation and torsade de pointes. Europace. 2007;9 Suppl 4:iv4-15. doi: 10.1093/europace/eum166. PMID: 17766323.

178. Tse G, Chan YW, Keung W, Yan BP. Electrophysiological mechanisms of long and short QT syndromes. Int J Cardiol Heart Vasc. 2017;14:8-13. doi: 10.1016/j.ijcha.2016.11.006. PMID: 28382321.

179. Meregalli PG, Wilde AA, Tan HL. Pathophysiological mechanisms of Brugada syndrome: Depolarization disorder, repolarization disorder, or more? Cardiovasc Res. 2005;67(3):367-78. doi: 10.1016/j.cardiores.2005.03.005. PMID: 15913579.

180. Behr ER, Ben-Haim Y, Ackerman MJ, Krahn AD, Wilde AAM. Brugada syndrome and reduced right ventricular outflow tract conduction reserve: A final common pathway? Eur Heart J. 2021;42(11):1073-81. doi: 10.1093/eurheartj/ehaa1051. PMID: 33421051.

181. Mohler PJ, Schott JJ, Gramolini AO, Dilly KW, Guatimosim S, duBell WH, et al. Ankyrin-B mutation causes type 4 long-QT cardiac arrhythmia and sudden cardiac death. Nature. 2003;421(6923):634-9. doi: 10.1038/nature01335. PMID: 12571597.

182. Ter Keurs HE, Boyden PA. Calcium and arrhythmogenesis. Physiol Rev. 2007;87(2):457-506. doi: 10.1152/physrev.00011.2006. PMID: 17429038.

183. Landstrom AP, Dobrev D, Wehrens XHT. Calcium signaling and cardiac arrhythmias. Circ Res. 2017;120(12):1969-93. doi: 10.1161/CIRCRESAHA.117.310083. PMID: 28596175.

184. Carnicer R, Suffredini S, Liu X, Reilly S, Simon JN, Surdo NC, et al. The subcellular localisation of neuronal nitric oxide synthase determines the downstream effects of NO on myocardial function. Cardiovasc Res. 2017. doi: 10.1093/cvr/cvx002. PMID: 28158509.

185. Tomek J, Hao G, Tomkova M, Lewis A, Carr C, Paterson DJ, et al. Beta-adrenergic receptor stimulation and alternans in the border zone of a healed infarct: An ex vivo study and computational investigation of arrhythmogenesis. Front Physiol. 2019;10:350. doi: 10.3389/fphys.2019.00350. PMID: 30984029.

186. Choi BR, Salama G. Simultaneous maps of optical action potentials and calcium transients in guinea-pig hearts: Mechanisms underlying concordant alternans. J Physiol. 2000;529 Pt 1:171-88. doi: 10.1111/j.1469-7793.2000.00171.x. PMID: 11080260.

187. Tomek J, Wang ZJ, Burton RB, Herring N, Bub G. COSMAS: A lightweight toolbox for cardiac optical mapping analysis. Sci Rep. 2021;11(1):9147. doi: 10.1038/s41598-021-87402-9. PMID: 33911090.

188. Osadchii OE. Effects of Na+ channel blockers on the restitution of refractory period, conduction time, and excitation wavelength in perfused guinea-pig heart. PLoS ONE. 2017;12(2):e0172683. doi: 10.1371/journal.pone.0172683. PMID: 28231318.

189. Jacquemet V, Virag N, Kappenberger L. Wavelength and vulnerability to atrial fibrillation: Insights from a computer model of human atria. Europace. 2005;7 Suppl 2:83-92. doi: 10.1016/j.eupc.2005.03.017. PMID: 16102506.

190. Heijman J, Algalarrondo V, Voigt N, Melka J, Wehrens XH, Dobrev D, et al. The value of basic research insights into atrial fibrillation mechanisms as a guide to therapeutic innovation: A critical analysis. Cardiovasc Res. 2016;109(4):467-79. doi: 10.1093/cvr/cvv275. PMID: 26705366.

191. Thomas G, Killeen MJ, Gurung IS, Hakim P, Balasubramaniam R, Goddard CA, et al. Mechanisms of ventricular arrhythmogenesis in mice following targeted disruption of KCNE1 modelling long QT syndrome 5. J Physiol. 2007;578(Pt 1):99-114. doi: 10.1113/jphysiol.2006.118133. PMID: 17095567.

192. Eloff BC, Lerner DL, Yamada KA, Schuessler RB, Saffitz JE, Rosenbaum DS. High resolution optical mapping reveals conduction slowing in connexin43 deficient mice. Cardiovasc Res. 2001;51(4):681-90. doi: 10.1016/s0008-6363(01)00341-8. PMID: 11530101.

193. Beauchamp P, Yamada KA, Baertschi AJ, Green K, Kanter EM, Saffitz JE, et al. Relative contributions of connexins 40 and 43 to atrial impulse propagation in synthetic strands of neonatal and fetal murine cardiomyocytes. Circ Res. 2006;99(11):1216-24. doi: 10.1161/01.RES.0000250607.34498.b4. PMID: 17053190.

194. Sikkel MB, Francis DP, Howard J, Gordon F, Rowlands C, Peters NS, et al. Hierarchical statistical techniques are necessary to draw reliable conclusions from analysis of isolated cardiomyocyte studies. Cardiovasc Res. 2017;113(14):1743-52. doi: 10.1093/cvr/cvx151. PMID: 29016722.

195. Nguyen TP, Qu Z, Weiss JN. Cardiac fibrosis and arrhythmogenesis: The road to repair is paved with perils. J Mol Cell Cardiol. 2014;70:83-91. doi: 10.1016/j.yjmcc.2013.10.018. PMID: 24184999.

196. Selvaraj RJ, Picton P, Nanthakumar K, Mak S, Chauhan VS. Endocardial and epicardial repolarization alternans in human cardiomyopathy: Evidence for spatiotemporal heterogeneity and correlation with body surface T-wave alternans. J Am Coll Cardiol. 2007;49(3):338-46. doi: 10.1016/j.jacc.2006.08.056. PMID: 17239715.

197. Nearing BD, Wellenius GA, Mittleman MA, Josephson ME, Burger AJ, Verrier RL. Crescendo in depolarization and repolarization heterogeneity heralds development of ventricular tachycardia in hospitalized patients with decompensated heart failure. Circ Arrhythm Electrophysiol. 2012;5(1):84-90. doi: 10.1161/CIRCEP.111.965434. PMID: 22157521.

198. King JH, Huang CL, Fraser JA. Determinants of myocardial conduction velocity: Implications for arrhythmogenesis. Front Physiol. 2013;4:154. doi: 10.3389/fphys.2013.00154. PMID: 23825462.

199. Jongsma HJ, Wilders R. Gap junctions in cardiovascular disease. Circ Res. 2000;86(12):1193-7. doi: 10.1161/01.res.86.12.1193. PMID: 10864907.

200. Beardslee MA, Laing JG, Beyer EC, Saffitz JE. Rapid turnover of connexin43 in the adult rat heart. Circ Res. 1998;83(6):629-35. doi: 10.1161/01.res.83.6.629. PMID: 9742058.

201. Beardslee MA, Lerner DL, Tadros PN, Laing JG, Beyer EC, Yamada KA, et al. Dephosphorylation and intracellular redistribution of ventricular connexin43 during electrical uncoupling induced by ischemia. Circ Res. 2000;87(8):656-62. doi: 10.1161/01.res.87.8.656. PMID: 11029400.

202. Ahern GP, Hsu SF, Klyachko VA, Jackson MB. Induction of persistent sodium current by exogenous and endogenous nitric oxide. J Biol Chem. 2000;275(37):28810-5. doi: 10.1074/jbc.M003090200. PMID: 10833522.

203. Iravanian S, Uzelac I, Herndon C, Langberg JJ, Fenton FH. Generation of monophasic action potentials and intermediate forms. Biophys J. 2020;119(2):460-9. doi: 10.1016/j.bpj.2020.05.039. PMID: 32645291.

204. Antzelevitch C, Sicouri S, Litovsky SH, Lukas A, Krishnan SC, Di Diego JM, et al. Heterogeneity within the ventricular wall. Electrophysiology and pharmacology of epicardial, endocardial, and M cells. Circ Res. 1991;69(6):1427-49. doi: 10.1161/01.res.69.6.1427. PMID: 1659499.

205. Li GR, Feng J, Yue L, Carrier M. Transmural heterogeneity of action potentials and Ito1 in myocytes isolated from the human right ventricle. Am J Physiol. 1998;275(2):H369-77. doi: 10.1152/ajpheart.1998.275.2.H369. PMID: 9683422.

206. Brunet S, Aimond F, Li H, Guo W, Eldstrom J, Fedida D, et al. Heterogeneous expression of repolarizing, voltage-gated K+ currents in adult mouse ventricles. J Physiol. 2004;559(Pt 1):103-20. doi: 10.1113/jphysiol.2004.063347. PMID: 15194740.

207. Patel SP, Campbell DL. Transient outward potassium current, 'Ito', phenotypes in the mammalian left ventricle: Underlying molecular, cellular and biophysical mechanisms. J Physiol. 2005;569(Pt 1):7-39. doi: 10.1113/jphysiol.2005.086223. PMID: 15831535.

208. Spitzer KW, Pollard AE, Yang L, Zaniboni M, Cordeiro JM, Huelsing DJ. Cell-to-cell electrical interactions during early and late repolarization. J Cardiovasc Electrophysiol. 2006;17 Suppl 1:S8-S14. doi: 10.1111/j.1540-8167.2006.00379.x. PMID: 16686687.

209. Bryant SM, Wan X, Shipsey SJ, Hart G. Regional differences in the delayed rectifier current (Ikr and Iks) contribute to the differences in action potential duration in basal left ventricular myocytes in guinea-pig. Cardiovasc Res. 1998;40(2):322-31. doi: 10.1016/s0008-6363(98)00133-3. PMID: 9893726.

210. Shattock MJ, Park KC, Yang HY, Lee AWC, Niederer S, MacLeod KT, et al. Restitution slope is principally determined by steady-state action potential duration. Cardiovasc Res. 2017;113(7):817-28. doi: 10.1093/cvr/cvx063. PMID: 28371805.

211. O'Hara T, Rudy Y. Quantitative comparison of cardiac ventricular myocyte electrophysiology and response to drugs in human and nonhuman species. Am J Physiol Heart Circ Physiol. 2012;302(5):H1023-30. doi: 10.1152/ajpheart.00785.2011. PMID: 22159993.

212. Nerbonne JM. Studying cardiac arrhythmias in the mouse--a reasonable model for probing mechanisms? Trends Cardiovasc Med. 2004;14(3):83-93. doi: 10.1016/j.tcm.2003.12.006. PMID: 15121155.

213. Nerbonne JM, Nichols CG, Schwarz TL, Escande D. Genetic manipulation of cardiac K(+) channel function in mice: What have we learned, and where do we go from here? Circ Res. 2001;89(11):944-56. doi: 10.1161/hh2301.100349. PMID: 11717150.

214. Lampe PD, Lau AF. The effects of connexin phosphorylation on gap junctional communication. Int J Biochem Cell Biol. 2004;36(7):1171-86. doi: 10.1016/S1357-2725(03)00264-4. PMID: 15109565.

215. Pogoda K, Kameritsch P, Retamal MA, Vega JL. Regulation of gap junction channels and hemichannels by phosphorylation and redox changes: A revision. BMC Cell Biol. 2016;17 Suppl 1:11. doi: 10.1186/s12860-016-0099-3. PMID: 27229925.

216. Majmundar AJ, Buerger F, Forbes TA, Klambt V, Schneider R, Deutsch K, et al. Recessive NOS1AP variants impair actin remodeling and cause glomerulopathy in humans and mice. Sci Adv. 2021;7(1). doi: 10.1126/sciadv.abe1386. PMID: 33523862.

217. Chen J, Pan L, Wei Z, Zhao Y, Zhang M. Domain-swapped dimerization of ZO-1 PDZ2 generates specific and regulatory connexin43-binding sites. EMBO J. 2008;27(15):2113-23. doi: 10.1038/emboj.2008.138. PMID: 18636092.

218. Palatinus JA, O'Quinn MP, Barker RJ, Harris BS, Jourdan J, Gourdie RG. ZO-1 determines adherens and gap junction localization at intercalated disks. Am J Physiol Heart Circ Physiol. 2011;300(2):H583-94. doi: 10.1152/ajpheart.00999.2010. PMID: 21131473.

219. Nademanee K, Raju H, de Noronha SV, Papadakis M, Robinson L, Rothery S, et al. Fibrosis, connexin-43, and conduction abnormalities in the Brugada syndrome. J Am Coll Cardiol. 2015;66(18):1976-86. doi: 10.1016/j.jacc.2015.08.862. PMID: 26516000.

220. Chatterjee D, Pieroni M, Fatah M, Charpentier F, Cunningham KS, Spears DA, et al. An autoantibody profile detects Brugada syndrome and identifies abnormally expressed myocardial proteins. Eur Heart J. 2020. doi: 10.1093/eurheartj/ehaa383. PMID: 32533187.

221. Hulsmans M, Clauss S, Xiao L, Aguirre AD, King KR, Hanley A, et al. Macrophages facilitate electrical conduction in the heart. Cell. 2017;169(3):510-22 e20. doi: 10.1016/j.cell.2017.03.050. PMID: 28431249.

222. Bezzina C, Veldkamp MW, van Den Berg MP, Postma AV, Rook MB, Viersma JW, et al. A single Na(+) channel mutation causing both long-QT and Brugada syndromes. Circ Res. 1999;85(12):1206-13. doi: 10.1161/01.res.85.12.1206. PMID: 10590249.

223. Seddon M, Shah AM, Casadei B. Cardiomyocytes as effectors of nitric oxide signalling. Cardiovasc Res. 2007;75(2):315-26. doi: 10.1016/j.cardiores.2007.04.031. PMID: 17568574.

224. Wood MW, Hastings RC, Sygowski LA. A homogeneous fluorescent cell-based assay for detection of heterologously expressed nitric oxide synthase activity. J Biomol Screen. 2005;10(8):849-55. doi: 10.1177/1087057105280640. PMID: 16234340.

225. Combet S, Balligand JL, Lameire N, Goffin E, Devuyst O. A specific method for measurement of nitric oxide synthase enzymatic activity in peritoneal biopsies. Kidney Int. 2000;57(1):332-8. doi: 10.1046/j.1523-1755.2000.00839.x. PMID: 10620216.

226. Wijesurendra RS, Casadei B. Mechanisms of atrial fibrillation. Heart. 2019;105(24):1860-7. doi: 10.1136/heartjnl-2018-314267. PMID: 31444267.

227. Riley G, Syeda F, Kirchhof P, Fabritz L. An introduction to murine models of atrial fibrillation. Front Physiol. 2012;3:296. doi: 10.3389/fphys.2012.00296. PMID: 22934047.

228. Schuttler D, Bapat A, Kaab S, Lee K, Tomsits P, Clauss S, et al. Animal models of atrial fibrillation. Circ Res. 2020;127(1):91-110. doi: 10.1161/CIRCRESAHA.120.316366. PMID: 32716814.

229. Verheule S, van Batenburg CA, Coenjaerts FE, Kirchhoff S, Willecke K, Jongsma HJ. Cardiac conduction abnormalities in mice lacking the gap junction protein connexin40. J Cardiovasc Electrophysiol. 1999;10(10):1380-9. doi: 10.1111/j.1540-8167.1999.tb00194.x. PMID: 10515563.

230. Blana A, Kaese S, Fortmuller L, Laakmann S, Damke D, van Bragt K, et al. Knock-in gain-of-function sodium channel mutation prolongs atrial action potentials and alters atrial vulnerability. Heart Rhythm. 2010;7(12):1862-9. doi: 10.1016/j.hrthm.2010.08.016. PMID: 20728579.

231. Watanabe H, Yang T, Stroud DM, Lowe JS, Harris L, Atack TC, et al. Striking in vivo phenotype of a disease-associated human SCN5A mutation producing minimal changes in vitro. Circulation. 2011;124(9):1001-11. doi: 10.1161/CIRCULATIONAHA.110.987248. PMID: 21824921.

232. Nielsen JB, Thorolfsdottir RB, Fritsche LG, Zhou W, Skov MW, Graham SE, et al. Biobank-driven genomic discovery yields new insight into atrial fibrillation biology. Nat Genet. 2018;50(9):1234-9. doi: 10.1038/s41588-018-0171-3. PMID: 30061737.

233. Ntalla I, Weng LC, Cartwright JH, Hall AW, Sveinbjornsson G, Tucker NR, et al. Multi-ancestry gwas of the electrocardiographic PR interval identifies 202 loci underlying cardiac conduction. Nat Commun. 2020;11(1):2542. doi: 10.1038/s41467-020-15706-x. PMID: 32439900.

234. Verheule S, Sato T, Everett Tt, Engle SK, Otten D, Rubart-von der Lohe M, et al. Increased vulnerability to atrial fibrillation in transgenic mice with selective atrial fibrosis caused by overexpression of TGF-beta1. Circ Res. 2004;94(11):1458-65. doi: 10.1161/01.RES.0000129579.59664.9d. PMID: 15117823.

235. Knollmann BC, Schober T, Petersen AO, Sirenko SG, Franz MR. Action potential characterization in intact mouse heart: Steady-state cycle length dependence and electrical restitution. Am J Physiol Heart Circ Physiol. 2007;292(1):H614-21. doi: 10.1152/ajpheart.01085.2005. PMID: 16963611.

236. Hindricks G, Potpara T, Dagres N, Arbelo E, Bax JJ, Blomstrom-Lundqvist C, et al. 2020 ESC guidelines for the diagnosis and management of atrial fibrillation developed in collaboration with the European Association of Cardio-Thoracic Surgery (EACTS). Eur Heart J. 2020. doi: 10.1093/eurheartj/ehaa612. PMID: 32860505.

237. Hong K, Piper DR, Diaz-Valdecantos A, Brugada J, Oliva A, Burashnikov E, et al. De novo KCNQ1 mutation responsible for atrial fibrillation and short QT syndrome in utero. Cardiovasc Res. 2005;68(3):433-40. doi: 10.1016/j.cardiores.2005.06.023. PMID: 16109388.

238. Francis J, Antzelevitch C. Atrial fibrillation and Brugada syndrome. J Am Coll Cardiol. 2008;51(12):1149-53. doi: 10.1016/j.jacc.2007.10.062. PMID: 18355651.

239. Ghaleb R, Anselmino M, Gaido L, Quaranta S, Giustetto C, Salama MK, et al. Prevalence and clinical significance of latent Brugada syndrome in atrial fibrillation patients below 45 years of age. Front Cardiovasc Med. 2020;7:602536. doi: 10.3389/fcvm.2020.602536. PMID: 33330665.

240. Nielsen JB, Kuhl JT, Pietersen A, Graff C, Lind B, Struijk JJ, et al. P-wave duration and the risk of atrial fibrillation: Results from the Copenhagen ECG study. Heart Rhythm. 2015;12(9):1887-95. doi: 10.1016/j.hrthm.2015.04.026. PMID: 25916567.

241. Nielsen JB, Pietersen A, Graff C, Lind B, Struijk JJ, Olesen MS, et al. Risk of atrial fibrillation as a function of the electrocardiographic PR interval: Results from the Copenhagen ECG study. Heart Rhythm. 2013;10(9):1249-56. doi: 10.1016/j.hrthm.2013.04.012. PMID: 23608590.

242. Gajendragadkar PR, Von Ende A, Ibrahim M, Valdes-Marquez E, Camm CF, Murgia F, et al. Assessment of the causal relevance of ECG parameters for risk of atrial fibrillation: A Mendelian randomisation study. PLoS Med. 2021;18(5):e1003572. doi: 10.1371/journal.pmed.1003572. PMID: 33983917.

243. Lewis T. Report cxix. Auricular fibrillation: A common clinical condition. Br Med J. 1909;2(2552):1528. doi: 10.1136/bmj.2.2552.1528. PMID: 20764769.

244. Wolff L, Parkinson J, White PD. Bundle-branch block with short PR interval in healthy young people prone to paroxysmal tachycardia. Am Heart J. 1930;5(6):685-704. doi: https://doi.org/10.1016/S0002-8703(30)90086-5.

245. Lewis T. Oliver-Sharpey lectures on the nature of flutter and fibrillation of the auricle. Br Med J. 1921;1(3147):590-3. doi: 10.1136/bmj.1.3147.590. PMID: 20770267.

246. Moe GK, Abildskov JA. Atrial fibrillation as a self-sustaining arrhythmia independent of focal discharge. Am Heart J. 1959;58(1):59-70. doi: 10.1016/0002-8703(59)90274-1. PMID: 13661062.

247. Moe GK, Rheinboldt WC, Abildskov JA. A computer model of atrial fibrillation. Am Heart J. 1964;67:200-20. doi: 10.1016/0002-8703(64)90371-0. PMID: 14118488.

248. Jalife J. Deja vu in the theories of atrial fibrillation dynamics. Cardiovasc Res. 2011;89(4):766-75. doi: 10.1093/cvr/cvq364. PMID: 21097807.

249. Scherf D, Terranova R. Mechanism of auricular flutter and fibrillation. Am J Physiol. 1949;159(1):137-42. doi: 10.1152/ajplegacy.1949.159.1.137. PMID: 15391089.

250. Fraser HR, Turner RW. Auricular fibrillation; with special reference to rheumatic heart disease. Br Med J. 1955;2(4953):1414-8. doi: 10.1136/bmj.2.4953.1414. PMID: 13269883.

251. Leier CV, Meacham JA, Schaal SF. Prolonged atrial conduction. A major predisposing factor for the development of atrial flutter. Circulation. 1978;57(2):213-6. doi: 10.1161/01.cir.57.2.213. PMID: 618606.

252. Simpson RJ, Jr., Foster JR, Gettes LS. Atrial excitability and conduction in patients with interatrial conduction defects. Am J Cardiol. 1982;50(6):1331-7. doi: 10.1016/0002-9149(82)90471-4. PMID: 7148710.

253. Haissaguerre M, Jais P, Shah DC, Takahashi A, Hocini M, Quiniou G, et al. Spontaneous initiation of atrial fibrillation by ectopic beats originating in the pulmonary veins. N Engl J Med. 1998;339(10):659-66. doi: 10.1056/NEJM199809033391003. PMID: 9725923.

254. Wijffels MC, Kirchhof CJ, Dorland R, Allessie MA. Atrial fibrillation begets atrial fibrillation. A study in awake chronically instrumented goats. Circulation. 1995;92(7):1954-68. doi: 10.1161/01.cir.92.7.1954. PMID: 7671380.

255. Nattel S, Heijman J, Zhou L, Dobrev D. Molecular basis of atrial fibrillation pathophysiology and therapy: A translational perspective. Circ Res. 2020;127(1):51-72. doi: 10.1161/CIRCRESAHA.120.316363. PMID: 32717172.

256. Alcaraz R, Hornero F, Rieta JJ. Noninvasive time and frequency predictors of long-standing atrial fibrillation early recurrence after electrical cardioversion. Pacing Clin Electrophysiol. 2011;34(10):1241-50. doi: 10.1111/j.1540-8159.2011.03125.x. PMID: 21605132.

257. Zhao TX, Martin CA, Cooper JP, Gajendragadkar PR. Coarse fibrillatory waves in atrial fibrillation predict success of electrical cardioversion. Ann Noninvasive Electrocardiol. 2018;23(4):e12528. doi: 10.1111/anec.12528. PMID: 29271577.

258. Cheng Z, Deng H, Cheng K, Chen T, Gao P, Yu M, et al. The amplitude of fibrillatory waves on leads aVF and V1 predicting the recurrence of persistent atrial fibrillation patients who underwent catheter ablation. Ann Noninvasive Electrocardiol. 2013;18(4):352-8. doi: 10.1111/anec.12041. PMID: 23879275.

259. Lankveld T, Zeemering S, Scherr D, Kuklik P, Hoffmann BA, Willems S, et al. Atrial fibrillation complexity parameters derived from surface ECGs predict procedural outcome and long-term follow-up of stepwise catheter ablation for atrial fibrillation. Circ Arrhythm Electrophysiol. 2016;9(2):e003354. doi: 10.1161/CIRCEP.115.003354. PMID: 26823480.

260. Lankveld TA, Zeemering S, Crijns HJ, Schotten U. The ECG as a tool to determine atrial fibrillation complexity. Heart. 2014;100(14):1077-84. doi: 10.1136/heartjnl-2013-305149. PMID: 24837984.

261. Magnani JW, Johnson VM, Sullivan LM, Gorodeski EZ, Schnabel RB, Lubitz SA, et al. P wave duration and risk of longitudinal atrial fibrillation in persons >/= 60 years old (from The Framingham Heart Study). Am J Cardiol. 2011;107(6):917-21 e1. doi: 10.1016/j.amjcard.2010.10.075. PMID: 21255761.

262. Magnani JW, Zhu L, Lopez F, Pencina MJ, Agarwal SK, Soliman EZ, et al. P-wave indices and atrial fibrillation: Cross-cohort assessments from The Framingham Heart Study (FHS) and Atherosclerosis Risk In Communities (ARIC) study. Am Heart J. 2015;169(1):53-61 e1. doi: 10.1016/j.ahj.2014.10.009. PMID: 25497248.

263. Cheng S, Keyes MJ, Larson MG, McCabe EL, Newton-Cheh C, Levy D, et al. Long-term outcomes in individuals with prolonged PR interval or first-degree atrioventricular block. JAMA. 2009;301(24):2571-7. doi: 10.1001/jama.2009.888. PMID: 19549974.

264. Smith JW, O'Neal WT, Shoemaker MB, Chen LY, Alonso A, Whalen SP, et al. PR-interval components and atrial fibrillation risk (from the Atherosclerosis Risk In Communities study). Am J Cardiol. 2017;119(3):466-72. doi: 10.1016/j.amjcard.2016.10.016. PMID: 27889043.

265. Perez MV, Dewey FE, Marcus R, Ashley EA, Al-Ahmad AA, Wang PJ, et al. Electrocardiographic predictors of atrial fibrillation. Am Heart J. 2009;158(4):622-8. doi: 10.1016/j.ahj.2009.08.002. PMID: 19781423.

266. Dilaveris PE, Gialafos EJ, Chrissos D, Andrikopoulos GK, Richter DJ, Lazaki E, et al. Detection of hypertensive patients at risk for paroxysmal atrial fibrillation during sinus rhythm by computer-assisted P wave analysis. J Hypertens. 1999;17(10):1463-70. doi: 10.1097/00004872-199917100-00015. PMID: 10526908.

267. Sanders P, Morton JB, Davidson NC, Spence SJ, Vohra JK, Sparks PB, et al. Electrical remodeling of the atria in congestive heart failure: Electrophysiological and electroanatomic mapping in humans. Circulation. 2003;108(12):1461-8. doi: 10.1161/01.CIR.0000090688.49283.67. PMID: 12952837.

268. Rabkin SW, Cheng XJ, Thompson DJ. Detailed analysis of the impact of age on the QT interval. J Geriatr Cardiol. 2016;13(9):740-8. doi: 10.11909/j.issn.1671-5411.2016.09.013. PMID: 27899938.

269. Haycock PC, Burgess S, Wade KH, Bowden J, Relton C, Davey Smith G. Best (but oft-forgotten) practices: The design, analysis, and interpretation of Mendelian randomization studies. Am J Clin Nutr. 2016;103(4):965-78. doi: 10.3945/ajcn.115.118216. PMID: 26961927.

270. Davey Smith G, Davies NM, Dimou N, Egger M, Gallo V, Golub R, et al. STROBE-MR: Guidelines for strengthening the reporting of Mendelian randomization studies. PeerJ Preprints. 2019;7:e27857v1. doi: 10.7287/peerj.preprints.27857v1.

271. Bycroft C, Freeman C, Petkova D, Band G, Elliott LT, Sharp K, et al. The UK Biobank resource with deep phenotyping and genomic data. Nature. 2018;562(7726):203-9. doi: 10.1038/s41586-018-0579-z. PMID: 30305743.

272. Littlejohns TJ, Sudlow C, Allen NE, Collins R. UK Biobank: Opportunities for cardiovascular research. Eur Heart J. 2019;40(14):1158-66. doi: 10.1093/eurheartj/ehx254. PMID: 28531320.

273. Petersen SE, Matthews PM, Francis JM, Robson MD, Zemrak F, Boubertakh R, et al. UK Biobank's cardiovascular magnetic resonance protocol. J Cardiovasc Magn Reson. 2016;18:8. doi: 10.1186/s12968-016-0227-4. PMID: 26830817.

274. Khurshid S, Choi SH, Weng LC, Wang EY, Trinquart L, Benjamin EJ, et al. Frequency of cardiac rhythm abnormalities in a half million adults. Circ Arrhythm Electrophysiol. 2018;11(7):e006273. doi: 10.1161/CIRCEP.118.006273. PMID: 29954742.

275. Eastwood SV, Mathur R, Atkinson M, Brophy S, Sudlow C, Flaig R, et al. Algorithms for the capture and adjudication of prevalent and incident diabetes in UK Biobank. PLoS ONE. 2016;11(9):e0162388. doi: 10.1371/journal.pone.0162388. PMID: 27631769.

276. Bihlmeyer NA, Brody JA, Smith AV, Warren HR, Lin H, Isaacs A, et al. Exomechip-wide analysis of 95 626 individuals identifies 10 novel loci associated with QT and JT intervals. Circ Genom Precis Med. 2018;11(1):e001758. doi: 10.1161/CIRCGEN.117.001758. PMID: 29874175.

277. Dayem Ullah AZ, Oscanoa J, Wang J, Nagano A, Lemoine NR, Chelala C. SNPnexus: Assessing the functional relevance of genetic variation to facilitate the promise of precision medicine. Nucleic Acids Res. 2018;46(W1):W109-W13. doi: 10.1093/nar/gky399. PMID: 29757393.

278. Ashburner M, Ball CA, Blake JA, Botstein D, Butler H, Cherry JM, et al. Gene ontology: Tool for the unification of biology. The Gene Ontology Consortium. Nat Genet. 2000;25(1):25-9. doi: 10.1038/75556. PMID: 10802651.

279. The Gene Ontology Consortium. The Gene Ontology Resource: 20 years and still GOing strong. Nucleic Acids Res. 2019;47(D1):D330-D8. doi: 10.1093/nar/gky1055. PMID: 30395331.

280. Bycroft C, Freeman C, Petkova D, Band G, Elliott LT, Sharp K, et al. Genome-wide genetic data on ~500,000 UK Biobank participants. bioRxiv. 2017.

281. Mack S, Coassin S, Vaucher J, Kronenberg F, Lamina C, Apo AIVGC. Evaluating the causal relation of ApoA-IV with disease-related traits - a bidirectional two-sample Mendelian randomization study. Sci Rep. 2017;7(1):8734. doi: 10.1038/s41598-017-07213-9. PMID: 28821713.

282. Li B, Martin EB. An approximation to the F distribution using the Chi-square distribution. Computational Statistics & Data Analysis. 2002;40(1):21-6. doi: 10.1016/s0167-9473(01)00097-4.

283. Burgess S, Thompson SG, Collaboration CCG. Avoiding bias from weak instruments in Mendelian randomization studies. Int J Epidemiol. 2011;40(3):755-64. doi: 10.1093/ije/dyr036. PMID: 21414999.

284. Christophersen IE, Rienstra M, Roselli C, Yin X, Geelhoed B, Barnard J, et al. Large-scale analyses of common and rare variants identify 12 new loci associated with atrial fibrillation. Nat Genet. 2017;49(6):946-52. doi: 10.1038/ng.3843. PMID: 28416818.

285. Cardiovascular disease knowledge portal. [cited 2020 January]. Available from: http://www.kp4cd.org/dataset_downloads/mi#summary.

286. Burgess S, Bowden J, Fall T, Ingelsson E, Thompson SG. Sensitivity analyses for robust causal inference from Mendelian randomization analyses with multiple genetic variants. Epidemiology. 2017;28(1):30-42. doi: 10.1097/EDE.0000000000000559. PMID: 27749700.

287. Hartwig FP, Davey Smith G, Bowden J. Robust inference in summary data Mendelian randomization via the zero modal pleiotropy assumption. Int J Epidemiol. 2017;46(6):1985-98. doi: 10.1093/ije/dyx102. PMID: 29040600.

288. Verbanck M, Chen CY, Neale B, Do R. Detection of widespread horizontal pleiotropy in causal relationships inferred from Mendelian randomization between complex traits and diseases. Nat Genet. 2018;50(5):693-8. doi: 10.1038/s41588-018-0099-7. PMID: 29686387.

289. Staley JR, Blackshaw J, Kamat MA, Ellis S, Surendran P, Sun BB, et al. Phenoscanner: A database of human genotype-phenotype associations. Bioinformatics. 2016;32(20):3207-9. doi: 10.1093/bioinformatics/btw373. PMID: 27318201.

290. Brugada J, Katritsis DG, Arbelo E, Arribas F, Bax JJ, Blomstrom-Lundqvist C, et al. 2019 ESC guidelines for the management of patients with supraventricular tachycardia: The Task Force for the management of patients with supraventricular tachycardia of the European Society of Cardiology (ESC). Eur Heart J. 2020;41(5):655-720. doi: 10.1093/eurheartj/ehz467. PMID: 31504425.

291. Schnabel RB, Sullivan LM, Levy D, Pencina MJ, Massaro JM, D'Agostino RB, Sr., et al. Development of a risk score for atrial fibrillation (Framingham Heart Study): A community-based cohort study. Lancet. 2009;373(9665):739-45. doi: 10.1016/S0140-6736(09)60443-8. PMID: 19249635.

292. Alonso A, Krijthe BP, Aspelund T, Stepas KA, Pencina MJ, Moser CB, et al. Simple risk model predicts incidence of atrial fibrillation in a racially and geographically diverse population: The CHARGE-AF consortium. J Am Heart Assoc. 2013;2(2):e000102. doi: 10.1161/JAHA.112.000102. PMID: 23537808.

293. van Noord C, Eijgelsheim M, Stricker BH. Drug- and non-drug-associated QT interval prolongation. Br J Clin Pharmacol. 2010;70(1):16-23. doi: 10.1111/j.1365-2125.2010.03660.x. PMID: 20642543.

294. Holm H, Gudbjartsson DF, Arnar DO, Thorleifsson G, Thorgeirsson G, Stefansdottir H, et al. Several common variants modulate heart rate, PR interval and QRS duration. Nat Genet. 2010;42(2):117-22. doi: 10.1038/ng.511. PMID: 20062063.

295. Pfeufer A, van Noord C, Marciante KD, Arking DE, Larson MG, Smith AV, et al. Genome-wide association study of PR interval. Nat Genet. 2010;42(2):153-9. doi: 10.1038/ng.517. PMID: 20062060.

296. Janse MJ. Why does atrial fibrillation occur? Eur Heart J. 1997;18 Suppl C:C12-8. doi: 10.1093/eurheartj/18.suppl_c.12. PMID: 9152670.

297. Dan GA, Martinez-Rubio A, Agewall S, Boriani G, Borggrefe M, Gaita F, et al. Antiarrhythmic drugs-clinical use and clinical decision making: A consensus document from the European Heart Rhythm Association (EHRA) and European Society of Cardiology (ESC) working group on cardiovascular pharmacology, endorsed by the Heart Rhythm Society (HRS), Asia-Pacific Heart Rhythm Society (APHRS) and International Society of Cardiovascular Pharmacotherapy (ISCP). Europace. 2018;20(5):731-2an. doi: 10.1093/europace/eux373. PMID: 29438514.

298. Chen LY, Ballew JD, Herron KJ, Rodeheffer RJ, Olson TM. A common polymorphism in SCN5A is associated with lone atrial fibrillation. Clin Pharmacol Ther. 2007;81(1):35-41. doi: 10.1038/sj.clpt.6100016. PMID: 17185997.

299. Ellinor PT, Nam EG, Shea MA, Milan DJ, Ruskin JN, MacRae CA. Cardiac sodium channel mutation in atrial fibrillation. Heart Rhythm. 2008;5(1):99-105. doi: 10.1016/j.hrthm.2007.09.015. PMID: 18088563.

300. van den Boogaard M, Smemo S, Burnicka-Turek O, Arnolds DE, van de Werken HJ, Klous P, et al. A common genetic variant within SCN10A modulates cardiac SCN5A expression. J Clin Invest. 2014;124(4):1844-52. doi: 10.1172/JCI73140. PMID: 24642470.

301. Benditt DG, Pritchett LC, Smith WM, Wallace AG, Gallagher JJ. Characteristics of atrioventricular conduction and the spectrum of arrhythmias in Lown-Ganong-Levine syndrome. Circulation. 1978;57(3):454-65. doi: 10.1161/01.cir.57.3.454. PMID: 624155.

302. Lown B, Ganong WF, Levine SA. The syndrome of short PR interval, normal QRS complex and paroxysmal rapid heart action. Circulation. 1952;5(5):693-706. doi: 10.1161/01.cir.5.5.693. PMID: 14926053.

303. Vidaillet HJ, Jr., Pressley JC, Henke E, Harrell FE, Jr., German LD. Familial occurrence of accessory atrioventricular pathways (preexcitation syndrome). N Engl J Med. 1987;317(2):65-9. doi: 10.1056/NEJM198707093170201. PMID: 3587328.

304. Bunch TJ, May HT, Bair TL, Anderson JL, Crandall BG, Cutler MJ, et al. Long-term natural history of adult Wolff-Parkinson-White syndrome patients treated with and without catheter ablation. Circ Arrhythm Electrophysiol. 2015;8(6):1465-71. doi: 10.1161/CIRCEP.115.003013. PMID: 26480930.

305. Frey MK, Richter B, Gwechenberger M, Marx M, Pezawas T, Schrutka L, et al. High incidence of atrial fibrillation after successful catheter ablation of atrioventricular nodal reentrant tachycardia: A 15.5-year follow-up. Sci Rep. 2019;9(1):11784. doi: 10.1038/s41598-019-47980-1. PMID: 31409803.

306. Gollob MH, Jones DL, Krahn AD, Danis L, Gong XQ, Shao Q, et al. Somatic mutations in the connexin 40 gene (GJA5) in atrial fibrillation. N Engl J Med. 2006;354(25):2677-88. doi: 10.1056/NEJMoa052800. PMID: 16790700.

307. Boukens BJ, Rivaud MR, Rentschler S, Coronel R. Misinterpretation of the mouse ECG: 'Musing the waves of mus musculus'. J Physiol. 2014;592(21):4613-26. doi: 10.1113/jphysiol.2014.279380. PMID: 25260630.

308. Ramanathan C, Ghanem RN, Jia P, Ryu K, Rudy Y. Noninvasive electrocardiographic imaging for cardiac electrophysiology and arrhythmia. Nat Med. 2004;10(4):422-8. doi: 10.1038/nm1011. PMID: 15034569.

309. Zhang J, Sacher F, Hoffmayer K, O'Hara T, Strom M, Cuculich P, et al. Cardiac electrophysiological substrate underlying the ECG phenotype and electrogram abnormalities in Brugada syndrome patients. Circulation. 2015;131(22):1950-9. doi: 10.1161/CIRCULATIONAHA.114.013698. PMID: 25810336.

310. Nademanee K, Veerakul G, Chandanamattha P, Chaothawee L, Ariyachaipanich A, Jirasirirojanakorn K, et al. Prevention of ventricular fibrillation episodes in Brugada syndrome by catheter ablation over the anterior right ventricular outflow tract epicardium. Circulation. 2011;123(12):1270-9. doi: 10.1161/CIRCULATIONAHA.110.972612. PMID: 21403098.

311. Vijayakumar R, Silva JNA, Desouza KA, Abraham RL, Strom M, Sacher F, et al. Electrophysiologic substrate in congenital long QT syndrome: Noninvasive mapping with electrocardiographic imaging (ECGI). Circulation. 2014;130(22):1936-43. doi: 10.1161/CIRCULATIONAHA.114.011359. PMID: 25294783.

312. Westenbroek RE, Bischoff S, Fu Y, Maier SK, Catterall WA, Scheuer T. Localization of sodium channel subtypes in mouse ventricular myocytes using quantitative immunocytochemistry. J Mol Cell Cardiol. 2013;64:69-78. doi: 10.1016/j.yjmcc.2013.08.004. PMID: 23982034.

313. Shen MJ, Zipes DP. Role of the autonomic nervous system in modulating cardiac arrhythmias. Circ Res. 2014;114(6):1004-21. doi: 10.1161/CIRCRESAHA.113.302549. PMID: 24625726.

314. Mason JW, Ramseth DJ, Chanter DO, Moon TE, Goodman DB, Mendzelevski B. Electrocardiographic reference ranges derived from 79,743 ambulatory subjects. J Electrocardiol. 2007;40(3):228-34. doi: 10.1016/j.jelectrocard.2006.09.003. PMID: 17276451.

315. Choy L, Yeo JM, Tse V, Chan SP, Tse G. Cardiac disease and arrhythmogenesis: Mechanistic insights from mouse models. Int J Cardiol Heart Vasc. 2016;12:1-10. doi: 10.1016/j.ijcha.2016.05.005. PMID: 27766308.

316. Clauss S, Bleyer C, Schuttler D, Tomsits P, Renner S, Klymiuk N, et al. Animal models of arrhythmia: Classic electrophysiology to genetically modified large animals. Nat Rev Cardiol. 2019;16(8):457-75. doi: 10.1038/s41569-019-0179-0. PMID: 30894679.

317. Ashar FN, Mitchell RN, Albert CM, Newton-Cheh C, Brody JA, Muller-Nurasyid M, et al. A comprehensive evaluation of the genetic architecture of sudden cardiac arrest. Eur Heart J. 2018;39(44):3961-9. doi: 10.1093/eurheartj/ehy474. PMID: 30169657.

318. Tomek J, Bueno-Orovio A, Passini E, Zhou X, Minchole A, Britton O, et al. Development, calibration, and validation of a novel human ventricular myocyte model in health, disease, and drug block. Elife. 2019;8. doi: 10.7554/eLife.48890. PMID: 31868580.

319. Verweij N, Benjamins JW, Morley MP, van de Vegte YJ, Teumer A, Trenkwalder T, et al. The genetic makeup of the electrocardiogram. Cell Syst. 2020;11(3):229-38 e5. doi: 10.1016/j.cels.2020.08.005. PMID: 32916098.